

Development and Characterisation of a Carbon Based pH Microsensor and Studies on Polypyrrole Nanowires



Karen M. Herdman, B.Sc. (Hons.)

Thesis Submitted to the National University of Ireland, in Fulfilment of the
Requirements for the Degree of

Doctor of Philosophy

Based on research carried out in the
Department of Chemistry, Maynooth University

May 2016

Research Supervisors: Prof. Carmel B. Breslin and Dr. Niall J. Finnerty

Head of Department: Dr. John C. Stephens

Table of Contents

Table of Contents	i
Declaration	viii
Acknowledgments	ix
Dedication	xi
Abstract	xii
List of Abbreviations	xiv
Chapter 1: Introduction and Literature Review	1
1.1 Introduction	2
1.2 Objectives and Achievements	3
1.3 Electrochemical Techniques and Theory	3
1.3.1 Cyclic Voltammetry (CV).....	4
1.3.2 Linear Sweep Voltammetry (LSV)	9
1.3.3 Potentiostatic Techniques	9
1.3.4 Electrochemical Impedance Spectroscopy (EIS)	10
1.4 Experimental Techniques	12
1.4.1 Scanning Electron Microscopy (SEM)	12
1.4.2 Energy Dispersive X-ray (EDX)	14
1.4.3 Infra-Red Spectroscopy (FT-IR)	15
1.5 Electrochemical Properties of Polypyrrole	16
1.5.1 Conducting Polymers (CPs)	16
1.5.2 Polypyrrole (PPy)	18
1.5.2.1 Polymerisation of Pyrrole	18
1.5.2.2 Factors Affecting Polymerisation	21
1.5.3 Nanostructures	23
1.5.3.1 PPy Nanomaterials	25
1.6 Voltammetric pH Sensor Development	26
1.6.1 pH	26
1.6.1.1 pH and the Nernstian Equation	27
1.6.1.2 Temperature and pH	27

1.6.1.3 Physiological pH	28
1.6.2 Existing pH Sensors	30
1.6.2.1 Glass pH Electrodes	30
1.6.2.2 Metal Oxide pH Sensors	31
1.6.2.3 Ion Selective Field Effect Transistors (ISFET)	32
1.6.2.4 Optical pH Sensors	33
1.6.2.5 Voltammetric pH Sensors	35
1.6.3 Designing a Voltammetric pH Sensor	35
1.6.4 Carbon Electrodes	36
1.6.4.1 Carbon Paste Electrodes (CPEs)	36
1.6.4.2 Carbon Fibre Electrodes (CFEs)	37
1.6.5 Quinones and Aryl Diazonium Salts	38
1.6.5.1 FBRR	39
1.7 Summary	42
1.8 References	43
Chapter 2: Experimental	54
2.1 Introduction	55
2.2 Experimental Procedures	55
2.2.1 Chemicals and Electrode Materials	55
2.2.1.1 Chemicals and Materials for the Electrochemical Analysis of Polypyrrole (PPy)	56
2.2.1.2 Chemicals and Materials for the Development of a pH Sensor	56
2.2.2 Solutions	58
2.2.2.1 Solutions for the Electrochemical Analysis of PPy	58
2.2.2.2 Solutions for the Development of a pH Sensor	58
2.2.3 Instrumentation and Software	61
2.3 Electrochemical Cell Set Up	63
2.3.1 Preparation of Working Electrodes	65
2.3.2 Electrode Modification	67
2.3.3 Preparation of Electrodes for Surface Analysis	68

2.4	<i>In-Vivo</i> Experiments	69
2.4.1	Electrodes	69
2.4.2	Subjects.....	70
2.4.3	Surgical Protocol	70
2.4.3.1	Induction of Ischemia	71
2.4.3.2	Injection of Sodium Bicarbonate	71
2.4.3.3	Termination	72
2.5	Data Acquisition and Statistical Analysis	72
2.6	References	73

Chapter 3:	Electrochemical Properties of Bulk and Nanowire Morphologies of Polypyrrole.....	74
3.1	Introduction	75
3.2	Results and Discussion	76
3.2.1	PPy Morphologies	76
3.2.2	PPy Morphologies Deposited from Similar Electrochemical Conditions	77
3.2.2.1	PPy in Nanowire Morphology	77
3.2.2.2	Effect of Perchlorate Dopant Ions	79
3.2.2.3	PPy Chain Defects	80
3.2.2.4	PPy in Bulk Morphology	83
3.2.2.5	Electrochemical Properties	85
3.2.2.6	Surface Area of Nanowire and Bulk PPy	86
3.2.3	PPy Morphologies with Similar Electroactive Surface Area	90
3.2.3.1	Bulk PPy Film Thickness.....	91
3.2.4	Electrochemical Impedance Spectroscopy (EIS)	94
3.2.4.1	Comparison of Bulk and Nanowire Morphologies of PPy	95
3.2.4.2	Effect of Applied Potential on PPy Films	98
3.2.4.3	Effect of Electrolyte on Impedance	105
3.2.4.4	PPy Biocompatibility.....	106
3.3	Conclusion	107
3.4	References	111

Chapter 4:	CPE: Optimisation of Electrochemical Reduction of FBRR	115
4.1	Introduction	116
4.2	Results and Discussion	117
4.2.1	Carbon Paste Electrodes	118
4.2.2	Electrochemical Reduction and Cycling	120
4.2.3	Electro-reduction of FBRR	121
4.2.3.1	Stability of FBRR in TEABF ₄ /ACN	123
4.2.3.2	Stability of FBRR in H ₂ SO ₄	124
4.2.3.3	Deposition Scan Rate	125
4.2.3.4	Deposition Potential Range	127
4.2.3.5	Number of Deposition Sweeps	129
4.2.3.6	Evidence of FBRR Deposition	131
4.2.3.7	FBRR Concentration	134
4.2.3.8	Cycling LSV Modified CPEs in PBS	135
4.2.3.9	Scan Rate	135
4.2.3.10	Potential Window	139
4.2.3.11	Stability of Redox Peaks	143
4.2.3.12	Storage of CPEs	145
4.2.3.13	Storage of Modified CPEs	147
4.2.3.14	FBRR/H ₂ SO ₄ Storage	149
4.2.3.15	pH response	150
4.2.3.16	Second Oxidation Peak	156
4.2.3.17	Mitigation of ZnCl ₂	158
4.2.3.18	Real-Time pH Response	160
4.2.3.19	Changing pH using a Constant Flow Rate Pump System	161
4.2.3.20	Observation	162
4.3	Conclusion	164
4.4	References	167

Chapter 5:	<i>In-Vitro</i> Characterisation of CPE/FBRR/H₂SO₄	
	pH Sensor	170
5.1	Introduction	171
5.2	Results and Discussion:	172
5.2.1	Stability of FBRR/H ₂ SO ₄ Modified CPEs	172
5.2.1.1	FBRR/H ₂ SO ₄ Modified CPEs Stored in Air	173
5.2.1.2	FBRR/H ₂ SO ₄ Modified CPEs Stored in N ₂	175
5.2.2	Effect of Styrene on CPEs	177
5.2.2.1	Drying Time of SMCPEs	178
5.2.2.2	Carbon Paste:Styrene Ratio	179
5.2.2.3	Storage After FBRR Deposition.....	181
5.2.3	Biocompatibility	182
5.2.3.1	Bovine Serum Albumen	183
5.2.3.2	Phosphatidylethanolamine	189
5.2.3.3	Triton [®] X	195
5.2.3.4	Brain Tissue	198
5.2.4	Silicone Oil Content of CPEs and SMCPEs.....	201
5.2.4.1	Effect of Physiological Molecules on Oil Content	201
5.2.4.2	Silicone Oil Content during FBRR/CPE Preparation	203
5.2.4.3	Silicone Oil Content of SMCPEs	205
5.2.5	Real-Time pH Recording	208
5.2.6	Carbon Paste Samples	208
5.2.7	Physiological Interferences	211
5.2.7.1	Ascorbic Acid	212
5.2.7.2	Uric Acid	213
5.2.7.3	Dopamine	214
5.2.7.4	L-Cysteine	215
5.2.7.5	L-Tyrosine	217
5.2.7.6	Serotonin	218
5.2.7.7	L-Glutathione	220
5.2.7.8	Homovanillic Acid	221
5.2.7.9	DOPAC	223
5.2.7.10	5-Hydroxy-Indole Acetic Acid	224

5.2.8	Pharmacological Interferences	226
5.2.8.1	Acetaminophen	226
5.2.8.2	Acetylsalicylic Acid	227
5.2.9	Ionic Strength	228
5.2.10	Ion Effect	230
5.2.11	Temperature	232
5.2.12	Reference Electrode	234
5.3	Conclusion	237
5.4	References	240
Chapter 6:	<i>In-Vitro</i> Characterisation of CFE/FBRR pH Sensor	244
6.1	Introduction	245
6.2	Results and Discussion	246
6.2.1	Untreated CFEs	246
6.2.1.1	Electro-reduction of FBRR using CPE Parameters	247
6.2.2	Pre-treating CFEs	249
6.2.2.1	Pre-treatment with PBS.....	250
6.2.2.2	Pre-treatment with NaOH	253
6.2.2.3	Pre-treatment with H ₂ SO ₄	253
6.2.3	Characterising FBRR Modified CFEs	256
6.2.3.1	Deposition of FBRR	256
6.2.3.2	pH Response	257
6.2.3.3	Stability of FBRR/TEABF ₄ /ACN Modified CFEs in Air	259
6.2.3.4	Stability of FBRR/TEABF ₄ /ACN Modified CFEs in N ₂	261
6.2.3.5	Real-Time pH Study	262
6.2.4	Factors Affecting the Operation of a pH Sensor	264
6.2.4.1	Ionic Strength	265
6.2.4.2	Ion Effect	267
6.2.4.3	Temperature	268
6.2.4.4	Reference Electrode	270
6.2.4.5	Physiological Interferences	272
6.2.4.6	Pharmacological Interferences	273
6.2.5	Biocompatibility	274

6.2.5.1	Bovine Serum Albumen	275
6.2.5.2	Phosphatidylethanolamine	275
6.2.5.3	Triton [®] X	278
6.2.5.4	Brain Tissue	279
6.3	Conclusion	281
6.4	References	284
Chapter 7:	<i>In-Vivo</i> Characterisation of Carbon/FBRR pH	
	Sensors	287
7.1	Introduction	288
7.2	Results and Discussion	289
7.2.1	FBRR Modified CFEs	290
7.2.1.1	Effect of Lowering Tissue pH	290
7.2.2	FBRR Modified CPEs	293
7.2.2.1	Effect of Lowering Tissue pH	293
7.2.2.2	Oxygen and pH	300
7.2.2.3	Effect of Increasing Tissue pH	301
7.3	Conclusion	308
7.4	References	310
Chapter 8:	General Conclusions	313
8.1	Conclusions	314
8.2	References	321
8.3	Conference Presentations.....	324
8.4	Publication	324

Declaration

I hereby certify that this thesis has not been submitted before, in whole or part, to this or any other university for any degree, and is, except where stated otherwise, the original work of the author.

Signed _____

Date _____

Karen Herdman, B.Sc. (Hons)

Acknowledgements

Firstly, I would like to thank my supervisors, Professor Carmel Breslin and Dr. Niall Finnerty for their exemplary supervision over the past few years. I will forever be indebted to you both.

Carmel, your encouragement, support and vast knowledge are hugely appreciated. Thank you for convincing me that age was no barrier to undertaking a PhD. I sincerely appreciate all the time and opportunities you have afforded me, especially the invaluable trips to America. You are a great room-mate and mentor. I will always hold you in great esteem. Niall, thanks for taking a chance on me, for the confidence you instilled in me as an independent researcher. Your enthusiasm for your work is truly admirable. Thanks for the laughs and constant innuendos, the lab was never a dull place to work. I wish you success in your future endeavours as an amazing P.I.

I wish to express my appreciation to the Irish Research Council for funding my work for the past three years. Thanks also to Prof. John Lowry for the lab space and Dr. Fiachra Bolger for his expertise. Special thanks to all in the Biosensors lab, Michelle, Caroline and Dr. Keeley, for the daily chats and many laughs. I also must mention my past colleagues Drs. David, Emer and Orla, in my beloved home from home, the Electrochemistry lab. Thanks for welcoming me into the lab and all the invaluable discussions and help in my first year as a post-grad, and beyond. I wish you all success and happiness for your futures.

To Mr. Noel Williams, who showed me that humans can interact with computers (sometimes), and was always so willing to help. Thanks to all the technical staff, especially Ollie, for all your help with the SEM. To Donna and Carol, thanks for the chats while printing the many drafts of this thesis and delivering my internet shopping.

To my fellow post grads, (who I am not going to name individually for fear of omitting anyone), thanks for all the nights out and the tea room banter. Thanks Andrew Reddy for your help with referencing. The “extras” you put on my PC are forever etched in my memory. Emer, thanks for your endless singing and afternoon chats. I wish you all successful careers and much joy and happiness in your lives.

Moving away from Maynooth, I now need to thank all those who are closest to me. Mags, thanks for all the girlie weekend breaks, we have a lot of catching up to do. To

my buddy Lee, you are an inspiration, my Martini person (anytime, anyplace, anywhere), there are times I would not have got through without your affection and advice.

This is a journey I embarked on almost 9 years ago, and I couldn't have done it without the support of a wonderful family. Unfortunately, my parents are no longer on this Earth, but you both made me who I am today. Thank you, I miss you both very much every day. To my siblings and the in-laws, thanks for all the support and encouragement, cheesecake is back on the menu!!

Finally, to the men in my life, my darling husband Aidan and my two sons Alan and Brian. Aidan, for being so supportive, loving, patient and understanding (and my cash machine). Your endless puns and corny jokes always put a smile on my face. Alan and Brian, you both make me proud and happy every day. My wish for you is health and happiness. Keep dreaming until all your dreams come true, x.

Dedication

For Aidan, Alan and Brian, with love and pride.

“A setback means the path you took didn’t work. It doesn’t mean all roads are closed toward your dream, nor does it invalidate your effort”

Dodinsky

Abstract

In this thesis the electrochemical deposition of polypyrrole (PPy) into nanowire and bulk morphologies is reported. The electrochemical properties of the different conformations of PPy were examined in order to ascertain their conductivities and surface areas. This could determine the optimisation for further modification of the polymer with, e.g., copper structures forming an electrochemical sensor for the detection of the nitrate ion. PPy nanowires were electrodeposited onto gold electrodes using slightly acidic anions (Na_2HPO_4) and non-acidic anions (LiClO_4) at a fixed potential of 0.80 V *vs.* SCE. The nanowires produced had an average diameter of *ca.* 89.2 nm, $n = 50$. Bulk PPy was electrodeposited using similar conditions, but the pH of the solution system was reduced using concentrated HClO_4 . This resulted in a bulk polymer with a higher surface area, so a second bulk polymer, of similar surface area to the nanowire films, was formed by reducing the electrodeposition time/charge consumed. Both of these bulk polymers were compared with the nanowire morphology of PPy using the electrochemical techniques of cyclic voltammetry, (CV), and electrochemical impedance spectroscopy, (EIS). Impedance data were fitted to equivalent circuits and the polymer resistance, the double-layer capacitance and the polymer capacitance were determined. The results indicated that the electrochemical properties of the polymers changed as the polymers went from an oxidised to a reduced state, i.e., their resistances and ability to store energy, confirming their optimum working potential range.

The second section of this thesis seeks to develop a miniaturised analytical device that can deliver real-time information on changes in tissue pH. Many different pH probes exist, but they present many limitations including fragility, difficulty in miniaturising, potential drift, and difficulties in accurately measuring pH in solutions of varying ionic strength. There therefore remains a pressing need for more robust, pH sensors that can accurately sense pH changes in hostile surroundings, e.g., the highly resistive tissue found in the clinical environment.

In this study, carbon paste electrodes (CPEs) and carbon fibre electrodes (CFEs) were modified with a quinone containing diazonium salt, FBRR, by electrochemical deposition. In buffered media, the quinone/hydroquinone redox system involves

changes of the protonation state of the molecule, resulting in the observation that potentials vary with pH in a Nernstian manner. This behaviour was used as the basis of the electrochemical pH sensor. Various deposition conditions were employed to give the optimum and most efficient method, while organic and aqueous solvents were employed as the supporting electrolytes. Using either solvent the electrochemical techniques of CV, and linear sweep voltammetry, (LSV), were applied, optimising FBRR deposition by varying parameters such as potential window, scan rate and number of cycles/sweeps. Modified CPEs were calibrated for their pH response by CV, showing a response slope of -60.36 ± 0.89 mV/pH, $n = 23$. The surfaces of bare and derivatised CPEs were analysed by scanning electron microscopy, (SEM), coupled with energy dispersive X-ray, (EDX).

After *in-vitro* development of a working pH sensor, a full characterisation was carried out, over the required pH range. This aimed to assess the sensor sensitivity, operational and storage stability, biocompatibility, and the effects that multiple interferences, found in the *in-vivo* environment had on the sensor performance. *In-vivo* voltammetry conditions were mimicked by changing the operational temperature and using a physiologically suitable reference electrode. An extensive study into the effect that the carbon: silicone oil content of CPEs had on the electrochemical properties of the modified electrodes was carried out using CV and corroborated by SEM and EDX surface analyses. These analyses concluded that although the electrodes appeared to perform better when exposed to proteins and lipids, the level of improvement did not justify the additional two days required in the manufacturing process of the sensor.

The *in-vivo* application of the pH sensor was subsequently examined. The sensor was inserted into the hind limb muscle of anaesthetised rats. A pH change was induced locally to the limb by applying a tourniquet to restrict the blood flow and induce ischemia. This caused an increase in CO₂ levels thus reducing the pH. After a short period of time, ca. 10 minutes, the tissue pH was allowed to recover. To induce an increase in the pH, injections of NaHCO₃ were administered locally showing an immediate change in the observed potential, which recovered soon after. These changes in potential, of which pH was a contributing factor, were successfully recorded in real-time.

List of Abbreviations

5-HIAA	5-Hydroxy-Indoleacetic Acid
5-HT	5-Hydroxytyramine
AA	Ascorbic Acid
ACN	Acetonitrile
ACOP	Acetaminophen
ASA	Acetylsalicylic Acid
aCSF	Artificial Cerebrospinal Fluid
BSA	Bovine Serum Albumen
CPA	Constant Potential Amperometry
CPE	Carbon Paste Electrode
CFE	Carbon Fibre Electrode
CP	Conducting Polymer
CV	Cyclic Voltammetry
DA	Dopamine
DOPAC	3,4-Dihydroxyphenylacetic Acid
ECF	Extracellular Fluid
EDX	Energy Dispersive X-ray
EIS	Electrochemical Impedance Spectroscopy
FBRR	4-Benzoylamino-2, 5-Dimethoxybenzenediazonium Chloride Hemi Zinc Chloride
FT-IR	Fourier Transform Infrared Spectroscopy
HVA	Homovanillic Acid
IVV	<i>In-Vivo</i> Voltammetry
LSV	Linear Sweep Voltammetry
NPV	Normal Pulse Voltammetry
OCP	Open Circuit Potential
PBS	Phosphate Buffered Saline
PEA	3-sn-Phosphatidylethanolimine
PPy	Polypyrrole
PSS	Polystyrenesulfonate
RI	Refractive Index

SCE	Saturated Calomel Electrode
SEM	Scanning Electron Microscope
Sty	Styrene
TEABF₄	Tetraethyl Ammonium Tetra-Fluoroborate

Chapter 1

Introduction and Literature Review

1.1 Introduction

Within this thesis lies two separate domains. Chapter 3 of this thesis discusses the first of these. It describes the electropolymerisation of pyrrole in two different conformations, bulk and nanowire, specifically designed, (A) from the same electrochemical deposition parameters and (B) to have similar electroactive surface areas. Nanomaterials are attractive candidates for use as electrochemical sensors due to their high sensitivity and fast redox chemistry.¹ The use of nanostructured materials has led to increases in efficiencies of electron transfer rates compared to the typical 'bulk' morphology.² Herein, a study of their electrochemical properties is performed, using cyclic voltammetry, (CV), and electrochemical impedance spectroscopy, (EIS). The relationship between the charge passed during electropolymerisation and the thickness of polymer formed is investigated, along with the effect of electrolyte on the electrical properties of the polymers. This introduction makes reference to nanomaterials and their properties, gives an outline of conducting polymers (CPs) and a description of their polymerisation, in relation to polypyrrole (PPy).

The primary aim of the remaining chapters of the thesis, (Chapters 4-7) is the development of a carbon based sensor, electrochemically modified with a diazonium salt, capable of monitoring *in-vitro* pH changes, within the tightly regulated biological pH ranges, to a sensitivity of 0.01 pH units. The aim of this work is to develop a voltammetric pH sensor, which measures changes in the redox potential of an electroactive surface attached species, 4-Benzoylamino-2,5-dimethoxybenzenediazonium chloride hemi zinc chloride salt, also referred to as Fast Blue RR, (FBRR). Increasing medical and biological interest in cheap disposable analytical and diagnostic devices has driven research towards the development and adaptation of low-cost electronic sensing devices. Carbon-based sensing materials are attractive substrates for this application since they are intrinsically biocompatible, conductive, and appropriate for surface modification.³ The reduction of diazonium salts onto carbon surfaces,⁴⁻⁶ pioneered by Savéant and co-workers⁷ in the early 1990s is a well-characterised method for the selective *in-situ* attachment of organic molecules. This mechanism involves the electrochemical generation of a solution radical from the diazonium modifier and subsequent covalent linkage to the carbon surface, which possesses excellent stability to external stimuli.⁸

Chapter 7 details a targeted application of the developed pH sensor, where pH changes were recorded in the *in-vivo* environment.

1.2 Objectives and Achievements

The first objective of this work was to deposit PPy onto a gold substrate in two different morphologies, bulk and nanowire. These were formed from the same electrochemical parameters resulting in polymers of different surface area. A second bulk polymer was specifically designed to have a surface area close to that of the nanowire polymer. The electrochemical properties of the formed polymers were compared using CV and EIS. An electrochemical comparison was carried out in order to determine which surface morphology could be easiest modified with e.g., copper structures for the detection of the nitrate ion. The effect of electrolyte solution on the electronic properties of the polymers was also investigated. All of this work is contained in Chapter 3.

The main objective of the thesis was the development and characterisation of a voltammetric pH microsensor, suitable for *in-vivo* applications. Chapter 4 investigates the optimum electrodeposition parameters of FBRR onto carbon paste electrodes, (CPEs), resulting in a near Nernstian response over the biologically relative, pH range of 7.20 to 7.60. Following the optimisation of the electrode design, Chapter 5 applies a rigorous regime of test conditions to the pH sensor, to evaluate its suitability for use in the challenging *in-vivo* environment. These included stability testing and exposing the sensor to a range of conditions to determine its biocompatibility. As well as CPEs, carbon fibre electrodes, (CFEs), were also used as a substrate for the pH sensor design. Chapter 6 discusses their optimisation, including their suitability in the *in-vivo* setting. Finally, the modified sensors are applied *in-vivo*, where pH changes are induced in live tissue using *in-vivo* voltammetry (IVV).

1.3 Electrochemical Techniques and Theory

A number of different electrochemical techniques were employed throughout this thesis. In the formation and characterisation of the PPy films the electrochemical techniques of CV, CPA and EIS were employed. For the pH sensor development, the

techniques used included, CV, LSV and CPA. These techniques are described in this section.

1.3.1 Cyclic Voltammetry (CV)

CV was a technique used frequently throughout this thesis, for the electrochemical characterisation of PPy films, including scan rate analyses, deposition of FBRR, determination of the pH response and interference studies. It was also used for *in-vivo* experiments, known as *in-vivo* voltammetry (IVV). CV is one of the most useful and widely applied techniques in electrochemistry,⁹ which reveals information about the nature of the electrode and the reactions taking place at the electrode/electrolyte interface. It involves scanning the potential applied to the working electrode, between two potential limits, and recording the current as a function of the applied potential, see Figure 1.1(B).¹⁰ The applied potential is ramped at a scan rate, v , between two potential limits. The potential scan rate, usually varies from mV/s to V/s.¹¹ The initial applied potential, E_i , is swept to a vertex potential, E_v , where the scan is reversed and swept back to the final potential, E_f , producing a triangular waveform over time, as shown in Figure 1.1(A).

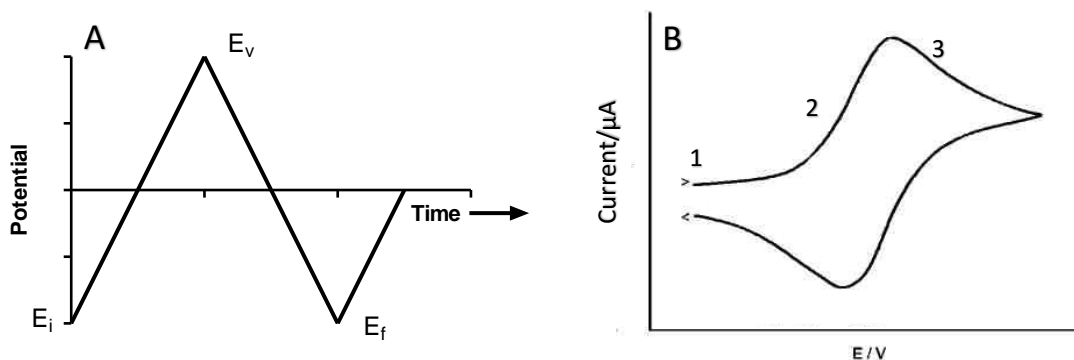


Figure 1.1: (A) Triangular waveform formed as potential is changed over time, and (B) typical CV showing the current/potential transient.

For a simple redox reaction, Equation 1.1, where only R (a reduced species) is present, the current response of the forward scan is the linear potential sweep voltammogram as R is oxidised to O (the corresponding oxidised species) which produces an anodic peak. On the reverse scan, the reduction of O to R occurs, resulting in a cathodic peak.



The oxidation and reduction peaks in CV are formed, as potentials that differ to the equilibrium potential, E_{eq} , are applied to the electrode/solution system. Figure 1.2(A) shows a system at equilibrium, where the highest occupied molecular orbital (HOMO) of the solution has the same energy as the Fermi level of the metal (working electrode, W.E.). As there is no net transfer of electrons, no current flows. Figure 1.2(B) shows the effect of applying a potential higher than the equilibrium potential, resulting in an oxidation reaction, of the solution species. Applying a potential, (E_{app}), more positive than the equilibrium potential (E_{eq}), reduces the energy of the electrons in the W.E., reducing the energy of the Fermi level. The higher energy electrons, in the solution HOMO, transfer to the Fermi level of the metal, resulting in an oxidation reaction.

Using the CV shown in Figure 1.1(B), it can be seen at (1) there is no current flowing as the applied potential is not far enough from equilibrium to induce electron transfer. As the potential is swept to more oxidising values, the oxidation of R to O begins, with a corresponding flow of current, (2). As the potential becomes even more positive, the concentration of R, at the electrode surface drops, causing a sudden influx of the reduced species to the electrode, and the current continues to rise, as R is converted to O with greater efficiency, until a peak maximum is reached. Once the applied potential becomes more positive than the system's standard potential, E_0 , the concentration of the reduced species tends to zero and the current then begins to diminish¹², as the diffusion layer thickens, (3). The potential then sweeps back through the equilibrium position gradually converting the oxidised species back to the reactant, by the corresponding reduction reaction.

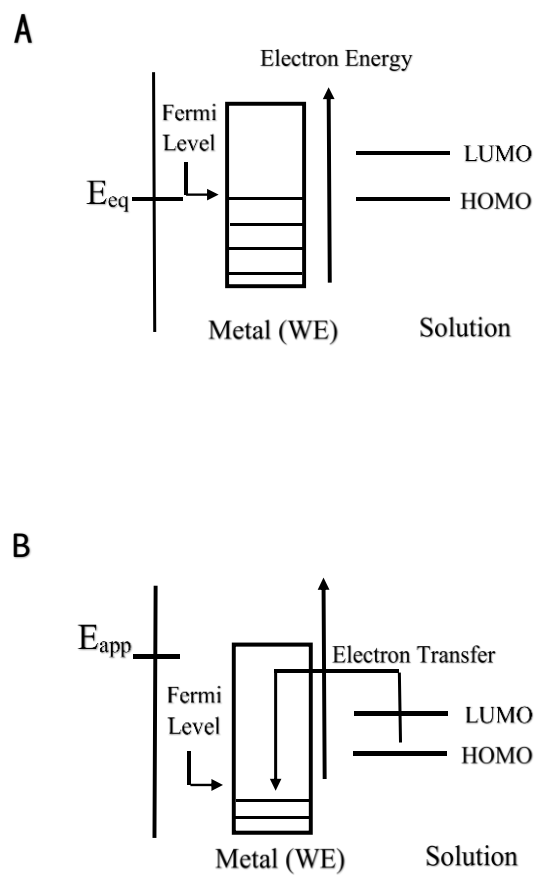


Figure 1.2: Schematic of (A) an electrode/solution in equilibrium, (B) an electrode/solution system undergoing an oxidation reaction.

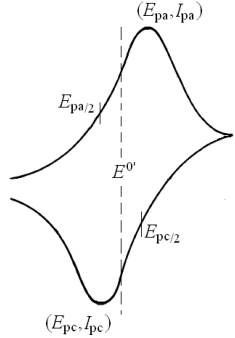
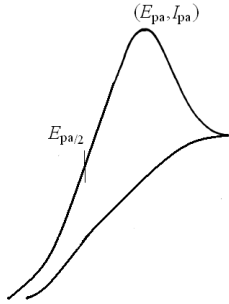
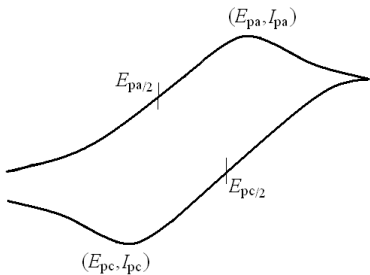
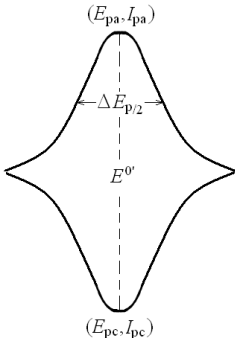
Reversible	Irreversible
 <p data-bbox="539 674 644 712">$I_p \propto v^{1/2}$</p> <p data-bbox="472 741 715 779">E_p independent of v</p> <p data-bbox="464 801 722 840">$E_p - E_{p/2} = 59/n \text{ mV}$</p>	 <p data-bbox="1102 674 1208 712">$I_p \propto v^{1/2}$</p> <p data-bbox="986 741 1324 779">E_p increases as v increases</p>
Quasi-reversible	Adsorption
 <p data-bbox="440 1350 746 1388">I_p not proportional to $v^{1/2}$</p> <p data-bbox="424 1417 762 1456">E_p increases as v increases</p>	 <p data-bbox="1114 1350 1193 1388">$I_p \propto v$</p> <p data-bbox="1034 1417 1276 1456">E_p independent of v</p>

Figure 1.3: ¹³ Typical CVs showing their respective peak current and peak potential responses.

As the system is scanned over the applied potential range, the changes in the current responses can be either faradaic, i.e., the oxidation and/or reduction of a species present, or non-faradaic, i.e., capacitive.¹⁴ Capacitance is defined as the ability of a material to store charge.¹⁵ There are three main parameters of interest, that describe a CV, the peak current, I_p , the peak potential (E_p), and the potential width at half peak

($E_P - E_{P/2}$). From these, various characteristics of the electrode/solution system can be defined, leading to four main CV responses, shown in Figure 1.3. Each response is characterised by a different shape of the corresponding CV. The dependence of each parameter on the scan rate, v , allows the characterisation of the electrochemical system. E_P does not change with v , for reversible systems. The I_P changes linearly with $v^{1/2}$ for diffusion controlled, reversible and irreversible systems, and with v for reversible adsorbed species. Generally, the voltammogram takes longer to record as the scan rate is decreased, this influences the diffusion layer thickness.¹⁶ At slow scan rates the diffusion layer grows much further from the electrode. The influx of ions, to the electrode surface, will be smaller, as there is a smaller concentration gradient and the current will be lower at slow scan rates and higher at high rates. The correlation between I_P and $v^{1/2}$ for *quasi*-reversible systems depends on the scan rate and the electron-transfer rate constant. Generally, there is no correlation between I_P and $v^{1/2}$ at high scan rates, and for reactions which display slow electron-transfer kinetics. If the peak occurs at the same potential, i.e., does not change with the scan rate, fast electron transfer kinetics are present, indicating a reversible electron transfer reaction. The diagnostic equations used to probe the redox characteristics have been described in many electrochemistry textbooks.^{9, 11, 17}

Throughout this thesis, different sized electrodes were used, ranging in diameter from 3 mm down to 7 μm . The CVs of microelectrodes are shaped differently to macroelectrodes as the geometry of an electrode dictates the mass transport to its surface.¹⁸ Therefore, diffusion dependant techniques, e.g., CV, effect the electrode response. The currents are lower at microelectrodes, due to their smaller surface area, but also the current goes to a steady-state¹⁹ value and is sigmoidal.²⁰ This is related to diffusional processes. Microelectrodes are considered as a “dot” with the diffusion layer being hemispherical in shape and extending out into the solution. The amount of electroactive species diffusing to the electrode surface is limited by the volume enclosed by the increasing hemisphere, not like a plane projecting into the solution for a macroelectrode, see Figure 1.4. The time scale of the experiment plays an important role in the size of the diffusion layer at microelectrodes, and hence, the shape of the resulting CV. For microelectrodes, the initial growth of the diffusion layer is similar to that of larger macroelectrodes, i.e., the diffusion layer is smaller than the electrode

surface and planar diffusion dominates. For short experimental times, e.g., fast scan CV, the size of the diffusion layer is smaller than that of the electrode, and planar/linear diffusion dominates, even at microelectrodes. Over longer experimental times, the dimensions of the diffusion layer exceed those of the microelectrode, and the diffusion becomes hemispherical.²¹

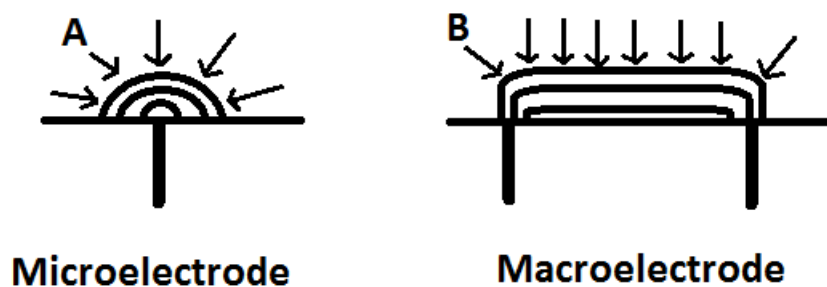


Figure 1.4: Diagrams depicting the growth of the diffusion layers at (A) a microelectrode, resulting in hemispherical diffusion and (B) a macroelectrode, resulting in planar diffusion.

1.3.2 Linear Sweep Voltammetry (LSV)

LSV is considered a special case of CV, in that a potential sweep is applied to the working electrode, but the potential is scanned only once, in one direction. It provides useful information about the system under investigation. LSV is conducted in a stationary solution, thereby only relying on diffusion as a means of mass transport.²² In this thesis, LSV was applied in the electro-reduction of FBRR onto carbon substrates.

1.3.3 Potentiostatic Techniques

Constant Potential Amperometry (CPA) involves the application of a constant potential to the working electrode, while monitoring the resultant current output, (I), with respect to time, (t). These plots are typically called transients to emphasise their time dependence. The potential at the working electrode is instantaneously stepped from the resting value, where no electrolysis occurs, to a value where conversion of

the reactants begins.^{22, 23} In this thesis, CPA was used in the formation of bulk and nanowire morphologies of PPy. An anodic potential, of 0.80 V *vs.* SCE, was applied to oxidise the monomer units, which polymerised and deposited onto the electrode surface. The resultant current was proportional to the rate of polymerisation occurring at the electrode surface.²⁴

A constant potential can be applied for a fixed period of time, (chronoamperometry), or until a desired charge is attained, (chronocoulometry). The charge passed can be calculated from the integral of the current.²⁵ The total charge passed, after an electrode reaction, can be related to the thickness of a polymer film.²⁶

CPA was also used to pre-treat CFEs prior to the electro-deposition of FBRR onto the electrode surface, a practice which improves the electrode kinetics.²⁷⁻²⁹ This was achieved by applying a potential of 2.0 V *vs.* SCE for 30 s followed by -2.0 V *vs.* SCE for 10 s.

1.3.4 Electrochemical Impedance Spectroscopy (EIS)

EIS is a method used to examine several factors at the working electrode surface, including, the stability, kinetics, and double layer capacitance.^{30, 31} Impedance measurements involve the application of a small perturbing sinusoidal potential of 5 or 10 mV, superimposed on the fixed baseline applied potential or versus the open-circuit potential, OCP. A shift in the phase and amplitude of this sinusoidal potential can occur, resulting in an AC current. A frequency response analyser measures the difference in amplitude and time lag, θ , over a range of frequencies. Any shift in the phase or amplitude of the potential results from variations occurring in the electrochemical cell. An advantage to EIS is its ability to operate over a wide frequency range, which allows processes, with different time scales, to be detected within the same experiment. Slow processes, e.g., the diffusion of ions inside the bulk of a conducting polymer, can be probed at low frequencies, whereas fast processes, e.g., the formation of a surface double-layer are examined at high frequency.

EIS was used in this thesis as an experimental method for characterising the electrochemical systems of bulk and nanowire conformations of PPy. Experiments were recorded over a frequency range from 65 kHz to 5 mHz at various applied potentials,

from -0.50 to 0.50 V *vs.* SCE including the OCP. As impedance is only applicable to electrochemical systems that behave linearly and are in a steady state condition, the polymer films were conditioned for 30 minutes to ensure the system was under steady-state conditions before the measurements were performed. The perturbing sinusoidal potential was maintained at 5 mV, which was low enough to keep the overall state of the system unchanged.

In an EIS experiment the input signal is an alternating potential and the output signal is the corresponding alternating current which has the same frequency but a different phase. The phase angle, θ , and impedance, Z , are computed. The impedance results are displayed in two different graphical formats, Nyquist and Bode plots. In the Nyquist, or complex plane plot, the real and imaginary components (Z' and Z'') are plotted as x and y axis in a Cartesian system. In the Bode plot the modulus and phase of the impedance ($|Z|$ and θ) are plotted against the frequency. Typical Nyquist and Bode plots, for a bulk PPy film, are shown in Figure 1.5.

These data are then fitted to equivalent electric circuits that represent real, physical components, of the electrical behaviour for the system under examination. Two main elements were used when fitting the data to equivalent circuits, resistors and constant phase elements. A resistor has no imaginary component and therefore, its value is equal to the impedance of the system. Resistors represent the resistive elements in the experimental system, e.g., solution resistance and the resistance of charge transfer. Constant phase elements, can be used to determine the capacitance of the interface and also diffusion processes in the polymer layer. Constant phase elements are often used in fitting impedance data, instead of pure capacitors, due to surface roughness and electrode porosity.³² A constant phase element is defined by two parameters, an actual value (T) and an exponent (P). The CPE-T value gives the physical value of the constant phase element. The CPE-P gives information on the physical process occurring. When CPE-P = 1.0, the CPE behaves as an ideal capacitor. However, values between 0.8 and 1.0 are values consistently obtained for a porous surface, like PPy. A value of 0.5 is indicative of a diffusion process and coincides with a phase angle of 45°.

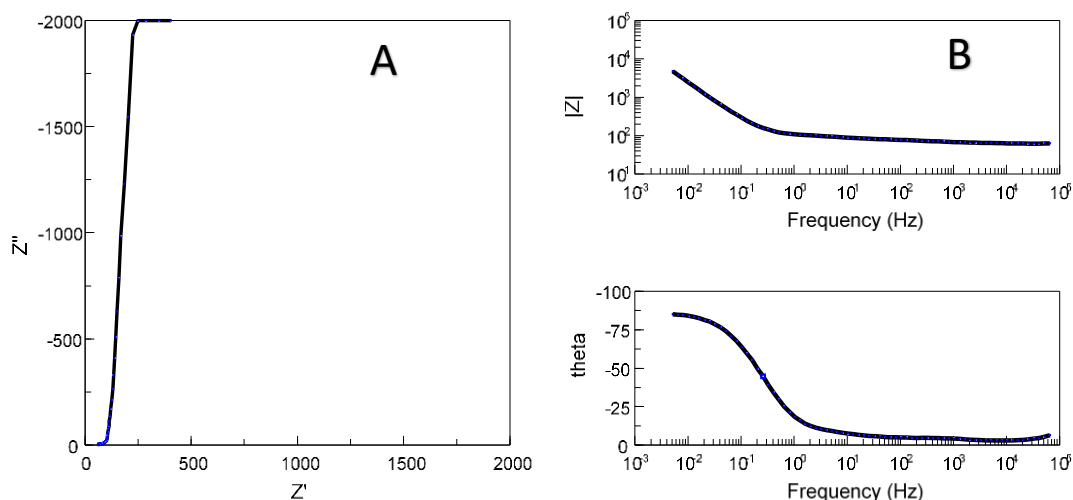


Figure 1.5: The impedance response of a typical PPy film (A) Nyquist plot and (B) Bode plots.

1.4 Experimental Techniques

1.4.1 Scanning Electron Microscopy (SEM)

An optical microscope has several limitations that are overcome by an SEM. Firstly, visible light has a long wavelength, *ca.* 550 nm, whereas with electron microscopes a voltage (kV) is applied to an electron gun, causing electrons to eject from a tungsten filament and accelerate down an optic column. The higher applied voltage, generates electrons with higher energy, and shorter wavelength, Equation 1.2. Also, an optical microscope has a poor depth of field caused by a large aperture angle. The aperture angle is defined as the angle between a line from sample to the lens centre and a line from the sample to the edge of the aperture opening.³³ An SEM has a large focal length and a small aperture opening, giving a large depth of field.

$$\lambda = \left(\frac{1.5}{V}\right)^{\frac{1}{2}} \quad 1.2$$

There are two main components to an SEM, the electron column and the control console. The electron column contains an electron gun and a series of lenses that direct the electrons down to the sample. The electron source, lenses and sample must be under vacuum as electrons cannot travel freely through air. The SEM uses a focused

beam of high-energy electrons, from the electron gun, to generate a variety of signals, categorised by elastic or inelastic interactions,³⁴ at the surface of solid specimens, as shown in Figure 1.6 ([http://www. Jeol.co.jp](http://www.Jeol.co.jp)). Many SEMs contain a tungsten filament that is heated by passing a current through it. The filament emits light and an electron cloud forms around it. Electrons emerge from the electron gun and are pushed down into the columns, by an accelerating voltage ranging from 1 to 30 kV, in a spray pattern, and are focussed to the sample through the series of electromagnetic lenses. The electron beam interacts (elastic interaction) with the sample to a depth of *ca.* 1 μm , emitting backscattered electrons from the sample surface, which generates a signal to create an image. The inelastic scattering which results from the deep interaction of the incident electrons with the nuclei and electrons of the material, generates other signals, including secondary electrons, X-ray emissions and auger electrons. These signals from the specimen give information about the sample including texture, chemical composition, and crystalline structure.³³ SEM analysis is considered to be "non-destructive"; that is, X-rays generated by electron interactions do not lead to volume loss of the sample, so it is possible to analyse the same materials repeatedly.

Two limitations to SEM are:

- (a) Samples must be solid and they must fit into the microscope chamber.
- (b) The sample must be conducting. An electrically conductive coating must be applied to electrically insulating samples before analysing unless the instrument is capable of operation in a low vacuum mode.

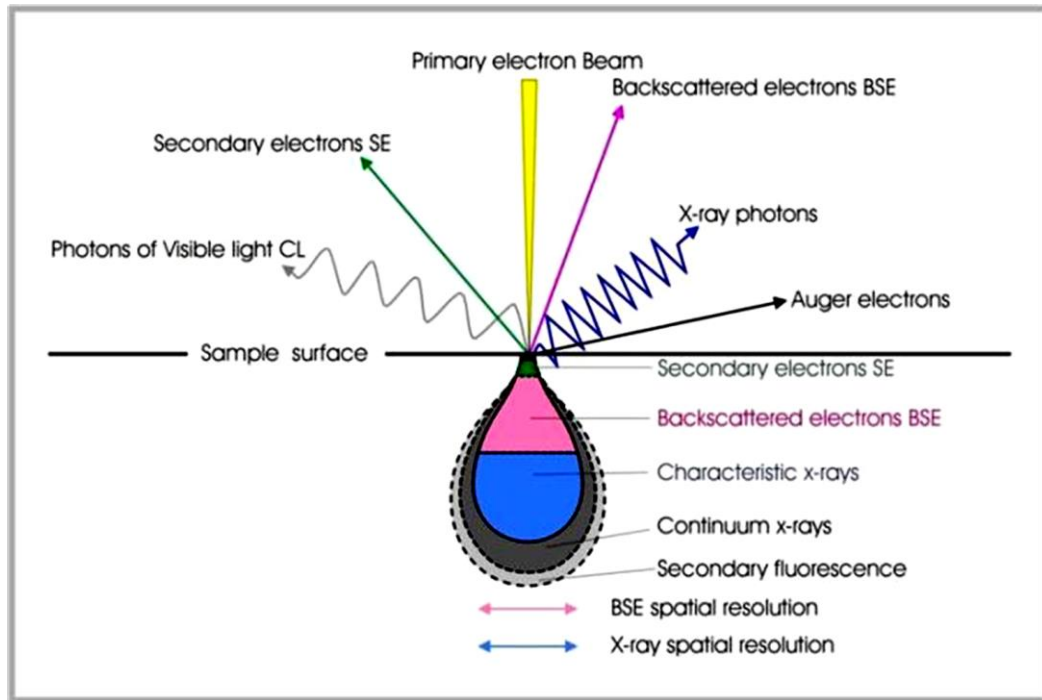


Figure 1.6: Schematic representation of electron-material interactions in the SEM. The volume of interaction of the electron beam with the sample surface and corresponding areas from which different signals originate. ([http://www. Jeol.co.jp](http://www.Jeol.co.jp)).

1.4.2 Energy Dispersive X-ray (EDX)

EDX is used in conjunction with SEM, as X-rays are generated when the electrons interact with the sample. When an electron beam interacts with a sample creating secondary electrons, it leaves thousands of the sample atoms, with holes in the electron shells, where the secondary electrons used to be. If these "holes" are in inner shells, then the atoms are not in a stable state, so electrons from the higher energy outer shells will drop into the vacant sites. These electrons, moving from higher to lower energy states, emit energy in the form of X-rays. Since each element has characteristic X-ray energy and wavelength, the elemental composition of a sample can be identified. This is a non-destructive technique, as is SEM. EDX can perform elemental analysis in areas, as small as $0.5 \mu\text{m}$ in size. The X-rays are emitted from a depth that depends on how deep the secondary electrons are formed. Depending on the sample density and incident beam, this is usually from 0.5 to $2 \mu\text{m}$ in depth.³³

EDX analysis can also quantify the elements it detects. This is carried out by calculating the area under the peak of each identified element of the sample.

Calculations convert the area under the peak into weight or atomic percentage. However, the quality of this quantitative analyses depends on the surface roughness of the sample,³³ so in this thesis it has been used for quantitative estimations.

1.4.3 Infra-Red Spectroscopy (FT-IR)

Fourier Transform Infrared spectroscopy (FT-IR) was used for the identification of carbonyl defects on the pyrrole polymer chain and their subsequent removal, (see Section 3.3.2.3). FT-IR was carried out using a Perkin Elmer 2000 FT-IR spectrometer. All samples were prepared by grinding with potassium bromide (KBr) and pressed into discs. The use of KBr limits the loss of information, as KBr does not contain IR bands in the mid-IR region of the electromagnetic spectrum.³⁵

FT-IR spectroscopy measures the vibrational motions of atoms, around their connecting bonds, when they are excited by electromagnetic radiation from the IR region of the electromagnetic spectrum. IR photons do not carry enough energy to cause electronic transitions, however, they have sufficient energy to cause groups of atoms to vibrate, with respect to the bonds between them. Since molecules absorb IR radiation at specific frequencies and wavelengths, the resulting vibrations are characteristic of certain energies, providing a means to identify the groups and species present in a material.³⁵ Every group has a characteristic frequency or band of absorption, determined by their wavelength, λ , or its reciprocal value, wavenumber, cm^{-1} .

The frequency of vibrations between two atoms depends on two quantities; the mass of the atoms involved, and the rigidity of the bonds between them. Heavier atoms vibrate slower than lighter atoms, and strong bonds, which tend to be more rigid, require more energy to stretch and/or compress the bonds between them. This leads to an IR spectrum, resulting in a characteristic, unique fingerprint of a compound.³⁶

1.5 Electrochemical Properties of Polypyrrole Films

This section gives an introduction to CPs, in particular PPy. The polymerisation mechanism for PPy is examined, along with the various factors which affect the chemical and physical properties of the resultant polymer. A brief introduction into the evolution of nanostructuring is given, with an emphasis on PPy nanowires.

1.5.1 Conducting Polymers (CPs)

Contrary to an article by Pople and Walmsley in 1962³⁷ stating that “Although it is not possible to synthesise very long polyenes (polyacetylene) at present...”, the first polymerisation of acetylene had been reported in the late 1950’s by Natta et al.³⁸ Up until the 1970s lots of literature, on the subject, was published by chemists and physicists, but it was not until 1977,³⁹ when chemists and physicists began to work together, that the first report of electrical conductivity in a conjugated polymer was achieved, by exposing the polymer to oxidising or reducing agents, i.e., dopants, which insert into the polymer backbone to enhance its conductivity. This breakthrough led to extensive research in the field of CPs. In 2000, the Nobel prize in Chemistry was awarded to MacDiarmid, Heeger, and Shirawaka, for their initial work on polyacetylene leading to the discovery and development of polymers that are electrically conducting.⁴⁰ The high electrical conductivity and good redox properties⁴¹ has led to extensive studies in the field.

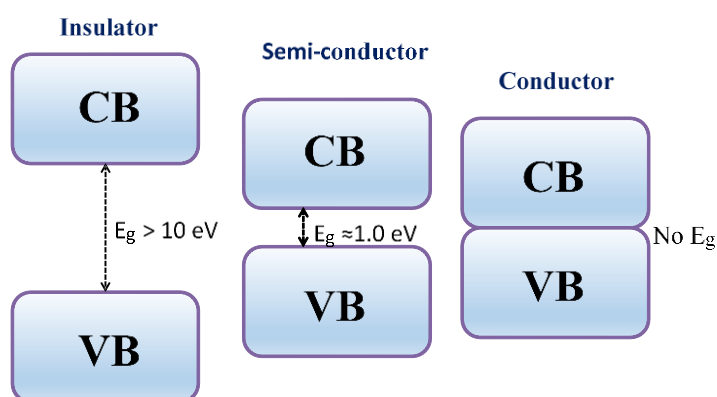


Figure 1.7: The energy differences between the valence band (VB) and conduction band (CB) for a conductor, semiconductor and insulator.

The conducting properties of polymers can be described using the band gap theory of solids,⁴² electron delocalisation and the choice of doping anions.^{43, 44} A schematic of a band gap energy diagram is shown in Figure 1.7. The highest occupied energy level for electrons is called the valence band (VB), and the lowest unoccupied level is the conduction band (CB). The energy required to excite an electron from the valence band into the conduction band is known as the band gap energy, E_g . If the band gap energy, between the conduction and valence bands, is large (>10 eV), electron promotion into the conduction band is inhibited and an insulator is formed. Similarly, if the valence and conduction bands overlap, there is no band gap energy, and a conductor results. If the energy gap is *ca.* 1.0 eV, then electrons can be promoted into the conduction band and the result is a semi-conductor. In general, the band gap energy of CPs is close to 1.0 eV, so they can be considered as semiconductors.

The conductivity of CPs is not entirely explained by the band gap theory. CPs are conjugated systems, giving a series of alternating double and single bonds. Electrons are delocalised over the conjugated system, so charge can spread over the polymer backbone⁴⁵ giving electrical conductivity. The conjugated double bonds along the backbone of CPs allow free movement of electrons within the polymer chain, making them electronically conducting.³¹ However in their neutral state, conductivity levels remain low. The increased conductivity of CPs results from the formation of charge carriers, when the polymer is oxidised (p-doped) and reduced (n-doped). Oxidation causes the formation of polarons, which form along the entire length of the polymer chain.²⁴ Figure 1.8 shows a schematic of the oxidation of a CP (PPy) resulting in the formation of a polaron. Upon the loss of a second electron, it is energetically more favourable to remove this electron from the polaron, rather than from the polymer chain. This leads to the formation of bipolarons instead of a pair of polarons⁴² and the polymer is now in its fully oxidised state. This process forms localised electronic states within the band gap.⁴² Bipolarons, are capable of movement along the polymer backbone, due to the conjugation,⁴⁶ and are associated with the incorporation of a counterion (A^-) to balance the charge generated. These counterions are commonly referred to as dopants.

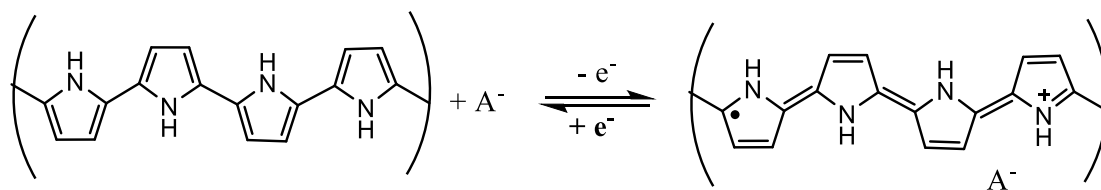


Figure 1.8: Diagram showing the formation of a polaron, resulting from the oxidation of a CP (PPy).

1.5.2 Polypyrrole (PPy)

PPy, see Figure 1.9, is a black insoluble material, which was first electrochemically synthesised by Dall'Olio *et al*⁴⁷ in 1969, but interest in the polymer was only developed after Diaz *et al*, produced a homogeneous electrically conducting material, 10 years later.⁴⁸ PPy is one of the most extensively studied CPs due to its easy oxidation. It is also environmentally stable with good redox properties¹⁰ and is highly conducting.⁴⁹ Its individual monomers consist of a 5 membered carbon ring with nitrogen replacing the 5th carbon. The carbon and nitrogen atoms are sp^2 hybridised, with each monomer unit containing an aromatic π delocalised system. This results from the overlapping of $2p_z$ orbitals and extends along the polymer backbone, resulting in a CP.

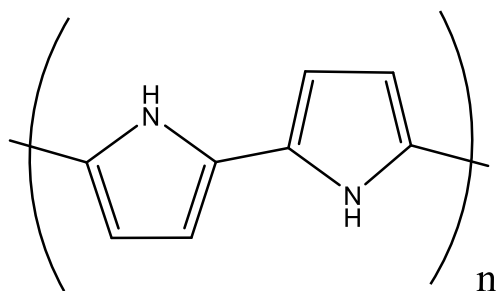


Figure 1.9: Structure of polypyrrole (PPy) repeating unit.

1.5.2.1 Polymerisation of Pyrrole

PPy can be formed by chemical or electrochemical polymerisation. The chemical synthesis of CPs uses chemical oxidants, such as ammonium peroxydisulfate, to oxidise the monomer, resulting in chemically active radicals of the monomer. These radicals react with the monomer to form an insoluble polymer.⁴⁷ A disadvantage to

this system is that most of the polymer precipitates into solution making it difficult to deposit onto a surface.⁴⁸ Generally the electrochemical method is the preferred synthesis, as it provides more control over the resulting film thickness, by controlling the charge passed, (see Section 3.3.3.1), morphology,⁴⁹ and leads to a cleaner polymer when compared to the corresponding chemical synthesis.⁵⁰

The electrochemical oxidation of pyrrole leads to a variety of chemical and electrochemical reactions which finally result in the CP being deposited onto the electrode surface. Possible electrochemical techniques include potentiostatic (constant potential), galvanostatic (constant current) and CV.⁵¹ Most literature refers to the polymerisation method described by Diaz *et al*⁵², although other initiation steps have been proposed.⁵⁰ The characteristic properties of an electrodeposited PPy film are highly dependent on the polymerisation conditions, therefore an understanding of the polymerisation reaction can lead to better control over the formed polymer. The main features of the Diaz method of electropolymerisation are described here, with a schematic shown in Figure 1.10.

The first, initiation, step is the oxidation of the pyrrole monomer, which results from the application of an anodic (oxidation) potential to the electrode, forming the pyrrole cation radical. This radical could combine with another monomer to propagate chain formation. However, the pyrrole at the electrode surface is mainly in its radical form, as the oxidation of pyrrole is a faster reaction than the diffusion rate of the monomer to the electrode surface. So, at the electrode surface, two radicals couple, with the loss of 2H^+ , to form a radical dication. With the loss of another 2H^+ (deprotonation) a neutral dimer is formed. This is further oxidised to form a radical dimer, with the unpaired electron delocalised over the two rings. This combines with a radical monomer, at the electrode surface, and is subsequently deprotonated to form a neutral trimer. Propagation continues as the trimer is oxidised and combines with a radical monomer forming oligomers and polymer chains. Termination of the reaction is brought about by reaction of the radical cation with water, or other nucleophiles.

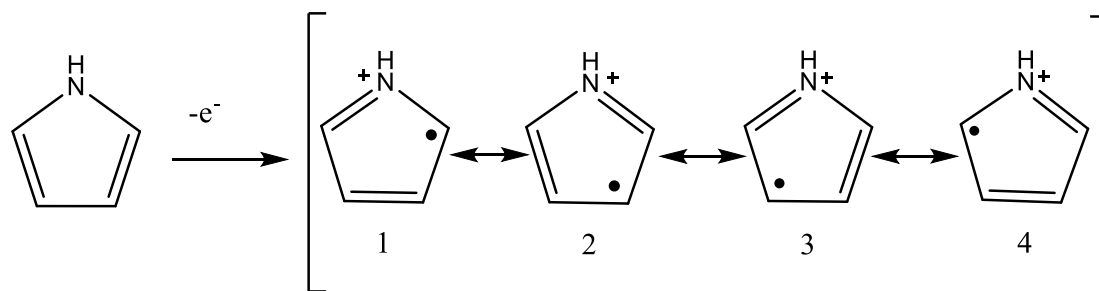


Figure 1.11: Resonance structures of the radical cation formed by the oxidation of pyrrole.

It is well documented that the dopant anion in polypyrrole plays a critical role in determining the physical and chemical properties of the polymer.⁵⁵ Dopant ions are generally incorporated into the film matrix during electropolymerisation. During doping the polymer structure distorts, due to the insertion and removal of the dopant. As previously stated, when the PPy is oxidised the dopant ion becomes inserted into the polymer to balance the charge. Similarly, when a reduction potential is applied, the dopant ion is expelled. This allows polymers to exchange dopants depending on the electrolytes in use.

The electrochemistry of PPy has been described as a “distributed double layer capacitor”,⁵¹ as the polymer charges and discharges during the application of redox potentials and dopant ions move in or out of the matrix, to balance this charge. The extent of oxidation/reduction is given by the doping level and this is generally expressed as the ratio of dopant anions, A^- (in this thesis the dopant anion was ClO_4^-), incorporated per monomer unit. For example, 1 A^- per 4 monomer units gives a doping level of 25%. The maximum doping level achievable with polypyrrole is 33%, i.e., 1 A^- per 3 pyrrole units.²⁴ It is important to point out that doping may not always be uniform; regions with high doping levels surrounded by areas with much lower doping levels are possible.

1.5.2.2 Factors Affecting Polymerisation

Many factors affect the polymerisation of pyrrole including, the nature of the electrode, the solvent, the concentration and nature of dopants, the pH of the electrolyte, the potential/charge attained during the electrochemical polymerisation and the method of

polarisation. All of these factors contribute to the final morphology and conductivity of the polymer film.⁵⁶

The nature of the substrate plays an important role in the formation of PPy. It is important that the working electrode is inert and does not compete with the oxidation of the monomer. Generally, platinum, gold and glassy carbon electrodes are used, however, a range of other metals which form oxides,⁵⁷ and non-metals,⁵⁸ have also been used, as well as composite electrodes.⁵⁹

The electrochemical polymerisation of pyrrole can be carried out using several techniques, including, normal pulse voltammetry (NPV),^{60, 61} CV⁶²⁻⁶⁴ and potentiometric techniques, where a constant potential is applied for a fixed period of time, known as chronoamperometry,⁶⁵ or until a desired charge is attained, chronocoulometry.¹⁶ PPy films formed from a constant current or potential, are found to be more porous and irregular than those deposited by CV. The surface morphology is better controlled when depositing the polymer by potentiostatic methods.⁶⁶ The morphology of the polymer is influenced by the applied potential and the charge attained during electropolymerisation. PPy prepared using lower current densities ($< 1.0 \text{ mA cm}^{-2}$) or lower anodic potentials ($< 0.80 \text{ V vs. SCE}$), forms more dense, homogeneous surfaces. While polymers deposited at higher current densities ($> 5.0 \text{ mA cm}^{-2}$) or higher anodic potentials ($> 0.90 \text{ V vs. SCE}$), form irregular, porous surfaces.⁶⁷ The thickness of the polymer film is also proportional to the charge passed,⁶⁸ (see Section 3.3.3.1).

If the applied potential is higher than the oxidation potential of PPy, or if the electrode is held at a potential for a long period of time, over-oxidation can occur, diminishing the electrical properties of the polymer.⁶⁹ Over-oxidation results from the nucleophilic attack (e.g., H_2O and OH^-) of the polymer backbone, resulting in the formation of carbonyl moieties on the chain which breaks the conjugation, and so is unavoidable when polymerising from aqueous solutions.⁷⁰ Over-oxidation also causes the ejection of dopant ions from the chain, forming a non-conducting polymer.

Since the electrochemical and mechanical properties of electrochemically deposited PPy are dependent on the dopants incorporated in the polymer, the choice of anions in

the supporting electrolyte is crucial. The mobility of the anions, in and out of the polymer backbone, depend on their size, with smaller anions, e.g., Cl^- , ClO_4^- and Br^- , having the best mobility. Larger, more bulky ions, e.g., polystyrenesulfonate (PSS), are unlikely to move out of the polymer, or be replaced.⁴³ However, the mobility of the anions is also affected by the applied polymerisation potential.⁷¹

The electrolyte pH is of critical importance to the PPy film formed from electropolymerisation.⁷² Alkaline solutions hinder polymerisation by deprotonating the radical cations, forming neutral radicals, thereby interfering with the coupling reaction described in Section 1.5.2.1.⁶² This leads to the formation of a non-conducting polymer. The electrolyte pH effect on the conductivity of the PPy film is dependent on the dopant anion used, with larger anions being less affected by the alkalinity of the solution.⁷³ PPy films have been successfully deposited from alkaline solutions,⁷⁴ as in the case for nanowire morphologies. This is discussed in Section 3.3.2.1. The coupling reaction between two radical cations releases two protons, which subsequently reduces the pH near the electrode surface. Zhou and Heinze found that a neutral or weakly acidic pH favours polymerisation.⁷⁵ Solution pH can also affect the already deposited PPy film. Alkali solutions, e.g., NaOH cause a loss of anions and, therefore, conductivity. The CP can be partially restored by immersion in an acidic solution.⁷⁶

1.5.3 Nanostructures

Nanomaterials are of the nanometre scale (10^{-9} m). The prefix nano- originates in the Greek “nanos” meaning dwarf. Because of their size, nanomaterials display several properties that are different to those displayed by their bulk material counterparts.⁷⁷⁻⁷⁹ This is due, in part, to surface effects. Smaller particles have a larger surface to volume ratio so most of their atoms lie along the surface. Surface atoms have fewer neighbours resulting in lower coordination numbers and sites available for bonding; therefore they are more reactive.⁸⁰

The band gap energy, described in Section 1.5.1, governs the properties of materials, including the conductivity. Changes in the energy gap between the valence and conduction bands, can alter the material’s physical and chemical properties. This occurs when the size of a substance is reduced to the nanometre scale. It has been well

established that the band gap of a semiconductor increases as the particle size is reduced.⁸¹⁻⁸³ In a bulk material, the conduction and valence bands are formed by many energy levels of the large number of atoms or molecules. As the material size decreases towards the nano scale, <10 nm, each entity is made up of a finite number of atoms, with less energy levels, therefore an increased energy band gap forms. In a single atom the bandgap is the distance between its ground state and first excited state, further decreasing the number of energy levels and increasing the band width. When an electron is promoted into the conduction band it leaves a “hole” (h^+) in the valence band. The energy gap in a semi-conductor is small enough that the electron and hole can recombine, so decreasing its reactivity. As nanomaterials have increased band gap energy, resulting in a lower probability of charge recombination, this increases their reactivity.⁸⁴ A schematic of the change in the energy band gap between nano- and bulk materials is shown in Figure 1.12.

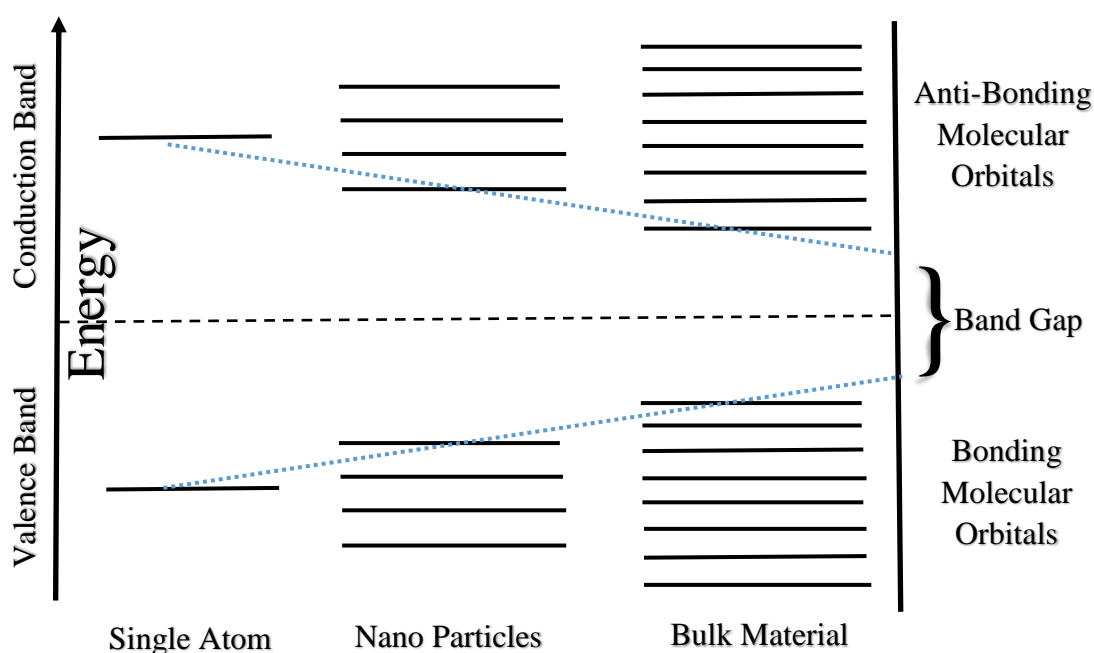


Figure 1.12: Energy band gap changes for bulk, nano and single atoms.

1.5.3.1 PPy Nanomaterials

Several methods for the fabrication of CPs on the nanometre scale have been developed.^{85, 86} One of the first methods, developed by Martin et al,⁸⁷ was based on the use of pore walls as templates, to guide the polymer growth. Using this method, an aluminium template is soaked in the monomer solution and polymerisation is initiated by applying a potential to the electrode. Tubules are formed as the monomer polymerises along the walls of the template, followed by solid wires as the tubules fill up. The template is removed by dissolution in acid, which is a harsh treatment and can degrade the polymer. Other disadvantages of the template method are the expense involved,⁸⁸ and often, when the template is removed, the formed nanowires collapse.⁸⁹ PPy has been successfully polymerised on the nanoscale, using the template method, and has shown higher conductivity and strength than the bulk material.^{90, 91} Some groups have reported that nanotubes form easier than nanowires when using a template method.⁴¹ Other procedures include a stepwise electrochemical assembly method,⁹² dilute chemical oxidative polymerisation⁹³ and biphasic electrochemical synthesis.⁹⁴ However, all these methods have proved to be very time consuming.⁹⁴

Template-free formation of nanowires offers many advantages including the removal of the construction and dissolution of the template. The morphology of the nanowires formed is controlled by the electrodeposition parameters. Massafera et al deposited PPy nanowires directly onto a gold substrate using NPV and potentiometry.⁶¹ They found that nanowires deposited from NPV were more conducting as they were shorter. Many other groups have developed simple template-free, environmentally friendly methods for electrodepositing PPy nanowires.^{74, 95, 96}

1.6 Voltammetric pH Sensor Development

The work undertaken in this section involves the modification and derivatisation of carbon substrates, namely CPEs and CFEs, with a quinone containing moiety, FBRR. The principle aim is to develop a miniaturised pH sensor, capable of detecting pH changes, with a sensitivity of 0.01 pH units, within biological pH ranges. This high level of sensitivity was suggested in consultation with a clinician as an extreme limit, although a sensitivity of 0.05 pH units would most likely suffice. Hence, this introduction refers to pH and its tight biological control; existing pH sensors, carbon electrodes, quinones as pH responsive moieties and FBRR, including the mechanism for its electro-reduction and its redox capabilities.

1.6.1 pH

pH is a measure of the concentration of hydrogen ions in a medium. The concept of pH was first mentioned, in 1909, by the Danish scientist Sorensen⁹⁷ and was defined as the negative logarithm of the concentration of hydrogen ions in an aqueous solution (Equation 1.3). This definition was based on the assumption that hydrogen ions were the only ions present. Therefore, in 1924, the definition was redefined in terms of the activity of hydrogen ions (Equation 1.4).

$$\text{pH} = -\log[\text{H}^+] \quad 1.3$$

$$\text{pH} = -\log [\text{a}_{\text{H}^+}] \quad 1.4$$

Here, $[\text{H}^+]$ is the hydrogen ion concentration, and $[\text{a}_{\text{H}^+}]$ is the hydrogen ion activity, i.e., it quantifies the hydrogen ion activity or concentration of an acid or base. The logarithmic relationship between pH and the hydrogen ion concentration means that a change of 1 unit of pH equals a tenfold change in the hydrogen ion concentration.

The pH quantity, as described in Equation 1.4, is not directly available, and requires determination by referencing it to other ion activities. Measurement by electrochemical methods has been the method of choice as electrochemical potentials are referenced to

standardised electrodes with great accuracy. The negative sign ensures that the pH of most solutions, except extremely acidic ones, is always positive.

1.6.1.1 *pH and the Nernstian Equation*

The definition of pH in Equation 1.4 was adopted because ion selective electrodes, which are used to measure pH, respond to activity. In an ideal situation the electrode potential, E , follows Nernstian values⁹⁸ which can be written as:

$$E = E^0 + (RT/F) \ln [a_{H^+}] \quad 1.5$$

$$= E^0 - (2.303RT/nF) \text{pH} \quad 1.6$$

where E is the measured potential, E^0 is the standard electrode potential, R is the universal gas constant, T is the temperature in kelvin, F is the Faraday constant and n is the number of electrons transferred. Therefore, potential is proportional to pH. Manipulation of the Nernst equation demonstrates that the observed potential for a redox system with m H^+ ions and n electrons transferred, will change by:

$$-m/n \text{ (59 mV) per pH unit at } 25^\circ\text{C}$$

The FBRR redox system, used throughout this thesis, involves $2 e^-$ and $2 H^+$, (see Section 1.6.5.1), therefore an ideally Nernstian pH response, for FBRR modified electrodes, is -59 mV/pH at 25°C .

1.6.1.2 *Temperature and pH*

Accurate measurement of pH is effected by temperature. An increase in the solution temperature results in a decrease in its viscosity and hence, an increase in the mobility of its ions in solution.⁹⁹ An increase in temperature can also lead to an increase in the number of ions in solution due to the dissociation of molecules.¹⁰⁰ As pH is a measure of the hydrogen ion concentration, a change in the temperature of a solution will be reflected by a subsequent change in the pH.¹⁰¹ The Rosenthal correction factor, which is recommended for clinical use, compensates for the change in pH due to the solution temperature, indicating a change of $0.015 \text{ pH units per } ^\circ\text{C}$.¹⁰²

By placing values in Equation 1.6, the following is obtained:

$$E = E_0 - 198 \times 10^{-6} T \text{ pH} \quad 1.7$$

From this equation, it can be seen that slope of an electrode is linearly dependent on the temperature. Because of this linear dependence the behaviour is fully predictable and can be compensated for by a pH meter and electrode with integrated temperature sensor.

1.6.1.3 *Physiological pH*

Real-time monitoring of physiological pH levels is important for many reasons. Physiological pH cannot fluctuate far from normal levels without possibly causing serious consequences. Normal human arterial blood has a pH of 7.40 at 37°C. At rest, venous blood is slightly more acidic, 7.38, than arterial blood, because of the uptake of CO₂ by the blood, as it perfuses the tissues.¹⁰³ Disturbance of the pH of blood is termed as acidosis or alkalosis. Acidosis occurs when the pH shifts to the acidic side of a normal pH value, < 7.36. There are two types of acidosis, classed by their primary cause, either metabolic or respiratory. Metabolic acidosis occurs when the concentration of blood bicarbonate, [HCO₃⁻], is too low. There are many causes for metabolic acidosis, including chronic diarrhoea.¹⁰⁴ Respiratory acidosis is caused by an increase in the CO₂ levels. Alkalosis occurs when blood pH is greater than 7.44, respiratory alkalosis being caused by a decrease in CO₂ levels and metabolic alkalosis caused by an increase in HCO₃⁻ levels.

Abnormal tissue pH, also referred to as interstitial fluid pH,¹⁰⁵ e.g., myocytes in muscle tissue, is an indicator of altered cellular metabolism in diseases including stroke¹⁰⁶ and cancer.¹⁰⁷ Tissue ischemic injury, i.e., reduced blood flow, is one of the most common types of injury in clinical medicine. Ischemic tissue is generally caused by obstruction of an artery. The affected tissue often becomes acidic due to increased anaerobic respiration leading to irreversible cellular damage. Hypoxia, on the other hand, is reduced availability of oxygen, generally caused by lower saturation or decreased amounts of haemoglobin. During hypoxia, energy generation by anaerobic glycolysis can continue, although not as efficiently as by oxidative pathways. Whereas during an ischemic episode, anaerobic energy generation ceases, as glycolysis is inhibited by the accumulation of various metabolites that would have been removed by normal blood

flow. Therefore, ischemia causes tissue damage faster than hypoxia.¹⁰³ Prolonged ischemia causes irreversible damage and necrosis to cell membranes, causing cell death. This can be caused by a large influx of Ca^{2+} ions into the cell, causing damage to cell membranes and DNA, resulting in cell death, mainly by necrosis, but also apoptosis. If cells are reversibly damaged, the restoration of blood flow can result in cell recovery. However, under certain circumstances, the restoration of blood flow to ischemic tissue can result in further damage. This is called ischemia-reperfusion injury.

The first investigations into the relationship between pH levels and ischemia was *ca.* 35-40 years ago, showing that tissue pH falls during an ischemic event.¹⁰⁸⁻¹¹³ Researchers agreed that tissue pH fell as the decrease in blood flow to the tissue resulted in anaerobic metabolism, which consequently produced lactate. The presence of lactate contributes to an increase in H^+ ion activity, which is proportional to a decrease in pH. Thus, pH can be used as an indication of a reduction of tissue perfusion.¹⁰⁸ Wolpert *et al.* compared serum pH measurements to that of tissue pH.¹¹⁰ They found that tissue pH, when compared to serum pH, had the advantages of reacting earlier to changes in tissue perfusion and it could be measured with minimal invasiveness. These studies involved miniaturised glass pH sensors, whose major disadvantages lie in the difficulty of miniaturisation,¹¹⁴ due to possible drift over time,¹¹⁵⁻¹¹⁷ fragility¹¹⁸ and electrode fouling,¹¹⁹ resulting in inaccurate measurements. Because of the expense of glass electrodes, they are not considered disposable. Glass pH sensors can only be disinfected, not heat or gas sterilised, therefore the risk of cross contamination with infectious diseases cannot be eliminated.¹²⁰ This makes the glass pH sensor undesirable for use in the *in-vivo* environment. An important study, carried out by Ye, investigated the relationship between pre-graft tissue pH and subsequent success of the tissue graft.¹²¹ It was found that the success rate increased if the pre-graft tissue pH was 7.4. This study was important as an accurate indication of whether surgery could be performed successfully, possibly avoiding many postoperative complications.

Patient monitoring, both during and after treatment is required in a clinical setting. *In-vivo* sensors can provide an instant evaluation of a biological parameter, e.g., pH, leading to quicker diagnosis and reducing hospital bed-time.¹²² For this purpose small

devices with low drift, easy calibration, immunity to electrode fouling and long life-time are required.

1.6.2 Existing pH Sensors

pH is a measurable parameter that is familiar to all in the scientific, industrial and medical fields.¹²³ pH can be measured using many techniques, from litmus paper, with low precision, to highly efficient potentiometric, e.g., glass electrode, pH meters. This section describes some of the existing pH sensors, their primary operating mechanism along with their advantages and disadvantages.

1.6.2.1 Glass pH Electrodes

The most commonly used pH sensor is the glass electrode. Modern glass pH meters combine a high impedance pH meter, along with a pH electrode and reference electrode, see Figure 1.13. The high impedance amplifier is required to measure the small voltage output.¹²⁴ The pH electrode consists of two electrodes, a hydrogen ion sensitive glass electrode and a reference electrode. The pH is observed by measuring the potential difference between the two electrodes,¹²⁵ making this a potentiometric sensor. The potential difference relevant to pH measurement builds up across the outside glass/solution interface. The glass membrane, is manufactured by blowing molten glass into a thin-walled bulb with a wall *ca.* 0.1 mm thick. The pH sensing ability of the glass electrode stems from the ion exchange property of its glass membrane. Glass is mostly amorphous silicon dioxide, with embedded oxides of alkali metals. The surface of the glass is protonated by both the internal and external solution until an equilibrium is achieved. Both sides of the glass are charged by the adsorbed protons, this charge is responsible for the potential difference. The glass electrode, develops a potential directly related to the H⁺ concentration of the solution. A second, standard potential, is provided by the reference electrode, which provides a stable potential against which the recording electrode can be compared. The reference electrode is generally contained in a 3 M KCl solution which completes the electric circuit. The potential difference between the recording and the reference electrode is converted to a pH value by using the electrode's specific calibration constants. Thus, electrodes must be calibrated in two or more buffers in order to convert the voltage

reading into a true pH value. By convention, the design of glass pH sensors is adapted such that the electrode potential reads 0 mV at pH 7 and 25°C. Commercially available micro glass pH sensors are available from World Precision Instruments (<http://www.wpiinc.com>) and Presens (<http://www.presens.de>). Their main disadvantages are fragility and difficulties in sterilisation, as explained in Section 1.6.1.3, making them an expensive electrode, suitable for single use only, so they are not suitable for use in a physiological environment.

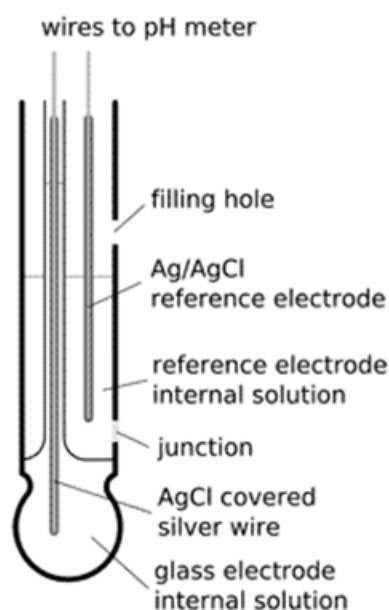


Figure 1.13: Schematic of a glass pH electrode, (<http://www.ph-meter.info/>).

1.6.2.2 Metal Oxide pH Sensors

In order to overcome the fragility of glass pH sensors, metal oxide sensors have been used for pH determination in physiological environments. The mechanically robust¹²⁶ electrodes can easily be miniaturised using modern technologies. Although many metal oxides have been examined, including, RuO_2 ,¹²⁷ TaO_5 ¹²⁸ and PbO_2 ,¹¹⁵ IrO_x is probably the most promising, due to its stability,¹²⁹ fast response and broad pH recording range.¹¹⁴ The potentiometric response of IrO_x to pH is due to the fluctuation between the two oxidation states Ir(III) oxide and Ir(IV) oxide. Depending on the method of electrode preparation, two variations on the IrO_x pH sensor can be produced, hydrous and anhydrous. Anhydrous iridium oxides are achieved by thermal oxidation or sputtering methods which showed pH response of -59 mV/pH, whereas

iridium oxides fabricated electrochemically are mainly hydrated iridium oxides, which result in a super-Nernstian response -90 mV/pH unit.¹³⁰

IrO_x , and other, pH micro sensors require reference electrodes, hence, problems associated with inserting two electrodes into the same position, *in-vivo*, exist.¹³¹ As they are based on potentiometric measurements they still suffer from substantial drift over time¹³² and are susceptible to electric noise.¹³³ They are more suitable for *in-vitro* measurements and are prone to interference from redox species, e.g., AA and DOPAC, making them unsuitable for *in-vivo* applications.¹³²

1.6.2.3 Ion Selective Field Effect Transistors (ISFET)

ISFETs were introduced as pH sensors by Bergveld¹³⁴ in 1970. Their operation is based on the surface adsorption of charges from the solution being tested.¹³⁵ In an ISFET, the metal gate is replaced by an ion-sensitive membrane, the solution to be measured and a reference electrode. Therefore, an ISFET combines, the sensing surface and a signal amplifier which produces a high current, low impedance output and allows the use of connecting cables without excessive shielding.¹²⁶ This pH sensitive gate electrode, which is situated between two semi-conducting electrodes (the drain and the sink), controls the current flowing between the two electrodes, by keeping drain current constant at a predefined value. If there is a pH change, there is a corresponding change in the gate potential. Although they can be miniaturised readily,¹³⁶ they are not suitable for clinical applications due to the brittle semi-conductor layer, often silicon.^{125, 135} For practical measurements in liquids, the electrical circuit must be closed with a reference electrode. Other disadvantages in using ISFET pH sensors are their substantial drift, due to the inherent contact of the gate with the liquid.¹³⁷ often slow response,^{128, 138} hysteresis effect, temperature dependence⁹⁸ expense¹²⁶ and difficulties with encapsulation.¹³⁹ ISFET pH sensors also have concerns relating to their power consumption, due to the FET operation requirements when used for *in-vivo* applications.¹²⁶ Despite these limitations, ISFETs are commercially available from several companies e.g., Orion, Orion Research, Boston, MA; Corning, New York, NY; Sentron Integrated Sensor Technology, The Netherlands, (<http://www.sentron.nl/>). The Sentron sensor is the only one that is FDA and CE approved, however its uses are limited due to its 5 mm diameter.

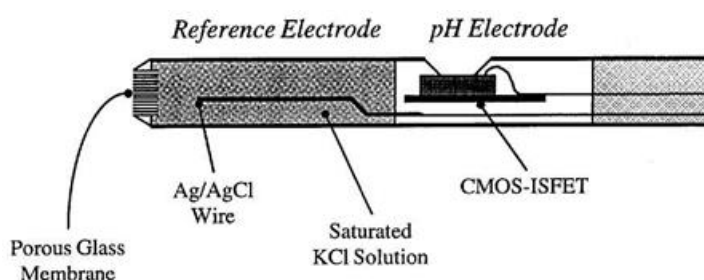


Figure 1.14: Schematic of an ISFET pH electrode, showing its major components.¹⁴⁰

1.6.2.4 Optical pH Sensors

Optical pH sensors use pH indicator dyes with distinct spectral properties. Their response is based on reversible changes of several parameters, mainly absorbance and reflectance, but sometimes fluorescence and refractive index (RI), due to changing pH of the solution.¹⁴¹ Measurements based on absorption are not very sensitive and require the application of a thick sensing layer or a high concentration of pH indicator dye.¹⁴² Several techniques have been reported for the immobilisation of indicator dyes, such as entrapment in sol-gel-based materials or polymers, with sensor sizes *ca.* 0.60 mm^{143, 144}, and wearable technology sensors^{145, 146} or dyes covalently bound to polymer matrices.^{147, 148} Covalently bound dyes, however, are prone to poor fluorescence properties and loss of dye sensitivity, whereas non-covalently (entrapped) dyes are not suitable for *in-vivo* use due to leeching problems.¹³⁵

The optical sensors have several advantages over glass electrodes including the possibility of miniaturisation and they are not affected by electrical interference.¹⁴² However, they require large sized analytical equipment, confining their use to static situations.¹³⁵ Other limitations include a restricted long term stability and they are particularly affected by large changes in ionic strength,¹³⁵ which is of particular importance when monitoring pH during blood dialysis.¹⁴⁹ They are also limited to a narrow pH range, usually *ca.* 2-3 pH units.¹⁵⁰ However, most biological systems operate over restricted pH ranges, so for the purpose of the sensor designed in this thesis, this is not necessarily a disadvantage. Despite their disadvantages, researchers continue to examine their possible use as pH sensors. Singh *et al* developed a sensor by coating the core of an optical fibre with three consecutive layers of silver, silicon, and a pH-sensitive hydrogel. The pH change in the fluid causes the swelling or

shrinkage of the hydrogel layer, which changes its RI.¹⁵¹ This sensor is capable of measuring pH values between 3 and 10, a substantial improvement in the operating range.

A commercially produced fibre optic sensor, the Paratrend[®] 7, boasted the ability to simultaneously measure PO₂, CO₂, pH and temperature. It consisted of three optical fibres, *ca.* 0.175 mm diameter each, with an outer membrane of a gas permeable polyethylene, which has a heparin compound covalently bound. Although the diameter of the sensor bundle was 0.5 mm, the four sensing components were located at intervals along the 25 mm length,¹⁵² (see Figure 1.15), and so was not designed to be inserted through a catheter. The covalent bonding eliminated any leeching problems and the heparin compound inhibited interference from proteins, although Hwang *et al*¹⁵³ and Jeevarajan *et al*¹⁵⁴ reported the formation of biofilms on the sensors, restricting gas permeation through the membrane. Each individual sensor was specifically modified for its purpose, e.g., the pH sensor had an acid-base indicator immobilised onto it. A problem associated with the sensor was the shut-down of all recordings once one of the sensors failed.¹⁵³ Also, significant differences, between actual and recorded values, were observed for pH and PCO₂, with $P = 0.001$ and 0.0003 respectively.¹⁵⁵ This sensor has now been discontinued due to these reasons as well as sterilisation and cost factors. Other commercially available fibre optic pH sensors are available from World Precision Instruments, Presens and Oceanoptics (<http://www.oceanoptics.com>), but all are specifically designed to cater for the pre-clinical market.

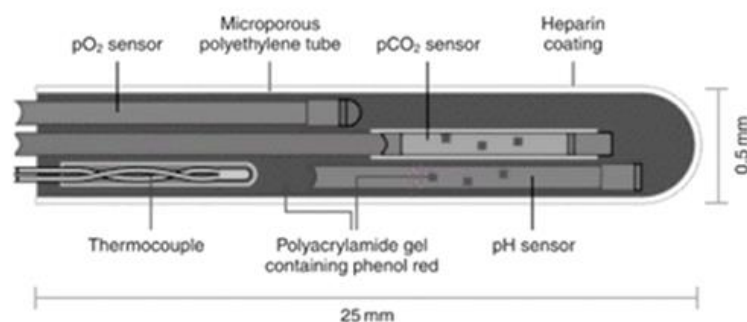


Figure 1.15: Schematic of the Paratrend 7[®] sensor.¹⁵³

1.6.2.5 Voltammetric pH Sensors

Electrochemical sensors have distinct advantages over optical pH sensors, including low cost, high stability and sensitivity.¹⁵⁶ It has been mentioned previously in this introduction, that electrochemical pH sensors, based on potentiometric measurements, suffer from excessive drift.¹⁵⁷ This potential drift is due to a reduced sensitivity towards H^+ activity as the glass membrane becomes dehydrated.¹⁵⁸ Voltammetric pH sensors, like the one used in this thesis, measure the redox potential of a pH dependent moiety, e.g., the quinone/hydroquinone redox couple of FBRR. Many other pH dependent redox systems have been investigated including nitrosophenyl compounds.¹¹⁷ The voltammetric response of the pH sensitive layer can be described by the Nernst equation, (see Equation 1.6).

1.6.3 Designing a Voltammetric pH Sensor

The design of pH sensors depends on their individual applications and as such is varied. In order to develop a novel miniaturised, voltammetric pH sensor, capable of continuous *in-vivo* measurements, certain criteria should be maintained. Firstly, the sensor should be easily miniaturised in order to inflict minimal trauma to the insertion site, thereby reducing the risk of infection to the subject. Biocompatible materials are required. If designing a clinical sensor it is imperative to avoid cross infection of, e.g., hepatitis B, hepatitis C and HIV, and as such, clinical pH sensors should ideally be single use and consequently the cost of production is of great importance. For physiological monitoring of tissue pH, the sensor response should be linear over the physiologically relevant range, and sensitive to at least 0.1, but preferably 0.01 pH units. It should also remain stable, with minimal drift, over a constant recording time of between 12 and 24 hours. The voltammetric response of the sensor should not be compromised by the presence of electrochemically active moieties such as ascorbic acid, (AA), uric acid, (UA) and dopamine, (DA) as well as pharmacological interferences, e.g., acetaminophen, (ACOP), and acetylsalicylic acid, (ASA). Excess, physiologically relevant, metal ions can also be detrimental to the voltammetric signal, e.g., Ca^{2+} and Mg^{2+} . Hence, a thorough examination into the effect of possible interferences should be undertaken. The effect of temperature should also be

ascertained, along with its ability to function efficiently in solutions of varying ionic strength.

1.6.4 Carbon Electrodes

Carbon based materials and sensors have been widely used in the field of electrochemistry, because of their good electrical conductivity,¹⁵⁹ ease of modification, low expense and relatively wide operating potential range. Oxygen readily adsorbs onto carbon surfaces to form carbon-oxygen complexes such as phenols, ortho- and para- quinones, carbonyls, lactones and carboxylic acids, especially on edge plane sites.¹⁶⁰ All of these groups are susceptible to redox reactions with other molecules in solution, including, protons,¹³² and as such, are capable of electron transfer processes.¹⁶¹ The type and quantity, of oxygen containing groups, is determined by the type of carbon and this can be altered by applying pre-treatments to the electrode.¹⁶²

Carbon materials can be functionalised in many different ways in order to achieve a pH sensing electrode. These include, the covalent attachment of the pH sensitive moiety,¹⁶³ either by chemical or electrochemical processes; chemical or physical adsorption of the pH sensing compound onto the surface; deposition of oxygen containing groups onto the electrode, or incorporation of the pH responsive substance into a composite electrode, e.g., CPEs.³ Many different carbon surfaces have been electrochemically modified with pH sensing elements, most notably, glassy carbon,¹⁶⁴ carbon fibres¹⁶⁵ and to a lesser extent, CPEs.

1.6.4.1 Carbon Paste Electrodes (CPEs)

CPEs are specialised heterogeneous carbon electrodes, containing a mixture of carbon powder and a binding fluid. One of the most quoted disadvantages of CPEs is that their operational success depends on the practical experience of the user.¹⁶⁶ Each prepared electrode is individual, due to the uneven distribution of carbon and binding liquid and the irregular surface formed. However, they are widely available, of low cost, and their ease of modification, giving them pre-determined properties, makes them useful as highly selective sensors.¹⁶⁷ The choice of carbon material and binding fluid also contribute to the flexibility when preparing carbon pastes with specific properties. Chemical or electrochemical modification, by introducing functional

groups onto the electrode surface, increases the number of chemical applications for CPEs. These attached groups can undergo chemical reactions with the analyte as well as electron transfer reactions.¹⁶⁸ Modification occurs through adsorption or covalent bonding of reagents or coverage with membranes or polymers. Modification of carbon paste electrodes can be achieved by the following methods,

- Modification *in-situ*.¹⁶⁹ The hydrophobic surface of the electrode can enhance the entrapment of some lipophilic modifiers.
- Mixing solid modifier into the bulk carbon paste.¹⁷⁰
- Impregnation of the graphite powder by soaking it in a solution of the modifier.¹⁷¹ After evaporation of the solvent the modified graphite is mixed with the binder, to form the paste.

Many CPEs have been used for *in-vivo* monitoring of brain tissue,¹⁷²⁻¹⁷⁴ an environment they are particularly suited to, as the interaction between the pasting liquid and brain lipids reduces the electrode fouling caused by proteins.¹⁷³ To the best of my knowledge, CPEs have not previously been adopted for *in-vivo* monitoring of muscle tissue pH.

1.6.4.2 Carbon Fibre Electrodes (CFEs)

CFEs were first described in 1979, by Ponchon et al, when they were designed for the electrochemical detection of catecholamines.¹⁷⁵ Today, their most common applications are still as sensors designed for monitoring neurotransmitters. They are considered as extremely suitable electrochemical sensors due to their inherent biocompatibility, relatively high mechanical strength¹⁷⁶ and their adaptability due to possible surface modification.¹⁷⁷ They can also be miniaturised to nano-dimensions and can therefore be utilised in low volume samples and in other more challenging environments, like those found in clinical situations, where they have been used for neurochemical monitoring of e.g., nitric oxide, (NO),¹⁷⁸ and dopamine, (DA).¹⁷⁹ The miniaturised electrodes have many advantages for biological applications, including, good electrochemical properties¹⁸⁰ and reduced tissue damage on implantation due to their small size,¹⁸¹ often less than 10 μm . Because of these many advantages, there is still a growing interest in the modification of the microelectrodes with various organic and inorganic materials including diazonium salts.^{182, 183}

When compared to metal electrodes, the electron transfer rates at carbon electrodes are relatively sluggish.²⁹ The electrochemical pre-treatment of carbon electrodes was first reported in the 1950s,¹⁸⁴ and has been shown to enhance the electrochemical response.¹⁸⁵ Improvements to CFEs have been achieved by pre-treating the electrodes prior to the attachment of quinones.¹⁸⁵

1.6.5 Quinones and Aryl Diazonium Salts

A quinone, shown in Figure 1.16, is an aromatic derivative of, e.g., benzene, with an even number of C-H bonds replaced by C=O, resulting in a conjugated cyclic dione. Quinones have shown strong adsorption onto various surfaces including platinum,¹⁸⁶ gold,¹⁸⁷ graphite^{116, 188} and glassy carbon^{189, 190} as well as carbon nanotubes^{191, 192} and are one of the most studied examples of an organic redox couple.¹⁹³ They are attached via diazonium attachment chemistry onto the required surface. *Para*-quinones undergo a reversible two electron reduction in aqueous buffered solutions, with alkaline, acidic and neutral pH values.¹⁹⁴ These reduction potentials are pH dependent, varying in a Nernstian manner.^{195, 196} However the number of protons transferred varies with pH in unbuffered media, therefore, the use of quinones for pH studies is suitable in buffered systems only.¹⁹⁷ Although many quinone modified electrodes respond to pH, few have been developed on biocompatible materials, that exhibit activity in a physiologically relevant pH range.¹⁰⁷

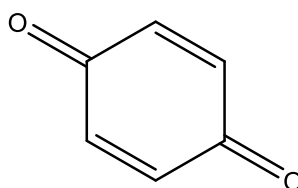
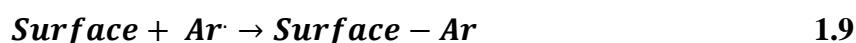


Figure 1.16: Structure of a *para*-quinone, 1, 4 benzoquinone.

The first reported reduction of an aryl diazonium salt onto carbon was in 1992 by Saveant et al.⁷ The electrochemical reduction of diazonium salts leads to a solid covalent attachment of aryl groups onto the substrate surface. The electrochemical reduction of diazonium salts is widely used for the modification of various electrode substrates. However, when reducing the salt onto metal surfaces, the surfaces should

be free of oxide groups to allow formation of the metal-carbon bond.¹⁹⁸ The diazonium salts are most stable in acidic and aprotic solutions, with the stability decreasing as the pH increases above 3 in aqueous solutions.¹⁹⁹ The first step, of the proposed mechanism, involves the electrochemical reduction of the aryl diazonium cation (Ar-N_2^+) to form the corresponding aryl radical (Ar^\cdot), with the loss of N_2 , as shown in Equation 1.8. This is a concerted reaction, therefore there are no intermediates formed between the cation and the radical formation, so the radical forms directly on the electrode surface. The electrochemical reduction that leads to the formation of the radical is relatively easy because of the electron withdrawing power of the diazonium group. The second step occurs when the radical reacts with the electrode surface, e.g., carbon, and a strong covalent C-C bond is formed. This is shown in Equation 1.9. In general, the electro-reduction of the diazonium salt onto a substrate results in a broad irreversible wave which disappears in the second sweep. This is due to the formation of the organic layer blocking the access of the electroactive moiety to the electrode surface. It is possible that the radical becomes further reduced to the anion, Ar^- , as in Equation 1.10, this leads to unfavourable conditions for the electrodeposition. In order to prevent further reduction of the radical to the anion the potential should not be brought to a too negative potential.



1.6.5.1 FBRR

4-Benzoylamino-2, 5-dimethoxybenzenediazonium chloride hemi zinc chloride salt also known as Fast Blue RR, (FBRR), is a quinone containing aryl-diazonium salt, as shown in Figure 1.17. Literature reports its main uses as a dye, with little reference to its electrochemical properties.

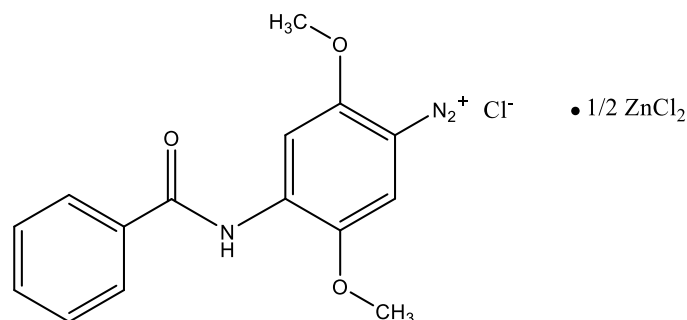


Figure 1.17: Chemical structure of FBRR.

The covalent bond formation of FBRR onto a carbon substrate follows the proposed mechanism described in Section 1.6.5, a schematic for which is depicted in Figure 1.18, forming a strong covalent C-C bond. This is a $1 e^-$, irreversible, reduction reaction, as shown by the cleavage of N_2 . The reduction of FBRR can be carried out in an aprotic or a protic solvent,⁵ using the same reduction mechanism.

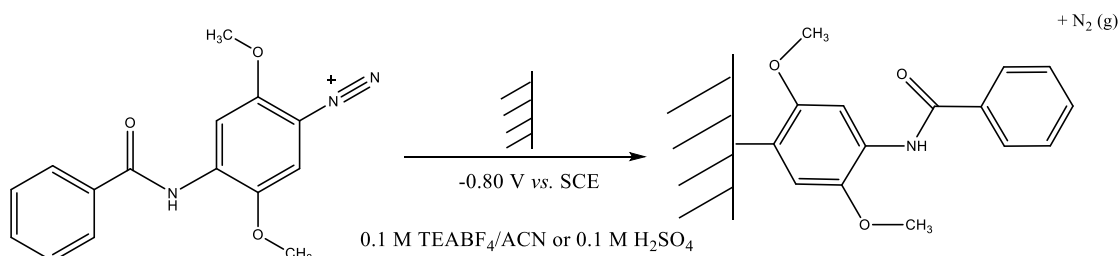


Figure 1.18: Schematic of the electrochemical reduction of FBRR onto an electrode surface, forming a strong covalent bond.

The electrochemical reduction of diazonium salts generally results in a layered deposition of the product onto the substrate, as opposed to monolayers.¹²³ These layers can vary in thickness from a few nm to several μm . The layers are formed when the radical attaches to the first layer of deposited FBRR. This happens when the radical attacks the *ortho*- position of an already surface bound aryl group, leading to the formation of multilayers.⁴ The multilayer formation is detrimental to the electron transfer rate, slowing it down. Bonding to the surface can also occur without the loss

of the diazonium group which results in a hydrazine (N_2H_4) attachment to the surface.²⁰⁰ As a result of the side reactions forming multi-layers and the hydrazine moiety, the surface generated from the electrochemical reduction of a diazonium salt is non-homogeneous.¹²³ However, these modified electrodes are reported to be remarkably stable. They have been reported to withstand sonication, are stable up to temperatures of at least $200^\circ C$ and can be stored for up to six months without losing their redox properties.²⁰¹

The mechanism for the oxidation/reduction reaction of FBRR, in buffered solutions, involves a $2e^-$ oxidation that converts the methoxy to the equivalent quinone, followed by a $2e^-/2H^+$ exchange to form the hydroxy-quinone. This is shown in Figure 1.19.

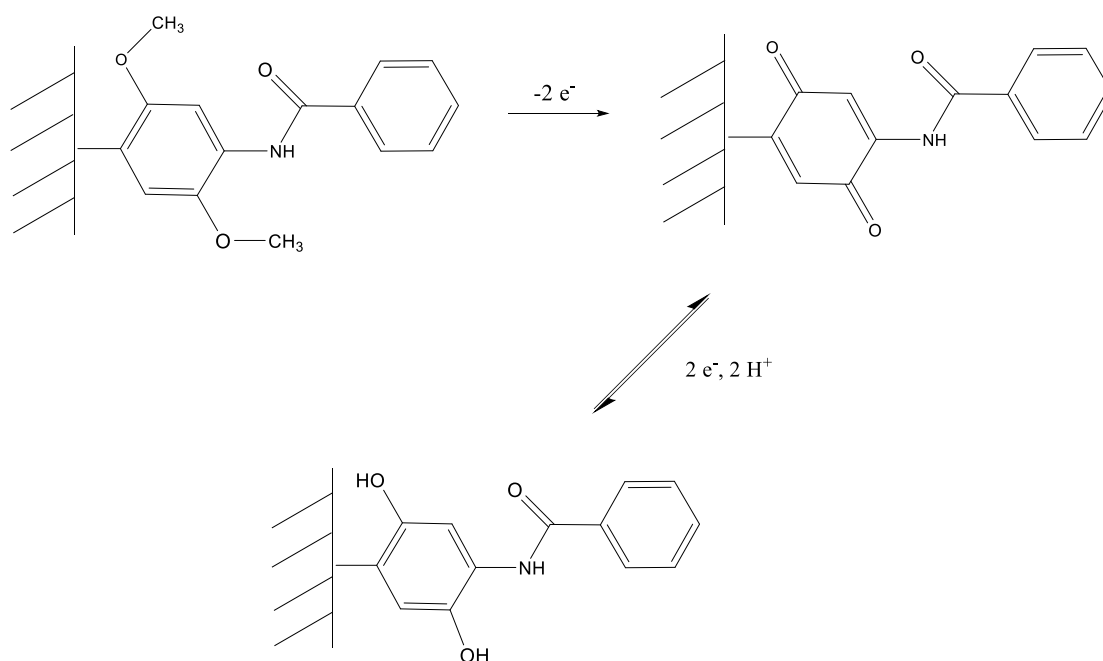


Figure 1.19: The redox reaction of FBRR electrodeposited on carbon substrates.

The potentials at which the redox reactions take place are pH dependent, as the oxidation induces a loss of protons. This deprotonation occurs more readily at higher pH values, resulting in, thermodynamically, more viable electron transfer, at more negative potentials.²⁰²

1.7 Summary

From the literature review it is clear that much research has been carried out into the electrochemical properties of PPy. The task here, was to prepare bulk and nanowire morphologies of PPy, (A) using the same electrochemical parameters and (B) with similar electroactive surface areas.

The development of a miniaturised pH sensor, capable of monitoring real-time changes in tissue pH, within the tightly regulated biological limits was challenging. Although many literature sources refer to miniaturised pH sensors, few have been developed that have received clinical approval. The advantages and disadvantages of various pH sensors have been discussed, and there appears to be opportunity to develop a voltammetric sensor based on the redox couple of quinones; one that is small enough to cause minimal patient discomfort, while eliminating as many disadvantages of other designed sensors, e.g., drift, ionic strength stability and expense.

1.8 References

1. C. Janaky and C. Visy, *Analytical and Bioanalytical Chemistry*, 2013, **405**, 3489-3511.
2. Y.-Z. Long, M.-M. Li, C. Gu, M. Wan, J.-L. Duvail, Z. Liu and Z. Fan, *Progress in Polymer Science*, 2011, **36**, 1415-1442.
3. H. C. Leventis, I. Streeter, G. G. Wildgoose, N. S. Lawrence, L. Jiang, T. G. J. Jones and R. G. Compton, *Talanta*, 2004, **63**, 1039-1051.
4. J. Pinson, *Chemical Society Reviews*, 2012.
5. M. Delamar, G. Desarmot, O. Fagebaume, R. Hitmi, J. Pinson and J. M. Saveant, *Carbon*, 1997, **35**, 801-807.
6. P. Allongue, M. Delamar, B. Desbat, O. Fagebaume, R. Hitmi, J. Pinson and J.-M. Saveant, *Journal of the American Chemical Society*, 1997, **119**, 201-207.
7. M. Delamar, R. Hitmi, J. Pinson and J. M. Saveant, *Journal of the American Chemical Society*, 1992, **114**, 5883-5884.
8. A. J. Downard, *Electroanalysis*, 2000, **12**, 1085-1096.
9. A. J. Bard and L. R. Faulkner, *Electrochemical Methods: Fundamentals and Applications*, John Wiley & Sons, 2001.
10. Y. J. Yuan, S. B. Adeloju and G. G. Wallace, *European Polymer Journal*, 1999, **35**, 1761-1772.
11. C. G. Zoski, *Handbook of Electrochemistry*, Elsevier Science, 2007.
12. A. C. Fisher, *Electrode Dynamics*, Oxford Science Publications, 2009.
13. E. Andreoli, PhD, NUIM, 2010.
14. R. S. Nicholson, *Analytical Chemistry*, 1965, **37**, 1351-1355.
15. D. Ross and D. Lowe, *Electronics All-in-One For Dummies*, John Wiley & Sons, 2013.
16. M. Zhou, M. Pagels, B. Geschke and J. Heinze, *Journal of Physical Chemistry B*, 2002, **106**, 10065-10073.
17. M. S. Milan Paunovic, *Fundamentals of Electrochemical Deposition*, Wiley, 2006, p. 52.
18. E. J. F. Dickinson, I. Streeter and R. G. Compton, *Journal of Physical Chemistry B*, 2008, **112**, 4059-4066.

19. L. K. Bieniasz, J. Gonzalez, A. Molina and E. Laborda, *Electrochimica Acta*, 2010, **56**, 543-552.
20. A. Molina, J. Gonzalez, E. Laborda, F. Martinez-Ortiz and L. K. Bieniasz, *Journal of Physical Chemistry C*, 2010, **114**, 14542-14551.
21. K. R. Ward, N. S. Lawrence, R. S. Hartshorne and R. G. Compton, *Physical Chemistry Chemical Physics*, 2012, **14**, 7264-7275.
22. C. M. A. Brett and A. M. O. Brett, *Electrochemistry: Principles, Methods and Applications*, Oxford University Press, 1993.
23. P. A. Christensen and A. Hamnett, *Techniques and Mechanisms in Electrochemistry*, Blackie Academic and Professional, 1994.
24. P. Chandrasekhar, *Conducting Polymers, Fundamental and Applications.*, Kluwer Academic Publishers, 1999.
25. V. Syritski, A. Öpik and O. Forsen, *Electrochimica Acta*, 2003, **48**, 1409-1417.
26. J. O. Iroh and G. A. Wood, *European Polymer Journal*, 1997, **33**, 107-114.
27. C. D. Allred and R. L. McCreery, *Analytical Chemistry*, 1992, **64**, 444-448.
28. J. X. Feng, M. Brazell, K. Renner, R. Kasser and R. N. Adams, *Analytical Chemistry*, 1987, **59**, 1863-1867.
29. P. M. Kovach, M. R. Deakin and R. M. Wightman, *Journal of Physical Chemistry*, 1986, **90**, 4612-4617.
30. E. Barsoukov and J. E. Macdonald, *Impedance Spectroscopy: Theory, Experiment and Applications*, Wiley-Interscience, 2005.
31. M. Ates, *Progress in Organic Coatings*, 2011, **71**, 1-10.
32. F. J. Iftikhar, P. G. L. Baker, A. M. Baleg, P. M. Ndangili, S. N. Mailu and E. I. Iwuoha, *Electrochimica Acta*, 2011, **56**, 5214-5221.
33. P. E. J. I. Goldstein, C. Joy, A. D. Romig, C. E. Lyman, C. Fiori and E. Lifshin., *Scanning Electron Microscopy and X-Ray Microanalysis*, Plenum Press, 1992.
34. Y. Ma, *Physical Review B*, 1994, **49**, 5799-5805.
35. B. C. Smith, *Fundamentals of Fourier Transform Infrared Spectroscopy*, CRC Press, 2011.
36. L. G. Wade, *Organic Chemistry*, Addison Wesley Longman, 1999.
37. J. A. Pople and S. H. Walmsley, *Molecular Physics*, 1962, **5**, 15-20.
38. G. Natta, G. Mazzanti and P. Corradini, *Atti della Accademia Nazionale dei Lincei. Classe di Scienze Fisiche, Matematiche e Naturali*, 1958, **25**, 3-12.

39. C. K. Chiang, C. R. Fincher, Jr., Y. W. Park, A. J. Heeger, H. Shirakawa, E. J. Louis, S. C. Gau and A. G. MacDiarmid, *Physical Review Letters*, 1977, **39**, 1098-1101.
40. A. J. Heeger, *Reviews in Modern Physics*, 2001, **73**, 681-700.
41. Y. F. Chen, J. Liu, H. J. Yao, D. Mo, J. L. Duan, M. D. Hou, Y. M. Sun, L. Zhang and K. Maaz, *Physica B* 2010, **405**, 2461-2465.
42. J. L. Bredas and G. B. Street, *Accounts of Chemical Research*, 1985, **18**, 309-315.
43. U. Johanson, M. Marandi, T. Tamm and J. Tamm, *Electrochimica Acta*, 2005, **50**, 1523-1528.
44. N. K. Guimard, N. Gomez and C. E. Schmidt, *Progress in Polymer Science*, 2007, **32**, 876-921.
45. J. Heinze, in *Electrochemistry IV*, Springer Berlin Heidelberg, 1990, pp. 1-47.
46. M. E. G. Lyons, *Advances in Chemical Physics, Polymeric Systems*, John Wiley & Sons, 1997.
47. A. Malinauskas, *Polymer*, 2001, **42**, 3957-3972.
48. A. Ramanavicius, A. Ramanaviciene and A. Malinauskas, *Electrochimica Acta*, 2006, **51**, 6025-6037.
49. M. Zhou and J. Heinze, *Electrochimica Acta*, 1999, **44**, 1733-1748.
50. S. Sadki, S. Philippe, N. Brodie and G. Sabouraud, *Chemical Society Reviews*, 2000, **29**, 283-293.
51. M. R. Warren and J. D. Madden, *Synthetic Metals*, 2006, **156**, 724-730.
52. E. M. Genies, G. Bidan and A. F. Diaz, *Journal of Electroanalytical Chemistry: Interfacial Electrochemistry*, 1983, **149**, 101-113.
53. J. Jang, J. H. Oh and X. L. Li, *Journal of Materials Chemistry*, 2004, **14**, 2872-2880.
54. P. Pfluger and G. B. Street, *Journal of Chemical Physics*, 1984, **80**, 544-553.
55. B. C. Thompson, S. E. Moulton, R. T. Richardson and G. G. Wallace, *Biomaterials*, 2011, **32**, 3822-3831.
56. C. Jerome, D. E. Labaye and R. Jerome, *Synthetic Metals*, 2004, **142**, 207-216.
57. S. B. Saidman and O. V. Quinzani, *Electrochimica Acta*, 2004, **50**, 127-134.
58. L. Tian, Y. Qi and B. Wang, *Journal of Colloid & Interface Science*, 2009, **333**, 249-253.

59. J. Wang, X. Mo, D. Ge, Y. Tian, Z. Wang and S. Wang, *Synthetic Metals*, 2006, **156**, 514-518.
60. K. Ghanbari, S. Z. Bathaie and M. F. Mousavi, *Biosensors and Bioelectronics*, 2008, **23**, 1825-1831.
61. M. P. Massafra and d. T. S. I. Cordoba, *Journal of Electroanalytical Chemistry*, 2012, **669**, 90-94.
62. S. Shimoda and E. Smela, *Electrochimica Acta*, 1998, **44**, 219-238.
63. P. M. Dziejowski and M. Grzeszczuk, *Journal of Physical Chemistry B*, 2010, **114**, 7158-7171.
64. S. Carquigny, O. Segut, B. Lakard, F. Lallemand and P. Fievet, *Synthetic Metals*, 2008, **158**, 453-461.
65. C. Jerome and R. Jerome, *Angewandte Chemie International Edition*, 1998, **37**, 2488-2490.
66. T. Hernandez-Perez, M. Morales, N. Batina and M. Salmon, *Journal of the Electrochemical Society*, 2001, **148**, C369-C375.
67. J.-M. Pernaut and J. R. Reynolds, *Journal of Physical Chemistry B*, 2000, **104**, 4080-4090.
68. S. M. Ebrahim, L. M. M. Abd-El, A. M. Gad and M. M. Soliman, *Thin Solid Films*, 2010, **518**, 4100-4105.
69. H. Ge, G. Qi, E. T. Kang and K. G. Neoh, *Polymer*, 1994, **35**, 504-508.
70. B. R. Saunders, R. J. Fleming and K. S. Murray, *Chemistry of Materials*, 1995, **7**, 1082-1094.
71. R. Bilger and J. Heinze, *Synthetic Metals*, 1993, **55**, 1424-1429.
72. A. Bhattacharya, A. De and S. Das, *Polymer*, 1996, **37**, 4375-4382.
73. Q. Pei and R. Qian, *Synthetic Metals*, 1991, **45**, 35-48.
74. C. Debiemme-Chouvy, *Electrochemical Communications*, 2009, **11**, 298-301.
75. M. Zhou and J. Heinze, *Journal of Physical Chemistry B*, 1999, **103**, 8443-8450.
76. Y. Li and R. Qian, *Synthetic Metals*, 1988, **26**, 139-151.
77. F.-L. Cheng, M.-L. Zhang and H. Wang, *Sensors*, 2005, **5**, 245-249.
78. M. E. T. Molares, V. Buschmann, D. Dobrev, R. Newmann, R. Scholz, I. U. Schuchert and J. Vetter, *Advanced Materials* 2001, **13**, 62-65.

-
79. J. Wang, X. Mo, D. Ge, Y. Tian, Z. Wang and S. Wang, *Synthetic Metals*, 2006, **156**, 514-518.
 80. Y.-P. Sun, K. Fu, Y. Lin and W. Huang, *Accounts of Chemical Research*, 2002, **35**, 1096-1104.
 81. K. K. Nanda, *Journal of Chemical Physics*, 2010, **133**, 545-568.
 82. D. Mohanta, S. S. Nath, A. Bordoloi, A. Choudhury, S. K. Dolui and N. C. Mishra, *Journal of Applied Physics*, 2002, **92**, 7149-7152.
 83. L. E. Brus, *Journal of Chemical Physics*, 1984, **80**, 4403-4409.
 84. O. L. Stroyuk, S. Y. Kuchmiy, A. I. Kryukov and V. D. Pokhodenko, *Nanoparticles*, 2010, 79-148.
 85. V. P. Menon, J. Lei and C. R. Martin, *Chemical Materials*, 1996, **8**, 2382-2390.
 86. T. Hernandez-Perez, M. Morales, N. Batina, J. Campos and M. Salmon, 2002.
 87. C. R. Martin, *Accounts of Chemical Research*, 1995, **28**, 61-68.
 88. J. Zang, C. M. Li, S.-J. Bao, X. Cui, Q. Bao and C. Q. Sun, *Macromolecules* 2008, **41**, 7053-7057.
 89. J. Huang, K. Wang and Z. Wei, *Journal of Materials Chemistry*, 2010, **20**, 1117-1121.
 90. Z. Cai and C. R. Martin, *Journal of the American Chemical Society* 1989, **111**, 4138-4139.
 91. S. Cuenot, S. Demoustier-Champagne and B. Nysten, *Physical Review Letters*, 2000, **85**, 1690-1693.
 92. L. Liang, J. Liu, C. F. Windisch, Jr., G. J. Exarhos and Y. Lin, *Angewandte Chemie International Edition*, 2002, **41**, 3665-3668.
 93. N.-R. Chiou, C. Lu, J. Guan, L. J. Lee and A. J. Epstein, *Nature Nanotechnology*, 2007, **2**, 354-357.
 94. M. Li, Z. Wei and L. Jiang, *Journal of Materials Chemistry*, 2008, **18**, 2276-2280.
 95. L. Al-Mashat, C. Debiemme-Chouvy, S. Borensztajn and W. Wlodarski, *Journal of Physical Chemistry C*, 2012, **116**, 13388-13394.
 96. D. Ge, S. Huang, R. Qi, J. Mu, Y. Shen and W. Shi, *Chemphyschem : a European journal of chemical physics and physical chemistry*, 2009, **10**, 1916-1921.
-

97. S. P. L. Sorensen and K. Linderstrom-Lang, *Biochemische Zeitschrift*, 1909, **8**, 1-168.
98. P. Kurzweil, *Sensors*, 2009, **9**, 4955-4985.
99. J. C. T. Kotz, P. M. and Weaver, G. C, *Chemistry & Chemical Reactivity*, Thomson Brooks/Cole, 2006.
100. J. J. A. Barron, C. & Geary, L., in *International Society of Electrochemistry*, Edinburgh, 2006.
101. S. S. Zumdahl, *Chemistry*, D. C. Heath & Co., 1993.
102. E. R. Ashwood, G. Kost and M. Kenny, *Clinical Chemistry* 1983, **29**, 1877-1885.
103. I. Khurana, *Textbook of Medical Physiology*, Elsevier, 2009.
104. S. Sabatini and N. A. Kurtzman, *Journal of the American Society of Nephrology*, 2009, **20**, 692-695.
105. B. R. Soller, N. Cingo and T. Khan, in *IEEE International Conference on Sensors*, Institute of Electrical and Electronics Engineers, 2002, vol. 1, pp. 266-269.
106. N. McVicar, A. X. Li, D. F. Gonçalves, M. Bellyou, S. O. Meakin, M. A. M. Prado and R. Bartha, *Journal of Cerebral Blood Flow & Metabolism*, 2014, **34**, 690-698.
107. M. A. Makos, D. M. Omiatek, A. G. Ewing and M. L. Heien, *Langmuir*, 2010, **26**, 10386-10391.
108. D. K. Harrison and W. F. Walker, *Journal of Physiology*, 1979, **291**, 339-350.
109. D. K. Harrison and W. F. Walker, *Journal of Medical Engineering and Technology*, 1980, **4**, 3-7.
110. P. W. Wolpert, D. Shaughnessy, D. N. Houchin, M. E. Baccari and F. A. Miller, *Archives of Surgery*, 1970, **101**, 308-313.
111. S. V. Rithalia, A. J. Hewer, J. Tinker and P. Herbert, *Journal of Biomedical Engineering*, 1980, **2**, 126-128.
112. C. C. Aickin, *Journal of Physiology*, 1984, **349**, 571-585.
113. D. Ellis and R. C. Thomas, *Journal of Physiology*, 1976, **262**, 755-771.
114. X.-r. Huang, Q.-q. Ren, X.-j. Yuan, W. Wen, W. Chen and D.-p. Zhan, *Electrochemistry Communications*, 2014, **40**, 35-37.
115. A. Eftekhari, *Sensors and Actuators, B*, 2003, **88**, 234-238.

116. I. Streeter, H. C. Leventis, G. G. Wildgoose, M. Pandurangappa, N. S. Lawrence, L. Jiang, T. G. J. Jones and R. G. Compton, *Journal of Solid State Electrochemistry*, 2004, **8**, 718-721.
117. L. Xiong, C. Batchelor-McAuley and R. G. Compton, *Sensors and Actuators, B*, 2011, **159**, 251-255.
118. T.-F. Kang, Z.-Y. Xie, H. Tang, G.-L. Shen and R.-Q. Yu, *Talanta*, 1997, **45**, 291-296.
119. D. O'Hare, K. H. Parker and C. P. Winlove, *Medical Engineering and Physics*, 2006, **28**, 982-988.
120. P. Duroux, C. Emde, P. Bauerfeind, C. Francis, A. Grisel, L. Thybaud, D. Armstrong, C. Depeursinge and A. L. Blum, *Gut*, 1991, **32**, 240-245.
121. R. C. Ye, *Plastic and Reconstructive Surgery*, 1957, **19**, 213-217.
122. M. J. Martin and P. Rolfe, *Analytical Processes*, 1986, **23**, 303-304.
123. J. J. Gooding, *Electroanalysis*, 2008, **20**, 573-582.
124. P. Vanysek, in *The Electrochemical Society Interface*, 2004.
125. C. Demuth, J. Varonier, V. Jossen, R. Eibl and D. Eibl, *Applied Microbiology and Biotechnology*, 2016, **100**, 3853-3863.
126. W.-D. Huang, H. Cao, S. Deb, M. Chiao and J. C. Chiao, *Sensors and Actuators, A*, 2011, **169**, 1-11.
127. Y.-H. Liao and J.-C. Chou, *Sensors and Actuators, B*, 2008, **128**, 603-612.
128. N. Uria, N. Abramova, A. Bratov, F.-X. Munoz-Pascual and E. Baldrich, *Talanta*, 2016, **147**, 364-369.
129. M. Wang, S. Yao and M. Madou, *Sensors and Actuators, B*, 2002, **81**, 313-315.
130. S. Kakooei, M. C. Ismail and B. Ari-Wahjoedi, *International Journal of Material Science Innovations*, 2013, **1**, 62-72.
131. A. M. Zimer, S. G. Lemos, L. A. Pocrifka, L. H. Mascaro and E. C. Pereira, *Electrochemistry Communications*, 2010, **12**, 1703-1705.
132. P. Takmakov, M. K. Zachek, R. B. Keithley, E. S. Bucher, G. S. McCarty and R. M. Wightman, *Analytical Chemistry*, 2010, **82**, 9892-9900.
133. H. Galster, *pH Measurement, Fundamentals, Methods, Applications, Instrumentation*, VCH, 1991.
134. P. Bergveld, *IEEE Transactions on Biomedical Engineering*, 1970, **17**, 70-71.

135. O. Korostynska, K. Arshak, E. Gill and A. Arshak, *IEEE Sensors Journal*, 2008, **8**, 20-28.
136. M. M. Maharbiz, W. J. Holtz, R. T. Howe and J. D. Keasling, *Biotechnology and Bioengineering*, 2004, **85**, 376-381.
137. C. Cane, I. Gracia and A. Merlos, *Microelectronics Journal*, 1997, **28**, 389-405.
138. J. A. Voorthuyzen and P. Bergveld, *Sensors and Actuators, B*, 1990, **1**, 350-353.
139. P. Bergveld, *Sensors and Actuators, B*, 2003, **88**, 1-20.
140. D. Armstrong, P. Duroux, C. Emde and A. L. Blum, *Barrett's Esophagus*, Oleso Knowledge, 1998.
141. X.-D. Wang and O. S. Wolfbeis, *Analytical Chemistry* 2013, **85**, 487-508.
142. J. Lin, *Trends in Analytical Chemistry*, 2000, **19**, 541-552.
143. Y. Hiruta, N. Yoshizawa, D. Citterio and K. Suzuki, *Analytical Chemistry* 2012, **84**, 10650-10656.
144. D. Jeon, W. J. Yoo, J. K. Seo, S. H. Shin, K.-T. Han, S. G. Kim, J.-Y. Park and B. Lee, *Optical Review*, 2013, **20**, 209-213.
145. P. Kassal, R. Surina, D. Vrsaljko and I. M. Steinberg, *Journal of Sol-Gel Science and Technology*, 2014, **69**, 586-595.
146. B. Schyrr, S. Pasche, E. Scolan, R. Ischer, D. Ferrario, J.-A. Porchet and G. Voirin, *Sensors and Actuators, B*, 2014, **194**, 238-248.
147. D. Aigner, S. M. Borisov, P. Petritsch and I. Klimant, *Chemical Communications*, 2013, **49**, 2139-2141.
148. L. H. Hutter, B. J. Muller, K. Koren, S. M. Borisov and I. Klimant, *Journal of Materials Chemistry C*, 2014, **2**, 7589-7598.
149. X.-D. Wang and O. S. Wolfbeis, *Analytical Chemistry*, 2015, 203-227.
150. D. Wencel, T. Abel and C. McDonagh, *Analytical Chemistry*, 2014, **86**, 15-29.
151. S. Singh and B. D. Gupta, *Sensors and Actuators, B*, 2012, **173**, 268-273.
152. D. Uhlmann, U.-C. Pietsch, S. Ludwig, J. Hess, B. Armann, G. Gaebel, E. Escher, L. Schaffranietz, A. Tannapfel, M. Fiedler, J. Hauss and H. Witzigmann, *Microvascular Research*, 2004, **67**, 38-47.
153. E. Y. Hwang, D. Pappas, A. S. Jeevarajan and M. M. Anderson, *Biomedical Microdevices*, 2004, **6**, 241-249.

154. A. S. Jeevarajan, S. Vani, T. D. Taylor and M. M. Anderson, *Biotechnology and Bioengineering*, 2002, **78**, 467-472.
155. R. B. Easley, T. R. Johnson and J. D. Tobias, *Clinical Pediatrics*, 2002, **41**, 351-355.
156. R. Sahney, S. Anand, B. K. Puri and A. K. Srivastava, *Analytica Chimica Acta*, 2006, **578**, 156-161.
157. S. Poeller and W. Schuhmann, *Electrochimica Acta*, 2014, **140**, 101-107.
158. M. Amiri, E. Amali, A. Nematollahzadeh and H. Salehniya, *Sensors and Actuators, B*, 2016, **228**, 53-58.
159. H. Kahlert, *Journal of Solid State Electrochemistry*, 2008, **12**, 1255-1266.
160. M. Lu and R. G. Compton, *Analyst*, 2014, **139**, 4599-4605.
161. X. Ji, C. E. Banks, A. Crossley and R. G. Compton, *Chemphyschem : a European journal of chemical physics and physical chemistry*, 2006, **7**, 1337-1344.
162. G. G. Wildgoose, P. Abiman and R. G. Compton, *Journal of Materials Chemistry*, 2009, **19**, 4875-4886.
163. J. C. Harfield, C. Batchelor-McAuley and R. G. Compton, *Analyst*, 2012, **137**, 2285-2296.
164. K. K. Shiu, F. Song and H. P. Dai, *Electroanalysis*, 1996, **8**, 1160-1164.
165. A. Anderson, J. Phair, J. Benson, B. Meenan and J. Davis, *Materials Science and Engineering, C*, 2014, **43**, 533-537.
166. I. Svancara and K. Schachl, *Chemische Listy*, 1999, **93**, 490-499.
167. K. K. I. Svancara, A. Walcarius and K. Vytras, *Electroanalysis with Carbon Paste Electrodes*, CRC Press, 2012.
168. K. Kalcher, I. Svancara, M. Buzuk, K. Vytras and A. Walcarius, *Monatshefte für Chemie*, 2009, **140**, 861-889.
169. I. Svancara, M. Hvizdalova, K. Vytras, K. Kalcher and R. Novotny, *Electroanalysis*, 1996, **8**, 61-65.
170. K. Kalcher, J. M. Kauffmann, J. Wang, I. Svancara, K. Vytras, C. Neuhold and Z. Yang, *Electroanalysis*, 1995, **7**, 5-22.
171. S.-S. Huang, Y.-D. Cheng, B.-F. Li and G.-D. Liu, *Mikrochimica Acta*, 1998, **130**, 97-101.
172. F. B. Bolger, R. Bennett and J. P. Lowry, *Analyst*, 2011, **136**, 4028-4035.

-
173. R. D. O'Neill, *Sensors*, 2005, **5**, 317-342.
174. J. P. Lowry, M. G. Boutelle and M. Fillenz, *Journal of Neuroscienc Methods*, 1997, **71**, 177-182.
175. J. L. Ponchon, R. Cespuglio, F. Gonon, M. Jouvet and J. F. Pujol, *Analytical Chemistry*, 1979, **51**, 1483-1486.
176. J. Wang, *Analytical Electrochemistry*, Wiley, New York, 2000.
177. X. J. Zhang, B. Ogorevc, G. Tavcar and I. G. Svegl, *Analyst*, 1996, **121**.
178. J.-P. Rivot, J. Montagne-Clavel and J. M. Besson, *European Journal of Pain*, 2002, **6**, 25-34.
179. Y. Yu, A. R. Wheeler, M. H. Shamsi, D. L. Krastev, M. D. M. Dryden and Y. Leung, *Lab on a Chip*, 2016, **16**, 543-552.
180. R. M. Wightman, M. R. Deakin, P. M. Kovach, W. G. Kuhr and K. J. Stutts, *Journal of the Electrochemical Society*, 1984, **131**, 1578-1583.
181. A. G. Ewing, M. A. Dayton and R. M. Wightman, *Analytical Chemistry*, 1981, **53**, 1842-1847.
182. M. Janin, J. Ghilane, H. Randriamahazaka and J.-C. Lacroix, *Electrochemical Communications*, 2009, **11**, 647-650.
183. Y. Song, T. Yang, X. Zhou, H. Zheng and S.-i. Suye, *Analytical Methods*, 2016, **8**, 886-892.
184. S. S. Lord, Jr. and L. B. Rogers, *Analytical Chemistry*, 1954, **26**, 284-295.
185. F. G. Gonon, C. M. Fombarlet, M. J. Buda and J. F. Pujol, *Analytical Chemistry* 1981, **53**, 1386-1389.
186. J. Ghilane, M. Delamar, M. Guilloux-Viry, C. Lagrost, C. Mangeney and P. Hapiot, *Langmuir*, 2005, **21**, 6422-6429.
187. A. Benedetto, M. Balog, P. Viel, F. Le Derf, M. Salle and S. Palacin, *Electrochimica Acta*, 2008, **53**, 7117-7122.
188. Y. Zhang and J. B. Zheng, *Electrochimica Acta*, 2007, **52**, 7210-7216.
189. S. Han, Y. Yuan, L. Hu and G. Xu, *Electrochemical Communications*, 2010, **12**, 1746-1748.
190. G. Shul, C. A. C. Ruiz, D. Rochefort, P. A. Brooksby and D. Belanger, *Electrochimica Acta*, 2013, **106**, 378-385.
191. J. L. Bahr, J. Yang, D. V. Kosynkin, M. J. Bronikowski, R. E. Smalley and J. M. Tour, *Journal of the American Chemical Society*, 2001, **123**, 6536-6542.
-

192. M. Raicopol, L. Necula, M. Ionita and L. Pilan, *Surface and Interface Analysis*, 2012, **44**, 1081-1085.
193. J. Q. Chambers, Wiley, 1988, vol. 2, pp. 719-757.
194. P. S. Guin, S. Das and P. C. Mandal, *International Journal of Electrochemical Science*, 2011, 816202, 816222 pp.
195. D. Menshykau, C. Batchelor-McAuley and R. G. Compton, *Journal of Electroanalytical Chemistry*, 2010, **651**, 118-130.
196. C. C. M. Neumann, C. Batchelor-McAuley, C. Downing and R. G. Compton, *Chemistry - A European Journal* 2011, **17**, 7320-7326.
197. M. Quan, D. Sanchez, M. F. Wasylkiw and D. K. Smith, *Journal of the American Chemical Society*, 2007, **129**, 12847-12856.
198. J. Pinson and F. Podvorica, *Chemical Society Reviews*, 2005, **34**, 429-439.
199. D. Belanger and J. Pinson, *Chemical Society Reviews*, 2011, **40**, 3995-4048.
200. C. Saby, B. Ortiz, G. Y. Champagne and D. Belanger, *Langmuir*, 1997, **13**, 6805-6813.
201. P. Allongue, M. Delamar, B. Desbat, O. Fagebaume, R. Hitmi, J. Pinson and J.-M. Saveant, *Journal of the American Chemical Society*, 1997, **119**, 201-207.
202. Q. Lin, Q. Li, C. Batchelor-McAuley and R. G. Compton, *Journal of Physical Chemistry C*, 2015, **119**, 1489-1495.

Chapter 2

Experimental

2.1 Introduction

The first results chapter of this thesis was concerned with the electrochemical deposition of different conformations of polypyrrole (PPy) onto gold electrodes. Nanowire, and the appropriately named “cauliflower” or bulk PPy, were examined by cyclic voltammetry (CV) and electrochemical impedance spectroscopy (EIS) to determine the electronic properties of the modified electrodes. Surface analyses of the various morphologies of PPy were performed using scanning electron microscopy (SEM).

The main objective of Chapters 4 to 7 was the development, characterisation and optimisation of a diazonium modified carbon substrate, which was suitable for the *in-vitro* and *in-vivo* monitoring of pH changes within acceptable biological ranges. Various electrochemical techniques were employed for the deposition of the diazonium salt onto various substrates, including CV, linear sweep voltammetry (LSV) and constant potential amperometry (CPA). The substrates modified during this study included carbon paste and carbon fibre electrodes. Surface analyses were carried out using SEM coupled with energy dispersive X-ray (EDX). Details of the electrodeposition and extensive characterisation and optimisation, as well as an *in-vivo* application are thoroughly explained in the respective chapters.

In this chapter, the electrochemical and analytical techniques used in the course of this study are described in detail. The electrochemical setup is outlined along with the experimental procedures used to modify the various substrates. The surgical protocol utilised is extensively described.

2.2 Experimental Procedures

2.2.1 Chemicals and Electrode Materials

The chemicals used throughout this thesis were mainly purchased from Sigma-Aldrich, and were of analytical grade. A list of all the chemicals and materials used throughout this research project is provided, alongside the relevant suppliers. For clarity the chemicals and materials are divided into sections depending on their use.

2.2.1.1 *Chemicals and Materials for the Electrochemical Analysis of Polypyrrole (PPy)*

Chemicals:

Ammonium Phosphate Monobasic	Sigma-Aldrich
Lithium Perchlorate	Sigma-Aldrich
Perchloric Acid	Sigma-Aldrich
Potassium Bromide FT-IR Grade ($\geq 99\%$)	Sigma-Aldrich
Potassium Chloride	Sigma-Aldrich
Potassium Chloride Suprapur [®] (99.999%)	Merck
Potassium Ferricyanide	Sigma-Aldrich
Pyrrole	Sigma-Aldrich
Sodium Perchlorate	Sigma-Aldrich
Sodium Phosphate Dibasic	Sigma-Aldrich
Sodium Phosphate Monobasic	Sigma-Aldrich

Electrode Materials:

Gold Working Electrode (99.99%)	GoodFellow
Platinum Wire	Fisher Scientific
Saturated Calomel Reference Electrode	Thermo Scientific

2.2.1.2 *Chemicals and Materials for the Development of a pH Sensor*

Chemicals:

4-Benzoylamino-2, 5-dimethoxybenzenediazonium chloride hemi (zinc chloride)	Sigma Aldrich
Acetonitrile	Sigma-Aldrich
Nitrogen Gas	BOC Gases
Potassium Chloride	Sigma-Aldrich
Sodium Chloride	Sigma-Aldrich
Sodium Hydroxide	Sigma-Aldrich
Sodium Phosphate Dibasic	Sigma-Aldrich
Sulfuric Acid 97%	BDH

Tetraethyl Ammonium Tetrafluoroborate	Sigma-Aldrich
Zinc Chloride	Sigma-Aldrich

Biocompatibility and Interference Studies:

3, 4-Dihydroxyphenylacetic acid	Sigma-Aldrich
5-Hydroxy-Indole Acetic Acid	Sigma-Aldrich
Acetaminophen	Sigma-Aldrich
Acetylsalicylic Acid	Sigma-Aldrich
Ascorbic Acid	Sigma-Aldrich
Bovine Serum Albumen	Sigma-Aldrich
Calcium Chloride	Sigma-Aldrich
Dopamine	Sigma-Aldrich
Homovanillic Acid	Sigma-Aldrich
L-Cysteine	Sigma-Aldrich
L-Glutathione	Sigma-Aldrich
L-Tyrosine	Sigma-Aldrich
Magnesium Chloride	Sigma-Aldrich
Phosphatidylethanolamine	Sigma-Aldrich
Serotonin	Sigma-Aldrich
Triton [®] X	Sigma-Aldrich
Uric Acid	Sigma-Aldrich

In-vivo Chemicals:

Isoflurane	Abbott Laboratories
Sodium Bicarbonate	Sigma-Aldrich

Electrode Materials:

Carbon Fibres	Kation Scientific
Graphite Powder	Sigma-Aldrich
Hydrochloric Acid	VWR
Platinum Wire	Fisher Scientific
Saturated Calomel Reference Electrode	Thermo Scientific
Silicone Oil	Sigma-Aldrich

Silver Wire	Advent Materials
Styrene	Sigma-Aldrich

2.2.2 Solutions

All aqueous solutions were prepared using distilled milli-Q water, assigned as H₂O throughout this thesis. The solutions used have been separated into sections, depending on their use.

2.2.2.1 Solutions for the Electrochemical Analysis of PPy

Preparation of Bulk and Nanowire PPy

Pyrrole monomer was distilled under vacuum and stored at -18°C under N₂, prior to use. To obtain a nanowire morphology, the monomer (0.15 M or 75 mM), was added to aqueous solutions containing the dopant salts, typically 2 mM LiClO₄ or NaClO₄, and 0.2 M NH₄H₂PO₄, NaH₂PO₄ or Na₂HPO₄. The pH of the solution was adjusted to *ca.* 5.5, with concentrated HClO₄, to achieve the bulk polymer.

Electrochemical Analyses of Ppy Films

CV studies were carried out in either 0.2 M KCl or 1 mM KFe(CN)₆/0.1M KCl solutions.

EIS studies were performed in 0.2 M solutions of KCl, LiClO₄, and Na₂HPO₄. The pH values of selected KCl and LiClO₄ solutions were increased using 1.0 M NaOH.

2.2.2.2 Solutions for the Development of a pH Sensor

All solutions in this section were N₂ saturated prior to their use, unless otherwise stated.

3, 4-Dihydroxyphenylacetic acid (DOPAC)

A 100 μM solution of DOPAC was prepared by dissolving 1.7 mg in 100 ml PBS (pH 7.4).

5-Hydroxy-Indole Acetic Acid (5HIAA)

A 100 μM solution of 5HIAA was prepared by dissolving 1.9 mg in 100 ml PBS (pH 7.4).

Acetaminophen (ACOP)

A 0.50 mM solution of ACOP was prepared by dissolving 7.6 mg in 100 ml PBS (pH 7.4).

Acetylsalicylic Acid (ASA)

A 0.50 mM solution of ASA was prepared by dissolving 9.0 mg in 100 ml PBS (pH 7.4).

Ascorbic Acid (AA)

500 μ M and 1.0 mM solutions of AA were prepared by dissolving 8.8 mg and 17.6 mg, respectively, in 100 ml PBS (pH 7.4).

Bovine Serum Albumen (BSA)

A 1% (w/v) solution of BSA was prepared by dissolving 50 mg in 5 ml H₂O.

Calcium Chloride (CaCl₂)

A 1.6 mM solution of CaCl₂ was prepared by dissolving 1.8 mg in 10 ml PBS (pH 7.2, 7.4 and 7.6).

Dopamine (DA)

A 0.1 mM solution of DA was prepared by dissolving 1.9 mg in 100 ml PBS (pH 7.4), 1 ml of this solution was then diluted in 1 litre of PBS, giving a 0.1 μ M solution.

FBRR/H₂SO₄

0.544 ml H₂SO₄ (98%) was added to 100 ml H₂O, forming a 0.1 M solution. 2 mM FBRR (7.7 mg) was added to 10 ml of the prepared 0.1 M H₂SO₄, before being sonicated for *ca.* 20 s. The solution was stored at 4°C when not in use.

FBRR/TEABF₄/ACN

TEABF₄/ACN was prepared by dissolving 0.1 M TEABF₄ (2.171 g) in ACN (100 ml). FBRR, 2 mM (7.7 mg), was added to 10 ml of the prepared solution and was sonicated for *ca.* 20 s. The solution was stored at 4°C when not in use.

Homovanillic Acid (HVA)

A 50 μM solution of HVA was prepared by dissolving 0.9 mg in 100 ml PBS (pH 7.4).

L-Cysteine

A 100 μM solution of L-Cysteine was prepared by dissolving 1.2 mg in 100 ml PBS (pH 7.4).

L-Glutathione

A 100 μM solution of L-Glutathione was prepared by dissolving 6.0 mg in 100 ml PBS (pH 7.4).

L-Tyrosine

A 200 μM solution of L-Tyrosine was prepared by dissolving 3.6 mg in 100 ml PBS (pH 7.4).

Magnesium Chloride (MgCl_2)

A 21 mM solution of MgCl_2 was prepared by dissolving 20 mg in 10 ml PBS (pH 7.2, 7.4 and 7.6).

Phosphate Buffered Saline (PBS)

PBS was prepared by dissolving 8.9 g NaCl (0.15 M), 1.76 g NaOH (44 mM) and 6.86 g $\text{NaH}_2\text{PO}_4 \cdot 2\text{H}_2\text{O}$ (44 mM) in 1 litre of H_2O . The pH was adjusted to 7.2, 7.4 or 7.6, using NaOH or NaH_2PO_4 .

PBS: Varied Ionic Strength (I)

I = 0.23 M: PBS was prepared by dissolving 4.38 g NaCl (75 mM), 0.88 g NaOH (22 mM) and 3.43 g $\text{NaH}_2\text{PO}_4 \cdot 2\text{H}_2\text{O}$ (22 mM) in 1 litre of H_2O . The pH was adjusted to 7.2, 7.4 or 7.6, using NaOH or NaH_2PO_4 .

I = 0.92 M: PBS was prepared by dissolving 17.52 g NaCl (0.30 M), 3.52 g NaOH (88 mM) and 13.72 g NaH₂PO₄·2H₂O (88 mM) in 1 litre of H₂O. The pH was adjusted to 7.2, 7.4 or 7.6, using NaOH or NaH₂PO₄.

Phosphatidylethanolamine (PEA)

A 1% (w/v) solution of PEA was prepared by dissolving 50 mg in 5 ml H₂O.

Serotonin (5-HT)

Solutions containing 1.0 and 10.0 μM 5-HT were prepared by dissolving 0.2 mg in 1 litre, and 0.2 mg in 100 ml, PBS (pH 7.4), respectively.

Sodium Bicarbonate (NaHCO₃)

A 45 mM solution was prepared by adding 0.378 g NaHCO₃ to 100 ml H₂O.

TritonX[®]

A 1% (w/v) solution of TritonX[®] was prepared by dissolving 50 mg in 5 ml H₂O.

Uric Acid (UA)

100 μM and 5.0 mM solutions of UA were prepared by dissolving 1.9 mg and 95 mg, respectively, in 100 ml PBS (pH 7.4).

Zinc Chloride (ZnCl₂)

0.5, 1.0, 2.0 and 5.0 mM solutions of ZnCl₂ were prepared in 0.1 M TEABF₄/ACN.

2.2.3 Instrumentation and Software

Electrochemical experiments for potentiometry and CV, relating to PPy, were performed on a Solartron SI 1287 potentiostat. The Solartron potentiostat used Scribner Associates Corrware[®] for Windows Version 2.1 and the resulting data were analysed using Scribner Associates CorrView[®] version 3.0. Electrochemical impedance spectroscopy (EIS) was undertaken on a Solartron SI 1287 potentiostat, coupled with a Solartron frequency response analyser model SI 1255B. Scribner Associates ZPlot[®] version 2.1 was the software used for the impedance experiments and all resulting data was analysed using ZView[®] 2.1.

For the pH sensor development, the potentiostat used was a 4 Channel Biostat from ACM instruments. This was used in conjunction with an 8 Channel PowerLab[®] 8/SP, which allowed digital-analogue and analogue-digital conversion between the computer and the potentiostat. Constant potential amperometry (CPA) was carried out using Chart 4 and LabChart 6 (AD Instruments, Oxford, UK). CV and LSV experiments were carried out using EChem 2 Application for Windows. All results were analysed using GraphPad Prism[®] 5.01.

A list of all other equipment used throughout this thesis is provided along with the relevant model numbers.

pH Meter

The pH meter used for all PPy experiments was a Jenway 370 Enterprise. A pH/Ion 510 (Eutech Instruments) was used for the development of the pH sensor.

Electronic Balance

The balance used for all PPy experiments was a Sartorius, Model TE 2145. A Sartorius, Model BP 310P, was used for the development of the pH sensor.

Sonicator

The sonicator used for all PPy experiments was a Branson 1510. A Fisherbrand FB 11002 was used for the development of the pH sensor.

FT-IR

The IR equipment used was a Perkin Elmer 2000.

Sputter Coater

The sputter coater used throughout this thesis was an Emitech K550 (Agar Scientific).

SEM

The SEM used was a Hitachi S-3200-N.

EDX

The EDX coupled to the SEM was an INCA x-act (Oxford Instruments).

Microscope

The microscope used in the preparation of all micro-electrodes was an Olympus stereo microscope SZ51 (Olympus America).

Constant Flow Micro Pump

A Univentor 801 syringe pump was used to change solution pH for the real-time *in-vitro* studies.

Vortex

The vortex used, to ensure homogeneous solutions, was Reax control from Heidolph.

Temperature Probe

A Yellowline TC1 temperature probe was used, in conjunction with a Yellowline MST basic C hotplate, to monitor and maintain the solution temperature at 37°C, when required.

2.3 Electrochemical Cell Set-Up

All surfaces in this thesis were electrochemically synthesised, on substrates with different surface areas. A standard three electrode cell was employed for all CV, EIS, LSV and CPA experiments, consisting of a working electrode, reference electrode and an auxiliary electrode. For the electrochemical analysis of PPy, the three electrodes included, a gold disc working electrode, diameter, $\varnothing = 3$ mm, a saturated calomel reference electrode (SCE) and a large surface area platinum auxiliary electrode. Current is passed through the auxiliary electrode during a redox reaction. If the surface area of the auxiliary electrode is smaller than that of the working electrode, it can impede the reaction taking place at the working electrode.¹ Therefore, an auxiliary electrode with a higher surface area than the working electrode is generally used for electrochemical experiments. For the development of the pH sensor, the working electrodes were either, carbon paste electrodes (CPEs) or carbon fibre electrodes

(CFEs) with $\text{Ø} = 0.27$ mm and $7 \mu\text{m}$, respectively. A platinum auxiliary wire was used for all *in-vitro* experiments, with a silver auxiliary wire used for *in-vivo* experiments.

Generally, a SCE was the reference electrode of choice for *in-vitro* experiments, except those designed to mimic *in-vivo* conditions, where a pseudo Ag/AgCl reference electrode was used. The pseudo Ag/AgCl reference was employed for all *in-vivo* experiments. The electrochemical cell was a glass cylinder, which included a Teflon[®] lid with openings for each of the electrodes. The three electrodes were immersed in the electrolyte solution with added analytes. A schematic of a typical three electrode cell is shown in Figure 2.1.² When not in use, the SCE was stored in a saturated solution of potassium chloride (KCl), to prevent the porous frit at the tip of the electrode from drying out. The electrode was rinsed with distilled water between experiments to avoid contamination of other electrolyte solutions with KCl. The electrode's internal KCl solution was refreshed on a weekly basis. The platinum counter electrodes were cleaned regularly with silicon carbide based abrasive paper (Buehler P2500). They were then sonicated in distilled milli-Q water and ethanol for 300 s, respectively.

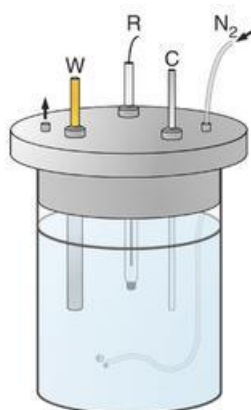


Figure 2.1: Schematic of a three electrode cell,² showing the working (W), reference (R) and auxiliary/counter (C) electrodes, with an inlet to enable N_2 saturation of the electrolyte solution.

2.3.1 Preparation of Working Electrodes

The preparation and maintenance of the working electrodes used throughout this thesis are described in this section.

Gold Electrodes

A gold (99.95%) rod ($\varnothing = 3$ mm) was cut into lengths of *ca.* 2 cm. An electrical contact between the metal and the external circuit was achieved by attaching a copper wire to the gold surface, with a conducting epoxy resin. The electrical contact was verified using a multimeter, with a resistance $\leq 1 \Omega$ required. The wire was then threaded through the Teflon[®] holder leaving the metal exposed at one end. The end of the electrode, with the copper wire, was sealed with silicone and the end of the electrode, with the metal exposed, was sealed using a non-conducting epoxy resin, see Figure 2.2. Prior to use, all electrodes were carefully polished to eliminate surface irregularities and scratches. They were manually polished using a succession of smaller diamond grade polishes, Buehler MetaDi Monocrystalline Diamond Suspension, from 30 μm to 1 μm , and a Buehler polishing micro cloth. Finally the electrodes were polished using an Al_2O_3 paste, 0.5 μm . The electrodes were sonicated in ethanol and H_2O between each grade of polish. This protocol was also used to remove polymers, exposing a clean reusable, electrode surface.

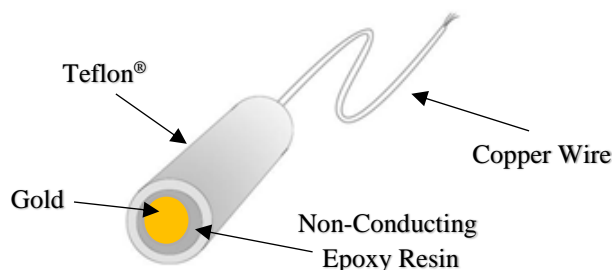


Figure 2.2: Schematic of a gold disc electrode.

Carbon Paste Electrodes (CPEs)

CPEs were prepared by thoroughly mixing graphite powder (0.71 g), with silicone oil (250 μl) using a pestle and mortar for up to three hours. Every 10 minutes, the sides of the container were scraped with a scalpel blade, collecting the paste together. A 5 cm length of Teflon insulated silver wire was cut. Approximately 1 mm of the Teflon insulation was removed from one end, exposing the bare silver wire. Using a tweezers,

the Teflon[®] was gently moved along the length of the wire, exposing a 1 mm cavity at the other end of the electrode. The exposed silver wire was then soldered into a gold clip, which served as the electrical connection. The cavity was subsequently packed by tapping it in the prepared carbon paste. A bare silver wire, with the same diameter, was used as a plunger, to ensure good electrical contact and that the paste was compactly packed. The packing procedure was repeated three times until the cavity was full. The surface was levelled by gently rubbing it on a clean, flat surface. A schematic of a CPE is shown in Figure 2.3.

After each use, the top 1 mm section, containing the carbon paste, was cut off. The gold clip was removed and the Teflon[®] was moved along the electrode exposing a new cavity. The gold clip was re-soldered into position, and the cavity was repacked as previously described.

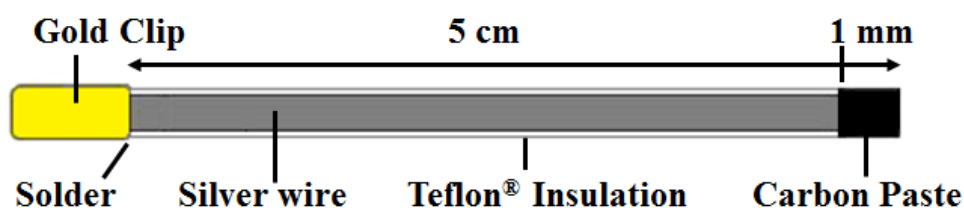


Figure 2.3: Schematic of a typical CPE.

Carbon Fibre Electrodes (CFEs)

CARBOSTAR-1 (E1011) standard CFEs were purchased from Kation Scientific, Kation Europa Bt., Hungary. The CFEs used in this thesis consisted of a 7 μm diameter single carbon fibre, which was held in a 1.5 mm diameter borosilicate glass capillary tubing. The carbon tip was conically shaped and protruded from the glass insulation by $20 \mu\text{m} \pm 5 \mu\text{m}$, leaving a cylindrical surface.

Before each use, the CFEs were pre-treated by applying a constant potential of 2.0 V *vs.* SCE for 30 s followed by -2.0 V *vs.* SCE for 10 s in PBS, 0.1 M NaOH or 0.1 M H₂SO₄. This enhanced their electrochemical performance^{3, 4} by either etching the surface thereby increasing the surface area, or forming surface oxides that could facilitate electron transfer.⁵ As the CFEs were covalently modified with FBRR, they

could not be re-used, so new CFEs were used in each experiment. Figure 2.4 shows an image of a CFE, the 7 μm carbon tip is not visible protruding from the glass capillary.



Figure 2.4: Image of a carbon fibre electrode as supplied by Kation Scientific.

2.3.2 Electrode Modification

Electropolymerisation of Pyrrole: Bulk and Nanowire Polymers

Nanowire PPy was obtained using 0.15 M/75 mM monomer in an aqueous solution containing 0.2 M Na_2HPO_4 and 2 mM LiClO_4 , at a constant potential of 0.80 V vs. SCE for 300 s. The bulk polymer was achieved by changing the solution pH to *ca.* 5.5 and applying a constant potential of 0.80 V vs. SCE for 300 s. A second, thinner, bulk polymer was deposited by applying the same potential until a charge of 0.01 C was attained. The electropolymerisation solution was formed by dissolving the LiClO_4 and NaH_2PO_4 in 10 ml H_2O . While stirring, the pyrrole was added, and stirring was continued for a few minutes.

Electrodeposition of FBRR onto CPEs

The FBRR modified CPE was obtained using a solution of 2 mM FBRR in 0.1 M H_2SO_4 , which was N_2 saturated for 20 minutes, before being electrochemically deposited by LSV, 5 sweeps, from 0.40 V to -0.80 V vs. SCE. The first 4 modified electrodes, from each freshly made solution, were not used for analyses (see Section 4.2.3.17). When not in use, the FBRR solution was stored at 4°C.

Electrodeposition of FBRR onto CFEs

CFEs were pre-treated in 0.1 M H₂SO₄ by applying constant potentials of 2.0 V *vs.* SCE for 30 s, followed by -2.0 V *vs.* SCE for 10 s. FBRR was then electrochemically reduced, onto the pre-treated CFEs, from a N₂ saturated solution of 2 mM FBRR in 0.1 M TEABF₄/ACN by LSV, 5 sweeps, from 0.40 V to -0.80 V *vs.* SCE. When not in use, the FBRR solution was stored at 4°C.

Styrene Modified CPEs (SMCPEs)

CPEs were prepared as described in Section 2.3.1. They were then stored overnight, in styrene, at 4°C, causing the carbon paste to contract within the Teflon[®] cavity. Quantities ranging from 12-25 µl of styrene were added to 0.025 g carbon paste, and repacked into the electrode cavity.⁶ The surface was levelled off by gentle rubbing on a clean, flat surface. SMCPEs were modified with FBRR as previously described.

2.3.3 Preparation of Electrodes for Surface Analysis

All SEM and EDX analyses were carried out using a Hitachi S-3200-N, with a tungsten filament electron gun. This has a maximum magnification of 200,000x and resolution of 3.5 nm. This microscope was equipped with an Oxford Instrument INCA x-act EDX system with silicon drift detector.

Preparation of PPy Samples

Once the polymers were prepared, the electrodes were rinsed with H₂O to remove any excess electrolyte from the modified surface. The electrodes were dried with a low pressure N₂ flow, before insertion into the sputter coater. A vacuum was applied for *ca.* 30 minutes to ensure no solvent remained within the polymer matrix. Sputter coating was performed, under argon, with an Au/Pd target, until a thickness of 20 nm was obtained. Copper tape was used to connect the surface of the modified electrode to the specially adapted aluminium holder, to reduce the build-up of incident electrons on the sample that can cause sparking within the SEM chamber.

Preparation of CPE Samples

After the FBRR was electro-reduced onto the surface, the electrodes were rinsed with H₂O, to remove any excess electrolyte. Once dried, a 5 mm long section was cut from the working end of the electrode. The Teflon was carefully removed from the bottom 2 mm, and the exposed silver wire was angled to 90° and placed onto 12 mm carbon adhesive tabs (Agar Scientific), mounted on 15 mm x 6 mm specimen stubs (Agar Scientific), so that the modified surface was *ca.* 90° to the mount, see Figure 2.5. The stubs were placed in the sputter coater and a vacuum was applied for 30 minutes. Sputter coating was performed, under argon, with an Au/Pd target, until a thickness of 5 nm was obtained.



Figure 2.5: Modified CPEs mounted on a specimen stub for imaging.

2.4 *In-Vivo* Experiments

This section describes, in detail, the materials and methods used for *in-vivo* testing of the pH sensor. All animal experiments were conducted under licence B100/2205, in accordance with the European Communities Regulations 2002 (Irish Statutory Instrument 566/2002 and U.K. Animals (Scientific procedures) Act 1986). Every effort was made to minimise any suffering caused to the animals used.

2.4.1 Electrodes

In-vivo experiments were performed using CPEs and CFEs. The auxiliary electrode used was a 5 mm long, 0.2 mm diameter silver wire. The SCE reference electrode was

used for the majority of *in-vitro* experiments, but because of the toxic mercury contained within,⁷ and difficulties in miniaturising, it was not suitable for *in-vivo* experiments. A pseudo Ag/AgCl reference electrode, manufactured on site, replaced the SCE for all *in-vivo* experiments.

To prepare the pseudo Ag/AgCl reference electrode, a 5 cm length of Ag wire was cut. The Teflon insulation was removed from 2 mm at one end and this was soldered into a gold clip, which served as an electrical contact and support for the electrode. A 5 mm section of Teflon was removed from the other end, exposing the bare silver wire. The wire was connected to the negative terminal of a 9 V battery (anode) and a Pt or Ag wire was connected to the positive terminal (cathode). The electrodes were immersed in 1.0 M HCl for 30 s, resulting in electroplating a layer of AgCl on the silver electrode surface, according to Equations 2.1 and 2.2.



2.4.2 Subjects

Male Wistar rats, (*rattus norvegicus*), were used for all *in-vivo* experiments (Charles River UK Ltd., Manston Rd., Margate, Kent CT9 4LT UK). The animals, weighing between 300 and 550 g were group housed, maximum of 3 animals per cage, in a strictly controlled environment. The temperature was maintained between 17 and 23°C, with humidity of 55 ± 10 %. A 12 hour light/dark regime was enforced. All animals had access to water and food ad libitum.

2.4.3 Surgical Protocol

Prior to any surgeries, all instruments and supplies to be used were sterilised by autoclaving at 126°C for 20 minutes. All other equipment to be used in the surgical procedures, e.g., microscope, operating lights and heating pad were cleaned with Virkon (5%) and allowed to dry. The recording equipment required for the procedure was subject to the same cleaning procedure.

Anaesthesia was induced in the gas chamber with an air-flow of 600-700 ml/minute and Isoflurane at 4%, for *ca.* 5 minutes. The animal was removed from the chamber, weighed and the upper hind limbs were shaved. The animal was then replaced in the induction chamber for a further 5 minutes. The subject was then placed, in the supine position, on a heating pad, in the nose-piece set-up, where the air-flow was set at 400-500 ml/minute and isoflurane at 2.0-2.5%, depending on the procedure's pain level. The rectal probe was positioned, ensuring a body temperature of 37°C. The shaved area of the hind limb was sterilised with an iodine solution to prevent the subject from getting any infection following introduction of the device into the muscle.

2.4.3.1 Induction of Ischemia

For experiments involving the CPEs, an 18 gauge needle, (inner $\text{\O} = 0.84\text{mm}$), containing the working, reference and auxiliary electrodes, was inserted through the skin of the exposed area and deep enough to reach muscle (minimum 1 cm). The needle tip was then retracted from the muscle and the pH sensor was left *in-situ*. CV recording was commenced. Once sufficient background cycling had occurred, *ca.* 45 minutes, a sterilised tourniquet was applied to the lower limb and was tightened to induce ischemia. The ischemic insult was continued over a 10 minute period, a duration sufficient to inflict ischemia without causing irreversible damage. After this time period the tourniquet was cut from the subject's limb to allow reperfusion of the muscle tissue. This reperfusion period was recorded for a 45 minute period, allowing comparison of pre- and post-ischemia potential recordings.

For experiments involving the CFEs, a 14 gauge needle, (inner $\text{\O} = 1.60\text{ mm}$) was used to insert the working electrode through the exposed skin and an 18 gauge needle, containing the reference and auxiliary electrodes, was inserted close in proximity to the working electrode. The needle tips were withdrawn, leaving the electrodes *in-situ*. The procedure then continued as described above.

2.4.3.2 Injection of Sodium Bicarbonate

The surgical protocol was carried out according to that described in Section 2.4.3. The working (CPE), reference and auxiliary electrodes were inserted into the animal's hind leg muscle using an 18 gauge needle, which was then withdrawn, leaving the recording

electrodes *in-situ*. CV recording commenced and background cycling lasted 45 minutes. Injections (0.1 ml) of sodium bicarbonate (45 mM) were administered directly into the tissue under investigation, close to the electrode location, after 50, 55 and 60 minutes. The limb was allowed to recover for a further 45 minutes. Recording continued throughout the experiment, lasting *ca.* 100 minutes in total.

2.4.3.3 Termination

Euthanasia was facilitated by administration of 1.0 ml of pentobarbitol sodium (euthatal) into the lower left or right quadrant of the abdomen of the animal.

2.5 Data Acquisition and Statistical Analysis

The data acquired from the experimental techniques used in Chapter 3 were translated into excel files (.xls) for mathematical and statistical analysis. The standard error bars are expressed in absolute units of measurement, represented by the standard error of the mean ($SE_{\bar{x}}$), i.e., standard deviation (s) divided by the square root of the sample size (n), as shown in Equation 2.3.

$$SE_{\bar{x}} = \frac{s}{\sqrt{n}} \quad 2.3$$

All pH experiments were analysed using linear regressions. All regression models fall between the two extremes of zero correlation and a perfect correlation, i.e., $0 \leq R^2 \leq 1$. In order to test whether two sets of results were statistically different, t -tests were used. A t -test is a statistical examination of two population means, resulting in a P -value. The P value is a probability, which helps to determine the significance of the results, where $0 \leq P \leq 1$. The standard 95% confidence interval was used for these tests, so a P -value less than 0.05 indicated a significant difference between the two data sets, whereas a P -value higher than 0.05 indicated no significant difference.⁸ These analyses were performed using GraphPad Prism[®], version 5.01.

2.6 References

1. P. M. S. Monk, *Fundamentals of Electroanalytical Chemistry*, John Wiley & Sons, 2001.
2. W. Ma, Y.-L. Ying, L.-X. Qin, Z. Gu, H. Zhou, D.-W. Li, T. C. Sutherland and H.-Y. Chen, *Nature Protocols*, 2013, **8**, 439-450.
3. A. L. Beilby, T. A. Sasaki and H. M. Stern, *Analytical Chemistry*, 1995, **67**, 976-980.
4. J. X. Feng, M. Brazell, K. Renner, R. Kasser and R. N. Adams, *Analytical Chemistry*, 1987, **59**, 1863-1867.
5. Z. Bartosova, D. Riman, P. Jakubec, V. Halouzka, J. Hrbac and D. Jirovsky, *Science World Journal.*, 2012, 295802-295806.
6. A. M. Wynne, Maynooth University, 2014.
7. M. W. Shinwari, D. Zhitomirsky, I. A. Deen, P. R. Selvaganapathy, M. J. Deen and D. Landheer, *Sensors*, 2010, **10**, 1679-1715.
8. R. D. De Veaux P. F. Velleman and D. E. Bock, *Stats: Data and Models*, Pearson Addison Wesley, 2008.

Chapter 3

Electrochemical Properties of Bulk and Nanowire Morphologies of Polypyrrole

3.1 Introduction

Polypyrrole (PPy) is one of the most extensively studied conducting polymers, due to its ease of preparation and its attractive range of properties, including high conductivity¹, redox activity,² and ion exchange capabilities.³ An additional feature of PPy is that it forms a biologically compatible polymer matrix.^{4,5} Therefore, it has been used in a wide range of biomedical fields including the development of biosensors,^{6,7} tissue engineering^{8,9} and implantable bio devices.⁴ Electrochemical polymerisation of pyrrole allows control over the film thickness and morphology, as well as permeation and charge transport by adjusting the electrochemical parameters.¹⁰ Furthermore, electropolymerised PPy films have a strong adherence to the electrode surface.^{11, 12} The properties of PPy depend on its morphologies which are in turn determined by the synthesis conditions,¹³ including, monomer concentration,¹⁴ applied potential,¹⁵ solvent and supporting electrolyte,¹⁶ dopant ions¹⁷ and pH.¹⁸ The morphology of bulk PPy formed at electrode surfaces is generally in “cauliflower” form.¹⁹

Because of their size, nanomaterials display several properties that are different to those displayed by their bulk material counterparts.^{19,20} The electrochemical, template free, formation of PPy nanowires was developed and characterised about 10 years ago,¹⁶ and was adapted in this thesis. In general, nanowires possess a higher surface area and shorter diffusion lengths than their analogous bulk materials, providing the wires with more attractive electrochemical properties.²¹ The aim of this chapter is to compare the properties of bulk and nanowire conformations of PPy using similar electropolymerisation conditions, and also bulk and nanowire conformations adapted to have similar electroactive surface areas. The polymers were designed with these specific objectives in mind, and do not represent the optimum conditions for polymer growth. Assuming the nanowire morphology afforded greater surface area and electrochemical properties than the bulk conformation, this would enhance their modification as they would possess a greater number of electrochemically active sites for the attachment of e.g. copper structures for the detection of nitrate ions. All polymer films formed were subsequently analysed for their electrochemical properties using cyclic voltammetry (CV) and electrochemical impedance spectroscopy (EIS). The influence of different electrolytes on the impedance was also examined.

In this section the electropolymerisation of pyrrole onto bare gold electrodes was investigated. A nanowire morphology was obtained by adopting a method developed by Debiemme-Chouvy.¹⁶ The conditions for the nanowire growth were then adapted to assess the effect of the perchlorate cation, Na^+ and Li^+ , on the nanowire diameter. Further amendments were carried out in order to reduce the length of the nanowires, as those formed from aqueous solutions tend to display “water defects” i.e., the inclusion of carbonyl groups into the polymer backbone, leading to decreased conductivity.

Once these growth conditions were confirmed, a simple change in the solution pH resulted in the corresponding bulk polymer, albeit of a substantially larger surface area. The electrochemical properties of both polymer films, bulk and nanowire, grown using the same conditions were analysed by CV and EIS. The bulk polymer growth conditions were then adapted to give a bulk polymer with a similar surface area to the nanowire films. The electrochemical properties of these two polymers were subsequently investigated by CV and EIS. Impedance experiments were also carried out in 0.2 M KCl, Na_2HPO_4 and LiClO_4 to examine the influence of the different electrolytes on the electrochemical properties of the polymers formed.

3.2 Results and Discussion

3.2.1 PPy Morphologies

The electrochemical polymerisation of pyrrole is affected by a wide range of parameters, among them the supporting electrolyte and its effect on the solution pH.²² Varying these conditions can lead to polymers of different physical morphologies, and therefore, electrochemical properties.

Electrochemical polymerisation of pyrrole was carried out in solutions of various pH, in order to observe the resulting morphology. This was achieved by changing the phosphate component of the electrolyte solution. It should be emphasised that the solution pH and the pH at the working electrode were not the same. Protons were released during polymerisation, two per monomer, which can cause the solution pH to

fall over time, at the electrode surface,^{16, 18} (see Section 1.5.2.1). The pH of the electrolyte solutions, measured just before polymerisation, is therefore, for comparison purposes only. Two contrasting morphologies of PPy, a bulk polymer, which has a distinct “cauliflower” appearance, or nanowires were formed. Table 3.1 lists the effect of varying phosphate in the electrolyte solution, giving the solution pH and the PPy morphology obtained. All solutions contained 0.15 M pyrrole, 2 mM ClO₄⁻ ions and 0.2 M of the relevant phosphate, in an aqueous solution.

Table 3.1: Variation of PPy morphology obtained by changing the phosphate component, and hence pH, of the electrolyte solution.

Phosphate (0.2 M)	pH	Morphology
NH ₄ H ₂ PO ₄	4.5	Bulk
Na ₂ HPO ₄	9.2	Nanowire
NaH ₂ PO ₄	4.5	Bulk
Na ₂ HPO ₄ / NaH ₂ PO ₄	7.7	Nanowire

3.2.2 PPy Morphologies Deposited from Similar Electrochemical Conditions

In order to compare the electrochemical properties of bulk and nanowire conformations of PPy, the polymers were formed using the same pyrrole concentration, in the same electrolyte solution, but different pH values. The electrochemical polymerisation was carried out using the same conditions, 0.80 V *vs.* SCE for 300 s. CVs of both polymer morphologies were examined.

3.2.2.1 PPy in Nanowire Morphology

It was found, in Section 3.2.1, that in order to obtain a nanowire morphology of PPy, the solution pH should be alkaline before the onset of polymerisation. On release of H⁺ ions during electropolymerisation, the pH at the electrode surface falls to a neutral/slightly acidic pH required for the successful formation of PPy nanowires.^{16, 23} An aqueous solution containing 0.15 M pyrrole, 0.2 M Na₂HPO₄ and 2 mM LiClO₄ was employed to deposit pyrrole onto the gold substrate, potentiostatically, at 0.80 V *vs.* SCE for 300 s. An advantage to using a constant potential method of deposition is

that no surface pre-treatment or template is required, as the method of nanowire growth relies only on the reactants and the potential applied to the working electrode.²⁴ Figure 3.1 shows the current-time plot obtained using the aforementioned conditions, alongside a SEM micrograph of the nanowires formed. In any polymerisation experiment, the application of the potential to the electrode leads to an initial charging current which arises from the charging of the double layer.²⁵ This charging current decays rapidly, depending on the conductivity of the solution, caused by the depletion of the monomer concentration at the electrode surface.²⁶ In this system the current continued to decay to a low value, indicating a slow rate of electropolymerisation at the electrode surface. The current output then stabilised indicating a steady rate of polymer growth.

These slow rates of electropolymerisation can be explained by the solution pH, which was recorded as 9.2. This corresponds to a relatively high concentration of OH⁻ ions in solution, which are known to terminate the propagation of pyrrole chains, leading to the formation of an over-oxidised polymer in unbuffered solutions.²⁷ However, a phosphate solution was used here, which was used as a buffer, to control the pH of the solution and subsequently the morphology of PPy nanowires.²⁴ Also, the release of H⁺ ions on polymerisation neutralises the OH⁻ ions leading to a relatively neutral pH at the electrode surface, for the optimum polymerisation conditions, hence the initial decrease was stabilised and uniform growth ensued. Although neutral to slightly acidic conditions are more favourable for PPy formation, solutions of high acidity can cause a reduction in the polymer conductivity, due to the acid catalysed formation of non-conjugated trimers.²⁸

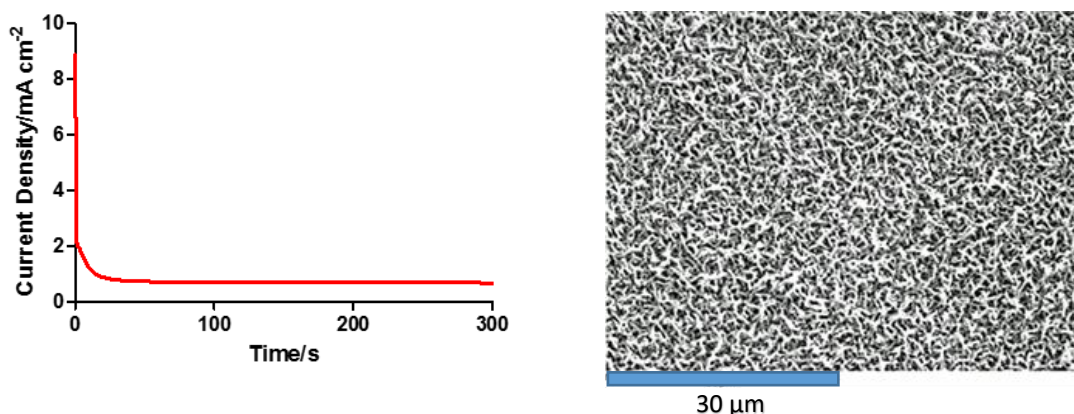


Figure 3.1: Current-time plot for the electropolymerisation of pyrrole and SEM micrograph of the resulting PPy nanowires, from a solution containing 0.15 M pyrrole, 0.2 M Na₂HPO₄ and 2 mM LiClO₄, for 300 s at 0.80V vs. SCE.

3.2.2.2 Effect of Perchlorate Dopant Ions

Electrochemical polymerisation of pyrrole results in the polymer being in an oxidised state, with a positive charge on the chain,²⁸ which is balanced by doping anions. This was explained in more detail in Section 1.5.1. Typical anionic dopants are chlorides, bromides, iodides, perchlorates, nitrates, sulfates, phosphates and para-toluene sulfonates.²⁹ The chemical nature of the dopant affects the electroactivity, as well as surface and bulk structural properties, of the polymer.^{17, 30, 31} A perchlorate anion was the anion of choice in this chapter. Although the ClO₄⁻ was present at very low concentrations, 2 mM, it was essential to the formation of the nanowires. In the absence of, or in higher concentrations of perchlorate, e.g., 0.1 M, PPy wires will not form. Since ClO₄⁻ is inserted into the polymer backbone as a dopant, it has a large impact on the growth rate achieved. Higher concentrations result in a higher growth rate leading to the formation of a bulk polymer.³²

In order to examine the effect of the cation bound to the perchlorate, on the deposited nanowires, electropolymerisation of pyrrole was carried out using Li⁺ and Na⁺ perchlorate salts. SEM micrographs were obtained and the diameters of a random selection of the formed nanowires were measured. The results are displayed in Table 3.2 and show that the smaller cation, Li⁺, resulted in significantly thinner nanowires, ($P = 0.0016$).

Table 3.2: Comparison of the diameters of nanowires obtained using Na⁺ and Li⁺ perchlorate dopant ions.

Cation	Mean Ø (nm)	SEM	<i>n</i>	<i>P</i> -value
Na ⁺	115.20	2.72	50	0.0016
Li ⁺	103.40	2.42	50	

3.2.2.3 PPy Chain Defects

Literature has shown that increasing the polymerisation time results in wires of longer length,^{19, 23} with no change in their diameter.³³ Contrary to some findings that the longer wires possess higher conductivity, due to the increased amount of conjugation, longer PPy nanowires formed from aqueous solutions have been found to have inferior conductivities.^{23, 34} The relatively high polymerisation potential, required when using aqueous solutions, causes the oxidation of water, forming OH radicals, which react with the polymer backbone by replacing the dopant anions. The resultant formation of carbonyl groups on the α -carbon of the pyrrole ring breaks the conjugation of the polymeric chain, leading to decreased electrochemical properties of the polymer.³⁵

In order to reduce the length of the nanowires formed, thereby reducing the number of carbonyl defects on the polymer backbone, the electropolymerisation time was reduced from 300 s to 100 s. The resulting current-time plot is shown in Figure 3.2, alongside the corresponding SEM micrograph. The current shows an initial decay to a very low value, indicative of a slow deposition rate at the electrode surface. Contrary to Section 3.2.2.1, where the current decay stabilised to give good nanowire formation, here the current continued to decay. Indeed, the current-time plot in Figure 3.2 would suggest the formation of an insulating polymer. However, on examination of the accompanying SEM micrograph in Figure 3.2, it was clear that 100 s was not a sufficient time span to allow the formation of the wires. Indeed for shorter times, < 300 s, the charge consumed is mainly used to coat the gold surface with a PPy sublayer from which the PPy nanowires start to grow.³⁶ There was evidence of the onset of sporadic nanowire formation. Further examination of the SEM micrograph gave evidence of a film formation that acts as a base from where the nanowire growth has initiated. This two-step nanowire formation has previously been suggested^{37,38} and involves an

instantaneous nucleation process resulting in a 3-dimensional growth pattern, followed by the 1-dimensional growth of the nanowires from this film support.^{16, 19}

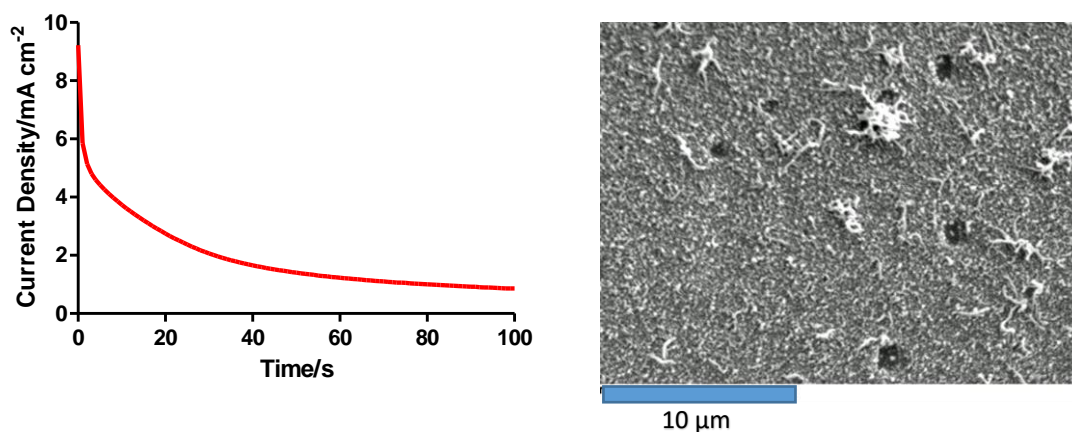


Figure 3.2: Current-time plot for the electropolymerisation of pyrrole and SEM micrograph of the resulting PPy nanowires, from a solution containing 0.15 M pyrrole, 0.2 M Na₂HPO₄ and 2 mM LiClO₄, for 100 s at 0.80V *vs.* SCE.

Several reports refer to the use of lower monomer concentrations resulting in shorter nanowire length.^{39 40} A monomer concentration of 75 mM was, therefore, electrodeposited onto gold electrodes for 300 s at 0.80 V *vs.* SCE from a solution containing 0.2 M Na₂HPO₄ and 2 mM LiClO₄. The current-time plot, in Figure 3.3., is almost identical to that described in Section 3.2.2.1, which resulted in a uniform coverage of the electrode surface with PPy nanowires. The SEM micrographs, in Figure 3.4, show various magnifications of the nanowires formed, with the electrode surface covered with a consistent mesh of fine wires.

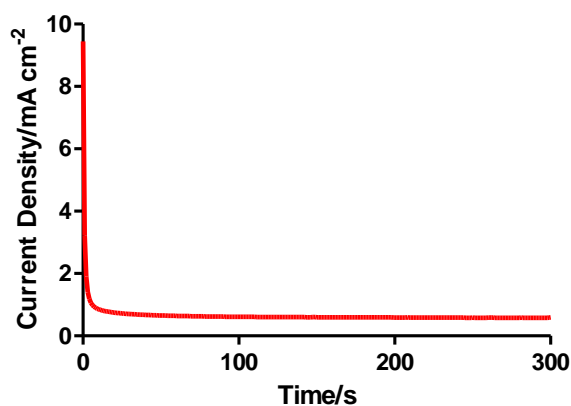


Figure 3.3: Current-time plot for nanowires formed from 75 mM pyrrole at 0.80 V vs. SCE for 300 s.

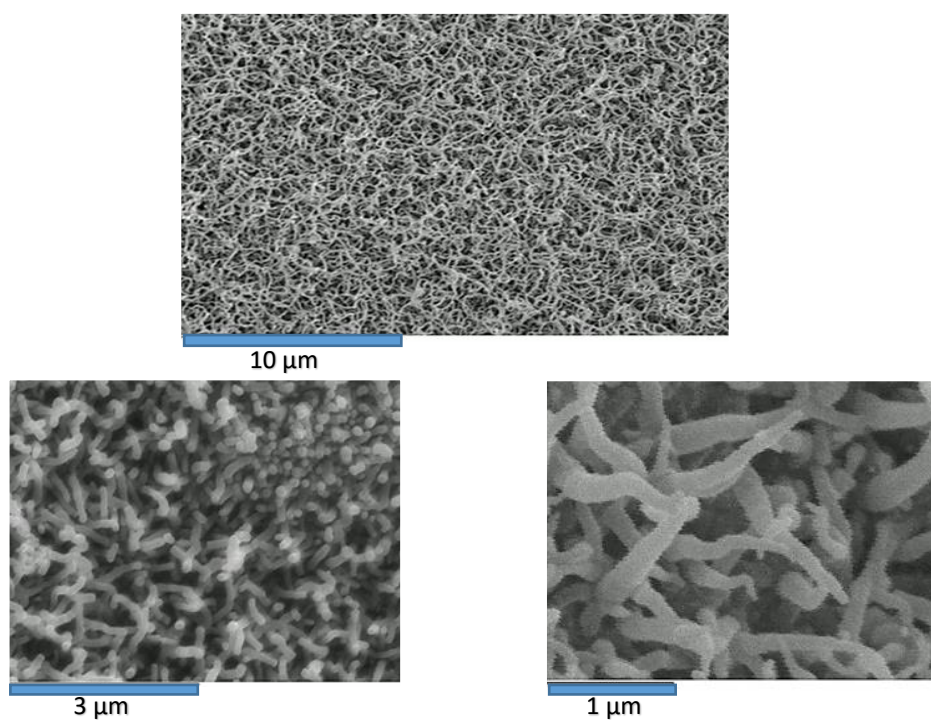


Figure 3.4: SEM micrographs of nanowires formed from 75 mM pyrrole at 0.80 V vs. SCE for 300 s.

FT-IR analyses of PPy nanowires grown from 0.15 M and 75 mM solutions of pyrrole, provided direct evidence for the development of carbonyl defects. Figure 3.5(A) shows the characteristic C=O band at *ca.* 1750 cm⁻¹ for nanowires generated from 0.15 M pyrrole. Figure 3.5(B), however, shows that this band was substantially reduced, although not totally eliminated, when a solution containing 75 mM pyrrole was employed. This confirmed that using a lower monomer concentration reduced the

amount of carbonyl defects along the PPy backbone, which should result in a polymer of higher conductivity.

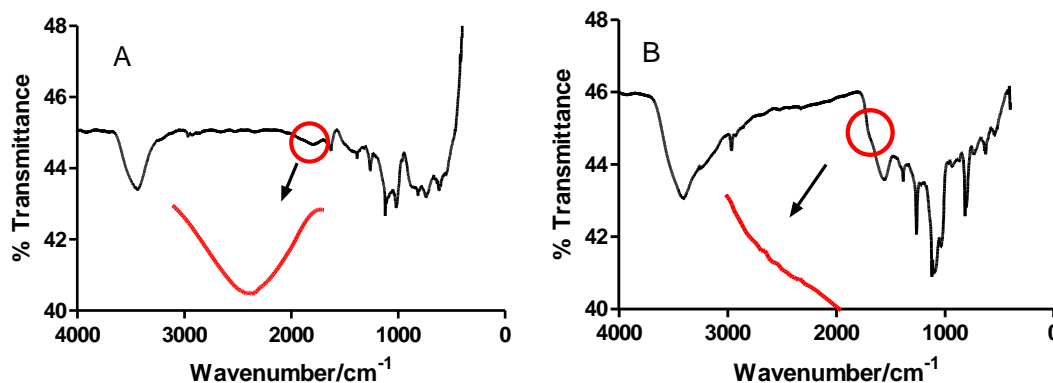


Figure 3.5: FT-IR spectra of PPy nanowires electrodeposited from aqueous solutions containing (A) 0.15 M and (B) 75 mM pyrrole.

3.2.2.4 PPy in Bulk Morphology

Sections 3.2.2.1-3 developed conditions for the electrochemical polymerisation of PPy nanowires onto a gold substrate. In order to compare their electrochemical properties with those of a bulk polymer grown using the same parameters, the solution pH was changed to a slightly acidic value, as directed by Table 3.1, using concentrated HClO_4 . The optimum growth conditions for a bulk polymer are at a neutral or slightly acidic pH.³⁴ For bulk PPy a solution that is too acidic or basic will interfere with conjugation, resulting in a polymer of lower conductivity.²⁸ Figure 3.6 shows the current time plot for the bulk polymer grown to the same conditions as the nanowires in Section 3.2.2.3. The corresponding plot for nanowires is also shown, for ease of comparison.

When compared to the current-time plot for nanowires, the region where the electrochemical current recovers and increases sharply is indicative of a rapid increase in the electrode surface area,¹⁴ as the PPy quickly nucleates and deposits onto the electrode surface, finally reaching a steady state, indicating efficient formation of the polymer. The mechanism behind the polymerisation of pyrrole at a constant potential has been well documented.^{26, 41}

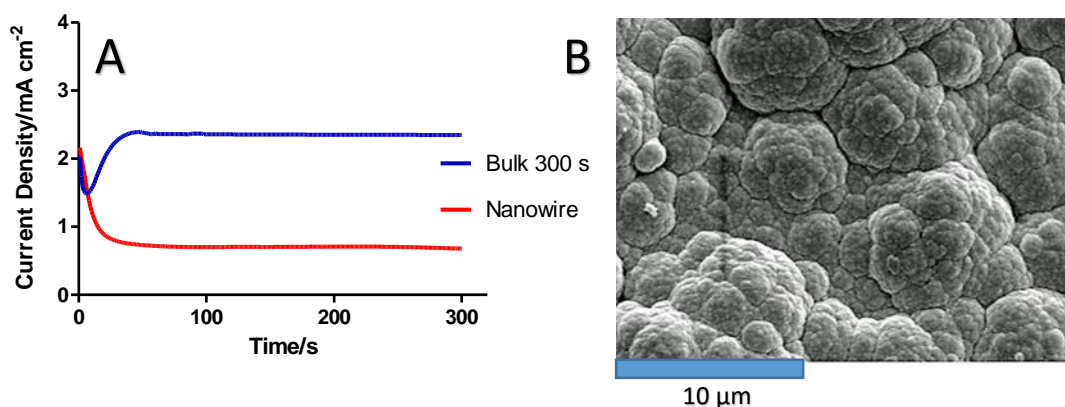


Figure 3.6: (A) Current-time plots for the electropolymerisation of bulk and nanowire morphologies of PPy grown at 0.80 V vs. SCE for 300 s, from a solution containing 75 mM pyrrole, 0.2 M Na₂HPO₄ and 2 mM LiClO₄. (B) SEM micrograph of the resultant bulk “cauliflower” PPy formed.

The current-time plots obtained during the polymerisation of pyrrole occur in three stages. The first stage, is the current spike whose decay is dependent on potential and is said to represent the electrode surface coverage with a monolayer of polymer film. The second stage, refers to the rise in current lasting for a number of seconds, indicating the rapid polymerisation at the electrode surface, and the third stage is represented by the continued steady state current flow for the remainder of the electrochemical deposition. These three stages were observed during the potentiostatic deposition of the bulk PPy film in Figure 3.6.

It is clear from a comparison of the two current-time transients, in Figure 3.6, that the bulk polymer was deposited at a high rate, and the nanowire film was formed at a much slower rate. It is this slow growth that leads to the formation of nanowires and not bulk PPy.

The surface morphology of the bulk polymer was examined by SEM. The micrograph, in Figure 3.6, shows the resulting polymer produced from the electrochemical polymerisation of pyrrole, from a solution containing 75 mM pyrrole, 0.2 M Na₂HPO₄ and 2 mM LiClO₄ (pH = 5.5), potentiostatically at 0.80 V vs. SCE for 300 s. It can clearly be seen that the polymer displayed the typical “cauliflower” morphology of PPy films.⁴²

3.2.2.5 Electrochemical Properties

The redox activity of the nanowire and bulk modified electrodes, as specified in Sections 3.2.2.3 and 3.2.2.4, respectively, was examined by CV in 0.2 M KCl, see Figure 3.7. It can be observed from the CVs, that the bulk PPy polymer had an increased electrochemical response compared to the nanowire polymer. This higher capacitance was attributed to the larger surface area of the bulk polymer, when compared to that of the nanowires.²⁶ Capacitive effects may originate from the higher surface area of the bulk polymer being able to store more charge. This in turn would require the formation of a larger double layer in solution, to counter balance this charge.²⁵ Further investigation into the polymer surface area will be carried out in Section 3.2.2.6.

Inspection of the CVs generated by the nanowires revealed a single anodic peak, E_p , at *ca.* 0.15 V *vs.* SCE which was due to the oxidation of the polymer, the corresponding, poorer defined, cathodic peak, E_c , was located at *ca.* -0.08 V *vs.* SCE. The peak separation of 0.23 V was indicative of a quasi-reversible process, which is typical of PPy.^{43, 44} Both peaks were relatively broad, indicating slow kinetics of the two redox processes. However, the reduction peak was less well defined than the oxidation peak. During oxidation of the polymer, the layer next to the electrode surface is oxidised first, giving a conducting layer, which facilitates oxidation of the adjacent layers. Conversely, on reduction of the polymer, the layer adjacent to the electrode is reduced first, giving an insulating layer, making the overall reduction process more difficult.⁴⁵

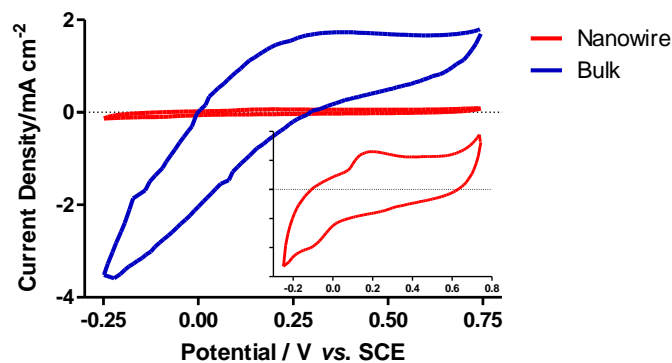


Figure 3.7: CVs of bulk and nanowire conformations of PPy electrodeposited at 0.80 V *vs.* SCE for 300 s from solutions containing 75 mM pyrrole, 0.2 M Na₂HPO₄ and 2 mM LiClO₄. The inset shows the magnified CV for the PPy nanowires.

3.2.2.6 Surface Area of Nanowire and Bulk PPy

It was clear from the CVs obtained in Figure 3.7, that the electroactive surface area of the bulk polymer formed was far greater than that of the nanowire PPy. The electroactive surface area is defined as the area that effectively transfers the charge of the species in solution.⁴⁶ In this section, experiments were carried out to estimate the surface areas of both polymers.

The PPy, nanowire and bulk, films were cycled in 0.2 M KCl at various scan rates. Diagnostic plots of the anodic and cathodic peak current against the square-root of the scan rate, from 0.50 V to -0.50 V *vs.* SCE, for the nanowire morphology of PPy, was linear across the whole range of scan rates tested, (5-200 mV/s), as shown in Figure 3.8, indicating a diffusion controlled processes. Correlation coefficients of 0.9704 and 0.9955 were obtained for the oxidation and reduction peaks for the nanowire film, respectively. However, because of the high capacitance of the bulk polymer, no redox peaks were visible in the CVs.

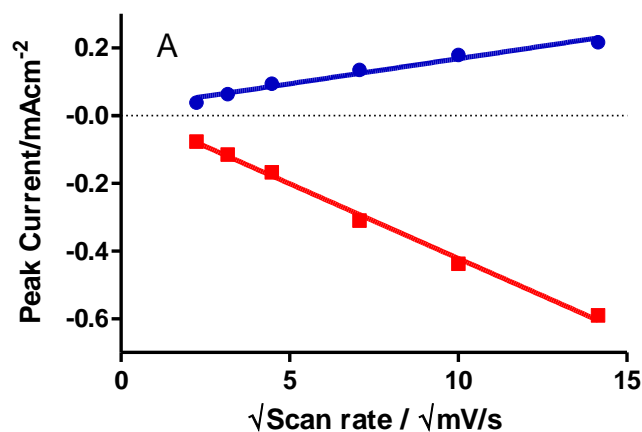


Figure 3.8: Plot of peak current density vs. $(\text{scan rate})^{1/2}$ for nanowire morphology of PPY. The anodic peak is represented by the blue line — and the cathodic peak by the red line. —

A linear relationship between the current and the square root of the scan rate was observed, this indicated that the oxidation and reduction processes were under diffusion control, and therefore, conform to the Randles-Sevcik relationship, described by Equation 3.1.

$$I_P = (2.69 \times 10^5) n^{3/2} A D^{1/2} \nu^{1/2} C \quad 3.1$$

where I_P is the peak current, n is the number of electrons transferred, ν is the scan rate, D is the diffusion coefficient, A is the surface area of the electrode and C is the concentration of the redox species.⁴⁷

Firstly, the diffusion coefficient of the $\text{Fe}^{3+}/\text{Fe}^{2+}$ redox couple was calculated at a bare gold electrode, using a 1.0 mM potassium ferrocyanide solution in a 0.10 M KCl solution. This was achieved by varying the scan rate as the electrode was cycled. The peak currents were measured at each scan rate, and the plot in Figure 3.9 was constructed. The slope of the plot was used, (Equation 3.2), to calculate the diffusion coefficient of ferrocyanide, $D = 9.87 \times 10^{-6} \text{ cm}^2 \text{ s}^{-1}$, which is close to the literature value.^{48, 49} Equation 3.2 was then used to estimate the surface area of the nanowire film as 0.14 cm^2 .

$$\text{Slope} = (2.69 \times 10^5) n^{3/2} A D^{1/2} C \quad 3.2$$

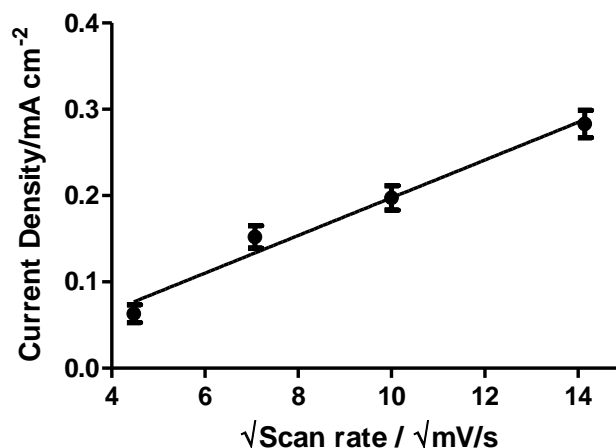


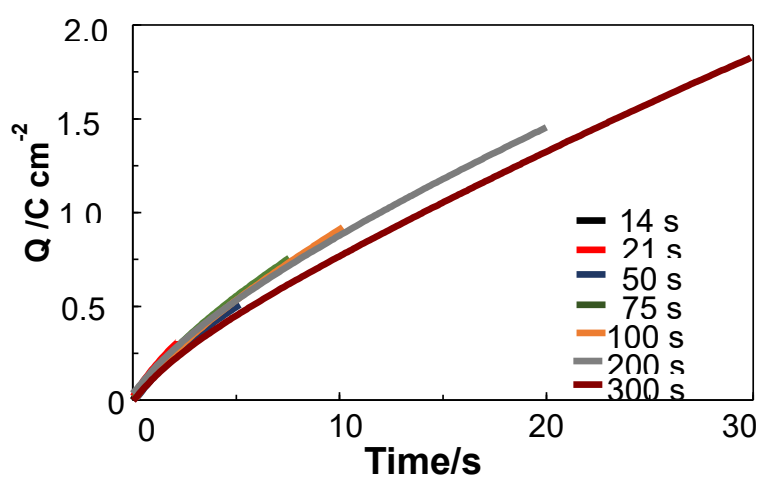
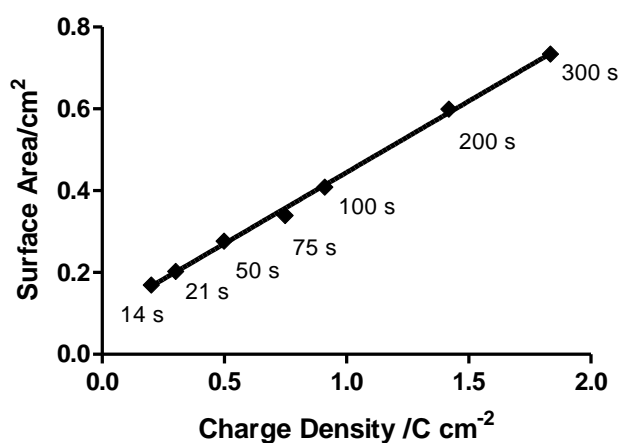
Figure 3.9: Plot of peak current density vs. square root scan rate for a bare gold electrode in 1.0 mM Fe(CN)₆/0.1 M KCl.

In order to estimate the surface area of the bulk PPy film, a calibration plot was prepared relating the polymer surface area, estimated using Equation 3.1, with the charge consumed during electropolymerisation. Bulk polymers were grown for various times, less than 300 s, and the charge consumed during the electropolymerisation was recorded, see Figure 3.10. Surface area estimations were made, using Equation 3.2. A plot of the charge density against the surface area, (data shown in Table 3.3), resulted in a straight line graph as shown in Figure 3.11, ($R^2 = 0.9969$), and the equation of the linear plot is given in Equation 3.3. This equation was subsequently used to estimate the surface area for the polymer grown for 300 s, which was calculated as 0.73 cm² (the charge density for a polymer grown for 300 s was 1.83 C cm⁻²).

$$y = 0.3505x + 0.0946 \quad 3.3$$

Table 3.3: Data from bulk PPy polymerisation experiments and surface area estimations using Equation 3.1.

Time (s)	Charge Density (C/cm^2)	Estimated Area (cm^2)
300	1.8343	0.7340
200	1.4184	0.5998
100	0.9108	0.4093
75	0.7478	0.3192
50	0.4987	0.2077
21	0.2986	0.2030
14	0.1970	0.1696

**Figure 3.10:** Plot of the charge densities attained for bulk PPy grown over various time periods.**Figure 3.11:** Calibration plot showing the relationship between the charge density consumed during electropolymerisation and the surface area of bulk PPy modified electrodes.

3.2.3 PPy Morphologies with Similar Electroactive Surface Areas

Section 3.2.2 discussed two different morphologies, nanowire and bulk, of PPy electrodeposited onto a gold substrate, using the same solution concentrations and electrochemical oxidation parameters. However, the CVs suggested that the bulk polymer had a far superior surface area, (0.73 cm^2), when compared with the nanowire PPy, (0.14 cm^2), and could therefore, contain more electroactive sites within the polymer film. In order to directly compare the electrochemical properties of nanowire and bulk morphologies of PPy, it was deemed necessary to develop a bulk polymer, with a surface area similar to that of the nanowire polymer film.

Using the plot obtained in Figure 3.11, and the estimated surface area of the nanowire modified electrode of 0.14 cm^2 , the estimated charge density for the bulk polymer was calculated as $Q = 0.13 \text{ C/cm}^2$, i.e., the bulk PPy should be grown to charge of 0.01 C. The resulting bulk polymer, shown in Figure 3.12, shows much smaller “cauliflower” morphology, and a more even surface, than that shown in Figure 3.6(B), for the bulk polymer grown for 300 s.

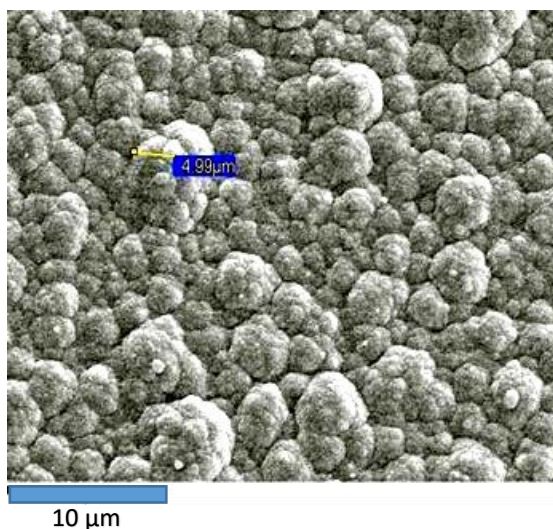


Figure 3.12: SEM micrograph of bulk PPy grown to a charge of 0.01 C.

The CVs, in 0.2 M KCl, (see Figure 3.13), show that the bulk polymer grown to a charge of 0.01 C had a more comparable surface area to that of the nanowire PPy grown for 300 s. The higher capacitance still indicated a slightly larger surface area for

the bulk polymer, suggesting a greater amount of dopant was interacting with the polymer, and possibly the presence of more electroactive sites within the polymer film.⁴⁴ Both films possessed electrochemical activity. The nanowire polymer exhibited a shift in the oxidation and reduction peak potentials to more favourable values, which may indicate better electrical properties of the nanowire film and thermodynamically more difficult electron transfer processes for the bulk material.⁵⁰ Both films exhibited quasi-reversible redox reactions, consistent with PPy films,^{43,44} with ΔE values of 0.25 V and 0.30 V for the nanowire and bulk polymers formed, respectively.

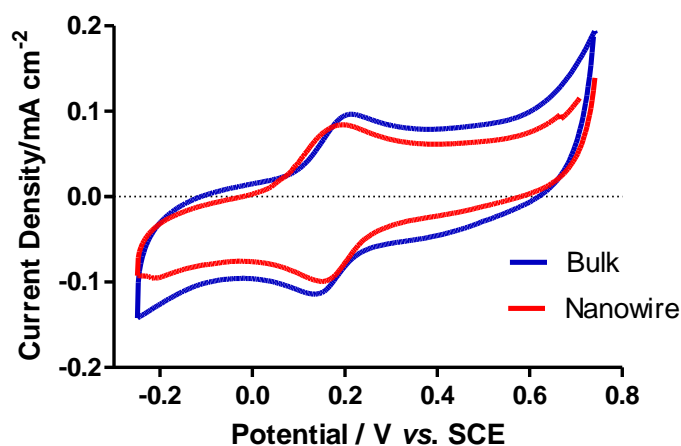


Figure 3.13: CVs, in 0.2 M KCl, of bulk and nanowire formations of PPy grown to have similar surface areas.

3.2.3.1 Bulk PPy Film Thickness

PPy film thickness is directly proportional to the charge consumed during electropolymerisation.⁵¹ In Section 3.2.3 bulk PPy was grown over various time periods and the charge consumed during electropolymerisation was recorded. Once the bulk PPy layer had formed, the electrode surface was scratched with a sharp scalpel blade, hence, using SEM, the film thickness could be obtained by scanning across the electrode surface and measuring the step height. Five separate thickness measurements were performed for each modified electrode and the results are presented in Table 3.4, with the corresponding plot of charge consumed against polymer thickness in Figure

3.14. The linear relationship, ($R^2 = 0.9794$), between the charge consumed and film thickness is given by Equation 3.4. SEM micrographs of a selection of the polymer films obtained are shown in Figure 3.15.

$$y = 2.919x - 0.1929 \quad 3.4$$

Table 3.4 shows that the thickness measurements at each charge were relatively reproducible, for the five thickness readings examined, indicating a consistent coverage over the electrode surface. Any discrepancies could be due to surface roughness of the film. It has been shown that the surface roughness of PPy films is dependent on the thickness of the film.^{52, 53} It was observed that the film thickness increased with the charge consumed during electropolymerisation. This was predicted by Diaz *et al.* who derived a relationship that assumes 1 C cm⁻² of charge is passed for each 2.5 μm of polymer growth.⁵⁴ Using Equation 3.4, 1 unit of charge (C cm⁻²) was calculated to result in 2.7 μm of PPy growth, which was in good agreement with the literature value. However, it is important to highlight that the relationship quoted by Diaz was for a chloride dopant, whereas a slightly larger dopant, ClO₄⁻, was used here. This may account for the variation in the values.

Table 3.4: Film thickness measurements for bulk Ppy films, grown at 0.80 V vs. SCE, to various electropolymerisation charges, $n = 5$.

Charge Density (C cm ⁻²)	Thickness (μm)	SEM	n
1.416	4.148	0.115	5
0.911	2.080	0.192	5
0.762	1.998	0.073	5
0.499	1.426	0.092	5
0.300	0.647	0.026	5
0.198	0.399	0.040	5
0.142	0.292	0.006	5

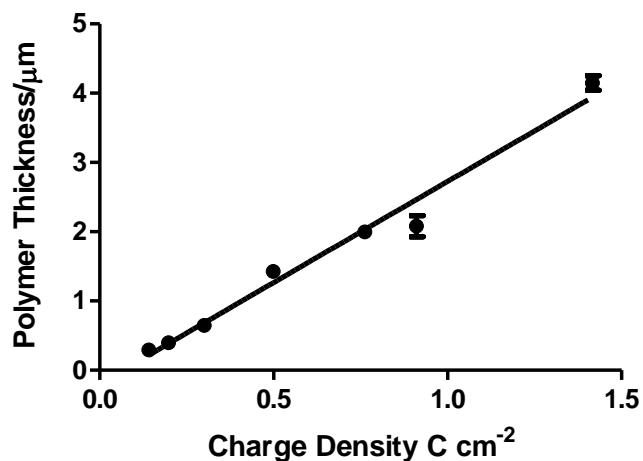


Figure 3.14: Plot of charge consumed during electropolymerisation vs. polymer thickness.

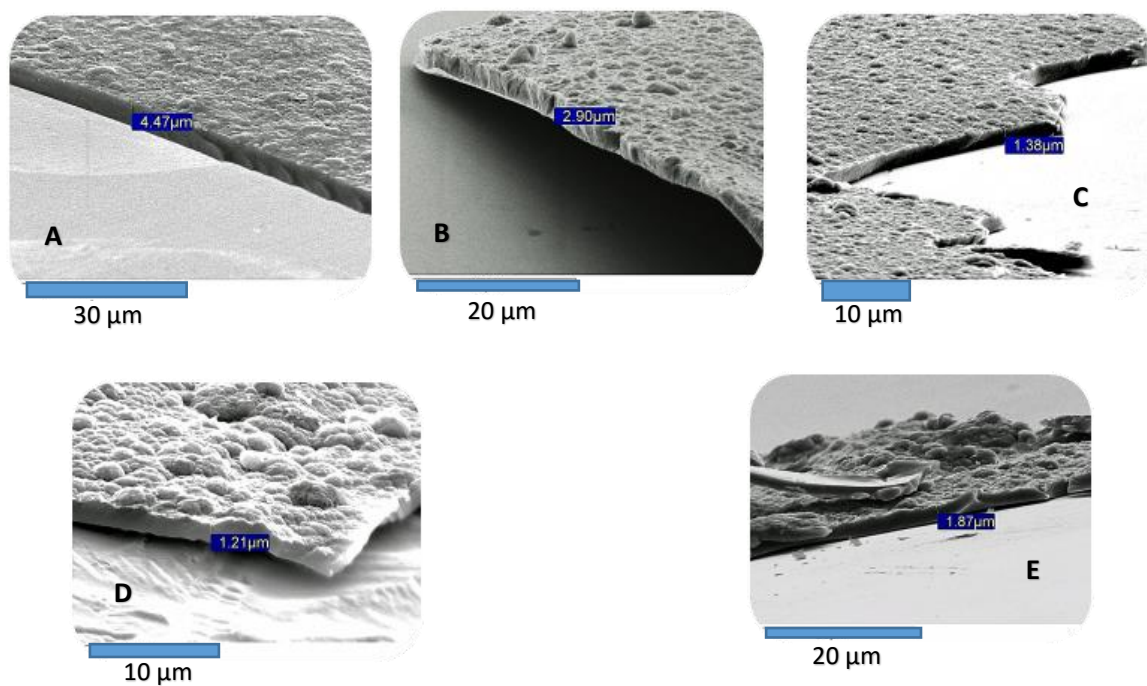


Figure 3.15: SEM micrographs of bulk PPy electropolymerised to (A) 0.91, (B) 0.73, (C) 0.20, (D) 0.14 and (E) 0.50 $C\ cm^{-2}$, respectively.

Alternatively, a theoretical calculation, using Equation 3.5, can be used to calculate the thickness of the PPy bulk films grown.

$$T = \frac{M(\text{Py}) + xM(\text{Dopant})}{d(2+x)F} q \quad 3.5$$

Here, T is the thickness of the film, $M(\text{Py})$ is the molar mass of the monomer, x is the number of dopant molecules per monomeric unit, $M(\text{Dopant})$ is the molar mass of the dopant (LiClO_4), d is the density of doped PPy, (assumed as 1.5 g cm^{-3}),^{1, 54} F is Faraday's constant and q is the charge passed during electropolymerisation. The maximum doping level achievable for PPy, with a ClO_4^- dopant, is one dopant unit per 3.3 monomer units, i.e., $x = 0.3$.^{55, 56}

Using Equation 3.5, 1 C cm^{-2} of charge is passed for each $2.97 \text{ }\mu\text{m}$ of polymer growth. This deviation from the experimental value obtained, $2.7 \text{ }\mu\text{m}$, was possibly due to the maximum doping level not being achieved. Another reason for the lower experimental mass per unit charge is the formation of dimers or oligomers, which in turn consume the current and, consequently, the charge, but are not involved in the deposition of the polymer to give the corresponding mass increase.⁴⁵

3.2.4 Electrochemical Impedance Spectroscopy (EIS)

EIS is one of the most effective, reliable techniques used to investigate the electrochemical characteristics of an electrochemical system, including double-layer capacitance, diffusion, solution resistance and the determination of the rate of charge transfer processes.⁵⁷ In this section, EIS studies of nanowire and bulk PPy modified electrodes were carried out in 0.20 M solutions of KCl , LiClO_4 and Na_2HPO_4 . All of the impedance measurements were carried out with the applied potential varying from -0.50 V vs. SCE to 0.50 V vs. SCE , with a perturbation signal of 5 mV and a frequency range of 65 kHz to 5 mHz . The potential range was restricted to $\pm 0.50 \text{ V vs. SCE}$ to avoid degradation of the polymer.⁵⁸ Each PPy modified electrode was examined immediately after electropolymerisation and was held at the given potential, prior to the study, for 30 minutes, to ensure a steady state had been reached. The computerised results were plotted and compared with equivalent circuits that model the electrical responses of the system over a range of frequencies. The individual elements of the circuit model represent the electrochemical parameters of the polymer/electrode system.⁵⁹ The influence of different electrolytes on the impedance was also examined.

3.2.4.1 Comparison of Bulk and Nanowire Morphologies of PPy

EIS experiments were carried out on a bare gold electrode, nanowire and bulk PPy, (0.01C), modified electrodes, in aqueous solutions of 0.2 M KCl, LiClO₄ and Na₂HPO₄. In Figure 3.16, Nyquist plots obtained for bare gold, bulk (grown to 0.01 C) and nanowire PPy modified electrodes were compared. The data shown were recorded at open circuit potentials, (O.C.P.), in 0.2 M KCl solutions. The O.C.P.s recorded for the PPy modified surfaces were almost identical at 54 and 58 mV vs. SCE, for the nanowire and bulk morphologies, respectively. The bare Au electrode O.C.P. was slightly higher at 64 mV vs. SCE. Considerable differences in the impedance spectra were observed. The EIS of both PPy modified electrodes, included a semicircle portion observed at the higher frequency range, representing the electron transfer limited process,⁶⁰ and a linear segment at lower frequencies representing the diffusion limited process. The intercept of the semi-circle with the Z' (real) axis in the high frequency region indicated the solution resistance. The diameter of the semi-circular portion is equal to the charge transfer resistance, (R_{CT}), which reflects conductivity. In general R_{CT} is the sum of polymer resistance to electron transport, R_e , and ion transport, R_i .⁶¹ It was obvious that the bare Au electrode exhibited the lowest R_{CT} value and consisted of an almost straight line due to the good conductivity of the bare metal.

The bulk PPy modified electrode had the largest R_{CT} value, indicating that the electron transfer ability of the nanowire modified electrode showed great improvement over that of the bulk PPy modified surface. The nanowire polymer had a region where the slope of the graph was approximately 45°, this is characteristic of ion diffusion in the porous structure of the polymer.⁵⁷ The low frequency response for both polymers was almost a vertical line indicating that the polymers are almost purely capacitive.

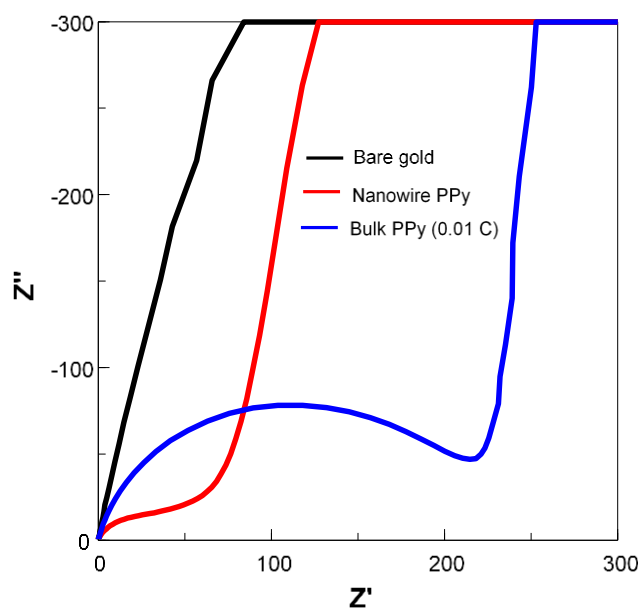


Figure 3.16: Nyquist plot of bare Au, bulk PPy, and PPy nanowires over a frequency range of 5 mHz–65 kHz in 0.2 M KCl, recorded at O.C.P., $n = 4$.

One advantage of EIS is that homogenous and porous surface models can fit the same experimental results.⁵⁷ The resulting impedance data for the bare electrode, bulk and nanowire conformations of the PPy modified electrode, were fitted to the same equivalent circuit shown in Figure 3.17, where R_s represents the solution resistance,⁵⁹ defined as the sum of resistances due to the ohmic resistance of the solution and electrical contacts.⁶² CPE1 is a constant phase element that represents the double layer capacitance of the polymer/electrolyte interphase. A constant phase element is used here to model the capacitive behaviour instead of a capacitor, as the interface between the electrode and the electrolyte solution is not smooth and contains a large number of surface defects.⁶³ Constant phase elements allow for the roughness of the interface⁶⁴ and to the non-ideal behaviour of the polymer films, which is due to inhomogeneity of the conductance or dielectric constant inside the layer.⁶⁵ A constant phase element is defined by two parameters, an actual value (T) and an exponent (P). The CPE-T value gives the physical value of the constant phase element. The CPE-P gives information on the physical process occurring. When CPE-P = 1.0, the constant phase element behaves as an ideal capacitor. However, values between 0.8 and 1.0 are values

consistently obtained for a porous surface, like PPy. A value of 0.5 is indicative of a diffusion process. R_1 (R_{CT}), represents the polymer/ionic resistance and CPE2 is a constant phase element representing the capacitance of the polymer. The parallel combination of polymer resistance, R_1 , and constant phase element, CPE1, accounts for the movement of electrons from the conductive polymer to the metal electrode.⁷

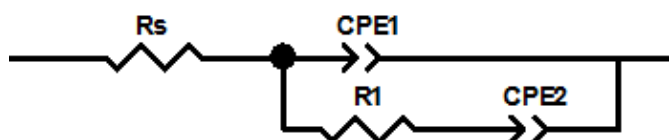


Figure 3.17: Equivalent circuit used to model the electrical parameters of a bare gold electrode, and electrodes modified with nanowire and bulk (0.01C and 300 s) conformations of PPy.

A summary of the data derived from the equivalent circuit fitting is shown in Table 3.5. The electron transfer resistance (R_1) of the bare Au electrode was estimated to be 1395 Ω . After modification with the bulk, cauliflower-like, PPy, the resistance dramatically decreased to 228 Ω . When the bare Au was covered by the PPy nanowire network, the value further decreased to 0.074 Ω . These results suggest that the formation of PPy, especially PPy nanowire network, effectively improved the electron transfer between the solution and electrode.⁶⁶ Generally, the greater surface area, of nanowires, and therefore the larger surface interaction with the electrolyte, leads to a shorter diffusion length for the dopant ions. Both capacitance values, double layer and polymer capacitance, were lower for the nanowire PPy modified electrode.

Table 3.5: Equivalent circuit values for bare gold, nanowire and bulk PPy (0.01 C) modified electrodes at O.C.P. in 0.2 M LiClO₄, $n = 4$.

Surface	CPE1/mF cm ⁻²	R1/ Ω cm ²	CPE2/mF cm ⁻²
Bulk PPy (0.01C)	0.99	228	6.92
Nanowire PPy	0.45	74	3.73
Bare Au	5.30x10 ⁻³	1395	0.27

3.2.4.2 Effect of Applied Potential on PPy Films

Gold electrodes coated with a bulk PPy morphology were prepared as described in Section 3.2.3. Complex plane impedance plots for the bulk PPy, (300 s), at various potentials are shown in Figures 3.18 and 3.19. All impedance results shown were carried out in 0.2 M LiClO₄, over a frequency range of 65 kHz to 5 mHz. The experiments were performed over a range of applied potentials, from -0.50 V to 0.50 V vs. SCE, and at the O.C.P. The O.C.P. value, for bulk PPy, after 30 minutes was 58 mV vs. SCE.

In Figure 3.18, the impedance plots recorded at various negative potentials are shown. The high frequency x-axis, Z' , intercept corresponds to the solution resistance, R_s . Table 3.6 shows all these values to be relatively consistent, as the same electrolyte solution had been employed, although the resistance value increased when the film became reduced at -0.50 V vs. SCE. As the potential was decreased the impedance plot began to shift along the real, x-axis. This indicated that the film's electronic resistance had increased, from 228 to 423 and 558 $\Omega \text{ cm}^2$ at O.C.P., -0.10 and -0.30 V vs. SCE, respectively. These values corresponded with the increase in the semi-circle diameter, as expected.

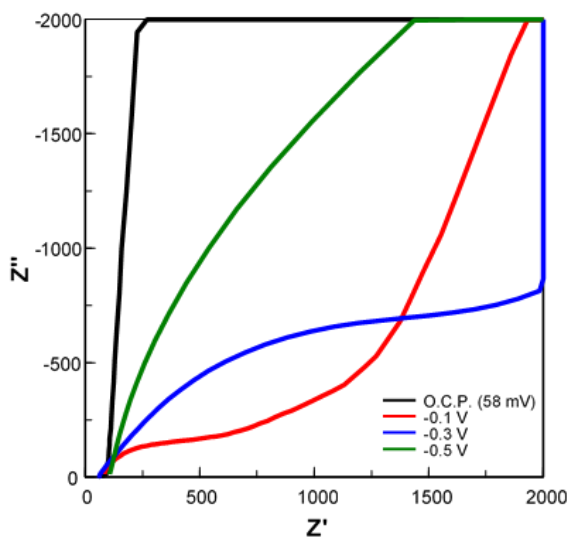


Figure 3.18: Nyquist impedance plots for bulk PPy, grown for 300 s, at various negative potentials in 0.2 M LiClO₄, $n = 4$.

On further reduction of the applied potential, to -0.50 V *vs.* SCE, there was a substantial change in the slope of the low frequency constant phase element. This may be an indication of increased inhomogeneity in the ionic diffusion coefficient in the reduced state, as the slope of a constant phase element is generally related to the porosity of the polymer film.⁶⁴ Ren and Pickup determined that the electronic resistance, R_e , of PPy is generally negligible, and does not, therefore, contribute to the overall R_{CT} of the polymer.⁶⁷ At potentials between O.C.P. and -0.30 V *vs.* SCE, a significant portion of the PPy film was oxidised, however, at -0.50 V *vs.* SCE the polymer was largely reduced and the contribution of R_e to the overall impedance of the polymer became apparent.⁶⁸

In Figure 3.19, the impedance data recorded at O.C.P., 0.10, 0.30 and 0.50 V *vs.* SCE, for the bulk PPy grown for 300 s, are presented. The high frequency semi circles were due to an electron transfer resistance at the electrode/polymer interface. It was evident from these data that the resistance of the bulk PPy film was, in general, lower at these potentials than at the negative potential values in Figure 3.18. The polymer resistance increased as the potential was increased from O.C.P. (58 mV) to 0.50 V *vs.* SCE from 88 to 370 Ω cm^2 , respectively.

Up to, and including, potentials of 0.30 V *vs.* SCE the bulk PPy behaved like a simple capacitor, with negligible resistance, and the Nyquist impedance plot was almost vertical. At an applied potential of 0.50 V *vs.* SCE, the Nyquist plot displayed evidence of the onset of over-oxidation. PPy over-oxidises irreversibly at potentials higher than 0.50 V *vs.* SCE.⁶⁹ This leads to a decrease in its redox activity and electronic conductivity as the β -carbon of pyrrole is oxidised to $\text{C}=\text{O}$.³⁵

These data were fitted to the equivalent circuit presented in Figure 3.17, which consisted of a solution resistance ($R_s \approx 7$ Ω cm^2) at the high frequency intercept. The CPE1 values represented the high frequency capacitance, or double layer capacitance, in parallel with R_1 .

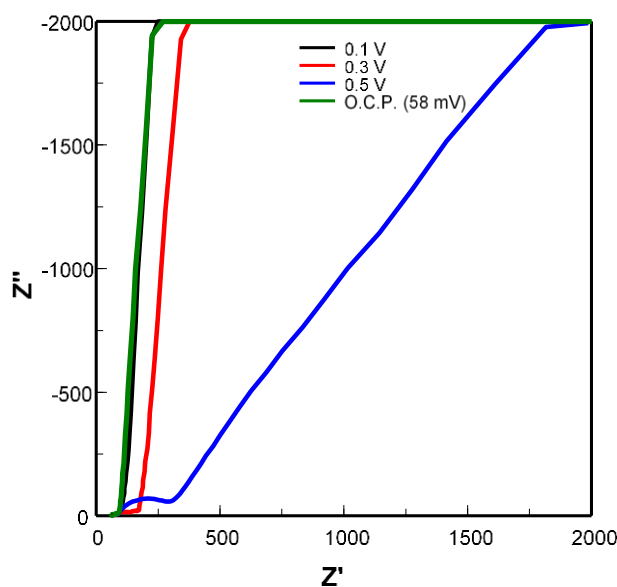


Figure 3.19: Nyquist impedance plots for bulk PPy, grown for 300 s, at various positive potentials in 0.2 M LiClO₄, $n = 4$.

The values relating to the resistance and capacitance values, of the two bulk polymers formed, (0.01 C and 300 s) are presented in Tables 3.6 and 3.7. On examination it was clear that the polymer resistance values followed similar trends, with the thicker polymer displaying slightly higher values, as expected. The polymer capacitance values display similar trends in the negative potential region, with the thicker polymer having lower capacitance. This could be due to a stronger screening effect in the thicker polymer.⁷⁰ There is evidence of some areas of over-oxidation in the thicker polymer from 0.30 V to 0.50 V vs. SCE, as it becomes less capacitive than the thinner PPy. Over-oxidation has been described as the nucleophilic attack of the polymer chains by nucleophilic species when the applied potential is higher than the oxidation potential of the polymer.⁷¹ The thicker polymer was grown for 300 s whereas the thinner polymer took *ca.* 11 s to reach a charge of 0.01C. It was possible, that exposing the surface to an electropolymerisation potential of 0.80 V vs. SCE, for a longer time period, resulted in much of the polymer becoming over-oxidised, hence reducing its ability to store energy. This is due to the fact that PPy has a lower oxidation potential compared to the monomer and indicates that over-oxidation of PPy is unavoidable if polymerisation takes place in the presence of nucleophilic species such as water.⁷¹ The

O.C.P. value for the thinner bulk polymer appears to be an outlier, and does not fit with the other data obtained. It was also observed that the thicker bulk polymer showed evidence of diffusion controlled processes, with CPE-P values closer to 0.50, whereas the thinner bulk polymer had corresponding values between 0.72 and 0.98, the expected values for a capacitive porous material.

Table 3.6: Parameters for the circuit elements evaluated by fitting the impedance data of bulk PPy, (300 s), in 0.2 M LiClO₄, at various potentials.

Potential (V)	R _s (Ω cm ²)	CPE 1-T (μF cm ⁻²)	CPE 1-P	R1 (Ω cm ²)	CPE 2-T (μF cm ⁻²)	CPE 2-P
O.C.P.	6.29	98.7	0.88	88.0	6862	0.75
0.10	5.31	404	0.84	97.8	4418	0.55
-0.10	6.30	274	0.83	422.7	4700	0.72
0.30	5.93	484	0.85	206.2	3546	0.50
-0.30	7.34	180	0.78	558.0	4257	0.60
0.50	8.57	469	0.82	369.6	2573	0.50
-0.50	13.84	427	0.80	119.5	2622	0.50

Table 3.7: Parameters for the circuit elements evaluated by fitting the impedance data of bulk PPy, (0.01 C), in 0.2 M LiClO₄, at various potentials.

Potential (V)	R _s (Ω cm ²)	CPE 1-T (μF cm ⁻²)	CPE 1-P	R1 (Ω cm ²)	CPE 2-T (μF cm ⁻²)	CPE 2-P
O.C.P.	6.67	971	0.72	203.14	6847	0.97
0.10	3.69	1460	0.65	3.69	1100	0.98
-0.10	5.86	587	0.71	112	2640	0.89
0.30	6.23	725	0.71	7.41	4280	0.95
-0.30	7.56	240	0.67	325	2620	0.78
0.50	5.68	297	0.91	144.5	4260	0.72
-0.50	11.21	104	0.74	272	20.6	0.72

Nanowire PPy modified gold electrodes were prepared as described in Section 3.2.2.3. Complex plane impedance plots for the resulting film, at various potentials, are shown in Figures 3.20 and 3.21. All impedance results shown were carried out in 0.2 M LiClO₄, over a frequency range of 65 kHz to 5 mHz. The experiments were carried out

over a range of applied potentials, from -0.50 V to 0.50 V *vs.* SCE, and at the O.C.P. (54 mV *vs.* SCE).

Figure 3.20 shows the impedance plots for nanowire PPy at various positive potentials, from O.C.P. to 0.50 V *vs.* SCE. It was clearly shown that the solution resistances were similar, with all high frequency x-axis intercepts located in the same region. As the applied potential was increased the corresponding Nyquist plot shifted along the x-axis, with broader semi-circular diameters, indicating increased polymer resistance. When compared to the Nyquist plot for the bulk (300 s) polymer in Figure 3.19, there was no evidence that the nanowire polymer had become over-oxidised at 0.50 V *vs.* SCE, indicating a more stable polymer was formed. It is well reported that the oxidation and reduction of PPy results from the insertion and removal of the dopant ions into the polymer backbone. This causes the polymer to swell and contract continuously. PPy nanowires are more able to withstand the strain caused by the constant swelling and contraction of the polymer, resulting in a more stable film.⁷²

In Figure 3.21, the impedance plots recorded at various negative potentials for the nanowire PPy are shown. Here, all the solution resistances were similar, as the same electrolytes were used. As the potential was decreased, the impedance plot generally shifted along the x-axis, similar to the corresponding plot in Figure 3.18 for the bulk polymer, indicating an increase in the polymer resistance, from O.C.P. to a potential of -0.30 V *vs.* SCE. These values corresponded to the increase in the semi-circle diameter, as expected. Further reducing the applied potential to -0.50 V *vs.* SCE, resulted in a change in the slope of the low frequency C.P.E, due to the reduction of the PPy film,⁶⁸ similar to the bulk PPy. The electronic parameters for the nanowire PPy were fit to the equivalent circuit shown in Figure 3.17.

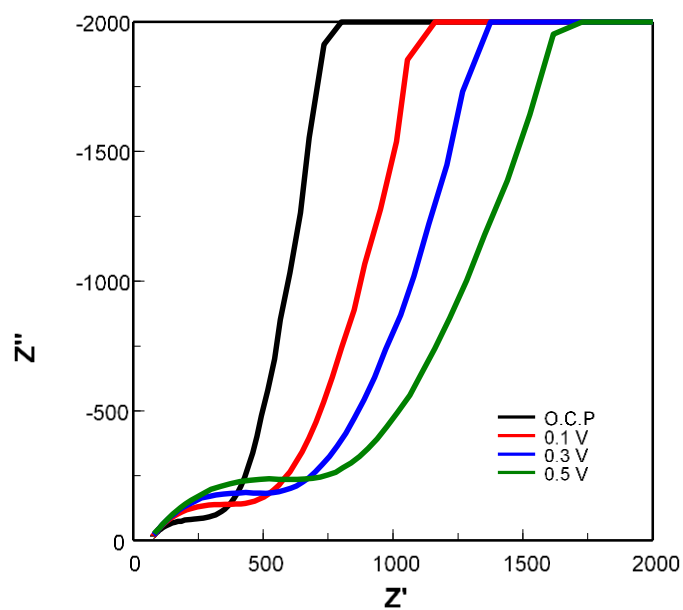


Figure 3.20: Nyquist impedance plots for nanowire PPy, at various positive potentials in 0.2 M LiClO₄, $n = 4$.

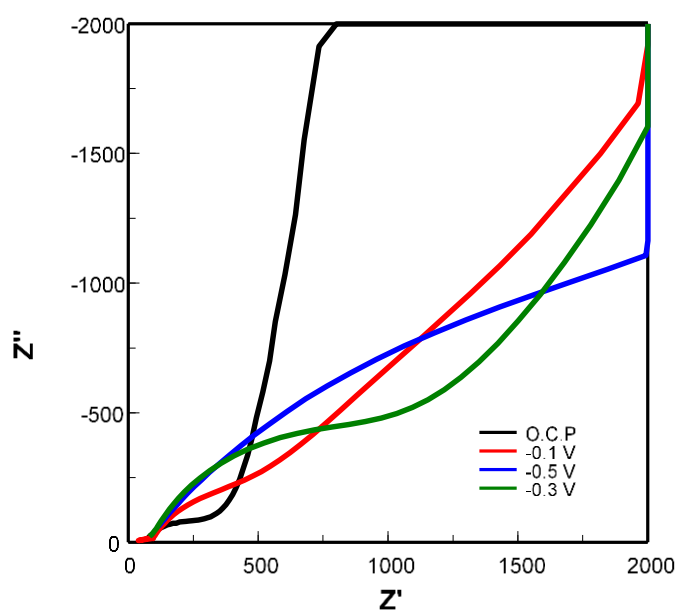


Figure 3.21: Nyquist impedance plots for nanowire PPy, at various negative potentials in 0.2 M LiClO₄, $n = 4$.

The resulting data, relating to the resistance and capacitance values, of the nanowire film are presented in Table 3.8. When compared with the thinner bulk data in Table 3.7, the double layer capacitance values, (CPE1), were larger for the bulk polymer, indicating a thicker layer had formed when depositing the bulk PPy onto the electrode. Overall, the polymer capacitance values were lower for the nanowire morphology of PPy, suggesting a lower electroactive surface area had formed on polymerisation. As a result, a poorly conducting nanowire polymer would have higher resistance values, which was evident from the results shown. This was possibly due to the pH of the electrolyte used for deposition. In general, to polymerise pyrrole, a solution pH that is slightly acidic is required.³⁴ However, to obtain the nanowire conformation, the electrolyte solution used had an alkaline¹⁶ pH of 9.2. In such alkaline conditions, reduced doping of the polymer backbone was likely, forming a less conducting polymer not capable of storing large amounts of charge. It is also possible that the nanowire modified electrodes were not sufficiently rinsed prior to running the EIS experiments, leaving excess alkaline solution on the functionalised surface, which could alter the pH of the electrolyte solution used for EIS studies. The effect of electrolyte solution pH on EIS will be examined in Section 3.2.4.3. The fragility of the nanowires formed from a relatively low concentration of monomer may also have resulted in the poor performance of the PPy nanowires in this section. This will be investigated in Section 3.2.4.4. The exponent, CPE-P, values for the nanowire polymer capacitance are similar to those obtained for the thinner bulk polymer, which are typical of porous materials, like PPy.

Table 3.8: Parameters for the circuit elements evaluated by fitting the impedance data of nanowire PPy, in 0.2 M LiClO₄, at various potentials.

Potential (V)	Rs ($\Omega \text{ cm}^2$)	CPE 1-T ($\mu\text{F cm}^{-2}$)	CPE 1-P	R1 ($\Omega \text{ cm}^2$)	CPE2 ($\mu\text{F cm}^{-2}$)	CPE 2-P
O.C.P.	72.5	398.7	0.58	76	6860	0.80
0.10	64.9	28.3	0.78	359	141.8	0.86
-0.10	57.4	14.0	0.72	542	38.9	0.92
0.30	73.2	19.9	0.68	589	127.2	0.86
-0.30	81.6	32.5	0.70	466	18.7	0.88
0.50	61.2	16.3	0.62	771	104.8	0.86
-0.50	106.1	7.6	0.56	239	11.0	0.72

3.2.4.3 Effect of Electrolyte on Impedance

In this section the effect of the nature of the electrolyte solution on the electrical parameters of bulk PPy modified electrodes was examined. The bulk polymer was electrodeposited onto gold substrates from aqueous solutions containing 75 mM pyrrole, 0.2 M Na₂HPO₄ and 2 mM LiClO₄, (pH adjusted to 5.5 with HClO₄), at 0.80 V vs. SCE, for 300 s. EIS studies were carried out on the modified electrodes in 0.2 M solutions of KCl, LiClO₄ and Na₂HPO₄ at an applied potential of 0.10 V vs. SCE over a frequency range from 65 kHz to 5 mHz. The resulting Nyquist plots are shown in Figure 3.22. The high frequency x-axis intercept, reflecting the solution resistance, R_s, increased with the increasing ionic strength of the three different electrolytes used, in the order, KCl < LiClO₄ < Na₂HPO₄. The electronic parameters for the impedance graphs were fitted to the equivalent circuit shown in Figure 3.17.

Table 3.9 shows the impedance of bulk PPy modified electrodes, recorded in KCl, LiClO₄, Na₂HPO₄ electrolyte solutions. The pH of these solutions ranged from 6.0 to 9.3. The data displayed a range of electrical behaviours. Similar double layer (5.6 and 0.6 μF cm⁻²) and polymer capacitances (67 and 51 mF cm⁻²) were obtained in the KCl (pH 6.1) and LiClO₄ (pH 6.0) solutions, respectively. The alkaline Na₂HPO₄ electrolyte, (pH 9.3), resulted in lower double layer and polymer capacitance values, 9.3x10⁻² μF cm⁻² and 1.2 mF cm⁻², respectively, indicating that the polymer stores less charge in an alkaline solution. This was likely due to OH⁻ ions in the alkaline solution interfering with the dopant ions, thereby reducing the conductivity and increasing the resistance of the film. This theory was examined by changing the pH of the KCl and LiClO₄ electrolyte solutions to that of Na₂HPO₄. As a result, similar capacitance values were observed on changing the pH, indicating the significant role of the pH of the solution, i.e., the addition of OH⁻ ions interfering with the dopant levels on the polymer backbone.

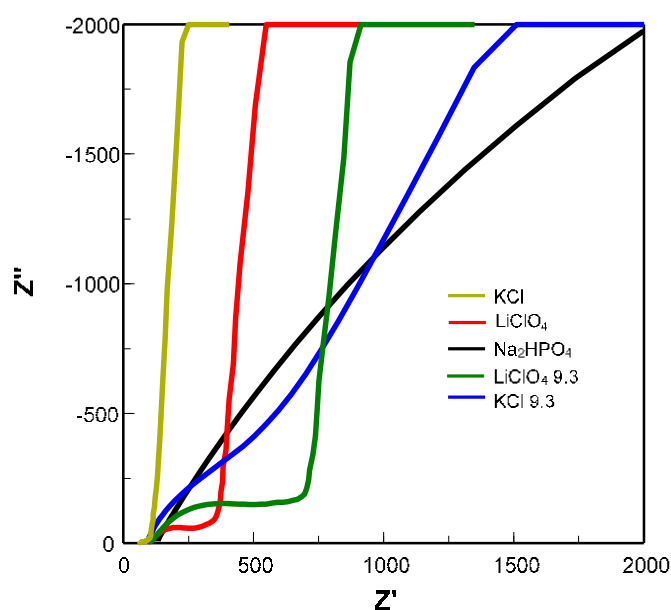


Figure 3.22: Nyquist impedance plots for bulk PPy, recorded at 0.1 V vs. SCE in 0.2 M solutions of various electrolytes, $n = 4$.

Table 3.9: Parameters for the circuit elements evaluated by fitting the impedance data for bulk PPy, recorded at 0.1 V vs. SCE in 0.2 M solutions of various electrolytes, $n = 4$.

Electrolyte	pH	CPE1 ($\mu\text{F cm}^{-2}$)	R1 ($\Omega \text{ cm}^2$)	CPE2 (mF cm^{-2})
KCl	6.1	5.6	3	67
LiClO ₄	6.0	0.6	101	51
Na ₂ HPO ₄	9.3	9.3×10^{-2}	318	1.2
KCl	9.3	6.1×10^{-2}	66	0.3
LiClO ₄	9.3	5.2×10^{-2}	177	5.4

3.2.4.4 PPy Biocompatibility

PPy is one of the most widely researched conducting polymers. One of the main advantages is its biocompatibility,^{4,5} although many of these studies were carried out *in-vitro*.⁷³ These included studies showing that PPy supported the adhesion of various kinds of cells, such as neuronal, endothelial and skeletal muscle cells.⁷⁴ To further evaluate the biocompatibility of PPy, Wang *et al* tested the suitability of PPy with nerve tissue *in-vitro* and *in-vivo*.⁷⁵ They demonstrated that the presence of PPy/biodegradable composites caused no abnormal tissue response. Other studies

concluded that PPy particles did not cause any cytotoxic effects to mouse peritoneum cells.⁷⁶ To my knowledge, no reports pertain to the stability of nanowire morphologies of PPy *in-vivo*. Bechara *et al* have coated nanostructures with PPy for stem cell research, but this study involved bulk PPy and was carried out *in-vitro*.⁷⁷ Fonner *et al* observed that although PPy doped with smaller ions had a high surface roughness it also de-doped rapidly, possibly leeching into surrounding tissue.⁷⁸ In contrast to other reports, Jiang *et al* confirmed that PPy coated fabrics caused some localised inflammation. They also recorded that thicker or clustered areas of PPy were damaged on implantation,⁷⁹ acknowledging the importance of achieving a thin, uniform PPy coating. In some reports, PPy was found to result in a brittle amorphous material.⁸⁰ Throughout the work carried out in this chapter, several SEM micrographs were recorded showing damaged PPy nanowire surfaces, casting doubt on the strength of the nanowires formed from a low monomer concentration (75 mM). Figure 3.23 shows some of the resulting images.

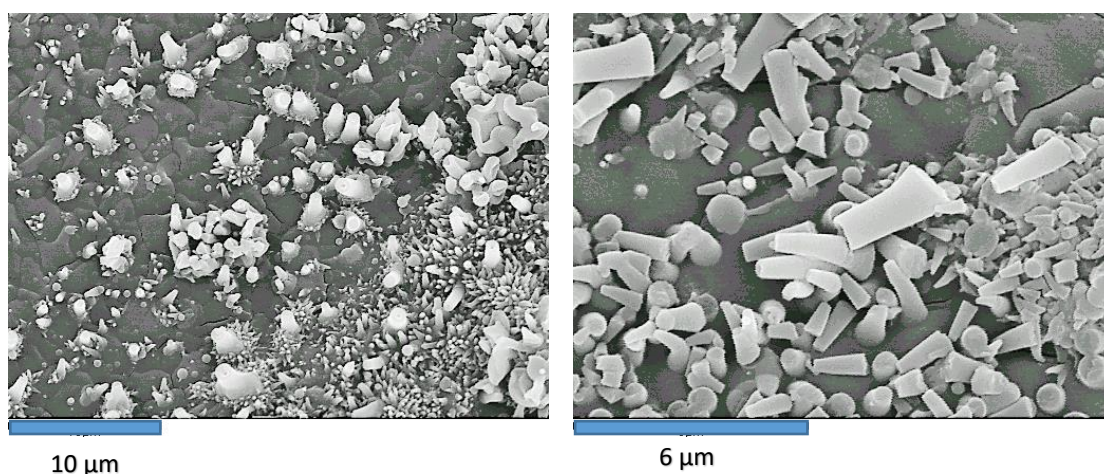


Figure 3.23: SEM micrographs showing damaged PPy nanowires resulting from an electropolymerisation solution containing 75 mM pyrrole.

3.3 Conclusion

The aim of this chapter was to compare the electrochemical properties of bulk and nanowire conformations of PPy. This would determine the ability to further modify the polymer with sensing agents, e.g., copper structures used for sensing the nitrate

ion. Sections 3.2.1 and 3.2.2 discussed the different morphologies of PPy electrografted onto gold electrodes. Two conformations, nanowire and bulk, were prepared using the same conditions, but reducing the electrolyte pH for the bulk polymer. In order to obtain a nanowire covering of the gold substrate the electrolyte solution needed to be slightly alkaline/alkaline in nature before the onset of polymerisation, the excess OH⁻ ions causing the slow growth conditions necessary to achieve the nanowire film, by mopping up excess H⁺ ions released during the electropolymerisation process.

The effect of dopant ions (ClO₄⁻) was examined, revealing that the larger cation, Na⁺, resulted in significantly thicker wires, ($\varnothing = 115.20$ nm), than Li⁺ ($\varnothing = 103.40$ nm), $P = 0.0016$. Longer PPy wires grown from aqueous solutions often display lower conductivities due to carbonyl defects interfering with the conjugation on the polymer backbone. To reduce these defects, the nanowires were grown from a lower pyrrole concentration. FT-IR spectra confirmed that most of the carbonyl defects had been removed. This would enable the formation of shorter more conducting wires.

Bulk polymers required the electrolyte pH to be slightly acidic in nature. The subsequent release of H⁺ ions on polymerisation led to a faster growth rate leading to a bulk conformation. The CVs of the two polymers, nanowire and bulk, revealed that the bulk PPy, when deposited for 300 s, had far superior capacitance and surface area than its nanowire counterpart. The surface areas of both polymers were estimated, and found to be 0.14 cm² for the nanowires and 0.73 cm² for the bulk PPy.

Section 3.2.3 discussed the preparation of bulk and nanowire conformations of electrodeposited PPy with similar surface areas. It was found that a nanowire morphology grown for 300 s, had a similar area to a bulk polymer grown to a charge of 0.01 C. CV confirmed the similar surface areas of the polymers, both displaying quasi-reversible electrode kinetics that is typical of PPy films. However, the nanowire modified electrode had a smaller ΔE value, and the location of the redox peaks indicated the facilitation of the oxidation and reduction reactions. This was indicative of enhanced electrochemical properties of the nanowire PPy.

A study of the thickness of the bulk PPy films formed from various electrodeposition times was carried out, by recording the charge consumed during electropolymerisation.

Polymer thickness measurements were recorded from SEM micrographs, and plotted against the charge density, $C\text{ cm}^{-2}$. The film thickness was experimentally found to be directly proportional to the charge consumed during polymerisation, each $C\text{ cm}^{-2}$ forming $2.7\text{ }\mu\text{m}$ of PPy. This was in good agreement with the literature value of $2.5\text{ }\mu\text{m}/C\text{ cm}^{-2}$. A mathematical equation was also used to evaluate the amount of polymer deposited per unit charge. This resulted in a polymer thickness formed of $2.97\text{ }\mu\text{m}/C\text{ cm}^{-2}$. Discrepancies between the experimental value and the literature and theoretical values were explained by the different dopant anion and the level of doping within the polymer backbone.

Section 3.2.4 of this chapter examined the electrical properties, of bulk and nanowire conformations of electrochemically deposited PPy, formed in Sections 3.2.2 and 3.2.3, by EIS. Studies carried out in Section 3.2.4.1 compared bare gold electrodes with those modified with nanowire and bulk morphologies of PPy. The Nyquist plots revealed considerable differences in the resulting impedance spectra. The results were fitted to the same equivalent circuit, enabling easy comparison of the electrical properties. The reduction of the polymer resistance, due to the modification with PPy, especially the nanowire network, showed the improvement in the electronic properties. Both nanowire and bulk films displayed almost purely capacitive behaviour, as indicated by the low frequency response being an almost vertical line.

The effect of the applied potential on the impedance spectra was discussed in Section 3.2.4.2. Three different polymers were examined, nanowires, bulk PPy grown for 300 s and bulk PPy grown to a charge of 0.01 C . The shape of the impedance Nyquist plots changed substantially with the negative shift in potential, indicating that the electrochemical properties of PPy films varied as a function of the applied potential, with the polymer changing from an oxidised to reduced state, over the potentials applied. The bulk polymer, grown for 300 s, displayed characteristics of over-oxidation that were not evident in the nanowire film.

Section 3.2.4.3 examined the effect of the electrolyte on the impedance characteristics of a bulk PPy grown for 300 s. Similar double layer and polymer capacitances were obtained in the solutions with similar pH, KCl (pH = 6.1) and LiClO_4 (pH = 6.0). The alkaline Na_2HPO_4 (pH 9.3) resulted in lower capacitance values, indicating that the polymer stored less charge in the alkaline solution. Similar capacitance values were

observed on changing the pH of the KCl and LiClO₄ solutions to that of Na₂HPO₄, indicating the significant role of the pH of the electrolyte solution.

In Section 3.2.4.4 the biocompatibility of PPy films and the stability of nanowire conformations were reviewed. Many reviewers reported PPy as a biocompatible matrix, however, many of these studies were carried out *in-vitro*. *In-vivo* studies support PPy as a biocompatible material, but the conditions of growth are important as smaller dopant ions may leech into surrounding tissue. The suitability of nanowire PPy for *in-vivo* studies was questioned as many samples produced in this thesis resulted in damaged surfaces.

In conclusion, bulk and nanowire conformations of PPy were successfully electrodeposited onto the gold substrate. The nanowire CV showed a more reversible system than the bulk material, indicating more efficient electrical properties. EIS again showed the better properties of nanowires with lower polymer resistance observed.

3.4 References

1. S. Carquigny, O. Segut, B. Lakard, F. Lallemand and P. Fievet, *Synthetic Metals*, 2008, **158**, 453-461.
2. U. Johanson, M. Marandi, T. Tamm and J. Tamm, *Electrochimica Acta*, 2005, **50**, 1523-1528.
3. P. M. Dziewoński and M. Grzeszczuk, *The Journal of Physical Chemistry B*, 2010, **114**, 7158-7171.
4. P. M. George, A. W. Lyckman, D. A. LaVan, A. Hegde, Y. Leung, R. Avasare, C. Testa, P. M. Alexander, R. Langer and M. Sur, *Biomaterials*, 2005, **26**, 3511-3519.
5. S. Geetha, C. R. K. Rao, M. Vijayan and D. C. Trivedi, *Analytica Chimica Acta*, 2006, **568**, 119-125.
6. J. Wang and M. Musameh, *Analytica Chimica Acta*, 2005, **539**, 209-213.
7. K. Ghanbari, S. Z. Bathaie and M. F. Mousavi, *Biosensors and Bioelectronics*, 2008, **23**, 1825-1831.
8. J. H. Collier, J. P. Camp, T. W. Hudson and C. E. Schmidt, *Journal of Biomedical Materials Research*, 2000, **50**, 574-584.
9. M. Martina and D. W. Hutmacher, *Polymer International*, 2007, **56**, 145-157.
10. R. Zhu, G. Li and G. Huang, *Materials and Corrosion*, 2009, **60**, 34-39.
11. M. D. Ingram, H. Staesche and K. S. Ryder, *Solid State Ionics*, 2004, **169**, 51-57.
12. A. Ramanavicius, A. Ramanaviciene and A. Malinauskas, *Electrochimica Acta*, 2006, **51**, 6025-6037.
13. J. Hegewald, L. Jakisch and J. Pionteck, *Synthetic Metals*, 2009, **159**, 103-112.
14. S. Demoustier-Champagne and P.-Y. Stavaux, *Chemistry of Materials*, 1999, **11**, 829-834.
15. C.-C. Hu and X.-X. Lin, *Journal of the Electrochemical Society*, 2002, **149**, A1049-A1057.
16. C. Debiemme-Chouvy, *Electrochemical Communications*, 2009, **11**, 298-301.
17. N. K. Guimard, N. Gomez and C. E. Schmidt, *Progress in Polymer Science*, 2007, **32**, 876-921.
18. S. Shimoda and E. Smela, *Electrochimica Acta*, 1998, **44**, 219-238.
19. J. Wang, X. Mo, D. Ge, Y. Tian, Z. Wang and S. Wang, *Synthetic Metals*, 2006, **156**, 514-518.
20. F.-L. Cheng, M.-L. Zhang and H. Wang, *Sensors*, 2005, **5**, 245-249.

21. Y.-Z. Long, M.-M. Li, C. Gu, M. Wan, J.-L. Duvail, Z. Liu and Z. Fan, *Progress in Polymer Science*, 2011, **36**, 1415-1442.
22. M. Zhou and J. Heinze, *Journal of Physical Chemistry B*, 1999, **103**, 8443-8450.
23. L. Al-Mashat, C. Debiemme-Chouvy, S. Borensztajn and W. Wlodarski, *Journal of Physical Chemistry C*, 2012, **116**, 13388-13394.
24. M. P. Massafra and d. T. S. I. Cordoba, *Journal of Electroanalytical Chemistry*, 2012, **669**, 90-94.
25. M. S. Milan Paunovic, *Fundamentals of Electrochemical Deposition*, Wiley, 2006, p. 52.
26. D. Ge, J. Wang, Z. Wang and S. Wang, *Synthetic Metals*, 2002, **132**, 93-95.
27. Y. Li and R. Qian, *Electrochimica Acta*, 2000, **45**, 1727-1731.
28. S. Sadki, S. Philippe, N. Brodie and G. Sabouraud, *Chemical Society Reviews*, 2000, **29**, 283-293.
29. C. Jin, F. Yang and W. Yang, *Journal of Applied Polymer Science*, 2006, **101**, 2518-2522.
30. U. Paramo-Garcia, J. G. Ibanez and N. Batina, *International Journal of Electrochemical Science*, 2011, **6**, 5172-5188.
31. W. K. Lee, Y. M. Song, J. M. Ha, H. Park, I. W. Lee, H. H. Chun and N. J. Jo, *Materials Research Innovations*, 2009, **13**, 235-238.
32. C. P. McCarthy, PhD, NUIM, 2013.
33. X.-l. Zhang, J.-x. Wang, Z. Wang and S.-c. Wang, *Sensors*, 2005, **5**, 580-593.
34. M. Zhou and J. Heinze, *Journal of Physical Chemistry B*, 1999, **103**, 8443-8450.
35. H. Ge, G. Qi, E. T. Kang and K. G. Neoh, *Polymer*, 1994, **35**, 504-508.
36. F. Miomandre, J. Saba, K. Wojcik and J. Bai, *Journal of Solid State Electrochemistry*, 2015, **19**, 2691-2699.
37. C. Jerome and R. Jerome, *Angewandte Chemie International Edition*, 1998, **37**, 2488-2490.
38. S. Asavapiriyant, G. K. Chandler, G. A. Gunawardena and D. Pletcher, *Journal of Electroanalytical Chemistry Interfacial Electrochemistry*, 1984, **177**, 229-244.
39. C. P. McCarthy, N. B. McGuinness, B. E. Alcock-Earley, C. B. Breslin and A. D. Rooney, *Electrochemical Communications*, 2012, **20**, 79-82.
40. X. Zhang, J. Zhang, W. Song and Z. Liu, *Journal of Physical Chemistry B*, 2006, **110**, 1158-1165.

41. C. K. Baker and J. R. Reynolds, *Journal of Electroanalytical Chemistry Interfacial Electrochemistry*, 1988, **251**, 307-322.
42. D. A. Reece, S. F. Ralph and G. G. Wallace, *Journal of Membrane Science*, 2005, **249**, 9-20.
43. S. B. Saidman and O. V. Quinzani, *Electrochimica Acta*, 2004, **50**, 127-134.
44. R. Ansari Khalkhali, *Journal of Electrochemistry*, 2005, **41**, 950-955.
45. G. Hendy, NUIM, 2009.
46. D. Salinas-Torres, F. Montilla, F. Huerta and E. Morallon, *Electrochimica Acta*, 2011, **56**, 3620-3625.
47. K. K. I. Svancara, A. Walcarius and K. Vytras, *Electroanalysis with Carbon Paste Electrodes*, CRC Press, 2012.
48. A. Morrin, A. J. Killard and M. R. Smyth, *Analytical Letters*, 2003, **36**, 2021-2039.
49. R. C. Fox, L. T. Nguyen, L. R. Henshaw and L. Yu, *ECS Electrochemistry Letters*, 2013, **2**, H40-H42.
50. A. C. Fisher, *Electrode Dynamics*, Oxford University Press, Oxford, 1996.
51. S. M. Ebrahim, L. M. M. Abd-El, A. M. Gad and M. M. Soliman, *Thin Solid Films*, 2010, **518**, 4100-4105.
52. T. Silk, Q. Hong, J. Tamm and R. G. Compton, *Synthetic Metals*, 1998, **93**, 59-64.
53. J. M. Fonner, C. E. Schmidt and P. Ren, *Polymer*, 2010, **51**, 4985-4993.
54. A. F. Diaz, J. I. Castillo, J. A. Logan and W. Y. Lee, *Journal of Electroanalytical Chemistry and Interfacial Electrochemistry*, 1981, **129**, 115-132.
55. J. H. Kaufman, K. K. Kanazawa and G. B. Street, *Physical Review Letters*, 1984, **53**, 2461-2464.
56. G. Maia, R. M. Torresi, E. A. Ticianelli and F. C. Nart, *Journal of Physical Chemistry*, 1996, **100**, 15910-15916.
57. M. Ates, *Progress in Organic Coatings*, 2011, **71**, 1-10.
58. G. Li and P. G. Pickup, *Journal of Physical Chemistry B*, 1999, **103**, 10143-10148.
59. P. Ferloni, M. Mastragostino and L. Meneghello, *Electrochimica Acta*, 1996, **41**, 27-33.
60. F. Meng, W. Shi, Y. Sun, X. Zhu, G. Wu, C. Ruan, X. Liu and D. Ge, *Biosensors and Bioelectronics*, 2013, **42**, 141-147.
61. X. Ren and P. G. Pickup, *Journal of Physical Chemistry*, 1993, **97**, 5356-5362.

62. F. Z. E. Sagirli, E. S. Kayali and A. S. Sarac, *Journal of the Electrochemical Society*, 2016, **163**, H205-H212.
63. F. J. Iftikhar, P. G. L. Baker, A. M. Baleg, P. M. Ndongili, S. N. Mailu and E. I. Iwuoha, *Electrochimica Acta*, 2011, **56**, 5214-5221.
64. M. R. Warren and J. D. Madden, *Synthetic Metals*, 2006, **156**, 724-730.
65. C. Pirvu, C. C. Manole, A. B. Stoian and I. Demetrescu, *Electrochimica Acta*, 2011, **56**, 9893-9903.
66. X. Ru, W. Shi, X. Huang, X. Cui, B. Ren and D. Ge, *Electrochimica Acta*, 2011, **56**, 9887-9892.
67. X. Ren and P. G. Pickup, *Journal of Physical Chemistry*, 1993, **97**, 3941-3943.
68. X. Ren and P. G. Pickup, *Journal of Electroanalytical Chemistry*, 1997, **420**, 251-257.
69. S. Ghosh, G. A. Bowmaker, R. P. Cooney and J. M. Seakins, *Synthetic Metals*, 1998, **95**, 63-67.
70. A. Hallik, A. Alumaa, J. Tamm, V. Sammelselg, M. Vaeærtou, A. Jaenes and E. Lust, *Synthetic Metals*, 2006, **156**, 488-494.
71. B. R. Saunders, R. J. Fleming and K. S. Murray, *Chemistry of Materials*, 1995, **7**, 1082-1094.
72. J. Huang, K. Wang and Z. Wei, *Journal of Materials Chemistry*, 2010, **20**, 1117-1121.
73. J. Upadhyay, A. Kumar, B. Gogoi and A. K. Buragohain, *Synthetic Metals*, 2014, **189**, 119-125.
74. A. Vaitkuvienė, V. Ratautaite, L. Mikoliūnaite, V. Kasetė, G. Ramanauskaite, G. Biziuleviciene, A. Ramanaviciene and A. Ramanavicius, *Colloids and Surfaces, A*, 2014, **442**, 152-156.
75. X. Wang, X. Gu, C. Yuan, S. Chen, P. Zhang, T. Zhang, J. Yao, F. Chen and G. Chen, *Journal of Biomedical Materials Research, Part A*, 2004, **68A**, 411-422.
76. A. Ramanaviciene, A. Kausaite, S. Tautkus and A. Ramanavicius, *Journal of Pharmacy and Pharmacology*, 2007, **59**, 311-315.
77. S. Bechara, L. Wadman and K. C. Popat, *Acta Biomaterials*, 2011, **7**, 2892-2901.
78. J. M. Fonner, L. Forciniti, H. Nguyen, J. D. Byrne, Y.-F. Kou, J. Syeda-Nawaz and C. E. Schmidt, *Biomedical Materials*, 2008, **3**, 034124.
79. Y. M. Xiaoping Jiang, Amidou Traoré, Dominic Tessier, Lê H. Dao, Robert Guidoin, and Ze Zhang, *Tissue Engineering*, 2004, **8**, 635-647.
80. A. I. Nazzal, G. B. Street and K. J. Wynne, *Molecular Crystals and Liquid Crystals*, 1985, **125**, 303-307.

Chapter 4

CPE: Optimisation of Electrochemical Reduction of 4-Benzoylamino-2, 5- dimethoxybenzenediazonium chloride hemi zinc chloride salt (FBRR)

4.1 Introduction

In this chapter the electrochemical deposition of FBRR in the presence of organic and aqueous solvents onto carbon paste electrodes (CPEs) is discussed. This was achieved by a one-step electrochemical deposition process using either LSV or CV techniques. The modified electrode characteristics and redox properties were subsequently analysed using CV. Surface analysis techniques of SEM and EDX were employed to confirm the modification of the substrate.

The evolution of various carbon surfaces has allowed the development of electrodes with advantages in catalytic, analytical and biological applications, e.g., electrocatalysts for the electrochemical reduction of oxygen.¹ Adaptations to carbon surfaces include the electrochemical covalent bonding of moieties to the substrate, for example, the electro-reduction of diazonium salts² and the development of CPEs.³ These advancements have enabled the development of electrodes for pH monitoring that have distinct advantages compared to other common methods used for the determination of solution pH,⁴ including their strength, reproducibility and low cost.

CPEs, were first introduced in 1958 by Ralph Norman Adams⁵ and have, since then, been widely used in analytical chemistry, notably in voltammetry.⁶ Carbon paste is prepared by mixing powdered graphite with a lipophilic, organic, liquid binding agent, e.g., silicone oil, forming a heterogeneous surface of carbon particles embedded in a pasting liquid. The resulting electrodes contain electrically conductive particles dispersed in an insulating binder.⁷ The purpose of the binder is to hold the particles together. Despite the presence of the non-conducting binder carbon pastes generally have a low ohmic resistance,^{8,9} this can be explained by the tight arrangement of the spherical particles within the paste.¹⁰ The active surface of a CPE is partially or completely covered by a thin film of the binding liquid. This causes the surface of a CPE to be, in general, lipophilic and therefore hydrophobic.¹¹ The hydrophobicity of a CPE is of great importance as it affects the character of the electrode and the electron processes that occur at its surface.¹²

The structure of a CPE depends on the properties of its main constituents.¹³ The binding liquid should be chemically inert, electrochemically inactive, of high viscosity and low volatility, minimally soluble in aqueous solvents and immiscible with organic

solvents.¹¹ Roughness varies in each individually prepared electrode, so each CPE has its own unique surface which leads to the fact that the surface area does not correspond to the geometrical area.³ The electroactive surface area depends on the graphite/binder ratio, smoothing methods and whether or not the electrodes have been pre-treated.¹⁴ The carbon/binder ratio used in this thesis was 0.71 g graphite: 250 μ l silicone oil.

4-Benzoylamino-2, 5-dimethoxybenzenediazonium chloride hemi zinc chloride salt also known as Fast Blue RR, FBRR, is a quinone containing (aryl) diazonium salt. Quinones have shown strong adsorption onto various surfaces including platinum, graphite and glassy carbon.¹⁵ They are attached by using diazonium attachment chemistry onto the required surface. The first reported reduction of an aryl diazonium salt onto carbon was in 1992 by Saveant et al.¹⁶ The electrochemical reduction of diazonium salts leads to a solid covalent attachment of aryl groups onto the substrate surface and generally results in a layered deposition of the product onto the substrate, not monolayers.¹⁷ These layers can vary in thickness from a few nm to several μ m.¹⁸ The layers are formed when the radical attaches to the first layer of deposited salt. This happens when the radical attacks the ortho-position^{2, 19} of an already surface bound aryl group, leading to the formation of multilayers.²⁰ The reduction of FBRR can be carried out in an aprotic solvent, e.g., 0.1 M TEABF₄ in ACN,²¹ or an aqueous solvent, e.g., 0.1 M H₂SO₄.²² Diazonium salts are stable in aqueous acidic solutions, but although their stability decreases as the pH increases above pH 2–3,²³ they have been reported as stable in acetonitrile.²⁰

The redox process involves changes in the protonation state between the quinone and the hydroquinone moieties meaning that potential values vary with pH in a Nernstian fashion.^{24, 25} Several quinone modified electrodes have been reported to respond to pH^{26, 27} but few have been developed on biocompatible materials that exhibit activity in a physiologically relevant pH range.²⁸

4.2 Results and Discussion

In this section the full characterisation of FBRR/CPEs for usage as voltammetric pH sensors was performed. FBRR was electrodeposited onto the prepared CPEs using the

electrochemical techniques of CV and LSV using both organic and acidic supporting electrolytes. All of the deposition parameters were examined along with the cycling conditions of modified CPEs in order to optimise the anodic and cathodic peaks obtained. The stability of the peak potentials were then investigated. Storage conditions for the solutions, bare and modified CPEs were reviewed. Finally the pH responses of the FBRR/CPEs were analysed.

4.2.1 Carbon Paste Electrodes

CPEs can usually be polarised up to between 1.0 V and 1.4 V vs. SCE¹⁰. This can be affected by the solvent medium. An increase in alkalinity will lead to a decrease in the positive potential limit⁵. Background currents are normally in the nA range and would seldom exceed 1 μ A.³ The background CV for a bare CPE in N₂ saturated PBS is shown in Figure 4.1. A background current level is described as the “mean current recorded in a blank electrolyte within the potential range of interest”.⁹ The currents are caused by several factors including, adsorbed oxygen in the paste and oxygen containing groups on the surfaces of the carbon particles.³ The electron transfer kinetics for CPEs is reduced due to the presence of the non-conducting binding oil. The less binding fluid included in the paste mixture results in higher background currents, i.e., less liquid content leads to a more rapid charge transfer at the electrode surface.¹¹

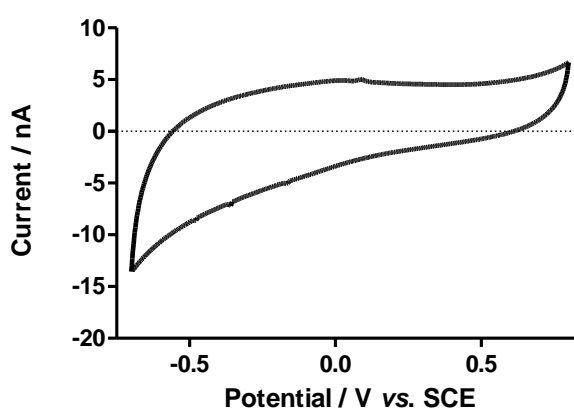


Figure 4.1: Average background CV of CPEs in N₂ saturated PBS pH 7.4, $n = 16$.

Over time the currents increased with cycling. Figure 4.2 shows a bare CPE cycled in PBS from -0.70 to 0.80 V vs. SCE at 100 mV/s for 400 cycles. This number of cycles was chosen due to the end application of the sensor being cycled in tissue for *ca.* 10-12 hours, so cycling for 400 cycles (3.5 hours) would give a good indication of how the sensor would perform. Wetting of the electrode surface has been reported to cause an initial increase in activity, especially over the first 2 minutes of cycling.²⁹ After this the gradual increase in currents obtained is possibly due to the binding oil leeching from the electrode²⁹ and less binding fluid results in increased conductivity¹¹. It could also be caused by the surface contracting, and therefore increasing in area, due to the leeching of the silicone oil.

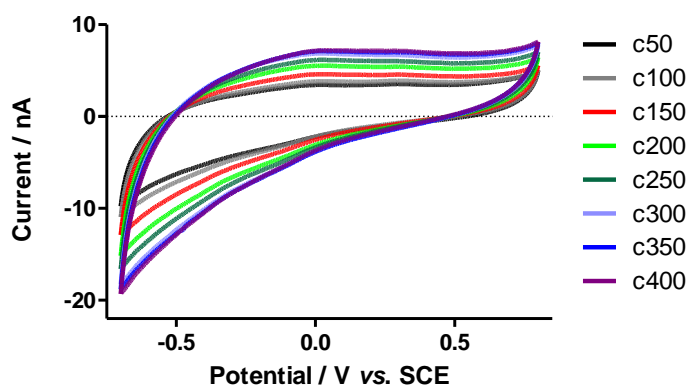


Figure 4.2: Increasing currents with cycling of bare CPEs cycled in PBS for 400 cycles from -0.70 to 0.80 V vs. SCE at 100 mV/s, $n = 4$.

It has been reported that carbon substrates can have many functional groups present on their surfaces which can react with atmospheric oxygen forming a series of electrochemically active groups.³⁰⁻³² Included in these functional groups are quinones which are pH dependent. In order to examine whether these groups were evident in the CVs of bare CPEs, they were cycled in PBS solutions of pH 7.2, 7.4 and 7.6 for 400 cycles in each solution. The resulting CVs are shown in Figure 4.3 and show no clear evidence of the existence of such species, a finding that has been supported by literature.³³ This confirms the requirement of depositing an electroactive species onto a CPE to develop a voltammetric pH sensor.

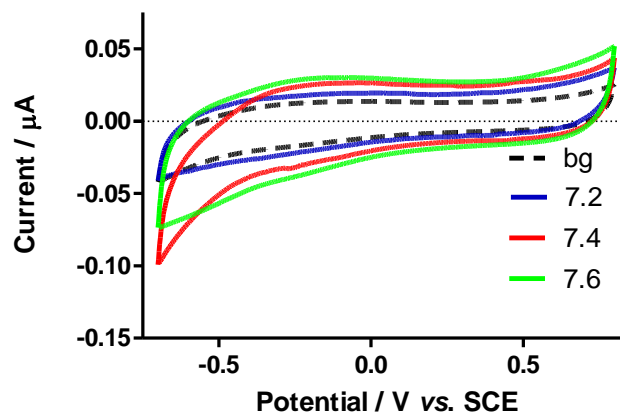


Figure 4.3: Bare CPEs cycled for 400 cycles in PBS solutions with pH 7.2, 7.4 and 7.6, $n = 4$.

4.2.2 Electrochemical Reduction and Cycling

In this section the electro-reduction of FBRR onto prepared CPE surfaces by CV and LSV from a 2 mM solution of the salt in an aprotic solvent, 0.1 M TEABF₄/ACN, and aqueous solvent, 0.1 M H₂SO₄, was examined. Several parameters were altered in order to obtain the optimum deposition, i.e., one that results in stable, sharp oxidation or reduction peaks. These included the age of the FBRR solution at the time of deposition, the number of sweeps applied, the potential range over which deposition took place and the scan rate at which CV or LSV was carried out.

As so many factors had an effect on the deposition of FBRR onto the substrate and the resulting CV of the modified electrodes, all of the variables were crossed examined. For example, for each day of FBRR use (1-5) several deposition scan rates were tested. Then each of the scan rates was used over a variety of potential ranges and number of linear sweeps. All of these deposition combinations were then subjected to similar permutations and combinations of scan rate and potential window in order to obtain the most stable and reproducible redox peaks when cycling the modified CPEs in PBS. A schematic of this process is shown in Figure 4.4.

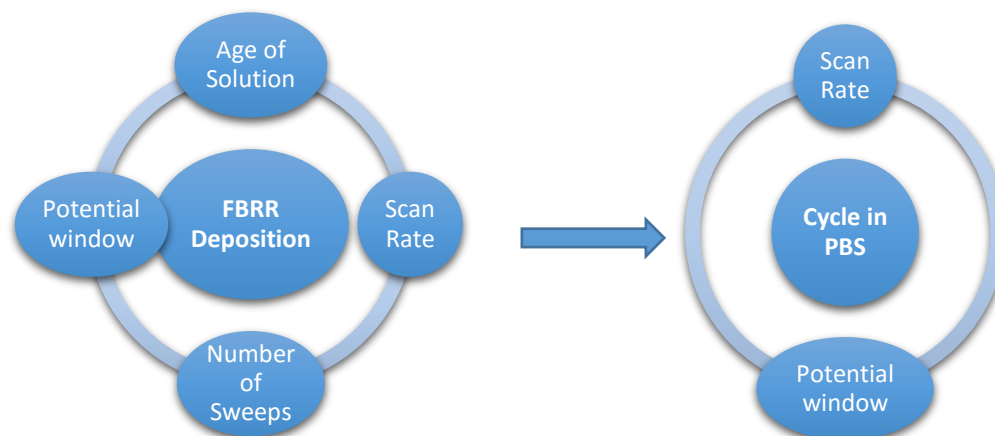


Figure 4.4: Schematic showing the combinations of deposition and cycling variables investigated in order to optimise the redox peaks of FBRR deposited by LSV from 0.1 M TEABF₄/ACN on CPEs.

The characterisation of the deposition parameters of FBRR onto the CPE substrate involved repeating a set of similar experiments four times, deposition by CV using TEABF₄/ACN, deposition by CV using H₂SO₄, deposition by LSV using TEABF₄/ACN and deposition by LSV using H₂SO₄. To avoid repetition the results in this section will display results from one system in full with reference made to the other three systems.

4.2.3 Electro-reduction of FBRR

This section shows the reduction profiles under various conditions and the effect on recycling the resulting modified electrode in PBS. Figure 4.5 shows the CV of a bare CPE in the background electrolyte, 0.1 M TEABF₄/ACN, compared to the first deposition cycle of 2 mM FBRR. An irreversible reduction wave is evident at approximately -0.35 V vs. SCE. This causes the radical formation of the FBRR and the subsequent covalent bond formation with the CPE surface.

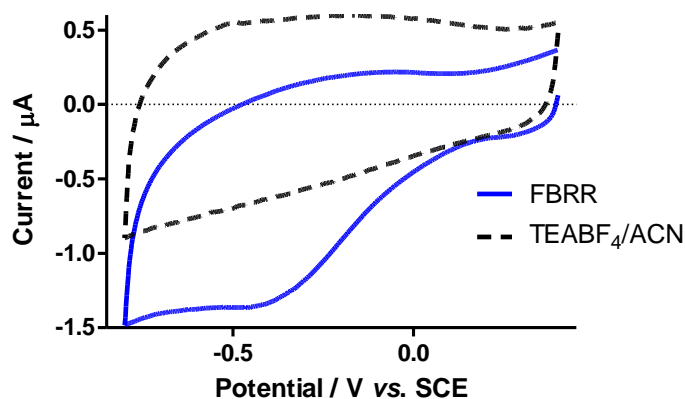


Figure 4.5: CVs of CPEs in TEABF₄/ACN and the first reduction cycle of 2 mM FBRR, $n = 4$.

As well as 0.1 M TEAFB₄ in ACN, FBRR can also be electrodeposited using 0.1 M H₂SO₄ as the supporting electrolyte.²² Figure 4.6 shows the CV of a bare CPE in the background electrolyte, 0.1 M H₂SO₄, compared to the first deposition cycle of 2 mM FBRR/ H₂SO₄. An irreversible reduction curve is evident. This causes the radical formation of the FBRR and the subsequent covalent bond formation with the CPE surface. When compared to the deposition in 0.1M TEABF₄/ACN, Figure 4.5, it can be seen that the currents obtained by cycling in the acid supporting electrolyte are substantially reduced, as well the currents for the FBRR deposition which are approximately one tenth that of the deposition in the aprotic solvent. Organic solvents are miscible with the hydrophobic layer on the surface of CPEs. This layer can become dissolved and eventually removed resulting in higher currents.¹⁴

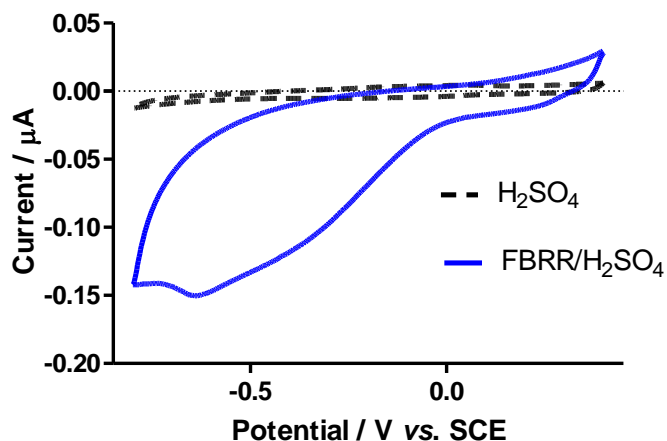


Figure 4.6: Bare CPE in background solvent and the first reduction cycle of 2 mM FBRR, $n = 4$.

4.2.3.1 Stability of FBRR in $\text{TEABF}_4/\text{ACN}$

The shelf life of diazonium salt solutions in aprotic media is approximately 5 days.¹⁸ In order to determine the effect that the age of the FBRR/ $\text{TEABF}_4/\text{ACN}$ solution had on the resulting CV scan the solution was prepared on day 1 before being electrodeposited onto a CPE by sweeping the applied potential over various ranges, scan rates and number of deposition sweeps. This procedure was repeated on 4 CPEs on 5 consecutive days using the same solution which was stored at 4°C when not in use. The resulting reduction LSV profiles for days 1-5 are shown in Figure 4.7. The FBRR was electrodeposited from 0.40 to -0.80 V vs. SCE for 5 sweeps, at a scan rate of 100 mV/s. Days 2-4 were identified as resulting in the best deposition of FBRR onto CPEs. The reduction of the salt is evident by the broad peak at approximately -0.35 V vs. SCE in Figure 4.7(A).

The modified CPEs were then cycled in PBS (pH 7.4). When the resulting CVs were compared, cycle 50, the best deposition resulted from the electrochemical reduction of FBRR on days 2-3. Figure 4.7(B) shows modified CPEs cycled between -0.50 and 0.80 V vs. SCE at 100 mV/s. The poorly defined redox peaks are highlighted within the solid rectangle. On day 1 the redox peaks were relatively broad, making it difficult to precisely locate the peak potential. A decrease in the peak height generated from depositing from the solution on days 4 and 5 was evident. This indicated that the FBRR concentration in solution had depleted, either due to the number of deposition

sweeps taken or due to the time taken for the number of depositions. A second oxidation peak (dashed rectangle) was observed at *ca.* 0.35 V *vs.* SCE in the CVs of FBRR/CPEs, this will be discussed later in this chapter, Section 4.2.3.16.

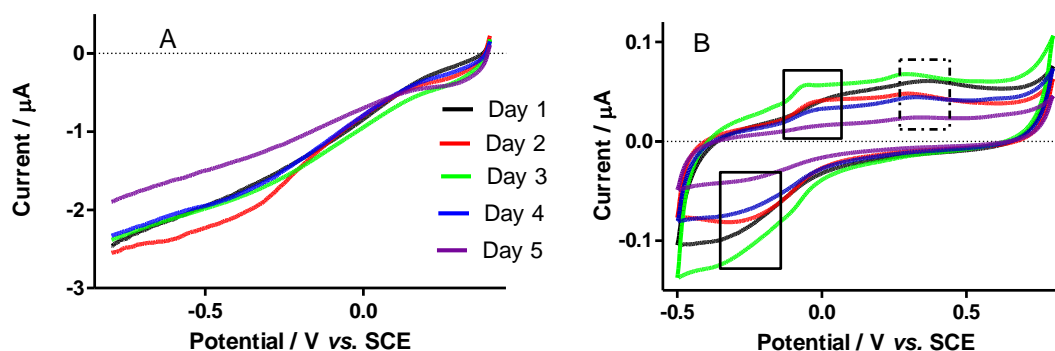


Figure 4.7: (A) Reduction profiles, 1st sweep, of 2 mM FBRR in 0.1 M TEABF₄/ACN over 5 days. (B) The modified electrodes cycled in PBS. All at 100 mV/s, $n = 4$.

4.2.3.2 Stability of FBRR in H₂SO₄

Similar to Section 4.2.2.1, an FBRR/H₂SO₄ solution was prepared on day 1 by dissolving 2 mM FBRR in 0.1 M H₂SO₄. This was then N₂ saturated before being electro-deposited onto a freshly prepared CPE. This procedure was repeated on 4 CPEs on 4 consecutive days using the same solution which was stored at 4°C when not in use.

The modified CPEs were then cycled in PBS. Figure 4.8 shows the 50th cycle of the resulting CVs with the characteristic anodic and cathodic peaks at approximately -0.07 and -0.15 V *vs.* SCE, respectively. When these were compared the sharpest redox peaks resulted from the electrochemical reduction of FBRR after the 1st day. On day 1 the redox peaks were relatively broad making it difficult to precisely locate the peak potential. On days 2 and 3 both the oxidation and reduction peaks appear sharp indicating a rapid electron transfer process. The sharpness of the peak makes it easier to extract the peak potential value for pH analysis. A decrease in the peak height generated from depositing from the solution on day 4 was evident. This indicated that the FBRR concentration in solution had depleted, due to the number of deposition

sweeps carried out. Other oxidation peaks were again observed here and will be dealt with in Section 4.2.3.16.

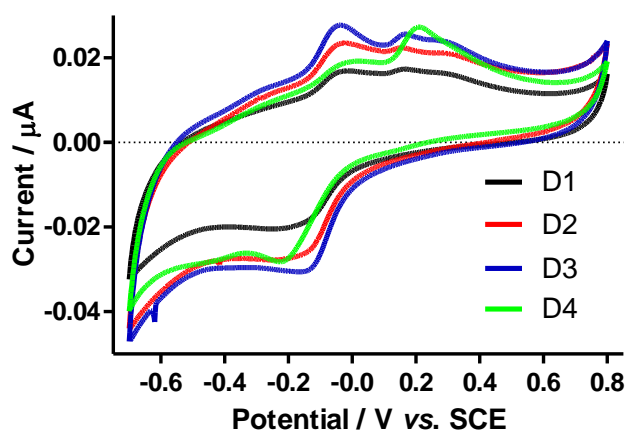


Figure 4.8: CVs resulting from the electro-reduction of FBRR/H₂SO₄ by LSV from 0.40 to -0.80 V vs. SCE at 100 mV/s over a period of 4 days, $n = 4$.

4.2.3.3 Deposition Scan Rate

Figure 4.9(A) shows the deposition profiles (CV) for 2 mM FBRR/H₂SO₄ electrodeposited from 0.40 to -0.80 V vs. SCE at various scan rates (mV/s). When the scan rate was decreased there was a corresponding decrease in the peak currents obtained during deposition. This occurs because the voltammogram takes longer to record each cycle as the scan rate is decreased, i.e., the cycles are recorded faster at higher scan rates. This influences the diffusion layer thickness. At slow scan rates the diffusion layer will grow much further from the electrode surface as it takes more time, so there will be a smaller concentration gradient between the surface and the solvent resulting in lower peak currents at slow scan rates and higher peak currents at higher scan rates. The increase in peak current with scan rate implies that a more capacitive film has been formed. For this reason the deposition curve with the largest peak current may not necessarily result in the best surface coverage with FBRR. It would appear from Figure 4.9(A) that the best FBRR deposition occurs at 100 mV/s, this is in agreement with the resulting CVs of the modified electrodes in PBS, Figure 4.9(B). Similarly, deposition by LSV from the aqueous electrolyte, and all depositions from the organic solvent showed 100 mV/s as the optimum scan rate to employ.

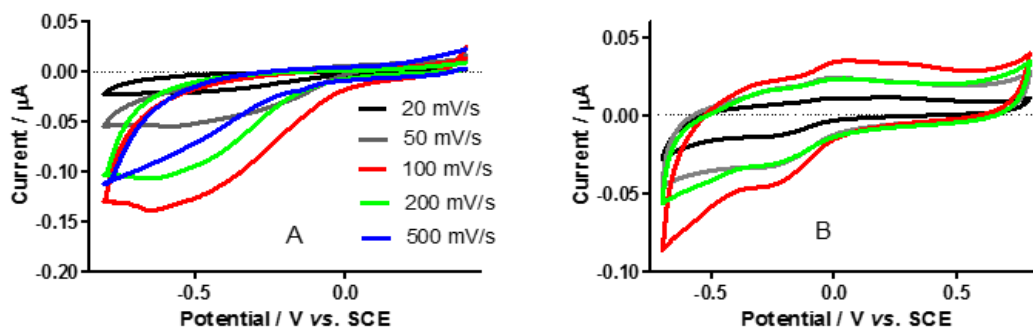


Figure 4.9: (A) Deposition profiles, 1st sweep, of 2 mM FBRR/H₂SO₄ at various scan rates (20-500 mV/s), and (B) the resulting CVs, 50th cycle, $n = 4$.

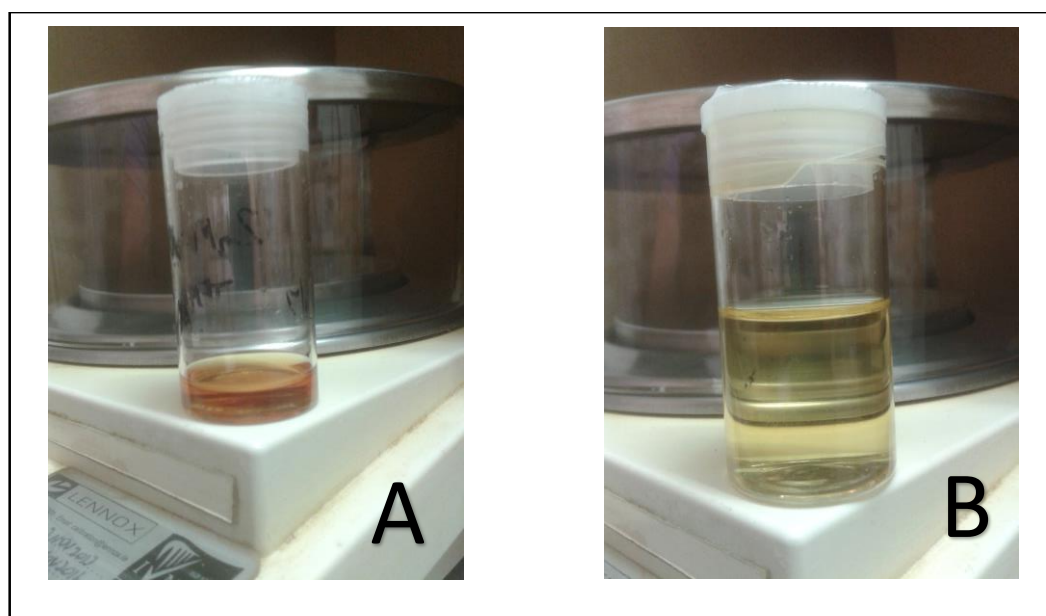


Figure 4.10: (A) 2 mM FBRR solution having been used for CV electrodeposition on 3 consecutive days and (B) a freshly prepared FBRR/TEABF₄/ACN solution.

It was previously observed that the day of deposition played a significant role in the deposition of FBRR and the clarity of the CVs subsequently produced so all of the above scan rates were applied to the deposition of FBRR on each of days 1-3. Figure 4.9 above shows the resulting CVs from day 2. The electrodeposition of FBRR by LSV was carried out over days 1-5. In the case of CV deposition each electrode was cycled 10 times and forward and reverse scans were performed increasing the time that the solution was in use. This resulted in the FBRR concentration and volume

diminishing by day 4. However, LSV deposition was carried out for 5 reduction sweeps only. Figure 4.10(A) shows the appearance of the FBRR/TEABF₄/ACN having been used for CV electrodepositions on 3 consecutive days. Image (B) shows how the solution appears when freshly prepared.

4.2.3.4 Deposition Potential Range

2 mM FBRR in 0.1 M H₂SO₄ was electrodeposited onto CPEs by CV varying both the anodic and cathodic potential ranges ($v = 100$ mV/s). Firstly the cathodic potential applied was varied between -0.60 and -1.00 V *vs.* SCE while maintaining the anodic potential limit to 0.40 V *vs.* SCE. The deposition reduction curves obtained, cycle 1, are shown in Figure 4.11(A) and the resulting CVs after deposition are in Figure 4.11(B). This procedure was repeated on days 1-4 after the FBRR solution had been prepared. The results shown below are from day 2. The best reduction peaks resulted from FBRR deposited between 0.40 and -0.80 V *vs.* SCE with a well-defined reduction peak at approximately -0.50 V *vs.* SCE. From the resulting CVs a similar pattern is observed with sharper more defined anodic and cathodic peaks obtained at approximately 0.03 and -0.20 V *vs.* SCE, respectively, for each of the potential ranges applied.

The limit of the reduction potential was subsequently chosen as -0.80 V *vs.* SCE. This avoided bringing the applied potential to too low a value resulting in the possible reduction of the aryl radical to the undesired anion,^{18, 34} forming a multi-layered surface.³⁵ Similar results were observed when depositing FBRR/H₂SO₄ by LSV, however, results from FBRR/TEABF₄/ACN formed poorly defined redox peaks.

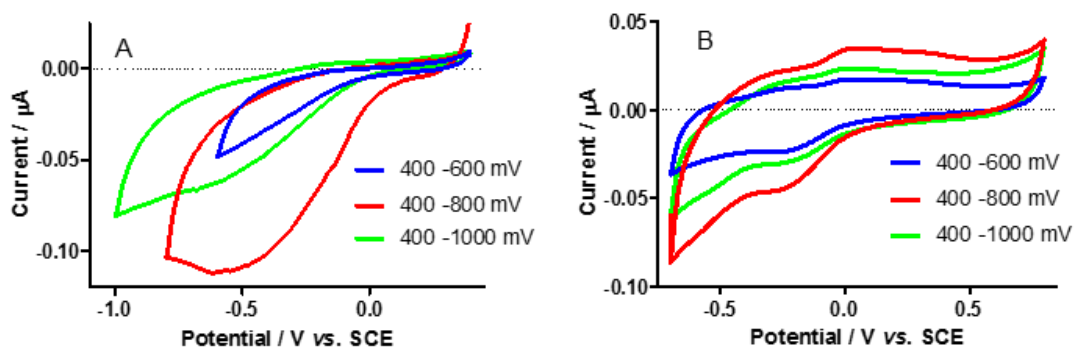


Figure 4.11: (A) Reduction profiles, cycle 1, for the deposition of 2 mM FBRR onto CPEs using various cathodic potentials and B the resulting modified electrodes cycled in PBS, $n = 4$.

The anodic potential was then varied from 0.20 to 0.80 V vs. SCE. The LSV deposition reduction profiles, sweep 1, for FBRR/ H_2SO_4 , are shown in Figure 4.12(A) with the resulting CVs, 50th cycle, after deposition in Figure 4.12(B). The reduction profiles, Figure 4.12(A), show a clear reduction at approximately -0.50 V vs. SCE. The resulting CVs indicate the variability in the oxidation and reduction peaks observed. The reduction peak appears broad across all the deposition potentials applied, this would make it difficult to extrapolate a precise peak potential value in order to determine a pH response. The oxidation peaks are, in general, sharper, indicating more efficient electron transfer processes. These experiments were performed using a FBRR solution aged between 1 and 4 days old, with the results shown in Figure 4.12 obtained when electro-reducing the FBRR/ H_2SO_4 onto CPEs from a 2 day old solution.

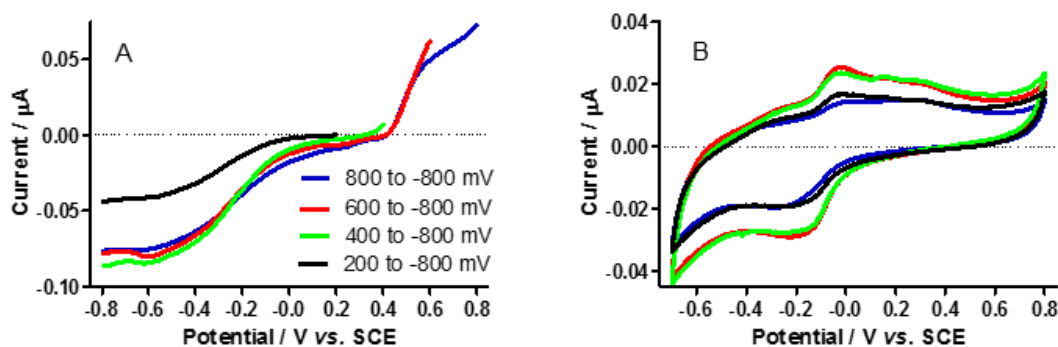


Figure 4.12: (A) LSV Deposition profiles for 2 mM FBRR/H₂SO₄ (day 2) over various anodic potential ranges and (B) the resulting CVs of the modified electrodes, all at 100 mV/s. The CVs all show the 50th cycle, $n = 4$.

The CVs resulting from all depositions involving TEABF₄/ACN were of poor quality, with ill-defined oxidation and reduction peaks of low current output, rendering them ineffective for the purpose of the sensor.

A potential range of 0.40 to -0.80 V vs. SCE was chosen as the optimum for all future electro-depositions of FBRR onto CPEs as this appeared to give more defined redox peaks when the results from all days were considered.

4.2.3.5 Number of Deposition Sweeps

The electrochemical reduction of diazonium salts generally results in a layered deposition of the product onto the substrate, not monolayers.³⁶ The application of more reduction sweeps normally produce thicker layers.³⁷ The formation of a uniformly distributed monolayer of FBRR on the substrate is desirable in order to minimise the diffusion layer thickness therefore increasing the electron transfer kinetics. Here, the effect of increasing the number of sweeps applied in CV and LSV was investigated.

FBRR was deposited by CV between 0.40 and -0.80 V vs. SCE at 100 mV/s. Figure 4.13(A) shows a typical CV for 10 cycles of deposition on a CPE from a solution containing 0.1 M TEABF₄ in ACN. It shows that most of the FBRR was deposited in the first cycle. The attachment of the aryl radical to the surface gives rise to the near disappearance of the reduction curve after the first reduction cycle has been performed, showing rapid blocking of the surface of the electrode by the organic layer.¹⁶ This is

likely the reason for the broadness of the wave; the surface being modified while the voltammogram is recorded.^{18, 34} In the following cycles, the reduction peak is absent which shows that the electrode is in a passive state and FBRR is no longer depositing onto the carbon paste surface.^{18, 34} The reduction of FBRR was then carried out for 1, 5, and 10 cycles. The resulting CVs are shown in Figure 4.13(B) with 10 deposition cycles giving the most defined peaks. Similar results were found when depositing FBRR/H₂SO₄ by CV, so all future CV electro-reductions involved cycling the CPEs in FBRR solutions for 10 cycles.

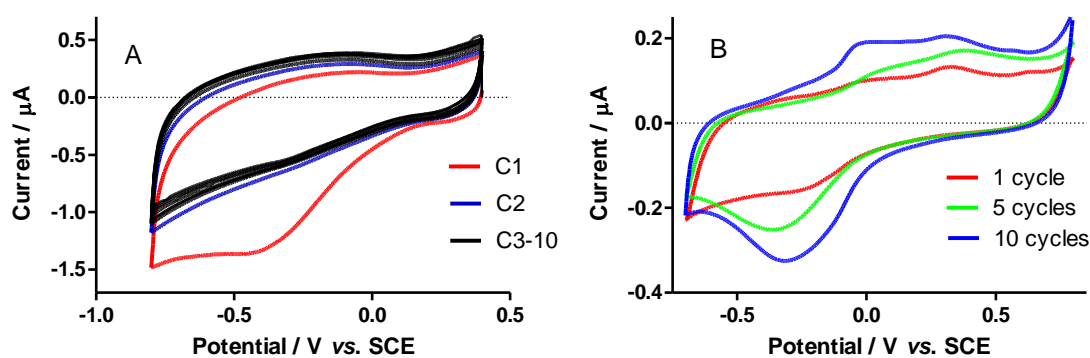


Figure 4.13: (A) Deposition CVs for 2 mM FBRR/TEABF₄/ACN, 10 cycles. (B) FBRR/CPEs cycled in PBS, pH 7.4, having been electrodeposited for 1, 5 and 10 cycles from 0.40 to -0.80 V vs. SCE, $n = 4$.

The effect of increasing the number of sweeps applied in LSV was then investigated across various anodic potential ranges, from 0.40 to 0.80 V vs. SCE. FBRR/H₂SO₄ was deposited by LSV for 2, 5 and 10 sweeps at 100 mV/s. The resulting CVs are shown in Figure 4.14(B-D). Across all potential ranges 5 sweeps gave the best results.

When the deposition profiles were reviewed there was still evidence of some FBRR deposition after the 2nd sweep, a small reduction peak is evident in Figure 4.14(A), and so 2 sweeps may give the maximum amount of FBRR on the CPE surface. 10 sweeps appeared to deposit too much FBRR on the surface, causing many layers to deposit onto the electrode. This thicker layer resulted in reduced electron transfer and therefore reduced peak currents. The peaks are also broader due to the slow rate of

electron transfer. Depositing from 0.40 to -0.80 V *vs.* SCE gave the best results which confirmed the results obtained in Section 4.2.2.4.

It was also found that depositing FBRR/TEABF₄/ACN by LSV for 5 sweeps gave the optimum electrode coverage.

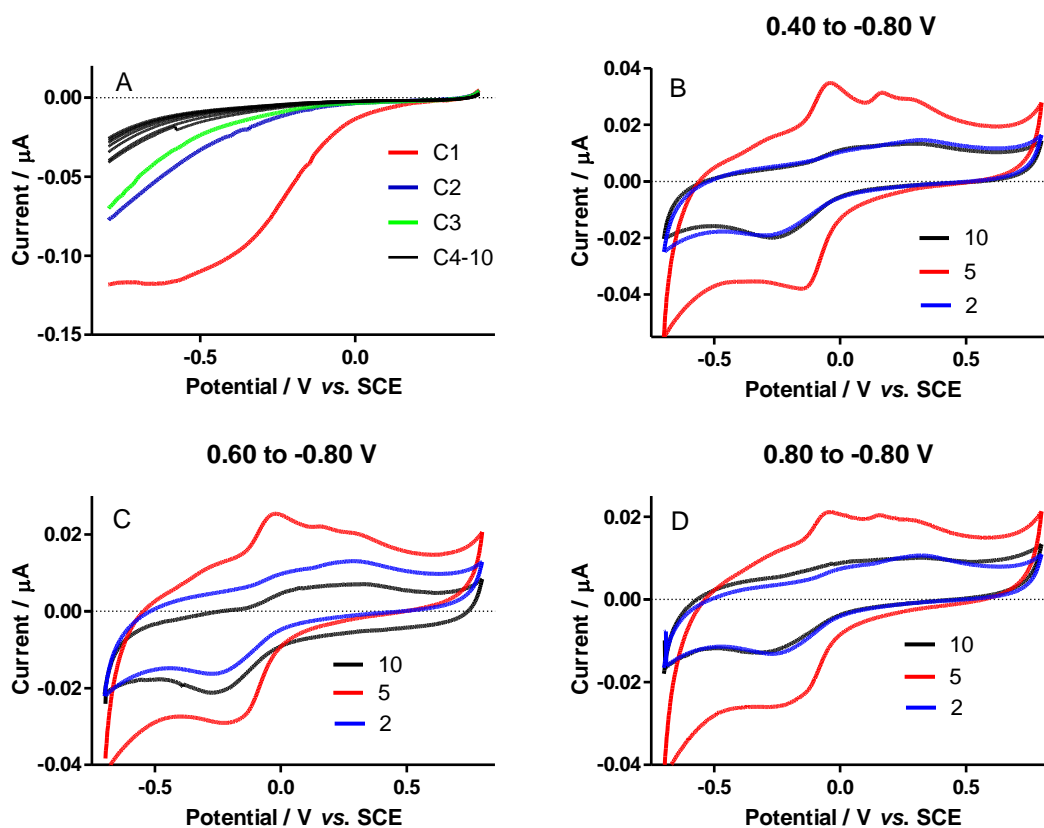


Figure 4.14: (A) Reduction profiles for FBRR/H₂SO₄, sweeps 1-10, with the resulting CVs of the modified CPEs in PBS having been electro-reduced for 2, 5 and 10 sweeps from (B) 0.40 to -0.80 V, (C) 0.60 to -0.80 V and (D) 0.80 to -0.80 V *vs.* SCE, $n = 4$.

4.2.3.6 Evidence of FBRR Deposition

Figure 4.15 demonstrates that the FBRR salt has been successfully electrodeposited onto the CPE surface. The plot shows three different CVs, all representing the 50th cycles. The innermost cycle shows the CV of a bare CPE in PBS. The centre CV shows the resulting CV once H₂SO₄ had been deposited (LSV, 5 sweeps; 0.40 to -0.80 V *vs.* SCE at 100 mV/s). These two CVs are almost identical other than a higher capacitance evident for the CPE modified in H₂SO₄. This suggests that the silicone oil

was drawn out when cycling CPEs resulting in a higher carbon: silicone oil ratio.¹¹ The outermost cycle shows the resulting CV after the reduction of FBRR onto the CPEs with the oxidation (-0.02 V) and reduction peaks (-0.15 V) of the diazonium salt clearly shown. This gives a ΔE_p value of 0.13 V vs. SCE. The redox pairs of quinones are generally classed as a quasi-reversible system, but this depends on the type of electrode used. At CPEs an irreversible behavior is generally observed.³⁸ It can be concluded therefore, that FBRR has been electro-deposited onto the electrode surface. Whether depositing FBRR by CV or LSV, from solutions of H₂SO₄ or TEABF₄/ACN, successful electro-reduction of the salt was shown by similar CVs.

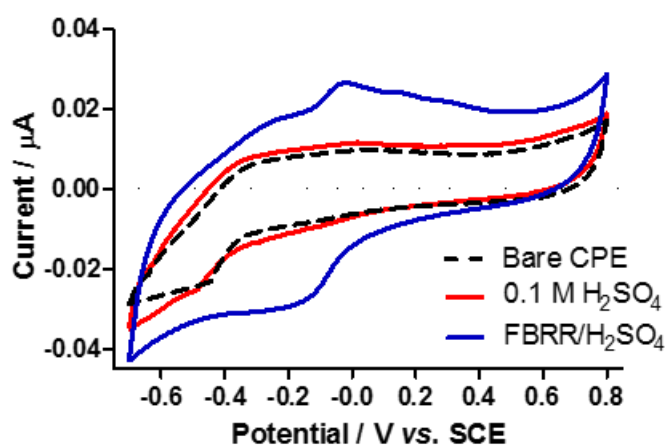


Figure 4.15: CVs comparing a bare CPE with ones modified with 0.1 M H₂SO₄ and FBRR/H₂SO₄ indicating that FBRR has been successfully electrodeposited, $n = 4$.

The SEM micrographs of a bare CPE (A) and one that has been modified with FBRR by LSV (B) are shown in Figure 4.16. Both images show irregularities on the surfaces leading to an inter-electrode variability in surface area. They also show the porous nature of CPEs. Obtaining a smoother surface would give more reproducible results.⁶

The corresponding EDXs shown directly below the images both show carbon and silicone, the two constituents of carbon paste. EDX (B) representing the FBRR/CPE has some zinc peaks resulting from the successful deposition of the diazonium salt.

There is no evidence of the nitrogen from the FBRR, this is because the nitrogen signal appears at 0.392 keV and cannot be resolved.

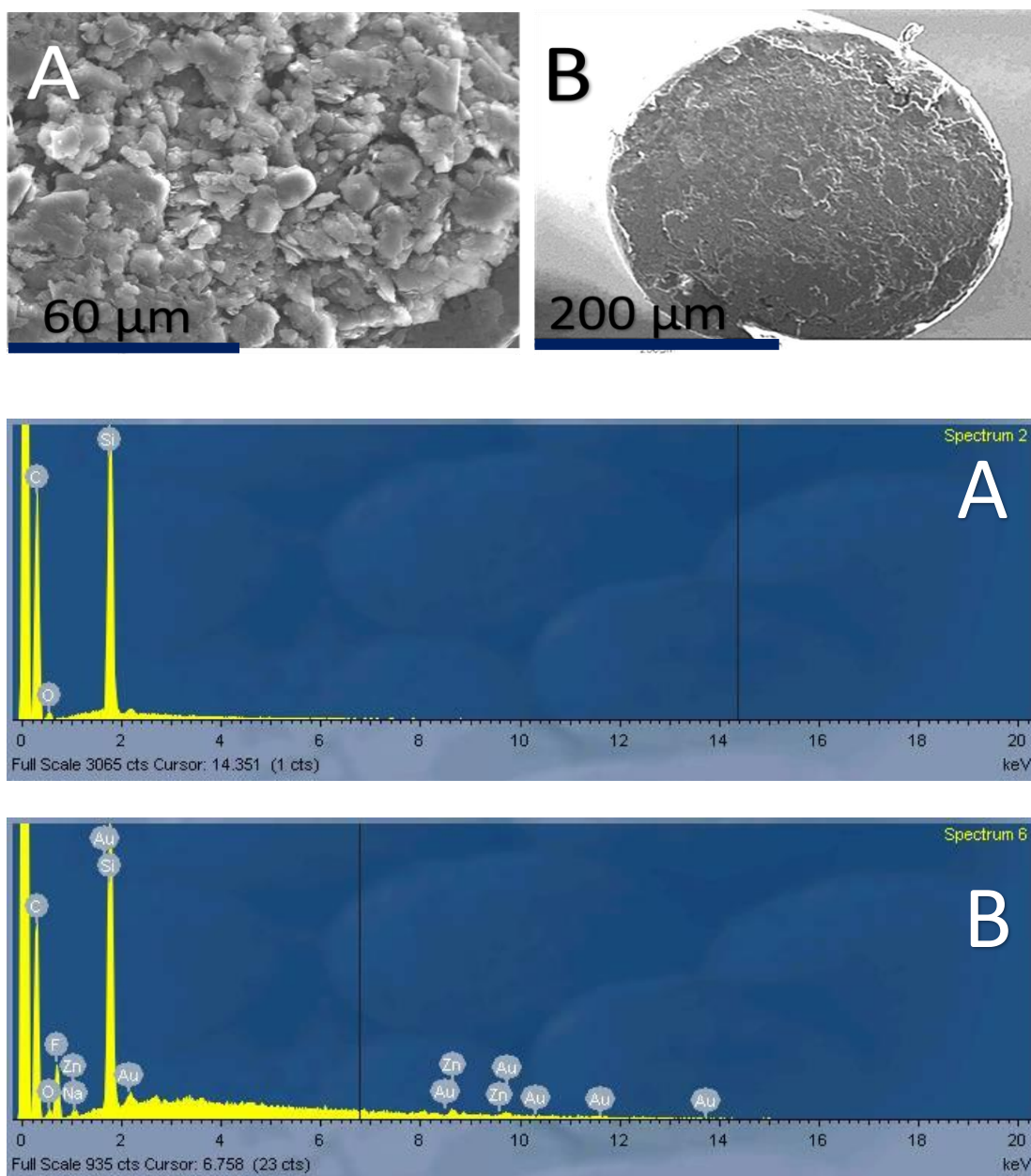


Figure 4.16: SEM micrographs with their corresponding EDX below. (A) A bare CPE, (B) an FBRR/CPE modified by LSV.

Unlike the CPEs modified by LSV the EDX of FBRR deposition by CV, in Figure 4.17, shows no definitive evidence of the existence of FBRR on the electrode surface, possibly indicating that significantly less FBRR was deposited by CV than LSV.

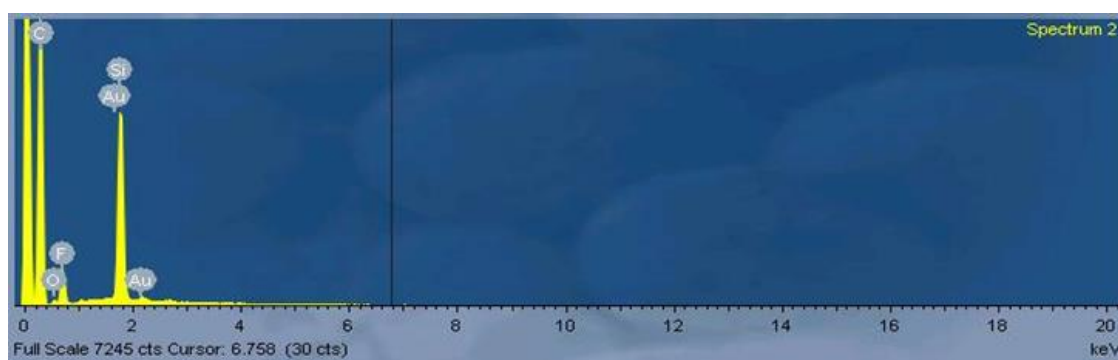


Figure 4.17: SEM micrograph and EDX of a FBRR CPE modified by CV in 0.1 M TEABF₄/ACN.

4.2.3.7 *FBRR Concentration*

The deposition of FBRR onto CPEs had up until now involved a FBRR concentration of 2 mM. Literature values for FBRR solutions in H₂SO₄ range from 1- 5 mM.¹⁶ In an attempt to deposit more FBRR onto the electrode surface, while maintaining a monolayer coverage, a solution containing 5 mM FBRR in 0.1 M H₂SO₄ was prepared and N₂ saturated before being reduced onto the electrode surface by CV, for 10 cycles at 100 mV/s from 0.40 to -0.80 V *vs.* SCE. The resulting electrodes were then cycled in PBS solutions with pH values of 7.2, 7.4 and 7.6 from -0.70 to 0.80 V *vs.* SCE at 100 mV/s over four days. Figure 4.18 shows the resulting CVs obtained from the FBRR/H₂SO₄ solution on day 3. The anodic and cathodic peaks obtained were broad, indicating slow electron transfer processes occurring at the electrode surface/solution interface. FBRR salt has a solubility in H₂O of 1.0 mg/ml, which equates to under 3 mM, therefore a solution above this concentration would be of no benefit. As increasing the concentration of FBRR did not enhance the redox peaks it was maintained at 2 mM for all experiments.

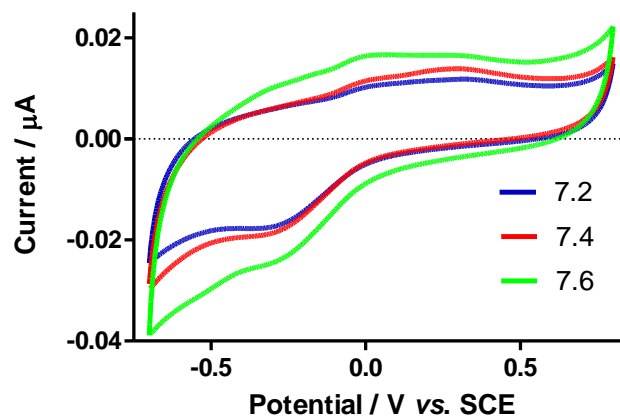


Figure 4.18: CVs showing the pH response of FBRR/H₂SO₄ modified CPEs using a 5 mM solution of FBRR, $n = 4$.

4.2.3.8 Cycling Modified CPEs in PBS

CPEs modified from aqueous and organic electrolytes, by LSV and CV, were examined by CV in order to ascertain that FBRR had been successfully deposited onto the electrode surface. It was also important to monitor the potentials at which the oxidation and reduction peaks occurred as a requirement was to develop a sensor that would respond to very small pH changes, between 7.20 and 7.60. In order to extrapolate these peak potentials a sharp, well-defined peak that is stable over time and responds to pH is desirable. The mechanism for the oxidation/reduction reaction of FBRR which is a $2 e^- / 2 H^+$ process³⁹ has been described in the introduction section. In this section the modified CPEs were cycled in PBS, varying the scan rates and potential ranges. The stability of the response over 400 cycles (3.3 hours) was also monitored along with the pH response of the redox peaks. Each of the aforementioned experiments were carried using the same FBRR solutions over several days. The storage conditions for bare and FBRR/CPEs was also examined.

4.2.3.9 Scan Rate

In order to determine the effect of the scan rate (v) on the resulting redox peaks, FBRR/H₂SO₄/CPEs were cycled at various scan rates, ranging from 50 to 500 mV/s. The resulting CVs of the modified electrodes in PBS (pH 7.4) are shown in Figure

4.19(A). As previously mentioned in Section 4.2.2.3, the currents achieved have increased with increasing scan rate. The results in Figure 4.19 show all the scan rates examined in graph (A). Graph (B) shows the scan rates from 20 to 100 mV/s. At higher scan rates the oxidation peak at approximately 0.03 V lost sharpness so a slower scan rate, 100 mV/s, was identified as the optimum scan rate for cycling FBRR/CPEs in PBS.

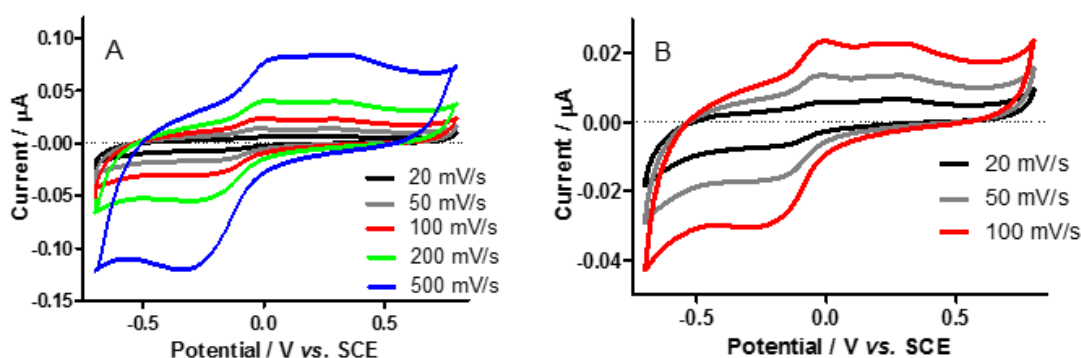


Figure 4.19: CVs showing CPEs modified with FBRR/H₂SO₄, cycled in PBS at scan rates between 20 and 500 mV/s (A) and from 20 to 100 mV/s (B) resulting in a better defined anodic peak at 100 mV/s, $n = 4$.

A linear dependence of the square root of the scan rate on the peak current (oxidation and reduction) indicates a diffusion controlled redox process whereas a surface controlled redox process results in a straight line plot of scan rate *vs.* peak current. Figure 4.20(A) plots the peak current, I_p , as a function of the scan rate, v . R^2 values of 0.997 and 0.998 for the oxidation and reduction peak currents, respectively, were achieved. Figure 4.20(B) plots the peak current, I_p , as a function of the square root of the scan rate, $v^{1/2}$. R^2 values of 0.980 and 0.975 for the oxidation and reduction peak currents, respectively, were achieved. As both these plots have straight line relationships a plot of the log of peak current *vs.* the log of the scan rate was constructed, Figure 4.20(C). This gave a linear dependence with slopes of 0.8181 and 0.9205 for the oxidation and reduction peaks, respectively. These values, between 0.5 and 1.0, confirm mixed mass transport, diffusion and adsorption,⁴⁰ resulting from thin-layer

diffusion.^{41, 42} This occurs when pockets of solution become trapped in the porous modified layer. As the electron transfer proceeds the currents decay over the potential cycle as there is a limited amount of FBRR in the trapped solution. These results are indicative of a quasi-reversible surface bound species that has been adsorbed onto the substrate surface.⁴³

As was observed previously the currents obtained increased with cycling. In order to eliminate any hysteresis effects in the above experiments the electrodes were cycled from a slow scan rate of 20 mV/s increasing up to 500 mV/s, the order was then reversed (cycling from high scan rate to low). By taking average peak currents of each scan rate better estimates of the currents were obtained.

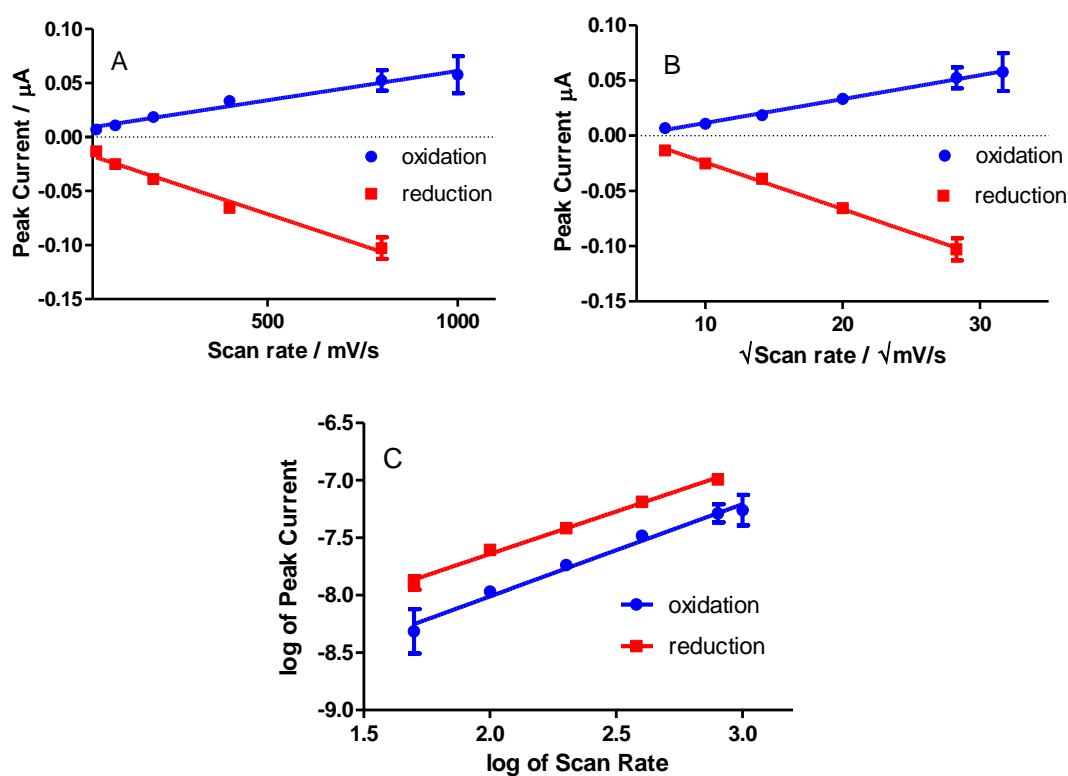


Figure 4.20: The plots of (A) I_p vs. v , (B) I_p vs. $v^{1/2}$ and (C) $\log I_p$ vs. $\log v$, for CV modified CPEs, all in PBS pH 7.4

Figure 4.21(A) shows the results obtained when FBRR/TEABF₄/ACN modified CPEs were cycled at various scan rates. The lower scan rates have been isolated in Figure 4.21(B) and show the oxidation and reduction peaks resulting from the FBRR salt. These peaks are not evident at higher scan rates as the faster scan rate has failed to differentiate the peaks during the cycle. Comparing Figures 4.19(A) and 4.21(A) reveals the differences in peak formations between the two supporting electrolytes used, with the FBRR/H₂SO₄ peaks much sharper than the FBRR/TEABF₄ peaks.

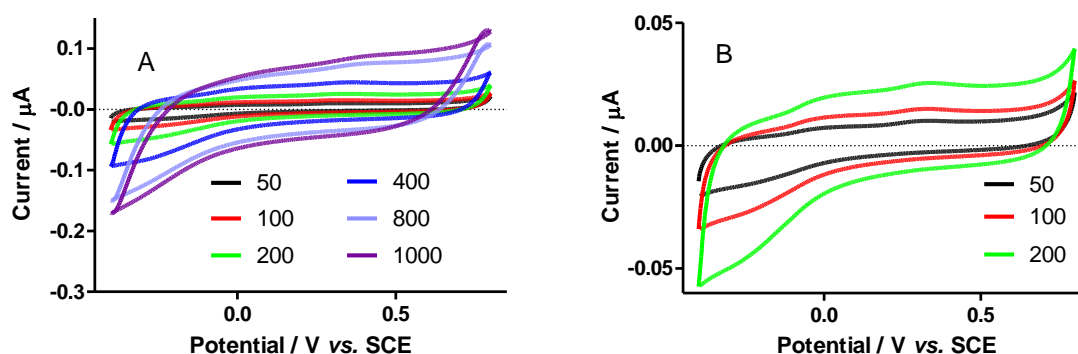


Figure 4.21: (A) FBRR modified electrodes cycled in PBS with varying scan rates between 50 and 1000 mV/s and (B) the lower scan rates expanded, $n = 4$.

Again, the peak currents for both the anodic and cathodic reactions are directly proportional to the scan rate indicating a surface controlled redox process, and vary linearly with the square root of scan rate indicating a diffusion-controlled process. Figure 4.22 (A) plots the peak current, I_p , as a function of the square root of the scan rate, $v^{1/2}$. Correlation coefficients of 0.996 and 0.997 for the anodic and cathodic peak currents, respectively, were achieved. Figure 4.22(B) plots the peak current, I_p , as a function of the scan rate, v . R^2 values of 0.979 and 0.984 for the anodic and cathodic peak currents, respectively, were achieved. The corresponding plot of the log of peak current vs. the log of the scan rate. Figure 4.22C, also revealed a linear dependence with slopes of 0.802 and 0.739 for the oxidation and reduction peaks, respectively, leading to Equations 4.1 and 4.2, indicative of thin layer diffusion.

$$\text{Anodic: } \log I_p = 0.802 \log v - 7.98; \quad R^2 = 0.9869 \quad 4.1$$

$$\text{Cathodic: } \log I_p = 0.739 \log v - 8.39; \quad R^2 = 0.9948 \quad 4.2$$

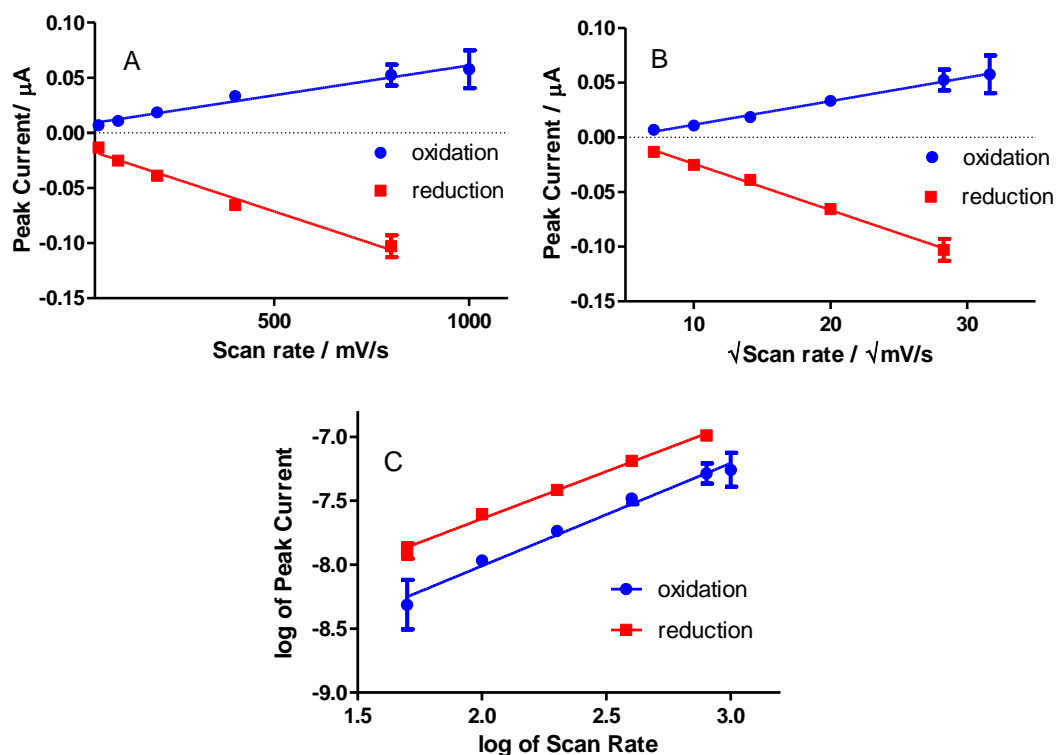


Figure 4.22: The plots of (A) I_p vs. v , (B) I_p vs. $v^{1/2}$ and (C) $\log I_p$ vs. $\log v$, for FBRR/TEABF₄/ACN modified CPEs, all in PBS pH 7.4.

4.2.3.10 Potential Window

FBRR/H₂SO₄ was deposited onto CPEs by LSV for 5 sweeps using the following potentials; (A) 0.40 to -0.80 V, (B) 0.60 to -0.80 V and (C) 0.80 to -0.80 V vs. SCE. The modified electrodes were then cycled in N₂ saturated PBS over various potential ranges, (-0.70 to 0.80 V, -0.50 to 0.50 V and -0.30 to 0.10 V vs. SCE) in this order to see if cycling over a wider window first affected the peaks when cycling over the subsequent narrower potential window. The modified electrodes were also cycled over each potential range individually. As the day of depositing FBRR played a significant role in the resulting CVs the listed experiments were carried out using the solution on days 2 and 3, which were previously found to be the optimum days for depositing FBRR/H₂SO₄. The resulting CVs for FBRR deposition on day 3 only are shown in this

section. Figures 4.23 A-C show the resulting CVs from modified electrodes being cycled over all the potential ranges in the order -0.70 to 0.80 V, -0.50 to 0.50 V and then -0.30 to 0.10 V *vs.* SCE for 50 cycles each (day 3). The results clearly show reduced peak definition and currents as the potential window was narrowed. They also show that a sharper peak is consistently obtained for the anodic peak making this the peak of choice for examination of peak potentials for pH analyses.

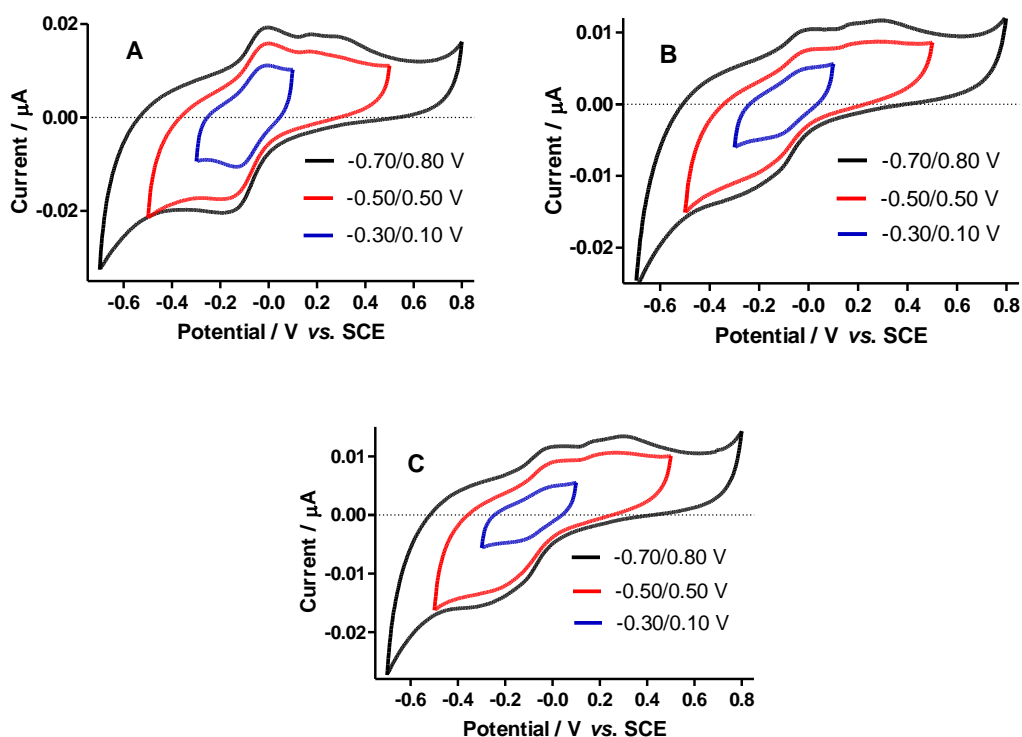


Figure 4.23: FBRR/H₂SO₄ deposited onto CPEs from (A) 0.40 to -0.80 V, (B) 0.60 to -0.80 V and (C) 0.80 to -0.80 V *vs.* SCE and subsequently cycled over various potential windows in the order -0.70 to 0.80 V, -0.50 to 0.50 V and -0.30 to 0.10 V *vs.* SCE. $n = 4$.

Electrodes were also FBRR modified and cycled through each of the above potential ranges individually, i.e. four electrodes were cycled from -0.70 to 0.80 V, another four were cycled from -0.50 to 0.50 V and finally four electrodes were cycled from -0.30 to 0.10 V. The average CVs are shown in Figure 4.24(A) (day 3). Again reduced peak definition and currents were obtained as the potential window was narrowed.

To check whether the order of cycling through each potential window had an effect on the resulting CVs, electrodes were first cycled from -0.30 to 0.10 V followed by -0.70 to 0.80 V *vs.* SCE for 50 cycles each. Figure 4.24(B) shows the final CVs (day 3) which clearly show no effect caused by the order of cycling.

It can be concluded from the results in this section that the most defined oxidation and reduction peaks are obtained on cycling the modified electrodes from -0.70 to 0.80 mV *vs.* SCE. These results also confirmed the optimal potential range of 0.40 to -0.80 V *vs.* SCE for the deposition of FBRR/H₂SO₄ onto CPEs by LSV.

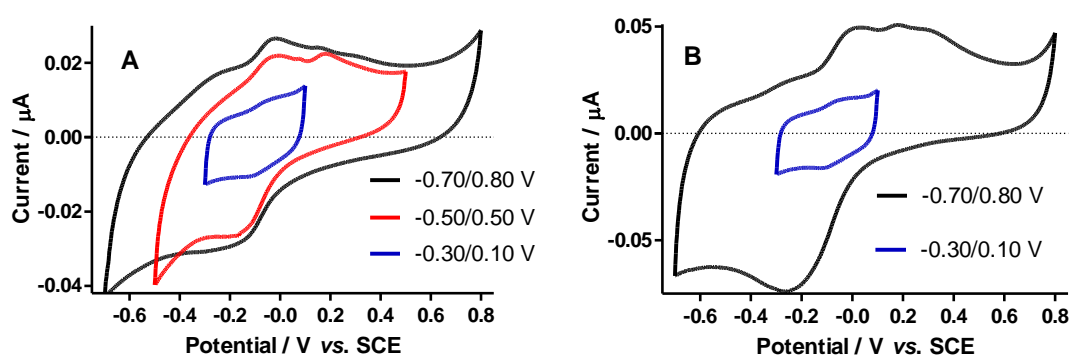


Figure 4.24: (A) CVs of CPEs modified from 0.40 to -0.80 V *vs.* SCE cycled over various potential ranges and (B) cycled over various potential windows in the order -0.30 to 0.01 V *vs.* SCE followed by -0.70 to 0.80 V *vs.* SCE, $n = 4$.

When FBRR/TEABF₄/ACN modified CPEs were cycled over various potentials it was noted that in order to observe the entire reduction peak the potential should be cycled to at least -0.50 V *vs.* SCE, this also results in improved anodic peaks. A further improvement in the sharpness of the redox peaks was observed when cycling the modified CPEs to -0.70 V *vs.* SCE, as increasing the cathodic potential has been shown to enhance the redox peaks.³⁷

As there were several parameters that affected the formation of sharp, reproducible redox peaks CPEs modified at various scan rates (20-100 mV/s) were cycled through various cathodic potentials (-0.10 to -0.70 V *vs.* SCE). The limit of the cathodic potential was set at -0.70 V *vs.* SCE as any lower would result in a longer time period taken for each cycle, increasing the response time of the sensor. This cathodic limit

would also eliminate the generation of H_2 at the electrode surface. Figure 4.25 shows the resulting CVs from CPEs having been modified at various scan rates then cycled to -0.50 V (A) and -0.30 V (B) *vs.* SCE. It can be seen that electrodes electro-reduced at 100 mV/s resulted in clearer redox peaks, making it easier to extrapolate the peak potential values required when testing the pH sensitivity of the FBRR/CPEs.

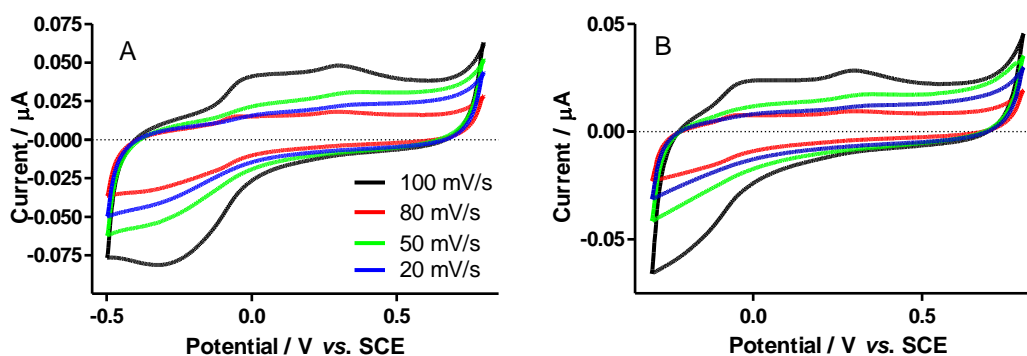


Figure 4.25: (A) CPEs modified at various scan rates and (B) cycled in PBS to cathodic potentials of -0.50 and -0.30 V *vs.* SCE, $n = 4$.

Figure 4.26 shows the results observed when CPEs were modified at 100 mV/s and then cycled in PBS over various cathodic potential windows. From the plot it can be seen that reducing the cathodic potential increases the current and gives more defined oxidation and reduction peaks. As a result all cycling of FBRR/CPEs was carried out at 100 mV/s between -0.70 and 0.80 V *vs.* SCE.

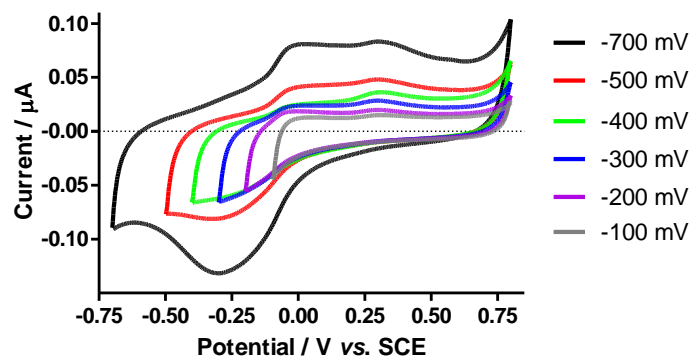


Figure 4.26: CPEs modified at 100 mV/s cycled in PBS through various cathodic potential windows, $n = 4$.

4.2.3.11 Stability of Redox Peaks

A requirement of a successful sensor is that its response remains stable over the time period required for use. A major problem with a lot of existing pH meters is that they tend to drift over time, therefore requiring frequent calibration.³⁰ In order to monitor the stability of the redox peaks obtained when CPEs were modified (LSV and CV) with FBRR/TEABF₄/ACN they were cycled in PBS for 400 cycles, (200 minutes) at 100 mV/s. As the age of the FBRR solution used and the potential range applied during electrodeposition were contributing factors to the resulting redox peaks the above procedure was carried out varying both of these parameters. The CVs resulting from cycling LSV modified CPEs from 0.40 to -0.80 V vs. SCE on days 1-3 are shown in Figure 4.27. Statistical analyses of their anodic and cathodic peak potentials are shown in Table 4.1 along with those obtained when depositing FBRR by CV. The CVs show every 50th cycle corresponding to a time period of 25 minutes. The peak potentials were recorded at this interval and analysed. Deposition of FBRR on days 2 and 3 resulted in peaks with similar currents, whereas FBRR deposited using the fresh solution had reduced currents reinforcing that the optimum days for using the FBRR solution are days 2 and 3. Other potential ranges were investigated in this manner. With regard to the results shown here the deposition of FBRR on day 1 resulted in peaks that were substantially different to those of days 2 and 3. It appears that the reduction peak potential (peak 2) $E_{p_{\text{cathodic}}}$, was more stable after 100 cycles had been applied, whereas the oxidation peak potential (peak 1) $E_{p_{\text{anodic}}}$, was stable from the 50th

cycle. It was also clear that the currents increased with cycling. Again, this was caused by the silicone oil leeching from the CPE.^{11, 29} When this happens it leaves a higher carbon:oil ratio in the paste resulting in a higher electron transfer rate.¹¹ Also the leeching of the binding fluid caused the CPE surface to contract, resulting in an increased surface area and therefore increased currents.

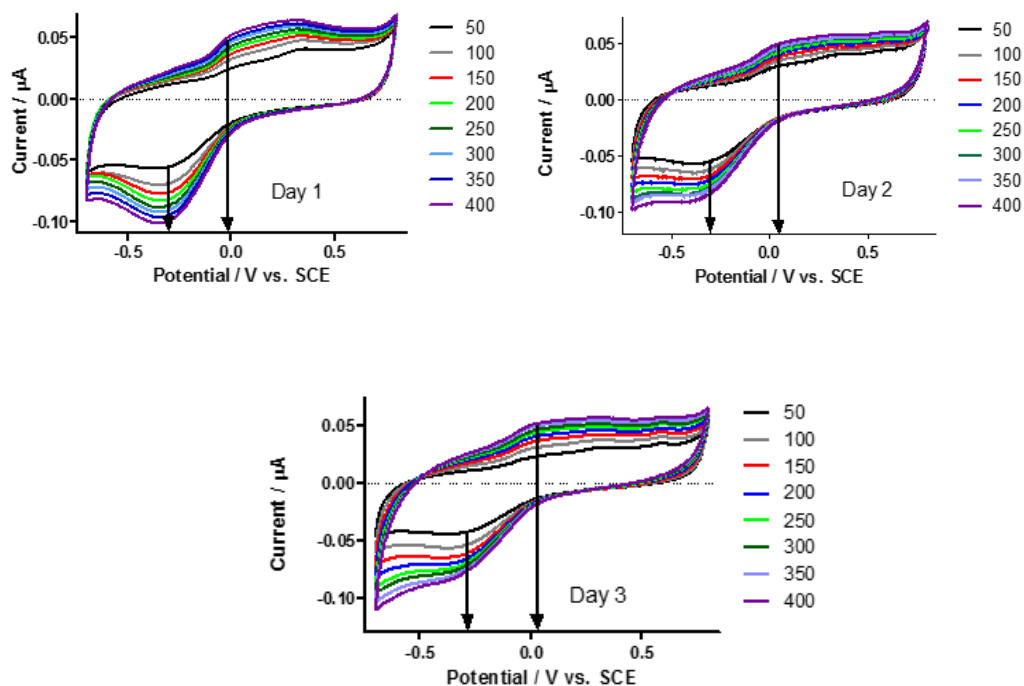


Figure 4.27: Stability of the oxidation and reduction peaks of FBRR deposited from 0.40 to -0.80 V vs. SCE showing 400 cycles on 3 different days..

Table 4.1: Analyses of peak potentials for FBRR/TEABF₄/ACN CPEs modified by LSV and CV.

	Peak	LSV			CV		
		E/V	SEM	<i>n</i>	E/V	SEM	<i>n</i>
Day 1	Ox.	-0.088	0.002	8	-0.03	0.002	16
	Red.	-0.305	0.002	8	-0.276	0.008	16
Day 2	Ox.	0.016	0.002	8	0.017	0.002	16
	Red.	-0.315	0.003	8	-0.302	0.004	16
Day 3	Ox.	0.025	0.002	8	0.025	0.002	8
	Red.	-0.274	0.002	8	-0.274	0.002	8

The typical voltammograms in the potential ranges chosen, at a FBRR/CPE, show pairs of redox peaks. An anodic peak, E_{p_a} , appears at approximately -0.03 V vs. SCE, which corresponds to the oxidation of the FBRR leading to the formation of its equivalent quinone.²⁴ In the reverse scan the cathodic peak, E_{p_c} , appears at approximately -0.30 V vs. SCE.

In order to examine the stability of the FBRR/H₂SO₄ electrodes with cycling and over time modified electrodes were cycled in PBS for 400 cycles. The CVs in Figure 4.28 show that the oxidation peak of interest appears stable at -0.028 ± 0.002 V vs. SCE ($n = 32$). A close up of the highlighted peaks confirmed that the peak was more stable from cycle 100 onwards, so this was the minimum number of cycles undertaken for future testing of FBRR/H₂SO₄ modified CPEs. Again the difference in peak quality is evident when comparing Figures 4.27 (TEABF₄/ACN) and 4.28 (H₂SO₄).

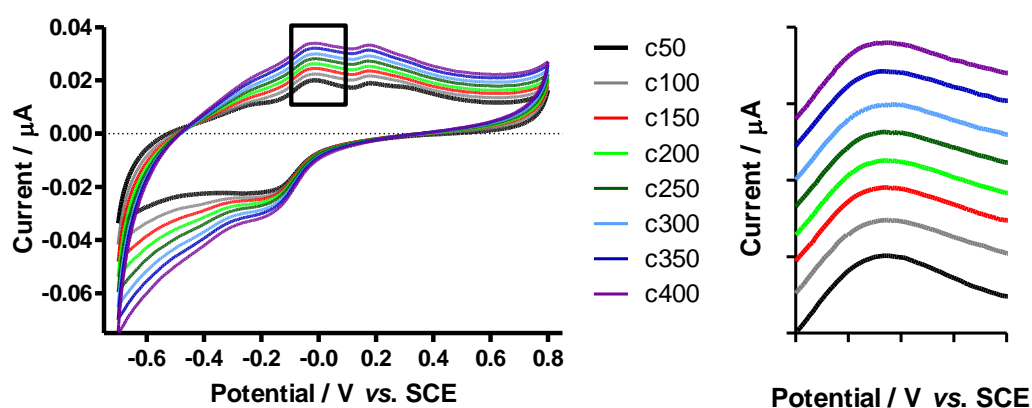


Figure 4.28: Stability of the peak potentials of FBRR/H₂SO₄ modified CPEs over 400 cycles, $n = 4$.

4.2.3.12 Storage of CPEs

Literature has reported that storing CPEs for 12-48 hours prior to use can enhance their performance.⁹ CPEs were prepared and used immediately, stored for 24 hours at room temperature or refrigerated at 4°C for 24 hours before being modified. (FBRR/TEABF₄/ACN). The resulting CVs of the modified electrodes, shown in Figure 4.29(A) with the anodic (B) and cathodic (C) peaks below, conclude that there

was no apparent advantage to storing the CPEs before depositing FBRR/TEABF₄/ACN. It does however show that the peaks appear at different potentials when stored overnight, with CPEs stored having lower potentials than those used immediately, indicating a more favourable oxidation. All electrodeposition used a FBRR solution on day 4 hence, the currents obtained were lower than expected.

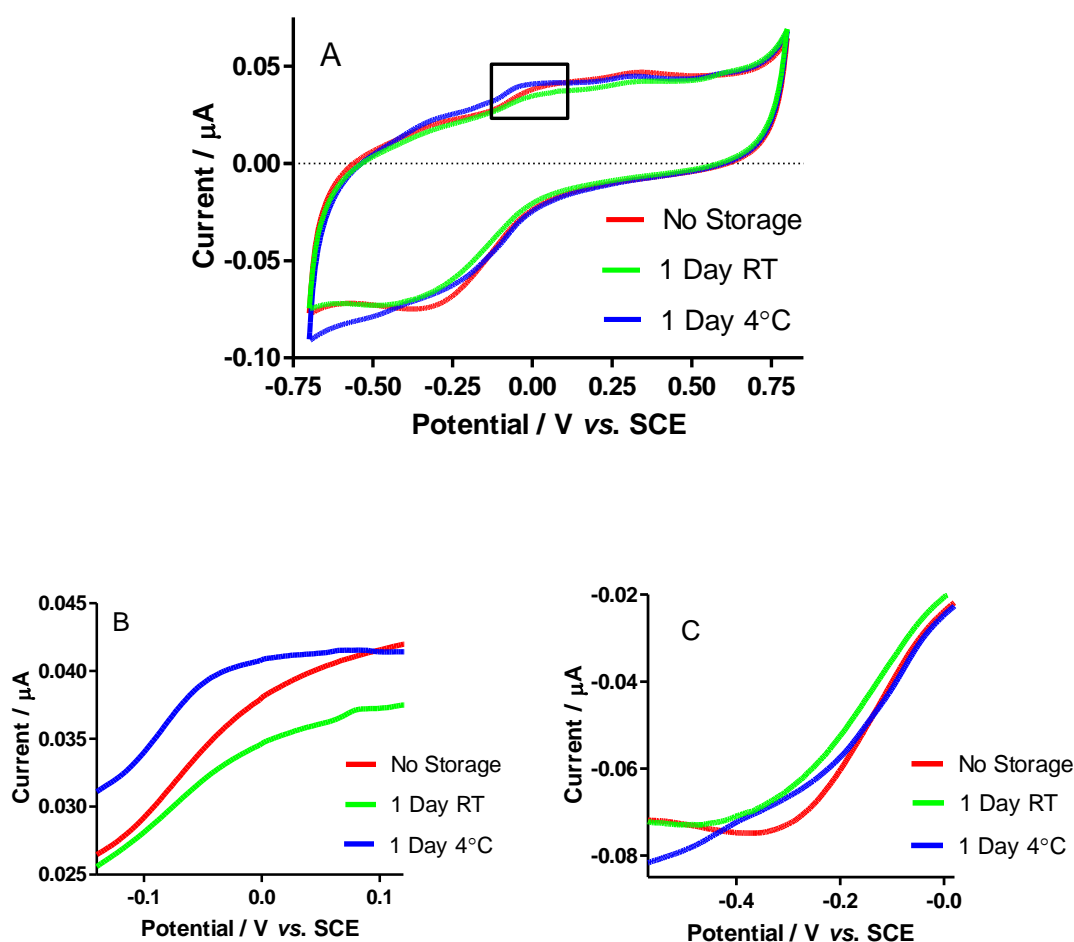


Figure 4.29(A): CVs showing the effect of storing CPEs at room temperature and 4°C before modification with FBRR/TEABF₄/ACN, $n = 4$. Close ups of the redox peaks are shown in (B) and (C) respectively.

Similarly, electrodes were modified with FBRR/H₂SO₄ having been stored at room temperature or refrigerated for 24 hours prior to FBRR electrodeposition. The resulting CVs (100th cycle) are shown in Figure 4.30 and also include the results for CPEs prepared and modified on the same day. These were stored at room temperature until

they were cycled. The most defined oxidation peak results from electrodes prepared and modified on the same day. Electrodes stored at room temperature resulted in broad ill-defined anodic peaks. When storing CPEs before use it is recommended that they are stored in distilled water.⁴⁴ The storage conditions employed in this section resulted in the “drying out” of the CPE.

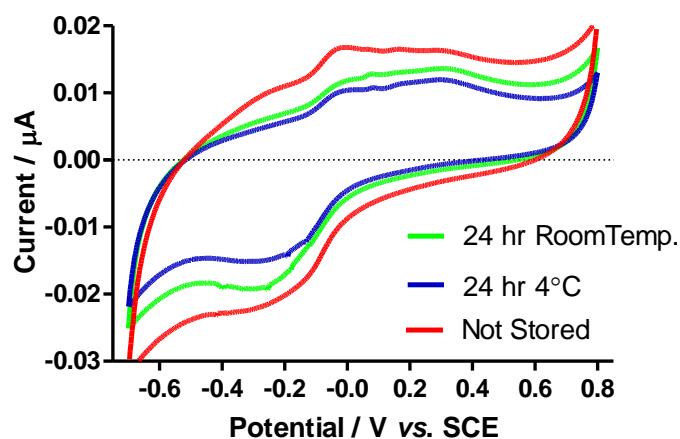


Figure 4.30: Effect of storing bare CPEs prior to electrodeposition of FBRR, $n = 12$.

When depositing FBRR from 0.1 M TEABF₄/ACN it was found that storing the bare CPE at room temperature overnight had no effect on the deposition. With the acid as solvent, better results were obtained when the electrodes were modified immediately after preparation as the formation of the oil layer on the surface may decrease the interaction between the organic layer and the aqueous solution therefore resulting in a reduction in the amount of FBRR deposited onto the carbon. Whereas when a layer of oil forms over the surface of the FBRR/TEABF₄/ACN modified electrode it allows the adsorption of FBRR from the organic solution.⁴⁵

4.2.3.13 Storage of Modified CPEs

To examine the effect of storage on the FBRR/TEABF₄/ACN CPEs, modified electrodes were either used immediately or stored overnight at room temperature or at 4°C before being cycled in PBS. The resulting CVs are shown in Figure 4.31. These

show that although storing the modified electrodes at 4°C gives better currents, the reduction peak was evident at a more negative potential, -0.45 V vs. SCE.

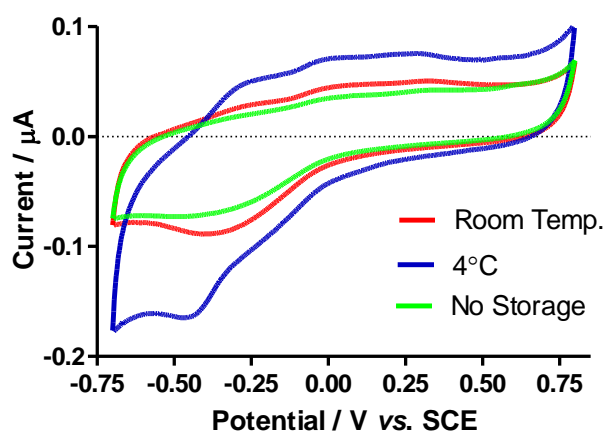


Figure 4.31: CVs showing the effect of storage on FBRR/ TEABF₄/ACN CPEs $n = 4$.

The resulting CVs for FBRR/H₂SO₄ electrodes are shown in Figure 4.32. They demonstrate that there is no advantage to storing the CPEs before depositing FBRR, in fact those stored at 4°C have lower current responses. This is because at temperatures below 5°C the reaction producing the aryl radical and anion has been slowed down.^{18,}

³⁴ All results here have used FBRR on day 2.

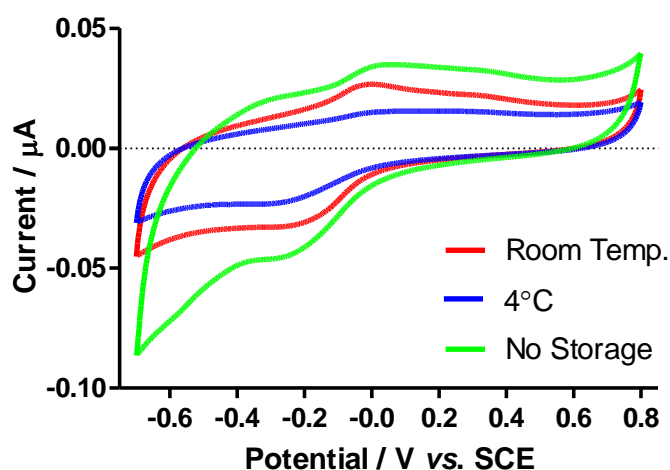


Figure 4.32: CVs showing the effect of storage of CPEs on FBRR/H₂SO₄ modified electrodes cycled in PBS pH 7.4, $n = 4$.

4.2.3.14 FBRR/H₂SO₄ Storage

Previously the FBRR/H₂SO₄ solution was always refrigerated when not in use. In order to investigate whether these were the optimum storage conditions a solution of 2 mM FBRR was prepared in 0.1 M H₂SO₄ and stored at room temperature. Because day 2 and 3 had previously been identified as giving the best results, the solution was prepared 24 hours before use. Solution A was stored in the refrigerator at 4°C. Solutions B and C were stored at room temperature. The resulting CVs are shown in Figure 4.33. Whereas there was no distinct difference between storage methods on day 2 (A), it was clear that storing the FBRR/H₂SO₄ solution at 4°C clearly prolonged the life of the solution by day 3 (B).

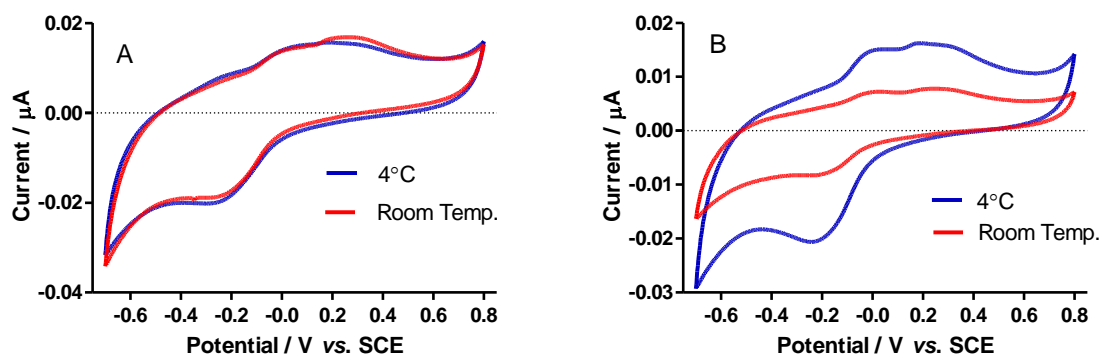


Figure 4.33: Resulting CVs from FBRR/H₂SO₄ solutions stored at either room temperature or 4°C, deposited on (A) day 2 and (B) day 3, $n = 8$.

The images in Figure 4.34 show how the salt fell out of solution when the FBRR/H₂SO₄ was stored at room temperature. After depositing FBRR on day 2, Figure 4.34(A), the solution still appeared pale yellow but upon agitation the salt did not go back into solution. After depositing FBRR on day 3, Figure 4.34(B), the solution was almost clear, again the salt did not go back into solution after stirring or sonication. In order to examine whether the electro-reduction caused the salt to fall from solution, a solution of FBRR/H₂SO₄ was stored for 3 days at room temperature. This solution was not used for any electrodeposition experiments. Again it can be seen that the salt fell from the solution and upon stirring did not go back into solution. In

contrast a solution refrigerated for 3 days slightly fell out of solution but upon stirring appeared to return to normal.



Figure 4.34: FBRR/H₂SO₄ solutions stored at room temperature and used for deposition on (A) day 2 and (B) day 3. Image (C) shows a solution stored for 3 days at room temperature not used for deposition.

4.2.3.15 pH Response

This chapter so far has detailed the parameters affecting the sharpness, stability and reproducibility of the redox peaks of FBRR/TEABF₄/ACN and FBRR/H₂SO₄ CPEs. In order to examine the pH response using the optimum conditions obtained the modified electrodes were cycled in PBS of pH 7.2, 7.4 and 7.6, the pH being altered using NaOH or NaH₂PO₄ as required. The oxidation/reduction reaction of FBRR involves a 2e⁻/2H⁺ exchange, so according to the Nernst equation when cycling FBRR modified electrodes in solutions of various pH an ideal Nernstian response of -59 mV/pH should be obtained.

Figure 4.35 shows modified CPEs, (TEABF₄/ACN), cycled for 50 cycles, in each pH PBS solution ($n = 4$). Figure A shows electrodes cycled in PBS (50th cycle) of pH 7.4 first followed by 7.2 and 7.6. Figure B shows electrodes cycled in order of increasing pH, 7.2, 7.4 and 7.6 (50th cycle).

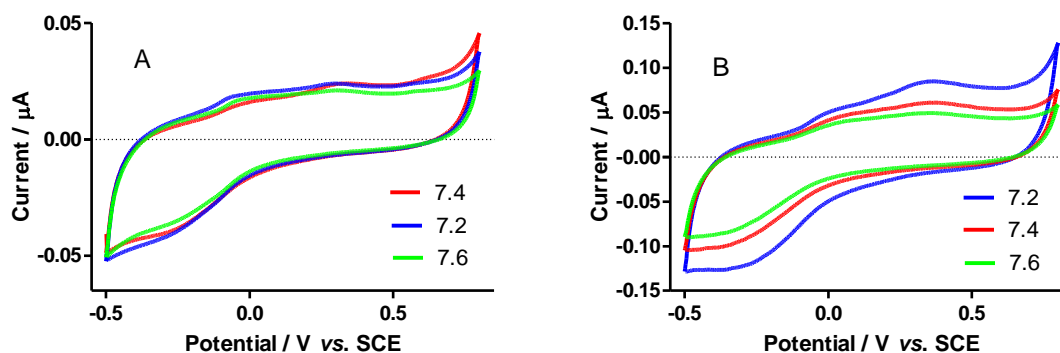


Figure 4.35: CVs of FBRR/CPEs (TEABF₄/ACN) cycled in PBS pH 7.2, 7.4 and 7.6. The order of cycling was specified as (A) 7.4, 7.2, 7.6 and (B) 7.2, 7.4, 7.6, $n = 4$.

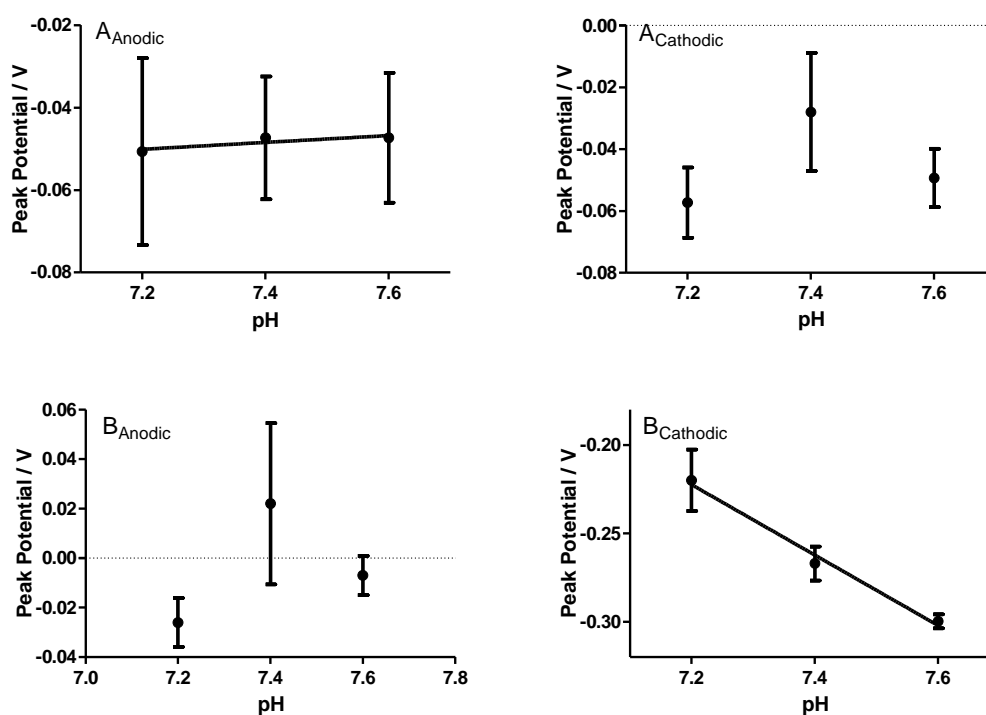


Figure 4.36: pH responses, anodic and cathodic, of FBRR/CPEs (TEABF₄/ACN), varying the order of the solution pH, $n = 4$.

Analyses of the peak potential responses to pH are also shown. As stated above a Nernstian response suggests an ideal pH response of -59 mV/pH unit . The responses displayed in Figure 4.36 show that the pH does not change with potential as expected,

for either the oxidation or reduction peaks. There are huge variations in the potential responses and large inter-electrode variabilities, shown in Table 4.2. Electrodes cycled in PBS pH 7.4, followed by 7.6 and 7.2 resulted in pH responses of +8 mV/pH for the anodic peak and a non-linear response for the cathodic peak whereas those cycled in order of increasing pH gave a non-linear response for the anodic peaks and a response of -20 mV/pH unit for the cathodic peaks. A possible source for these errors and non-linear pH responses was the formation of multilayers of FBRR onto the electrode surface. This was further corroborated by the CVs in Figure 4.35, where the broad peaks are indicative of a slow electron transfer due to an increased diffusion layer thickness.

Table 4.2: Summary of the pH responses of the anodic and cathodic peaks of FBRR/CPEs (TEABF₄/ACN).

pH Order	pH Response (Anodic)/mV	R ²	pH Response (Cathodic)/mV	R ²
7.4, 7.6, 7.2	+8.33	0.7500	Non-linear	_____
7.2, 7.4, 7.6	Non-linear	_____	-19.94	0.9895

As the results from this section were particularly poor it could not be determined whether the order of cycling in each pH PBS solution had any effect on the resulting peak potentials. From this point the order of cycling was randomly assigned in order to eliminate any possible hysteresis effects.

Various conditions for the deposition of FBRR onto CPEs, and their subsequent storage, were examined to see whether or not the modified electrodes had a Nernstian response (-59 mV/pH) to pH changes. These parameters included the age of the FBRR solution, the deposition scan rate and potential window applied during deposition, the number of deposition cycles, the potential range and scan rate used during cycling the modified CPEs and the storage conditions for bare and modified CPEs. An example of the resulting CVs is shown in Figure 4.37 with close-up images of the anodic and cathodic peaks. In the example shown FBRR/H₂SO₄ was electrodeposited on day 3 by CV, 2 cycles, from 0.40 to -0.80 V vs. SCE at 100 mV/s and subsequently cycled from

-0.70 to 0.80 V vs. SCE at 100 mV/s. The anodic peak response was -40 ± 0.1 mV/pH ($R^2 > 0.99$) and the cathodic peak response was -43 ± 17 mV/pH ($R^2 = 0.86$). The order of PBS pH was randomly chosen in all experiments in order to eliminate any hysteresis effects. A comprehensive set of the pH responses resulting from the aforementioned variables, from electrodes modified by CV in H_2SO_4 , is shown in Table 4.3. It shows the inconsistency in the pH responses obtained and also a wide range of errors between the individual modified electrodes.

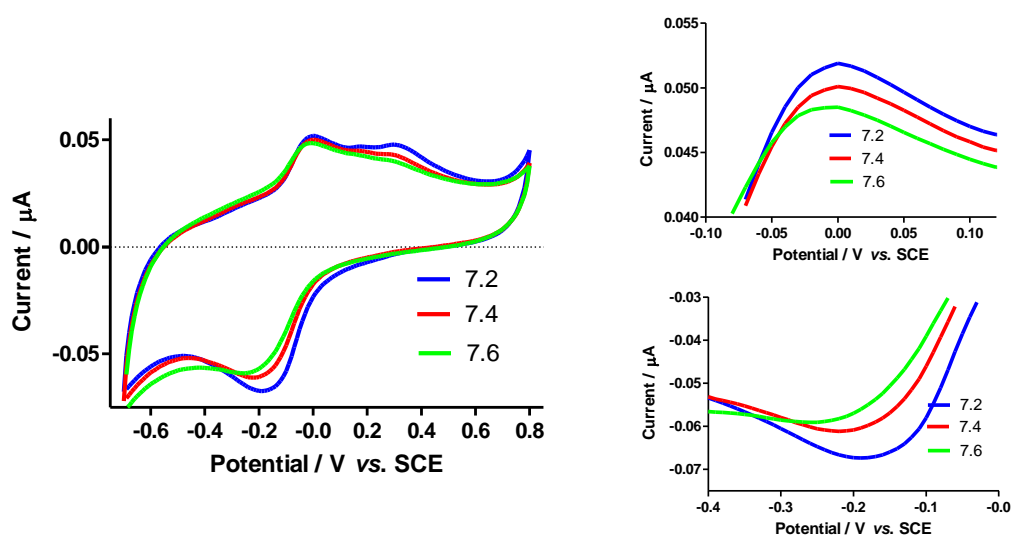


Figure 4.37: CV of the response to pH for FBRR/ H_2SO_4 CV modified CPEs with close-ups of the anodic and cathodic peaks, $n = 4$.

Table 4.3: pH responses of FBRR/H₂SO₄ CV modified CPEs under various deposition and cycling conditions.

Variable		Day FBRR	Oxidation			Reduction	
			Slope (mV/pH)	R ²	n	Slope (mV/pH)	R ²
Scan Rate (mV/s)	20	1	-127 ± 75	0.740	4	27 ± 10	0.885
	50	4	-73 ± 6	0.994	4	-28 ± 4	0.976
	100	1	-106 ± 6	0.996	4	-8 ± 7	0.519
	200	1	-28 ± 99	0.076	4	-6 ± 4	0.996
	500	1	-110 ± 19	0.912	4	-28 ± 4	0.976
Deposition Potential (V vs. SCE)	0.40/-1.00	2	-58 ± 5	0.993	4	-83 ± 24	0.367
	0.40/-0.80	3	-60 ± 2	0.997	4	-76 ± 12	0.876
	0.40/ -0.60	3	-95 ± 4	0.998	4	-55 ± 3	0.997
Number of Cycles	1	1	-44 ± 18	0.855	4	-43 ± 17	0.858
	2	3	-40 ± 0.1	1.000	4	-75 ± 1	0.999
	5	3	-43 ± 21	0.807	4	-75 ± 1	0.999
	10	3	-45 ± 12	0.925	4	-74 ± 2	0.978
Potential Range (V vs. SCE)	-0.50/0.50	2	-53 ± 2	0.999	4	-75 ± 5	0.996
	-0.70/0.80	2	-87 ± 8	0.992	4	-23 ± 15	0.697
Storage of CPEs (24 Hours)	22°C	2	-68 ± 13	0.968	4	-60 ± 4	0.996
	4°C	2	-100 ± 6	0.997	4	-38 ± 53	0.330
Storage of Modified CPEs (24 Hours)	22°C	1	-75 ± 3	0.999	4	-60 ± 9	0.980
	4°C	1	-5 ± 6	0.429	4	-50 ± 25	0.800
	Freezer	1	-91 ± 34	0.879	4	-15 ± 56	0.066

From Table 4.3 the most reliable pH response was obtained when depositing FBRR/H₂SO₄ from an anodic potential of 0.40 V *vs.* SCE to -0.80/-1.0 V *vs.* SCE. The optimum deposition conditions achieved throughout this chapter were then applied for CPE modification, i.e., LSV from 0.1 M H₂SO₄, from 0.40 to -0.80 V *vs.* SCE at 100 mV/s. The resulting CVs for both the 50th (A) and 100th (B) cycles are shown in Figure 4.38 with the insets showing close-up views of the anodic peaks of interest. They clearly show a shift in the peak potential on changing the pH of the PBS solution between 7.2 and 7.6.

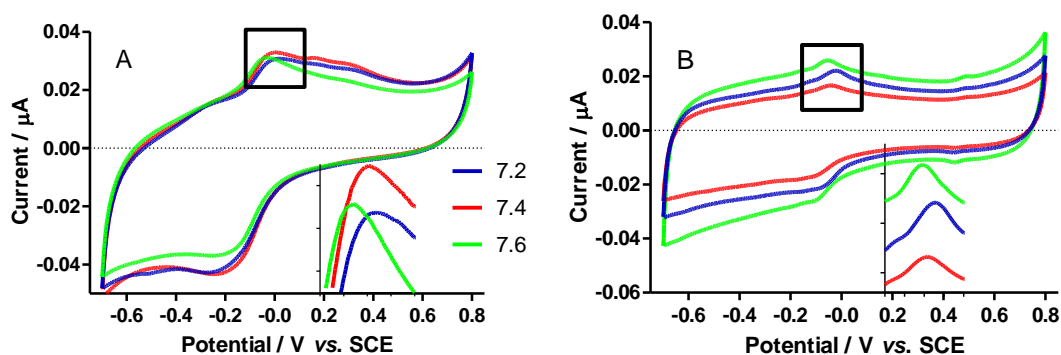


Figure 4.38: CVs of the variation of peak potential with changing pH having cycled the FBRR/H₂SO₄ modified CPEs for 50 cycles (A) and 100 cycles (B), $n = 4$.

The corresponding pH responses of the modified CPEs are shown in Figure 4.39. Having cycled the modified CPEs for 50 cycles (A) before each peak potential was recorded resulted in a straight line graph with a slope (pH response) of -72 ± 5 mV/pH, $R^2 > 0.99$, $n = 12$. This is substantially higher than the ideal Nernstian response of -59 mV/pH. After 100 cycles (B) the pH response and errors were substantially reduced to -59 ± 3 mV/pH, $R^2 > 0.99$, $n = 39$. These results confirmed that CPEs modified by LSV with FBRR/H₂SO₄ required 100 cycles before recording their peak potentials.

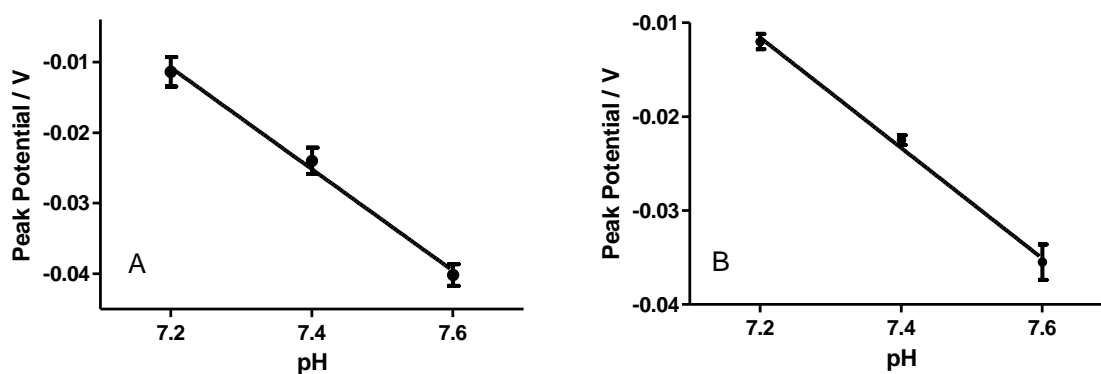


Figure 4.39: pH responses of FBRR/H₂SO₄ modified CPE cycled for 50 cycles (A) and 100 cycles (B), $n = 4$.

4.2.3.16 Second Oxidation Peak

When the modified electrodes were recycled in PBS a second oxidation peak at *ca.* 0.35 V *vs.* SCE was apparent, see Sections 4.2.2.1-2. The currents for this peak increased at a slower rate than the first (quinone) oxidation peak with cycling, and after 400 cycles were no longer distinguishable. In order to identify this peak the modified electrodes were held under different conditions. The electrodes were rinsed, immediately after FBRR deposition, with H₂O, ACN and N₂ saturated ACN to remove any loosely bound molecules that may be present. The resulting CVs are shown in Figure 4.40. The electrodes that were rinsed under the above mentioned conditions gave far inferior responses on cycling and the second oxidation peak was still evident (inset).

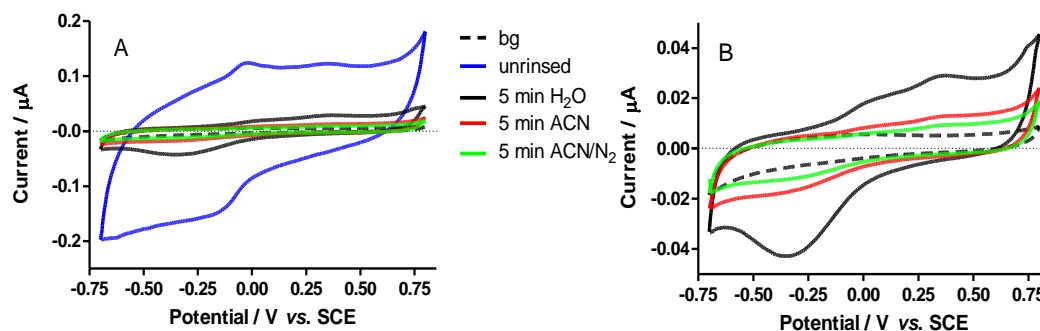


Figure 4.40: (A) CVs showing an unrinsed and various rinsing methods for a CPE after FBRR deposition. (B) The resulting CVs for various rinsed modified CPEs, $n = 4$.

The FBRR salt used in the experiments contains ZnCl_2 (4-Benzoylamino-2, 5-dimethoxybenzenediazonium chloride hemi zinc chloride). To examine whether or not the second peak could result from the ZnCl_2 various concentrations of ZnCl_2 were dissolved in 0.1 M $\text{TEABF}_4/\text{ACN}$ and electrodeposited onto CPEs by cycling between 0.40 and -0.80 V vs. SCE at 100 mV/s for 10 cycles. The electrodes were then cycled in PBS. The resulting CVs are shown in Figure 4.41. There is a second oxidation peak evident for 0.5, 1 and 2 mM ZnCl_2 . The 5 mM sample did not fully dissolve into solution. 1 mM is the corresponding amount of ZnCl_2 contained in 2 mM FBRR solution.

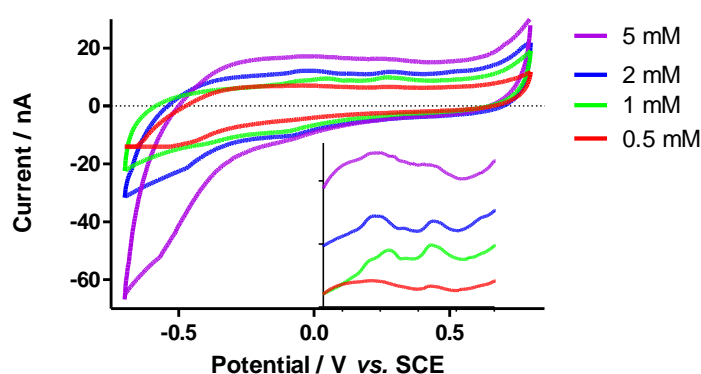


Figure 4.41: CVs showing various concentrations of ZnCl_2 in 0.1 M $\text{TEABF}_4/\text{ACN}$ and a close up of the oxidation peaks in the inset, $n = 4$.

A calibration curve of the concentration of ZnCl_2 against the peak current obtained was plotted and is shown in Figure 4.42. The relationship is not linear over the full range of concentrations used, but the inset shows good linearity between 0.5 and 2 mM ($R^2 > 0.99$). A method to diminish the effect of ZnCl_2 on the resulting CVs will be discussed later in this chapter, Section 4.3.5.11.

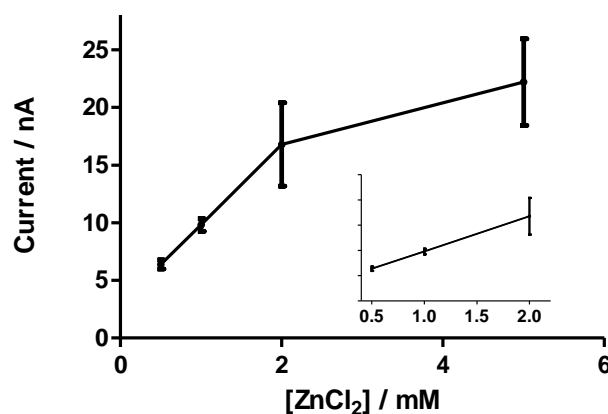


Figure 4.42: Calibration curve showing the response of various concentrations of ZnCl_2 in 0.1 M $\text{TEABF}_4/\text{ACN}$ electrodeposited onto CPEs, $n = 4$.

4.2.3.17 Mitigation of ZnCl_2

It has been confirmed throughout this section that FBRR deposited after day 1 gave the best results. It was thought that the ZnCl_2 might deposit onto the electrode more readily than the FBRR therefore blocking available sites on the electrode surface. “Pre reducing” the solution onto bare CPEs would reduce more ZnCl_2 onto the first set of electrodes; therefore in subsequent reductions less ZnCl_2 would deposit and so more sites for the FBRR to covalently bond onto the electrode surface would be available. If this was the case then Zn, although in small concentrations, would be more readily visible with EDX on the electrodes used for the “pre reduction”. Previous EDX rarely found Zn on the electrode surface, most notably from LSV reduction. However, the presence of zinc is evident from the EDX in Figure 4.44 which is shown alongside the corresponding SEM micrograph in Figure 4.43.

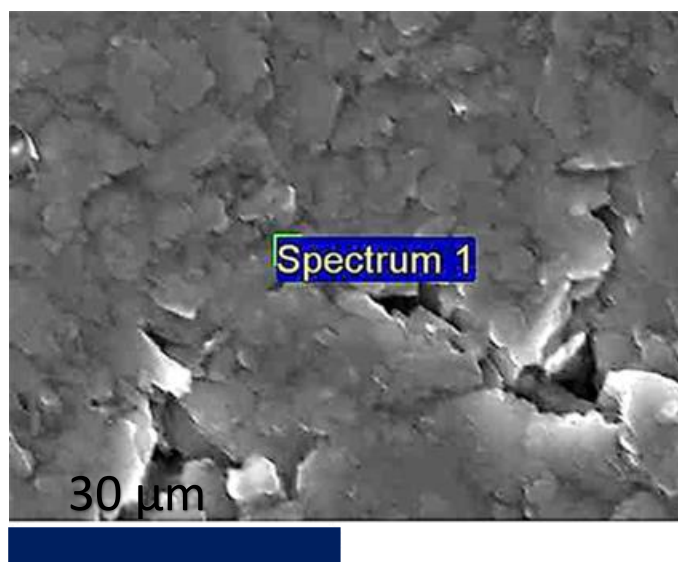


Figure 4.43: SEM micrograph from the first set of CPEs modified with FBRR/H₂SO₄ showing evidence of zinc deposition onto the surface.

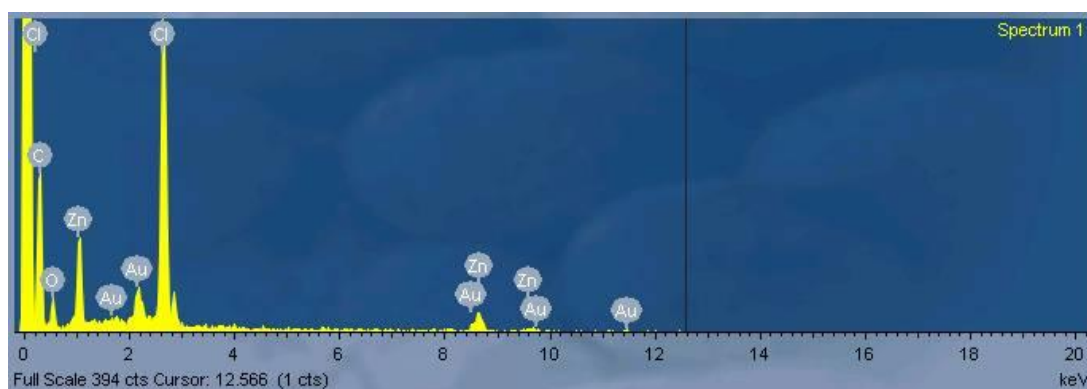


Figure 4.44: EDX from the first set of CPEs modified with FBRR/H₂SO₄ showing evidence of zinc deposition onto the surface.

As the results obtained when depositing FBRR/H₂SO₄ onto a CPE on day 1 were consistently poor, the solution was prepared as normal but stored in the refrigerator at 4°C overnight before being used for LSV electrodeposition on day 2. Figure 4.45 shows that this still resulted in poorly defined peaks (inner, dashed line). The same solution was used later that day, for deposition of FBRR by LSV (5 sweeps, from 0.40 to -0.80 V vs. SCE at 100 mV/s). This resulted in far superior results. Similar redox peaks were obtained when a FBRR/H₂SO₄ solution was “pre-reduced” by CV. It was therefore confirmed that the FBRR/H₂SO₄ solution required several pre-reduction

sweeps in order to obtain well defined peaks, so all future FBRR/H₂SO₄ solutions were “pre reduced” onto 4 CPEs by sweeping from 0.40 to -0.80 V vs. SCE at 100 mV/s for 5 sweeps before being used for any further studies.

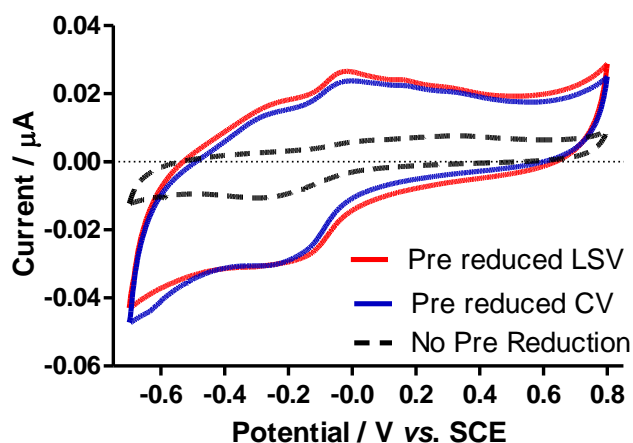


Figure 4.45: Effect of “pre-reducing” the FBRR solution (LSV and CV) onto 4 CPEs prior to electrodeposition on CPEs used for analysis, $n = 4$.

4.2.3.18 Real-Time pH Response

In the previous section the pH response of FBRR/H₂SO₄ modified CPEs was enhanced by cycling the electrodes for 100 cycles before recording the peak potentials. This gave the pH sensor an extremely long response time, one which would not be suitable for a marketable product. A contributing factor was that the electrodes were withdrawn from the N₂ saturated solutions for several seconds in order to change the solution to one with a different pH and it took several cycles for the electrodes to return consistent, stable CVs. In an attempt to reduce the settling period before recordings could be made a set-up whereby the modified CPEs were not removed from the solution between recordings was designed.

The pH response of CPEs modified with FBRR/H₂SO₄ by LSV was tested in N₂ saturated PBS with a pH between 7.2 and 7.6. The modified electrodes were cycled for either 50 or 20 cycles to settle before any peak potentials were observed. A commercial, glass pH probe was used to monitor the pH of the PBS solution while it

was altered by dropping small amounts of either 0.5 M NaOH or 0.5 M NaH₂PO₄. After the pH was altered the solution was stirred vigorously for a few seconds then the electrodes were cycled for a further 50 or 20 cycles before the peak potential and pH were recorded. During cycling the solution was slowly stirred to eliminate the possibility of pH drift. The magnetic stirrer was set to spin at approximately 45 rev/min. The results for both settling periods are shown in Figure 4.46. They show pH responses of -61 ± 3 mV/pH ($R^2 = 0.97$, $n = 4$) for 50 cycles (A) and -57 ± 2 mV/pH ($R^2 = 0.92$, $n = 16$) for 20 cycles (B). These results substantially improved the response time of the pH sensor.

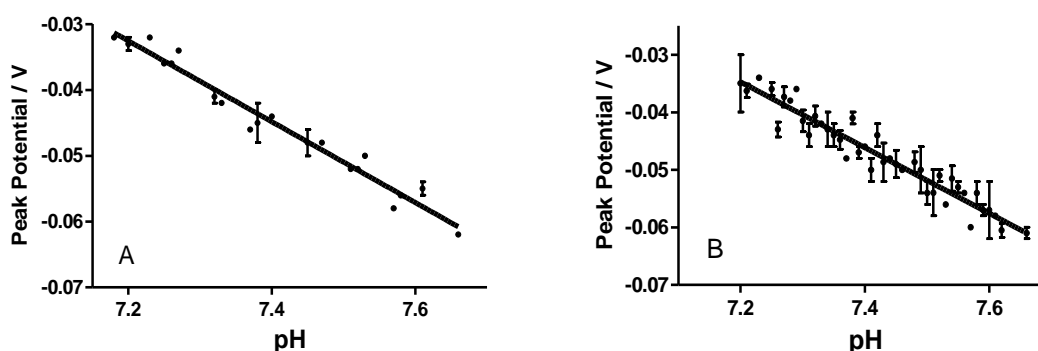


Figure 4.46: Real-time pH response of FBRR/CPEs with peak potentials recorded every 50 (A) and 20 (B) cycles, $n = 4$.

4.2.3.19 Changing pH Using a Constant Flow Rate Pump System

Tissue pH in living organisms is tightly regulated and should be maintained close to a value of 7.4.⁴⁶ As this pH sensor was designed to record physiological pH changes it needed to be sensitive to within 0.01 pH units between pH values 7.2 to 7.6. To test the sensitivity of the FBRR/H₂SO₄ electrode in a real-time situation CPEs were modified with FBRR as in Section 4.2.2.18. A similar setup to the real time study was used except a micro pump with a constant flow rate of 5 μ l/min was incorporated in order to change the pH of the PBS. The electrodes were allowed to settle for 50 cycles prior to any pH recordings. Either 0.5 M NaOH or 0.5 M NaH₂PO₄ was used to gradually change the pH. The CV was continuously recorded between the two pH

limits (7.20 and 7.60) while the solution was slowly stirred (45 rev/min). The cycle number and time were noted on each pH change of 0.01 pH units. The peak potentials were extrapolated after the experiment was completed. The results are shown in Figure 4.47 and show that the FBRR/CPE had a sensitivity of -56 ± 1 mV/pH ($R^2 > 0.95$, $n = 4$). The error bars in Figure 4.47 correspond to *ca.* 2 mV, which is equivalent to 0.03 pH units. These results demonstrated that the FBRR/H₂SO₄ modified CPE continuously measured pH changes *in-vitro*.

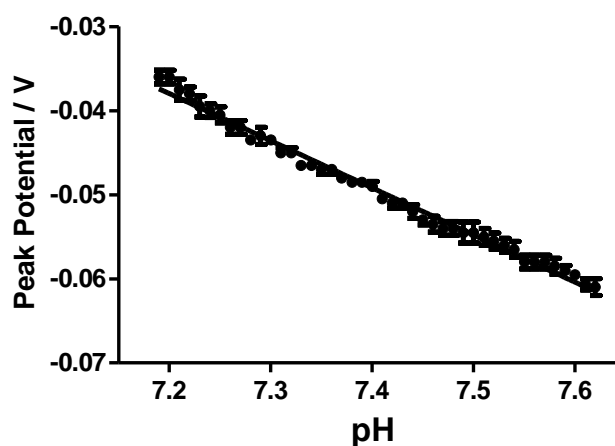


Figure 4.47: pH response of FBRR/CPEs using a controlled flow micro pump system to alter pH, $n = 4$.

4.2.3.20 Observation

It was observed throughout this chapter that modified CPEs exhibited inconsistent currents during cycling, demonstrated in Figure 4.48 which shows four CPEs (A-D) modified by CV in 0.1 M H₂SO₄, having been stored and cycled in PBS using the same conditions. These discrepancies are most likely a problem inherent with CPEs. Various currents are obtained due to the inconsistent compactness of the paste in the cavity caused by the manual packing of the paste,⁹ resulting in varied coverage of the adsorbed species onto the electrode surface between experiments.³⁹ The rougher surface may in fact result in more FBRR becoming embedded within the layers of the carbon paste. In the example shown below there is a shift in potential over the four modified CPEs. This would account for the large errors often found throughout this section.

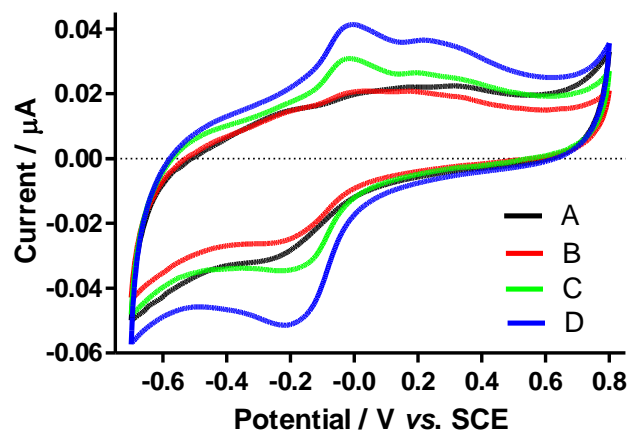


Figure 4.48: Example of the wide range of CVs obtained from FBRR/H₂SO₄ modified CPEs.

4.3 Conclusion

Throughout this chapter the modification of CPEs with FBRR was examined using either organic or aqueous solvents and varying the deposition technique between CV and LSV. Several deposition and CV parameters were investigated in order to achieve consistent, reproducible redox peaks with Nernstian pH responses. When depositing FBRR by LSV, using TEABF₄/ACN as the supporting electrolyte, it was confirmed that FBRR had deposited onto the electrode surface although the redox peaks were broad and ill-defined, indicative of slow electron transfer. This could result from the presence of the non-conducting silicon oil in the CPE or due to the formation of multi-layers of FBRR on the surface, increasing the diffusion layer thickness. This hindered the ability to precisely locate the peak potentials that were necessary to analyse the pH response. During testing it became apparent that the anodic peak gave more stable, consistent potential readings. The age of the FBRR solution at the time of electrodeposition greatly influenced the resulting redox peaks. When the functionalised CPEs were tested for their pH response, inconsistent non Nernstian values were obtained. Depositing FBRR onto CPEs proved more successful when electro-reduced by CV rather than LSV. The anodic peaks obtained resulted in a pH response that was relatively close to Nernstian values, see Table 4.4.

The electrodeposition of FBRR onto CPEs by CV using 0.1 M H₂SO₄ as the supporting electrolyte was also examined. The presence of FBRR on the CPEs was confirmed but the redox peaks remained relatively broad indicative of slow electron transfer. The pH sensitivities obtained gave some responses that were near Nernstian but were inconsistent, with a large inter-electrode variability. The best results obtained are included in Table 4.4. When depositing FBRR/H₂SO₄ by LSV the anodic peaks were consistently sharper and when analysed gave Nernstian pH responses of -59 mV/pH (see Table 4.4). Real-time pH studies were performed yielding linear responses with Nernstian values and reduced errors. The modification of CPEs with FBRR had successfully been optimised to produce a pH sensor capable of the real-time recording of pH changes *in-vitro*.

A second oxidation peak that was evident in many CVs was investigated as it was thought to interfere with the efficient deposition of FBRR when using a freshly prepared solution and it was concluded that it resulted from the ZnCl_2 present in the salt. A method to eliminate the effect of ZnCl_2 was performed when depositing from freshly prepared FBRR solutions.

Table 4.4: pH sensitivities for FBRR/CPEs using the electrochemical techniques of CV and LSV in organic and aqueous solutions.

ELECTROCHEMICAL TECHNIQUE	SUPPORTING ELECTROLYTE	pH RESPONSE (mV/pH)	SEM	<i>n</i>
LSV	0.1 M TEABF ₄ /ACN	-20	4.1	4
CV	0.1 M TEABF ₄ /ACN	-74	0.7	4
CV	0.1 M H ₂ SO ₄	-60	2.0	4
LSV	0.1 M H₂SO₄	-59	3.0	39

Using an aqueous solvent proved more beneficial to the final electrode design. The organic solvent, TEABF₄/ACN, has a similar polarity to the silicone oil contained in the CPEs. This causes the removal of some oil from the electrode surface leaving it more carbon-like which facilitates the reduction of FBRR onto the substrate, possibly forming multi-layers. The aqueous solvent, H₂SO₄, being opposite in polarity to the silicone oil, has no effect on the electrode surface. It is likely that less FBRR deposits onto the substrate, this is evident by the lower currents obtained when cycling FBRR/H₂SO₄ modified electrodes in PBS. Monolayers of FBRR are more likely to result, meaning a thinner diffusion layer is formed, facilitating electron transfer at the electrode surface. This was confirmed by the sharper redox peaks.

4.3.1 Final Design of Optimised CPE/FBRR pH Sensor

- Prepare CPE as described in Section 2.3.1, for best results use on day of manufacture.
- Prepare 2 mM solution of FBRR in 0.1 M H₂SO₄. Store at 4°C when not in use.
- N₂ saturate FBRR/H₂SO₄ prior to use.

- Pre-reduce FBRR onto 4 CPEs (LSV 5 sweeps, 0.40 to -0.80 V vs. SCE at 100 mV/s) and disregard.
- Electro-reduce FBRR onto CPEs (LSV 5 sweeps, 0.40 to -0.80 V vs. SCE at 100 mV/s).
- Cycle modified CPEs in N₂ saturated PBS for 100 cycles to stabilise (-0.70 to 0.80 V vs. SCE at 100 mV/s). This number of cycles can be reduced if the electrodes are not withdrawn from the solution between pH changes.
- Store at 4°C if required, see Section 5.3.1.1.

Figure 4.3.5.15 shows the CV for FBRR/CPEs prepared using the optimum conditions obtained in this section. The pH sensitivities were then determined using three different methods as described in Sections 4.3.5.12-14, all resulting in linear responses with near Nernstian values and small errors.

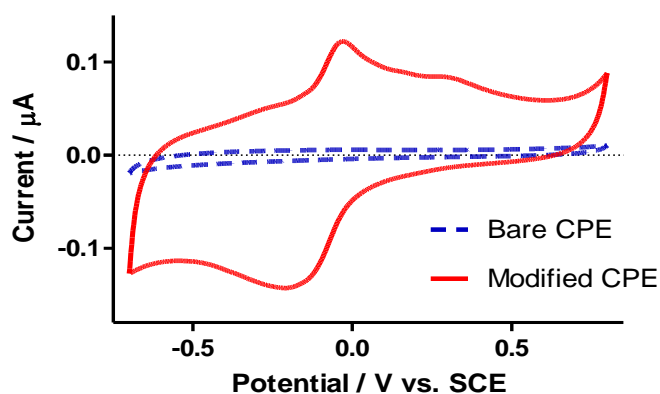


Figure 4.3.5.15: CVs comparing bare CPEs with those modified with FBRR using the optimum deposition and cycling parameters obtained throughout Chapter 4.

These conditions were the best design achieved for the development of FBRR/CPE voltammetric pH sensors. As the pH responses obtained had near Nernstian values of -59 mV/pH it was concluded that FBRR/CPEs had been developed that could successfully detect changes in pH to within 0.01 pH units in the *in-vitro* environment.

4.4 References

1. H. C. Leventis, I. Streeter, G. G. Wildgoose, N. S. Lawrence, L. Jiang, T. G. J. Jones and R. G. Compton, *Talanta*, 2004, **63**, 1039-1051.
2. A. J. Downard, *Electroanalysis*, 2000, **12**, 1085-1096.
3. K. Kalcher, I. Svancara, M. Buzuk, K. Vytras and A. Walcarius, *Monatshefte für Chemie*, 2009, **140**, 861-889.
4. H. Kahlert, *Journal of Solid State Electrochemistry*, 2008, **12**, 1255-1266.
5. R. N. Adams, *Analytical Chemistry*, 1958, **30**, 1576.
6. I. Svancara, M. Hvizdalova, K. Vytras, K. Kalcher and R. Novotny, *Electroanalysis*, 1996, **8**, 61-65.
7. J. Wang, T. Martinez, D. R. Yaniv and L. McCormick, *Journal of Electroanalytical Chemistry Interfacial Electrochemistry*, 1990, **286**, 265-272.
8. T. Mikysek, M. Stoces, I. Svancara and J. Ludvik, *RSC Advances*, 2012, **2**, 3684-3690.
9. I. Svancara and K. Schachl, *Chemické Listy*, 1999, **93**, 490-499.
10. I. Svancara, K. Vytras, K. Kalcher, A. Walcarius and J. Wang, *Electroanalysis*, 2009, **21**, 7-28.
11. K. Kalcher, J. M. Kauffmann, J. Wang, I. Svancara, K. Vytras, C. Neuhold and Z. Yang, *Electroanalysis*, 1995, **7**, 5-22.
12. Q. J. Chi, W. Gopel, T. Ruzgas, L. Gorton and P. Heiduschka, *Electroanalysis*, 1997, **9**, 357-365.
13. K. Kalcher, *Electroanalysis* 1990, **2**, 419-433.
14. M. E. Rice, Z. Galus and R. N. Adams, *Journal of Electroanalytical Chemistry Interfacial Electrochemistry*, 1983, **143**, 89-102.
15. H. Salehzadeh, D. Nematollahi, V. Khakyzadeh, B. Mokhtari and L. C. Henderson, *Electrochimica Acta*, 2014, **139**, 270-280.
16. M. Delamar, R. Hitmi, J. Pinson and J. M. Saveant, *Journal of the American Chemical Society*, 1992, **114**, 5883-5884.
17. B. Ortiz, C. Saby, G. Y. Champagne and D. Belanger, *Journal of Electroanalytical Chemistry*, 1998, **455**, 75-81.
18. J. Pinson and F. Podvorica, *Chemical Society Reviews*, 2005, **34**, 429-439.
19. J. J. Gooding, *Electroanalysis*, 2008, **20**, 573-582.

20. D. Belanger and J. Pinson, *Chemical Society Reviews*, 2011, **40**, 3995-4048.
21. M. A. Makos, D. M. Omiatek, A. G. Ewing and M. L. Heien, *Langmuir*, 2010, **26**, 10386-10391.
22. P. A. Brooksby and A. J. Downard, *Langmuir*, 2004, **20**, 5038-5045.
23. R. Pazo-Llorente, C. Bravo-Diaz and E. Gonzalez-Romero, *European Journal of Organic Chemistry*, 2004, 3221-3226.
24. Q. Lin, Q. Li, C. Batchelor-McAuley and R. G. Compton, *Journal of Physical Chemistry C*, 2015, **119**, 1489-1495.
25. P. S. Guin, S. Das and P. C. Mandal, *International Journal of Electrochemical Science*, 2011, 816202, 816222 pp.
26. C. Batchelor-McAuley, Q. Li, S. M. Dapin and R. G. Compton, *Journal of Physical Chemistry B*, 2010, **114**, 4094-4100.
27. V. G. H. Lafitte, W. Wang, A. S. Yashina and N. S. Lawrence, *Electrochemical Communications*, 2008, **10**, 1831-1834.
28. M. A. Makos, Y.-C. Kim, K.-A. Han, M. L. Heien and A. G. Ewing, *Analytical Chemistry*, 2009, **81**, 1848-1854.
29. P. D. Lyne and R. D. O'Neill, *Analytical Chemistry*, 1990, **62**, 2347-2351.
30. G. G. Wildgoose, M. Pandurangappa, N. S. Lawrence, L. Jiang, T. G. J. Jones and R. G. Compton, *Talanta*, 2003, **60**, 887-893.
31. M. Lu and R. G. Compton, *Analyst*, 2014, **139**, 2397-2403.
32. M. Lu and R. G. Compton, *Analyst* 2014, **139**, 4599-4605.
33. C. Apetrei, I. M. Apetrei, J. A. De Saja and M. L. Rodriguez-Mendez, *Sensors*, 2011, **11**, 1328-1344.
34. J. Pinson, *Chemical Society Reviews*, 2012.
35. J. K. Kariuki and M. T. McDermott, *Langmuir*, 2001, **17**, 5947-5951.
36. V. Hambate Gomdje, T. R. Ngono, H. Saadane, M. Ennachete, M. Khouili, A. Hafid, L. Benoit and A. Chtaini, *Pharmaceutica Analytica Acta*, 2013, **4**, 1000271/1000271-1000271/1000274, 1000274 pp.
37. M. Raicopol, L. Necula, M. Ionita and L. Pilan, *Surface and Interface Analysis*, 2012, **44**, 1081-1085.
38. J. Lindquist, *Journal of Electroanalytical Chemistry Interfacial Electrochemistry*, 1974, **52**, 37-46.

39. C. C. M. Neumann, C. Batchelor-McAuley, C. Downing and R. G. Compton, *Chemistry - A European Journal*, 2011, **17**, 7320-7326.
40. M. Hadi, *Analytical Methods*, 2015, **7**, 8778-8785.
41. I. Streeter, G. G. Wildgoose, L. Shao and R. G. Compton, *Sensors and Actuators, B*, 2008, **133**, 462-466.
42. G. Yildiz, Z. Aydogmus and J.-M. Kauffmann, *Electroanalysis*, 2013, **25**, 1796-1802.
43. M. J. Sims, N. V. Rees, E. J. F. Dickinson and R. G. Compton, *Sensors and Actuators, B*, 2010, **144**, 153-158.
44. C. Olson and R. N. Adams, *Analytica Chimica Acta*, 1963, **29**, 358-367.
45. N. A. Ulakhovic, *Zhurnal Analiticheskoi Khimii*, 1995, **48**.
46. O. Korostynska, K. Arshak, E. Gill and A. Arshak, *IEEE Sensors Journal*, 2008, **8**, 20-28.

Chapter 5

In-Vitro Characterisation of CPE/FBRR/H₂SO₄ pH Sensor

5.1 Introduction

Chapter 4 of this thesis discussed the optimisation of the electrochemical reduction of FBRR onto CPEs. The results obtained confirmed that FBRR had been electrodeposited onto the carbon paste substrate. The most favourable conditions are detailed in Section 4.2. By maximising these parameters the FBRR derivatised CPEs yielded electrodes capable of determining pH changes in a solution, giving a Nernstian response of *ca.* -57 to -61 mV/pH unit in an *in-vitro* environment. In order to bring this project forward towards the *in-vivo* application whereby real-time changes in pH values could be monitored, using *in-vivo* voltammetry, the modified electrodes were required to endure rigorous test procedures, exposing them to a range of different test conditions.

Living tissue contains a broad range of electroactive species, e.g., ascorbic acid (AA) and uric acid (UA), as well as lipids, proteins and surfactants. These can limit the mass transport rate,¹ diffusion and adsorption, at the electrode surface, thereby affecting the voltammetric signal produced by the functionalised CPEs. This is due to the lipophilic nature of biological tissue, which has been reported to remove the hydrophobic oil from the CPE surface,² thus altering the modified surface.

Conventional CPEs are simple and cheap to prepare, hence their widespread use in electrochemical sensors. However, their reproducibility and stability, due to their easily corrupted surface, is flawed.³ The ease at which the FBRR functionalised CPEs become modified by the various physiological substances (lipids, proteins and surfactants), see Section 5.2.3, was a concern, mainly resulting from the loss of silicone oil changing the morphology of the electrode surface and the electron transfer at the solution/electrode interface. In order to create a more robust device, a styrene (Sty) modification was applied to the paste, before the electrochemical reduction of FBRR. This has previously been shown to improve the electrochemical properties of the carbon based electrodes.^{4, 5} The ability to incorporate monomers into the electrode design in an attempt to create a sturdier sensor capable of withstanding the harsh *in-vivo* environment, has been investigated in our laboratory previously.⁶ Carbon pastes represent one of the most convenient materials for the preparation of modified electrodes.⁷

In contrast to the relatively complicated modifications of solid-state electrodes, the preparation of modified CPEs is very simple, and can be carried out by various procedures.⁸ Modifiers can be dissolved directly in the binding oil⁹ or physically mixed into the paste during its homogenisation.¹⁰ Modification can also be carried out by soaking the graphite particles in a solution of the required modifier.¹¹ Finally, prepared pastes can be modified *in-situ*.¹² In this chapter the incorporation of the monomer, Styrene (Sty) into prepared CPEs (SMCPEs) is investigated and the comparative results between FBRR/CPEs and FBRR/SMCPEs are shown alongside each other.

Various metal ions, e.g., Mg^{2+} and Ca^{2+} , are prevalent in biological environments, and have been recorded as affecting the peak potentials of several quinone derivatives.¹³ The effect of ionic strength, operational temperature of the sensor and choice of reference electrode are also investigated in this chapter.

5.2 Results and Discussion:

In preparation for *in-vivo* testing the FBRR/ H_2SO_4 modified CPE was subjected to a range of tests. These included the “shelf-life” of modified electrodes and suitable storage conditions. Several parameters that are unique to the *in-vivo* environment required investigation so these conditions were mimicked *in-vitro*. These included testing the biocompatibility of the FBRR/CPE, FBRR/SMCPE and the effects of known physiological and pharmacological interferences on the FBRR anodic signal. The effects of ionic strength and the introduction of metal ions into the testing solution were also examined. Finally the recording temperature and reference electrode were altered to mimic physiological conditions.

Also included in this chapter is a comprehensive study into the carbon:silicone oil ratio present in CPEs and SMCPEs and how this ratio affects bare and modified electrodes when exposed to lipids, proteins, surfactants and *ex-vivo* brain tissue.

5.2.1 Stability of FBRR/ H_2SO_4 Modified CPEs

In this section the stability of the pH response of FBRR/ H_2SO_4 modified CPEs was examined over a time period of up to 1 month.

5.2.1.1 FBRR/H₂SO₄ Modified CPEs Stored in Air

Figure 5.1 shows the resulting pH responses of FBRR/CPEs at calibration and after storage in air.

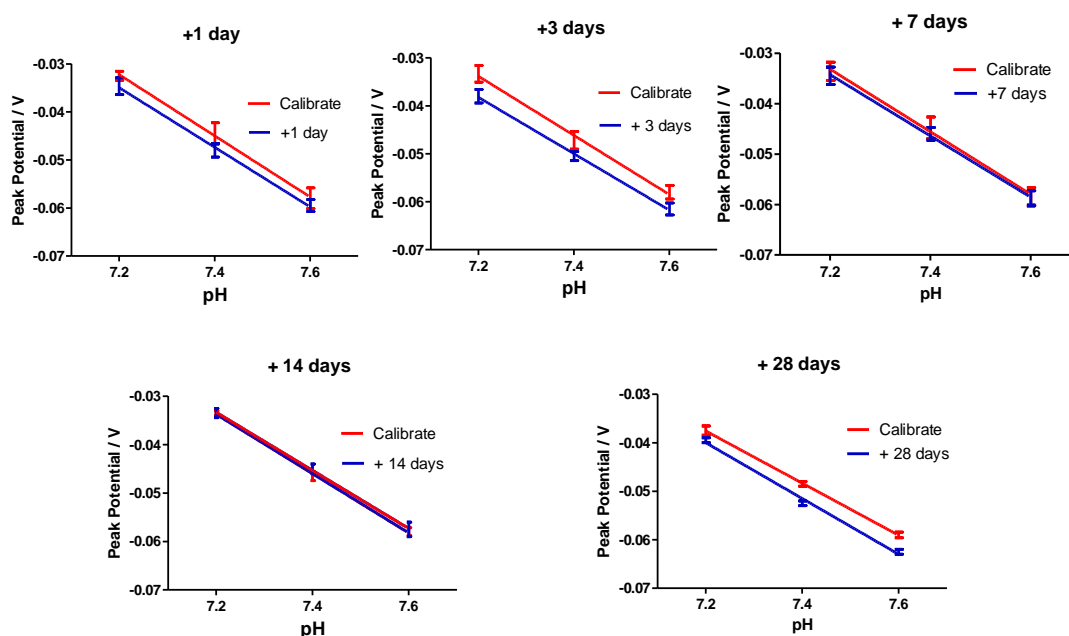


Figure 5.1: pH response of modified CPEs calibrated and stored at 4°C for 1, 3, 7, 14 and 28 days, $n = 4$.

Table 5.1 shows analysed data for all the calibrations, pre and post storage. It was noted that the slope (pH response) shifted towards a more Nernstian value after storage, suggesting the modified electrodes needed time to settle once prepared. This is most likely due to the carbon paste becoming more homogenised.¹² The slopes of each set of electrodes, before and after storage, have been compared using unpaired t-tests. Although the results in Table 5.1 suggest an improvement in the pH response after storage, the analyses indicate that there was no significant difference in the pH sensitivities of the modified electrodes after storage at 4°C, for the times specified, ($P > 0.05$).

The changing pH response over time is shown in Figure 5.2. The sensitivity of the modified electrodes remained relatively stable, pre and post storage, for the first two weeks, but drifted after 28 days. However, the calibration sensitivity was lower than

expected here, and may have affected the results. The differences in calibration slopes were due to inter-electrode variability, a problem inherent in CPEs. Also, it was notable that the errors had generally reduced post storage.

Table 5.1: Statistical analyses of modified CPE pH response before and after storage at 4°C.

	Slope mV/pH	SEM	R ²	n	P-value
Calibrate	-63.8	2.2	0.9988	4	0.6426
+ 1 Day	-62.1	2.6	0.9982	4	
Calibrate	-61.7	4.4	0.9949	4	0.6033
+ 3 Days	-58.8	2.2	0.9986	4	
Calibrate	-62.0	3.5	0.9969	4	0.7618
+ 7 Days	-60.8	1.9	0.9990	4	
Calibrate	-61.3	2.2	0.9988	4	0.6479
+ 14 Days	-60.0	1.4	0.9994	4	
Calibrate	-56.3	0.7	0.9998	4	0.7854
+ 28 Days	-57.5	4.3	0.9944	4	

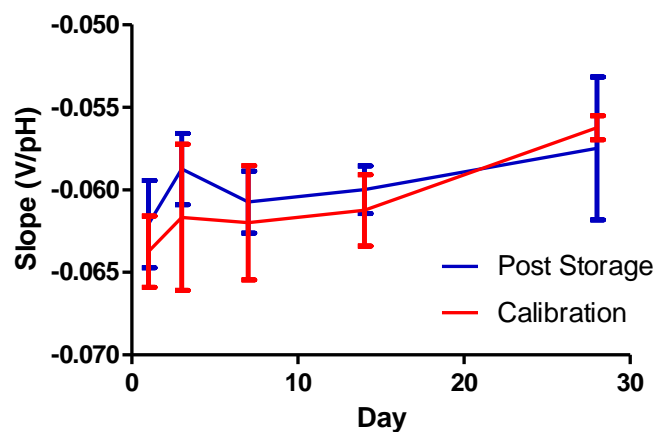


Figure 5.2: Variability in pH sensitivities of FBRR/H₂SO₄ modified CPEs, pre and post storage, at 4°C.

Figure 5.3 shows the isolated anodic peaks of modified electrodes cycled in pH 7.2, 7.4 and 7.6 for 100 cycles each, before and after storage for 3 days (A) and 14 days (B). They clearly indicate that there was a potential shift with changing pH and that the peak potentials remained reasonably stable.

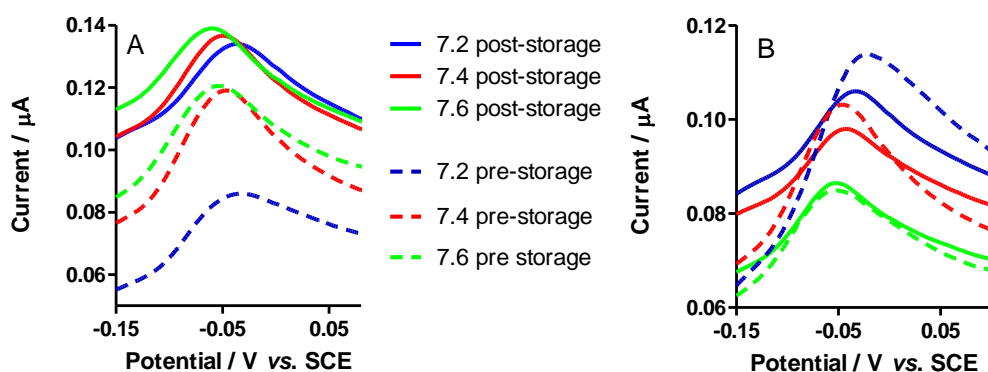


Figure 5.3: Modified CPEs cycled in PBS pH 7.2, 7.4 and 7.6, before and after storage for 3 days (A) and 14 days (B) at 4°C.

5.2.1.2 FBRR/H₂SO₄ Modified CPEs Stored in N₂

Figure 5.4 shows the pH response of FBRR/CPEs at calibration and after storage in N₂ for various time periods. There was a clear difference in sensitivity on days 1 (60.0 to 52.5 mV/pH) and 7 (68.8 to 53.8 mV/pH), and to a lesser extent on day 14 (67.5 to 63.3 mV/pH).

Table 5.2 shows analysed data for all the calibrations. It was observed that the sensor's sensitivity towards pH decreased after storage, with the only exception being after 28 days. The slopes of each set of electrodes, before and after storage, were compared using unpaired t-tests. Some of the results gave a P -value > 0.05 meaning that there was no significant difference in the pH response of the modified electrodes after storage at 4°C for the times specified. However, after storing under N₂ for 1 and 7 days, the mean slopes were significantly different, with P -values of 0.0020 and 0.0119, respectively.

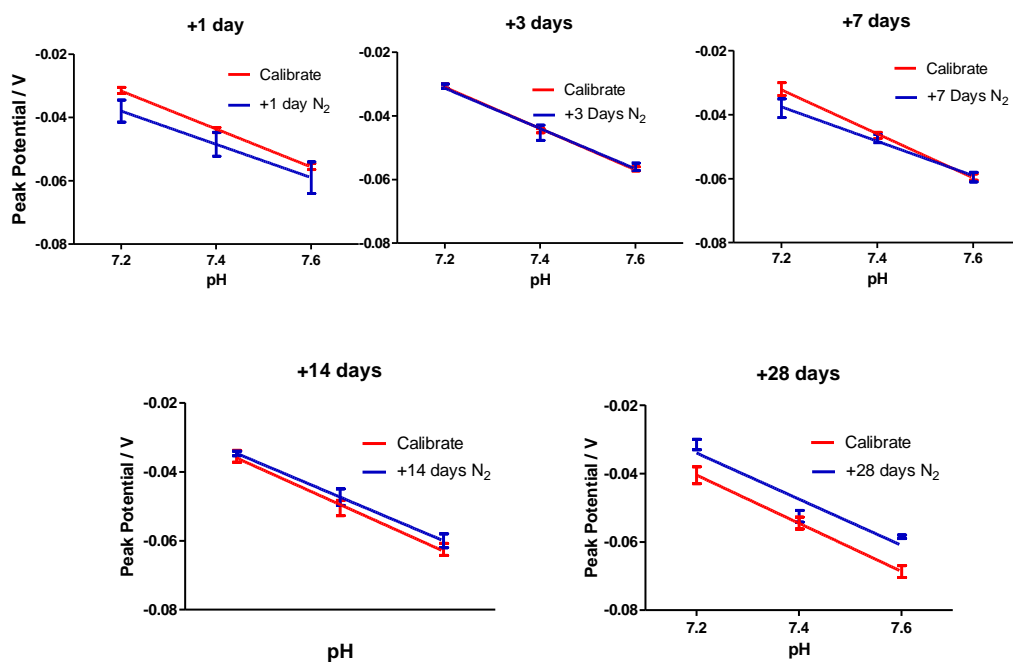


Figure 5.4: pH response of modified CPEs calibrated and stored at 4°C under N₂, for 1, 3, 7, 14 and 28 days, $n = 4$.

Table 5.2: Statistical analyses of the pH response of FBRR/CPEs before and after storage at 4°C in N₂.

	Slope V/pH	SEM	R ²	n	P -value
Calibrate	-60.0	1.4	0.9994	4	0.0020**
+ 1 Day	-52.5	0.0	1.0000	4	
Calibrate	-65.0	2.8	0.9980	4	0.8045
+ 3 Days	-63.3	5.8	0.9918	4	
Calibrate	-68.8	2.2	0.9990	4	0.0119*
+ 7 Days	-53.8	3.6	0.9955	4	
Calibrate	-67.5	4.3	0.9959	4	0.3727
+ 14 Days	-63.3	0.0	1.0000	4	
Calibrate	-66.3	2.2	0.9989	4	0.1041
+ 28 Days	-67.5	21.7	0.9067	4	

Figure 5.5 shows how the pH response changed over time. It can be seen that over all the storage periods examined the pH responses were not uniform and the errors had substantially increased after 28 days, similar to electrodes stored in air (see Figure 5.2).

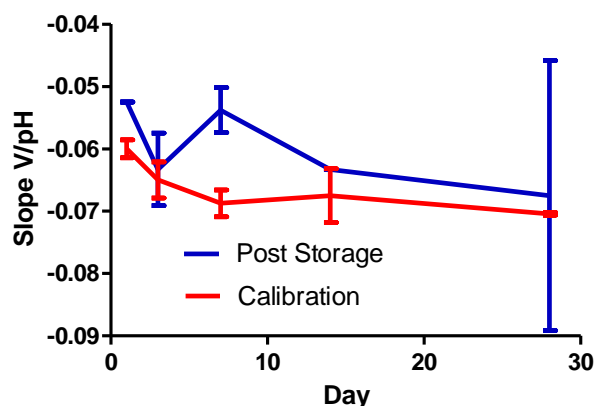


Figure 5.5: Variability in pH sensitivities of FBRR/H₂SO₄ modified CPEs pre and post storage at 4°C in N₂, $n = 4$.

5.2.2 Effect of Styrene on CPEs

It was identified, from previous group members, that functionalising CPEs with Sty, (SMCPEs), causes the carbon paste to contract, leaving a larger surface area, see Figure 5.6. The CV in Figure 5.7(A) indicates the increased capacitance of CPEs once stored in Sty, which is indicative of the increased surface area. This was reduced once the surface had been smoothed off by repacking the cavity with the carbon paste/Sty mixture Figure 5.7(B).

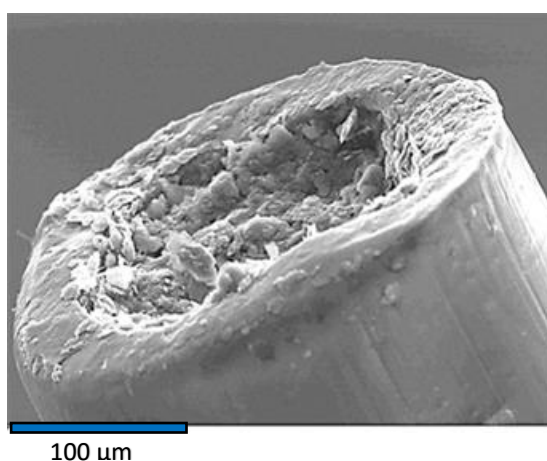


Figure 5.6: SEM micrograph of CPE stored overnight in styrene.

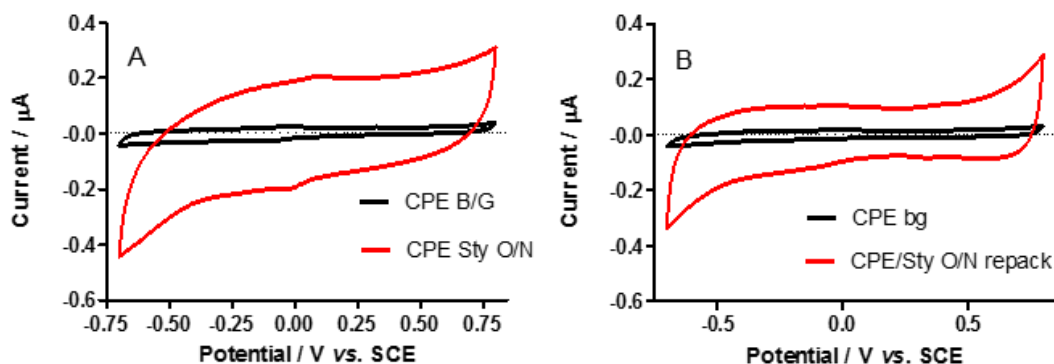


Figure 5.7: Effect of Sty on CPEs before (A) and after (B) repacking the cavity with the carbon paste/Sty mixture, $n = 4$.

5.2.2.1 Drying Time of SMCPEs

SMCPEs were dried for various amounts of time, at 4°C, before being modified with FBRR/H₂SO₄, using the same procedure described in Section 4.3. They were cycled in PBS solutions with pH values of 7.2, 7.4 and 7.6. The results are shown in Figure 5.8 with their corresponding pH responses in Table 5.3. It was found that electrodes modified after 2 and 6 hours displayed an array of unidentified anodic and cathodic peaks. The characteristic FBRR redox peaks were well defined and located at potentials *ca.* -0.04 and -0.10 V vs. SCE. The ΔE value of 60 mV indicated a reversible redox reaction. In Section 4.2.3.6, the FBRR/H₂SO₄ modification of CPEs resulted in a quasi-reversible reaction process. The change to reversibility of the system confirmed that the Sty modification had facilitated electron transfer at the solution/electrode interface. After an 18 hour drying period the CVs were cleaner, with reversible anodic and cathodic peaks. These were the only electrodes that showed a good pH response with a sensitivity of -56 ± 14 mV/pH, $n = 16$.

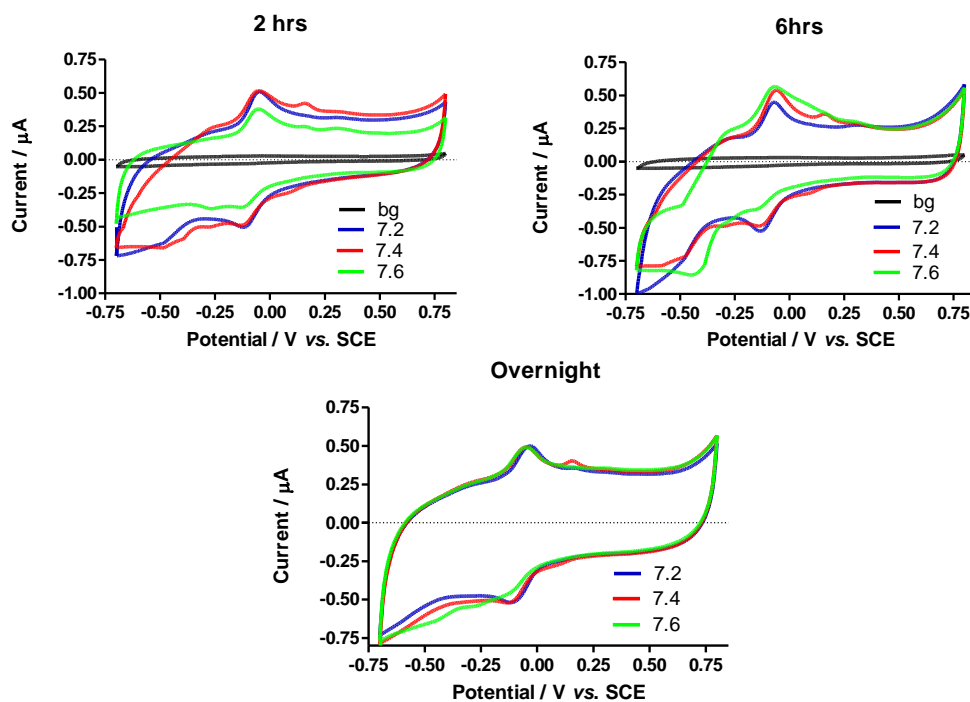


Figure 5.8: SMCPs dried for 2 hours ($n = 4$), 6 hours ($n = 4$) and 18 hours (overnight) ($n = 16$), before electrodeposition of FBRR/ H_2SO_4 .

Table 5.3: pH sensitivities of FBRR modified SMCPs stored over various time periods before electrodeposition of FBRR.

Drying Time (Hours)	SLOPE (mV/pH)	SEM	R ²	n
2	-45	14	0.901	4
6	+28	6.0	0.960	4
18	-56	14	0.944	16

5.2.2.2 Carbon Paste: Styrene Ratio

The amount of modifier in the paste usually varies between 10-30% (w/w),⁸ depending on the character of modifying agent and its capability of forming enough active sites in modified paste.¹²

The most promising result in Section 5.2.2.1 was obtained when the repacked electrodes were dried overnight at 4°C before being modified with FBRR, although errors were still high. In an attempt to reduce these errors various ratios of carbon

paste: Sty were used in the manufacturing process of electrodes. The volumes of Sty (>99%) used were 12, 14 and 18-22 μl , while the mass of carbon paste was a constant 0.025 g. The resulting CVs for 19 and 20 μl are shown in Figure 5.9, with the anodic peaks of interest highlighted, along with their corresponding pH responses. The pH sensitivities of FBRR modified SMCPEs using all Sty volumes are shown in Table 5.4.

The results have shown that using 18-20 μl oil: 0.025 g paste gave the best pH response, with substantially reduced errors for 20 μl . However, the pH sensitivities showed no improvement over FBRR/ H_2SO_4 modified CPEs.

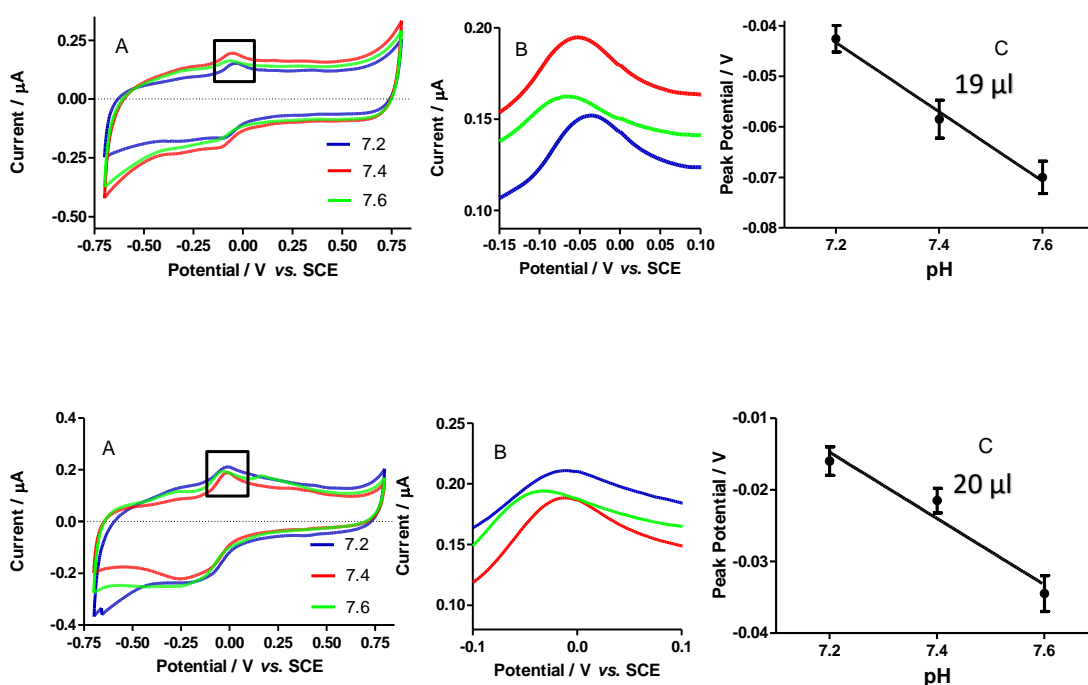


Figure 5.9: (A) CVs of FBRR modified SMCPEs using 19 and 20 μl Sty in 0.025 g paste, (B) close-up of their anodic peaks and (C) pH sensitivities.

Table 5.4: pH responses of FBRR modified SMCPEs using various Sty: paste ratios.

STY (μl)	SLOPE (mV/pH)	SEM	R ²	n
12	-40	10	0.945	4
14	-50	25	0.039	4
18	-56	14	0.944	4
19	-46	11	0.948	4
20	-69	6	0.991	10
21	-35	3	0.993	4
22	-43	16	0.876	4

5.2.2.3 Storage after FBRR Deposition

FBRR/SMCPE modified electrodes were stored at 4°C for various amounts of time after deposition of FBRR and before being calibrated. The pH responses of these electrodes are shown in Figure 5.10 and clearly show that the best pH sensitivity was obtained when the electrodes were stored for a period of 1 day before carrying out a calibration. These gave a pH response of 50 mV/pH with a correlation of 0.94, shown in Table 5.5. The lower time period was insufficient due to impurities within the styrene, which evaporated off over time, and the longer time period possibly caused the removal of some FBRR salt from the modified surface.

Table 5.5: pH responses of FBRR/SMCPEs stored for various time periods before calibration, $n = 4$.

	Slope (mV/pH)	SEM	R ²	n
+2 Hours	-28.3	2.2	0.1946	4
+1 Day	-50.0	3.5	0.9408	4
+2 Days	-38.3	4.6	0.9100	4

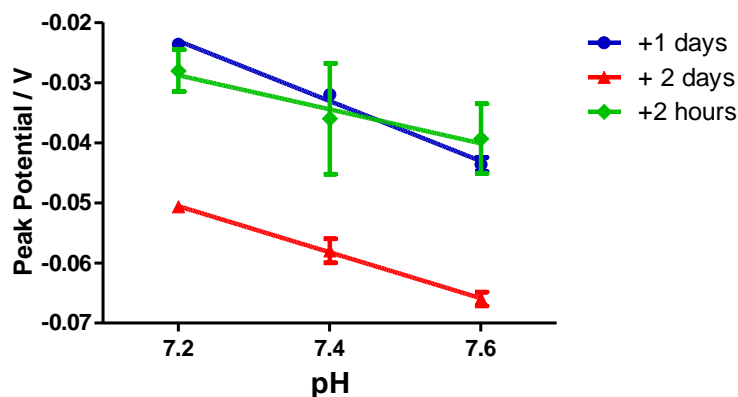


Figure 5.10: pH sensitivities of FBRR/SMCPEs stored for up to 2 days before calibration, $n = 4$.

The protocol for making FBRR/SMCPEs was:

- Store CPEs in Sty overnight at 4°C
- Repack the electrode surface with 20 μ l Sty in 0.025 g carbon paste
- Store SMCPEs overnight at 4°C
- Electrodeposit 2 mM FBRR in 0.1 M H₂SO₄, by LSV x5, from 0.40 to -0.80 V vs. SCE at 100 mV/s.
- Store FBRR/SMCPEs overnight at 4°C, before calibrating

5.2.3 Biocompatibility

Calibrated electrodes were stored in PBS solutions of Bovine Serum Albumen, BSA, 1% (protein), Phosphatidylethanolamine, PEA, 1% (lipid), Triton[®] X 1% (surfactant) or homogenised brain tissue, for various time periods (1, 3, 7 and 28 days). As the modified electrodes were stored in aqueous solutions, they were first stored in PBS and H₂O at 4°C for 3 days to examine any resulting effects. After storage the electrodes were rinsed and cycled in PBS pH 7.2 for 100 cycles, $n = 4$. The results, showing the effect of storing FBRR/CPEs in PBS and H₂O are indicated in Figure 5.11, demonstrate that although the currents increased due to wetting of the electrode² resulting in increased activity, all peaks were retained.

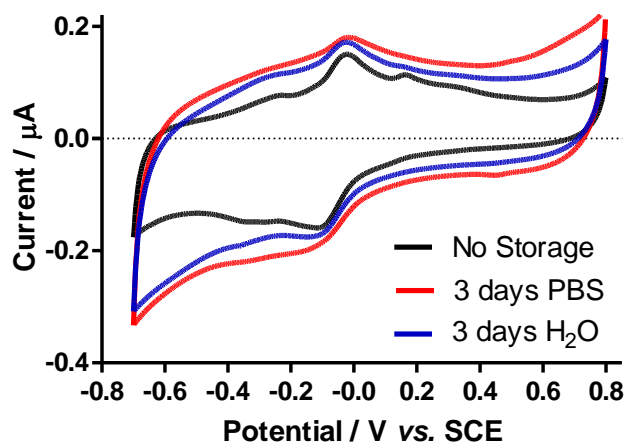


Figure 5.11: Effect of storing modified CPEs in PBS and H₂O for 3 days.

5.2.3.1 Bovine Serum Albumen (BSA)

BSA is a protein, which is readily purified from bovine blood, and is often used to mimic protein concentrations in laboratory scenarios. A major problem of the practical application of the FBRR/CPE results from the adsorption of surface active molecules, present in proteins, onto the electrode surface. The tendency is to build up a layer inhibiting electron processes resulting in altered voltammograms.¹⁴

The centre graph in Figure 5.12 shows typical calibration CVs for FBRR/CPEs at pH 7.2, 7.4 and 7.6 with the post-storage CVs surrounding it. After all days, 1-28, poorly defined, broad peaks were evident which appeared to shift with pH, in a non-Nernstian fashion, but at a more positive potential than the calibration peaks. This suggested that the BSA modification made the oxidation of FBRR at the CPE interface less thermodynamically viable.¹⁵ These potential values are shown in Table 5.6. The potential difference between 7.2 and 7.4 had an average value of 14 mV, $n = 3$, which would give a near Nernstian value of -70 mV/pH. It was the final 100 cycles, therefore, that resulted in most fouling, the average potential difference between pH 7.4 and 7.6 is 32.6 mV giving a sensitivity of over 160 mV/pH. The values for 7 days were omitted as the peaks were too broad to give a good estimate of potential. It was also clear from Figure 5.12 that the currents attained increased with storage time. There was an initial increase in currents after day 1, which appeared to reach a maximum after 7 days, and

then remained stable. This relationship was also confirmed by the Si % data, see Section 5.2.4.1, which demonstrated that after storage the Si % reduced initially and then remained relatively stable.

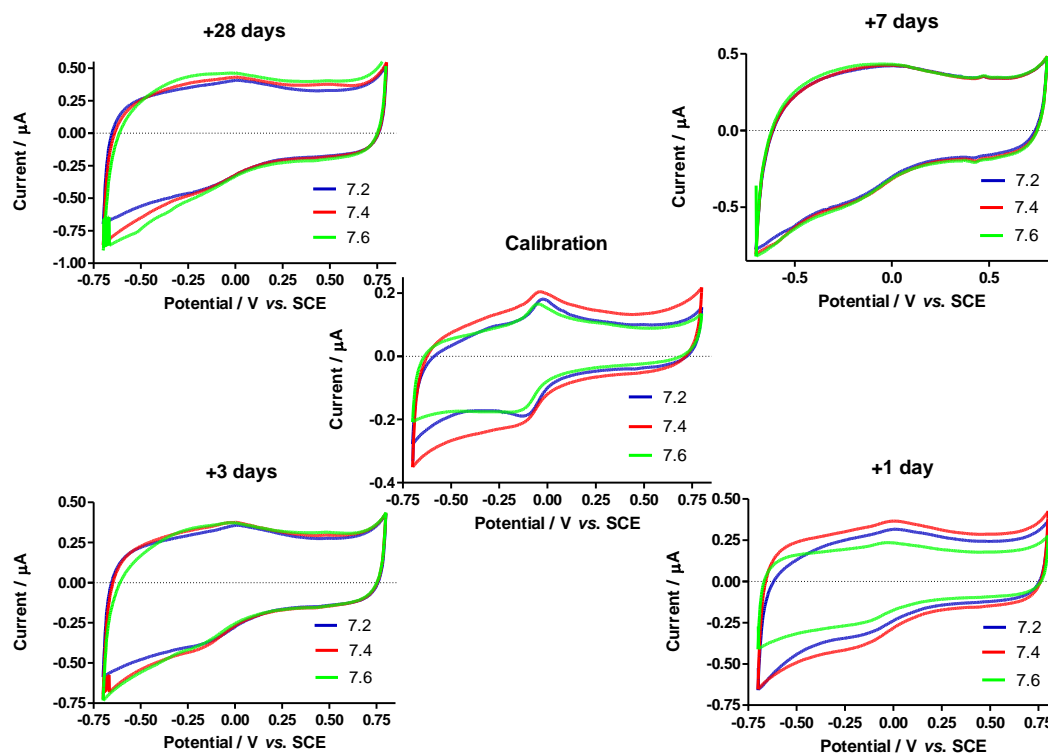


Figure 5.12: CVs showing the effect of storing FBRR/H₂SO₄ modified CPEs in 1% BSA.

Table 5.6: Shift in peak potentials when storing FBRR/H₂SO₄ modified CPEs in 1% BSA.

	pH 7.2 (mV)	pH 7.4 (mV)	pH 7.6 (mV)	<i>n</i>
Calibration	-28	-38	-50	4
+1 Day	-2.0	-18	-52	4
+3 Days	-12	-22	-58	4
+7 Days	-----	-----	-----	4
+28 Days	-1.0	-16	-44	4

For comparison, calibrated FBRR/SMCPEs were stored in a 1% BSA solution at 4°C overnight, before being recalibrated. The resulting CVs are shown in Figure 5.13, (A) pre-storage and (B) post-storage. An increase in the capacitive current, approximately 67%, was observed, (maximum I_p ca. 0.18 μ A) but not quite as large an increase as reported in for FBRR/CPEs (maximum I_p ca. 0.30 μ A). This implied that not as much

BSA had adsorbed onto the electrode surface, allowing more efficient electron transfer. There was a clear shift in the anodic peak to a more positive potential, from -0.050 V vs. SCE for FBRR/CPEs to -0.020 V vs. SCE for FBRR/SMCPEs. This indicated that the Sty modification had made the oxidation of FBRR, at the electrode surface, less thermodynamically favourable, by increasing its required potential. It was also noted that the redox peak potentials did not shift with pH in a Nernstian fashion.

FBRR/CPEs were stored in BSA for up to 28 days. As no obvious improvement was made to the resulting CVs of FBRR/SMCPEs having been stored for 1 day in BSA, it could be postulated that the inclusion of Sty would not change 3, 7 and 28 day exposure, so no further investigations were carried out.

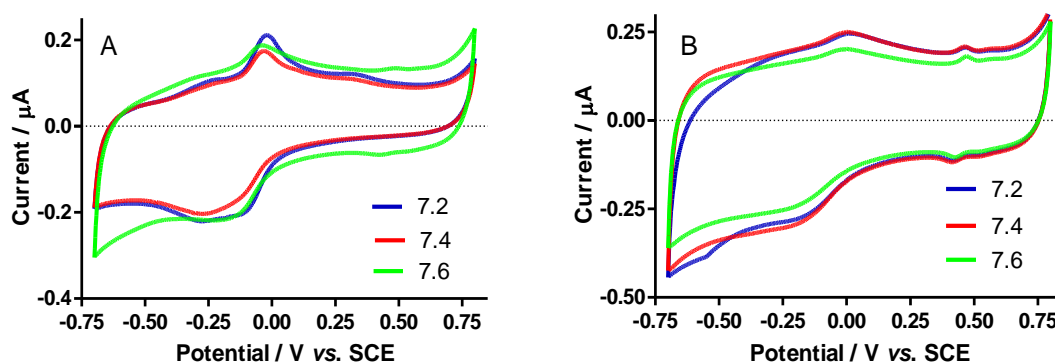


Figure 5.13: (A) Calibration CVs for FBRR/SMCPEs before storage and (B) after storage in a 1% solution of BSA for 1 day, $n = 4$.

The SEM micrographs in Figure 5.14 show FBRR/CPEs after storing in 1% BSA for 1, 3, 7 and 28 days. After day 1 the electrode appeared reasonably intact, with many areas fairly smooth allowing consistent electron transfer. This was also reflected in the CVs in Figure 5.13 where the peaks were clearly visible and the currents were lower than any other days. Days 3 and 28 show overhead views of the electrode surfaces that had a more powder-like and less organised surface. The concave shape can be clearly seen. The image for day 7 shows a side view of the electrode, where the edges have come away from the Teflon[®] support, increasing the surface area.

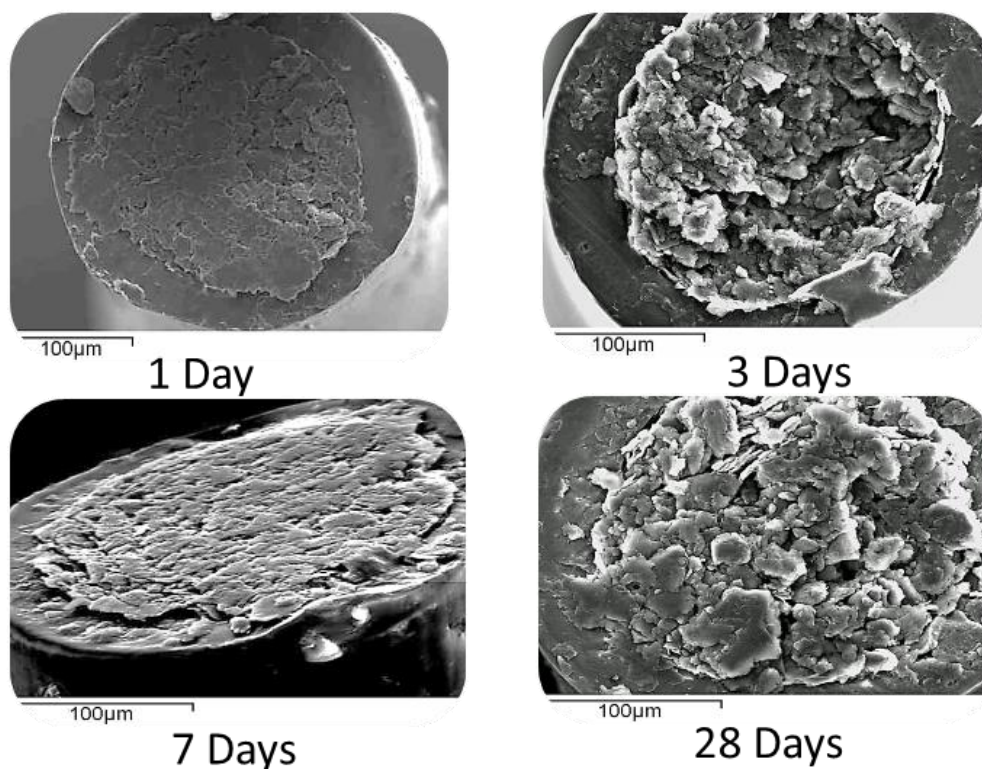


Figure 5.14: SEM micrographs of FBRR/CPEs stored in 1% BSA between 1 and 28 days.

The EDX of the electrode surface, after 3 days storage in 1% BSA, Figure 5.15, shows evidence of silicone oil, although its quantity has been reduced when compared to the EDX of a freshly modified CPE (see Table 5.7).

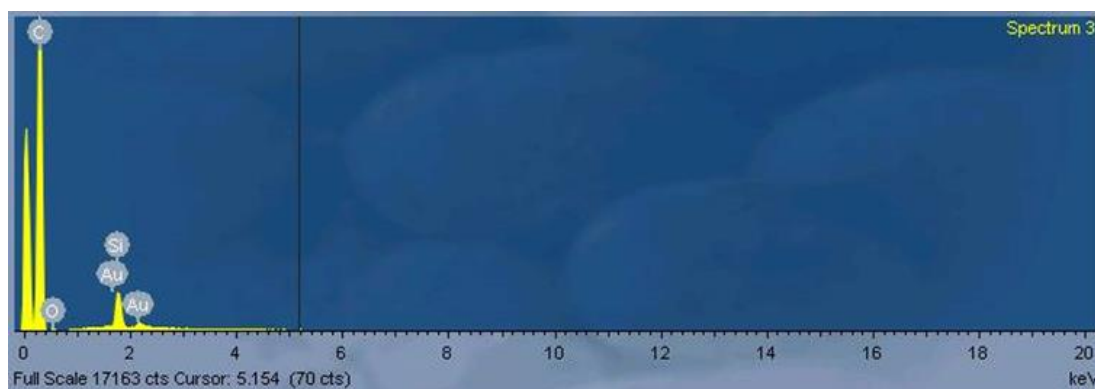


Figure 5.15: EDX of FBRR/CPEs stored in 1% BSA for 3 days.

Poor results were obtained when the FBRR/CPEs were stored in BSA (1%). One of the main aims of developing this sensor was to monitor real-time pH changes. This, ideally, would be carried out for a maximum period of 12-24 hours, and would involve the constant application of oxidation and reduction potentials.

The differing CVs obtained when cycling and storing FBRR/CPEs in BSA are shown in Figure 5.16. The functionalised CPEs cycled in the BSA solution for 3.5 hours are shown in Figure 5.16 (A), with the anodic peaks alongside (A_1). Figure (B) shows the electrodes after storage in the BSA solution for 3.5 hours with the corresponding anodic peaks in (B_1). Electrodes stored in BSA show similar results to those in Figure 5.12, with a shift in the peak potential and a gradual broadening and height decrease in the peaks. This is indicative of the build-up of the protein on the electrode surface over time, resulting in a decrease in the electron transfer rate. However, electrodes cycled in the BSA solution show far superior peak sharpness with an increase in peak height over time. This clearly suggests that the constant application of an oxidation potential followed by a reduction potential does not allow the protein layer to build-up on the electrode surface. It is likely that trace amounts of BSA were present on the electrode surface enhancing the electron transfer.¹⁶ Alternatively, the BSA had removed the silicone oil from the CPE surface making it more powder-like, therefore increasing the electron transfer rate at the electrode/solution interface.²

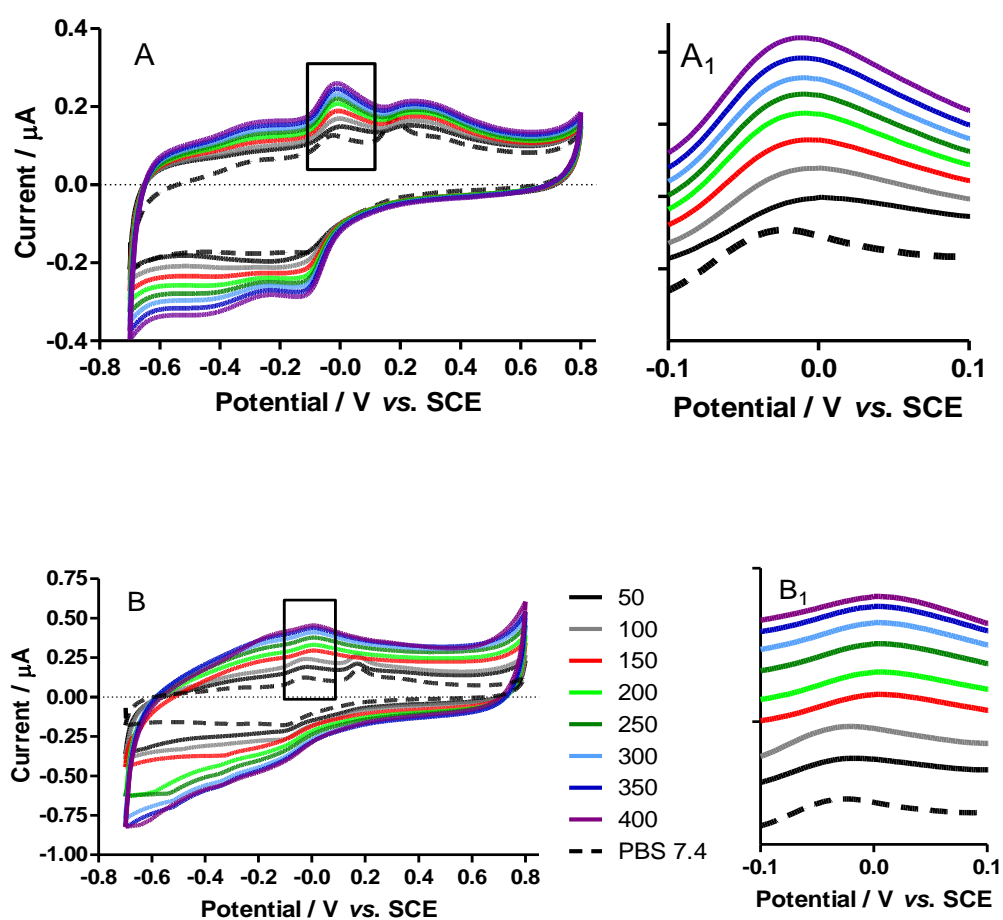


Figure 5.16: CVs of FBRR/CPEs cycled (A) and stored (B) in 1% BSA/PBS for 3.5 hours with the corresponding anodic peaks in (A₁) and (B₁), $n = 4$.

The FBRR/SMCPEs were similarly cycled in the BSA solution for 3.5 hours to examine if cycling the electrodes was less severe than storing them in the protein. The CVs, in Figure 5.17, show every 50th cycle, gave no apparent enhancement of the peak sharpness.

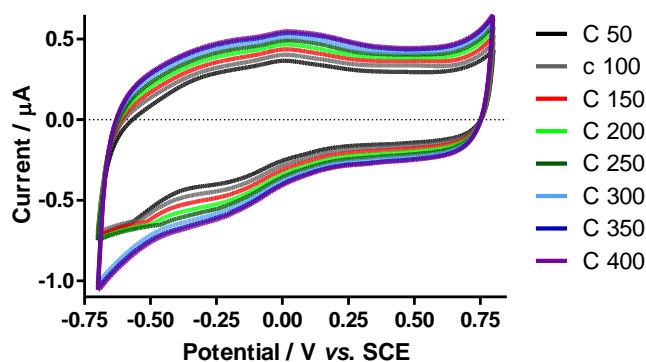


Figure 5.17: FBRR/SMCPEs cycled in a 1% BSA solution for 3.5 hours, $n = 4$.

Figure 5.18 shows how the FBRR/CPEs behaved when cycled in a 1% BSA solution for 12 hours, a similar time span required for physiological monitoring of tissue pH. The anodic peak, highlighted in (A), was still observed and increased in sharpness with cycling, (B). This implied that there was no fouling of the electrode surface, only enhancement of electrode kinetics by the protein.

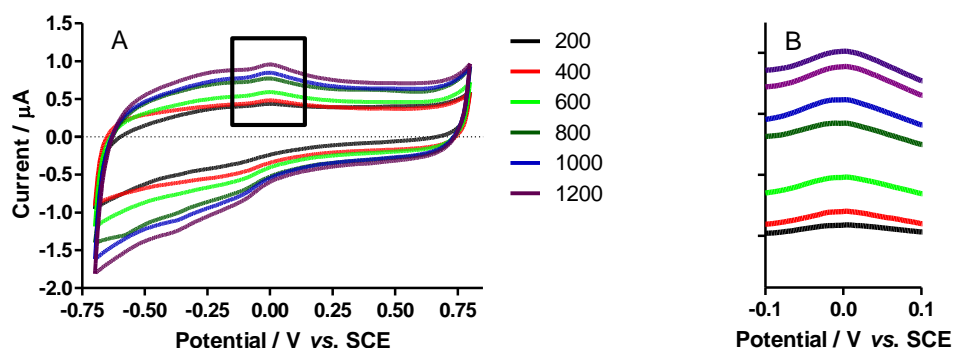


Figure 5.18: CVs of FBRR/CPEs cycled in 1% BSA for 12 hours (A), with the corresponding anodic peaks (B), $n = 4$.

5.2.3.2 Phosphatidylethanolamine (PEA)

PEA is a phospholipid found in all living cells. It was utilised in this section to examine the behaviour of the FBRR/H₂SO₄ modified CPEs when exposed to lipids.

The centre graph in Figure 5.19 shows typical calibration CVs at pH 7.2, 7.4 and 7.6 with the post-storage CVs, in PEA, surrounding it. Some broad peaks were visible at more positive potentials than the original calibration. It was noticeable that the currents increased the longer the electrodes had been stored in PEA. This was due to fouling of the electrode and the removal of silicon oil which is also shown in Section 5.2.4.1.

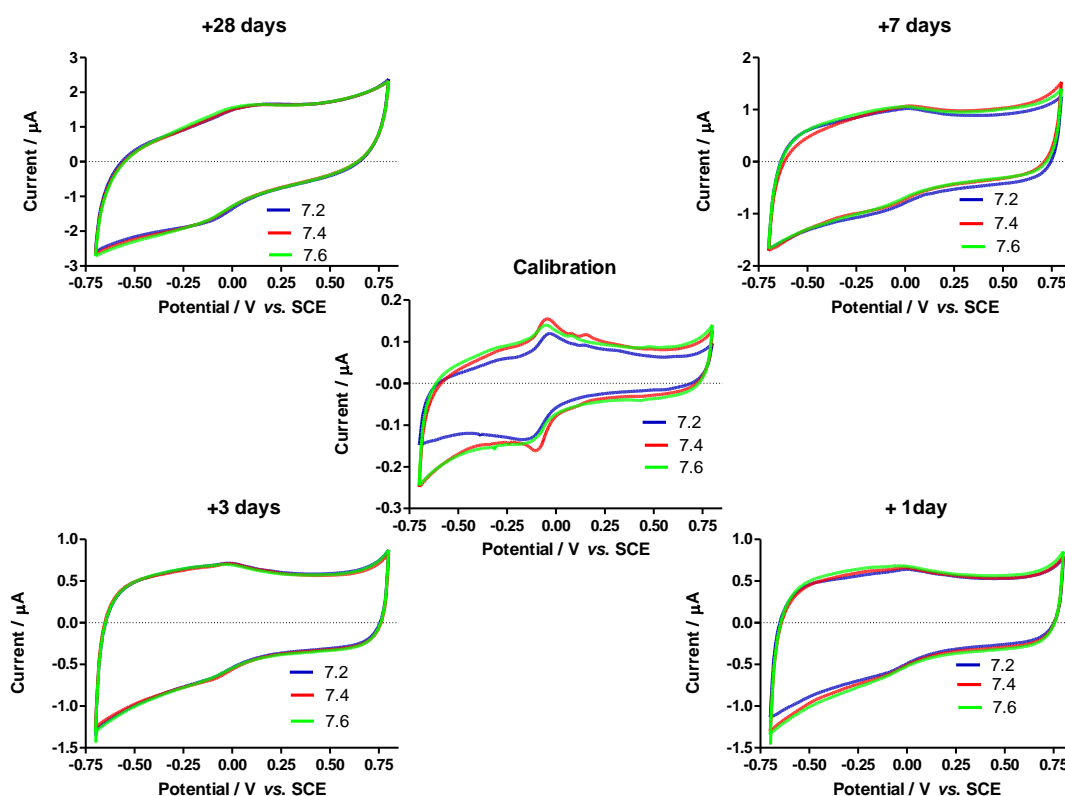


Figure 5.19: CVs showing the effect of storing FBRR/H₂SO₄ modified CPEs in 1% PEA.

FBRR/SMCPEs were stored in PEA solutions overnight for comparison. Graph (A) in Figure 5.20 shows typical calibration CVs at pH 7.2, 7.4 and 7.6 with the post-storage CVs in (B). Some broad peaks were visible at more positive potentials than the original calibration, similar to FBRR/CPEs in PEA, showing the hindering of FBRR oxidation once the CPEs were modified with Sty.

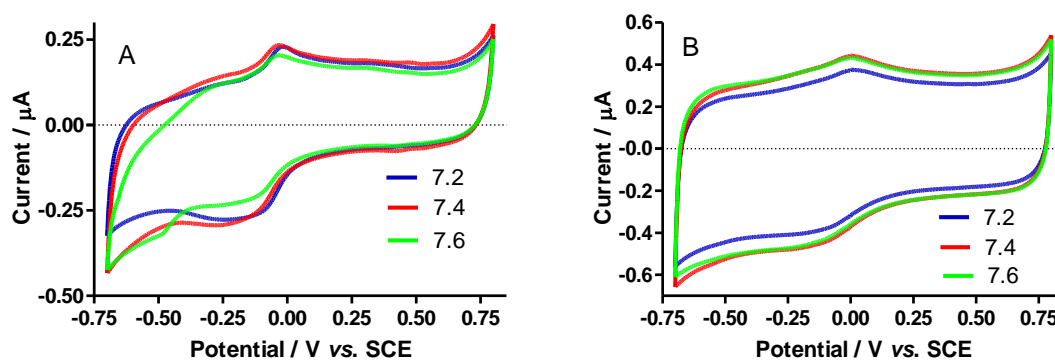


Figure 5:20: (A) Calibration CVs for FBRR/SMCPEs before storage and (B) after storage in a 1% solution of PEA for 1 day, $n = 4$.

FBRR/CPEs were stored in PEA for up to 28 days. With the corresponding FBRR/SMCPEs, only a slight improvement was made to the resulting CVs having been stored for 1 day in PEA, but the peak potentials did not appear to give a Nernstian response to changes in pH, so no further investigations over longer time periods were carried out.

SEM micrographs of modified CPEs stored in PEA for between 1 and 28 days are displayed in Figure 5.21. They demonstrate, clearly, that the silicone oil had been removed from the CPE leaving concave surfaces, this was especially noticeable from day 3. When the CVs in Figure 5.19 were directly compared to their corresponding image it shows that the higher currents (7 and 28 days) are obtained for CPEs that have a more concave surface, i.e., more silicone oil removed.

The EDX of the electrode surface, after 3 days storage in 1% PEA, Figure 5.22, shows evidence of silicone oil, although its quantity has been reduced when compared to the EDX of a freshly modified CPE (see Table 5.7). The currents obtained for the modified electrodes, stored in PEA, agree with the % Si quantitative analysis, showing an initial drop in % Si after day 1, leading to a gradual increase in currents for days 3 and 7, which further increase to a maximum level after day 28.

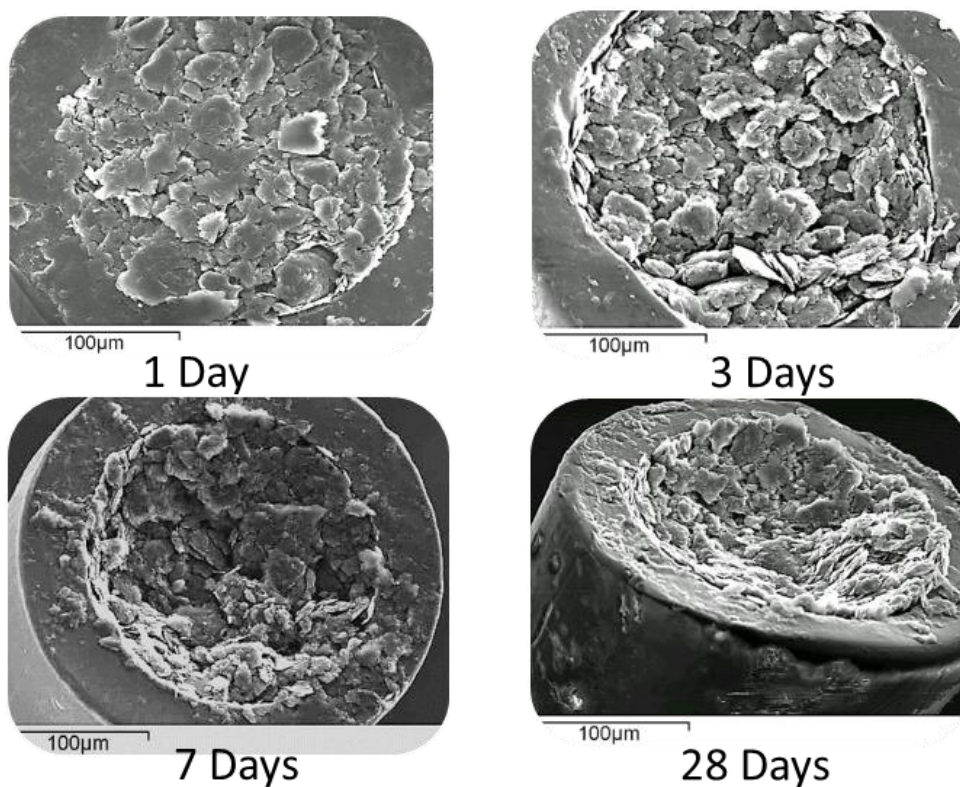


Figure 5.21: SEM micrographs of FBRR/CPEs stored in 1% PEA for between 1 and 28 days.

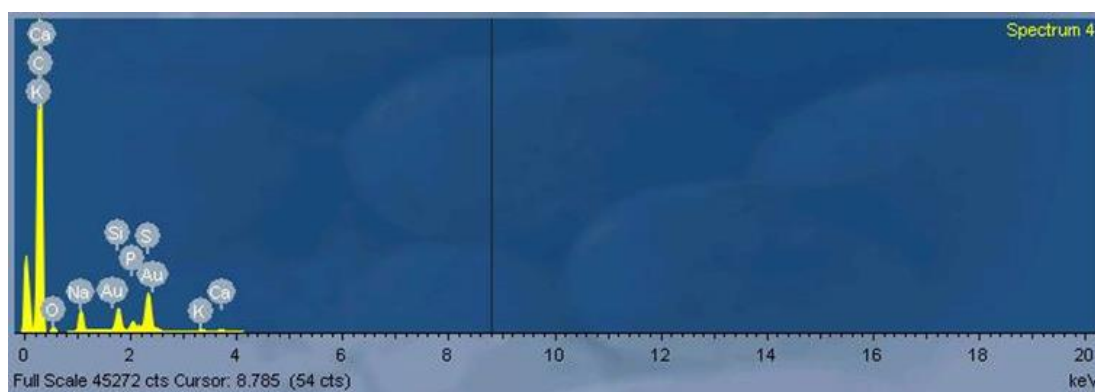


Figure 5.22: EDX of FBRR/CPEs stored in 1% PEA for 3 days.

The application of this pH sensor was to monitor real-time pH changes in living tissue, so in reality the modified electrodes would never be stored in lipids. To mimic the *in-vivo* application of the FBRR/CPE required continuous cycling in the lipid solution.

The resulting CVs, shown in Figure 5.23, were compared. Figure 5.23(A) shows the electrodes cycled in PEA, every 50th cycle is shown, with the corresponding anodic peaks in (A₁). The anodic peaks (highlighted) are clear and improve with time, indicating that the PEA had not fouled the electrode, conversely, it had enhanced the electron transfer kinetics. This was similar to BSA in Section 5.2.3.1. The application of oxidation and reduction potentials allowed trace amounts of PEA to adsorb onto, and desorb from the electrode surface, preventing any build-up of the lipid layer. Figure 5.23(B) shows the CVs of electrodes that were stored in the PEA solution for 3.5 hours, with the anodic peaks in (B₁). These are very similar to those in Figure 5.19, with broad peaks, resulting from a build-up of lipid on the electrode surface, effectively blocking the electron transfer between the solution and the electrode surface.

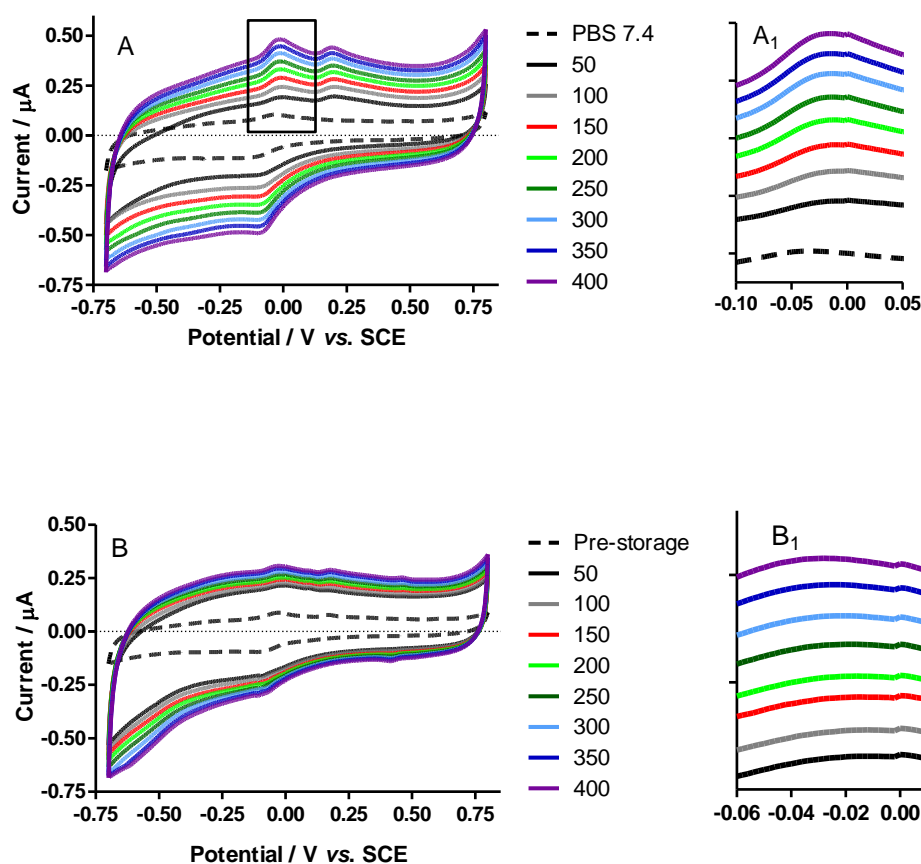


Figure 5.23: CVs of FBRR/CPEs cycled (A) and stored (B) in 1% PEA for 3.5 hours with the corresponding anodic peaks in (A₁) and (B₁), $n = 4$.

Similarly, FBRR/SMCPEs were cycled in the PEA solution for 3.5 hours. The resulting CVs, every 50th cycle, are shown in Figure 5.24. The anodic peaks remained broad, showing no improvement over storing the FBRR/SMCPEs in PEA. This may be because the Sty limited the oil loss during storage to levels found when cycling electrodes in PEA.

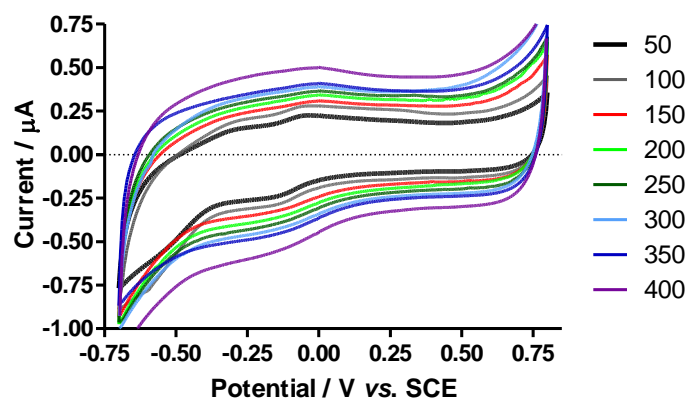


Figure 5.24: FBRR/SMCPEs cycled in a 1% PEA solution for 3.5 hours, $n = 4$.

To further test the effect of lipids on modified CPEs, they were cycled in the PEA solution for 12 hours, corresponding to the time period that would be required for physiological monitoring of tissue pH. The resulting CVs can be seen in Figure 5.25, showing every 200th cycle. The anodic peaks of interest were still visible, while the peak height appeared to slightly increase with time. A second oxidation peak appeared from cycle 1200, this resulted from O_2 entering the system. The N_2 flow was reduced as it caused the PEA solution to foam, wetting the electrode contacts, so the solution was no longer N_2 saturated.

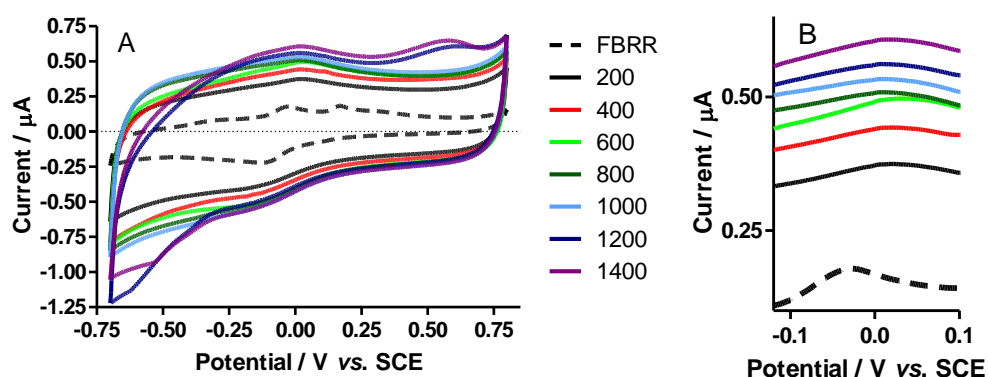


Figure 5.25: CVs of FBRR/CPEs cycled in 1% PEA for 12 hours (A), with the corresponding anodic peaks (B), $n = 4$.

5.2.3.3 Triton[®] X

Triton[®] X is a non-ionic surfactant¹⁷ that has a hydrophilic polyethylene oxide chain and an aromatic hydrocarbon lipophilic or hydrophobic group. Moieties containing hydrophilic heads and hydrophobic tails can form lipid bilayers, which make up the cell walls surrounding almost all living organisms, confirming the choice of Triton[®] X for the biocompatibility studies. CPEs functionalised with low concentrations of Triton[®] X have been shown to improve their electrochemical activity¹⁶⁻¹⁸ by forming a monolayer¹⁶ of surfactant on the electrode surface, but higher concentrations result in fouling of the substrate.¹⁴

CPEs were modified with FBRR and calibrated for pH response. They were then stored in Triton[®] X, 1%, at 4°C for 1, 3, 7 and 28 days. Calibration gave the expected anodic peaks with a pH response of approximately -58 mV/pH unit. On recycling the electrodes it was found that the currents had increased approximately 10 fold. These large currents, caused by surface fouling, masked the FBRR peaks and they were no longer visible in the CVs as shown in Figure 5.26. In contrast to electrodes stored in BSA and PEA, Sections 5.2.3.1-2, where the currents increased with time of storage, the currents for Triton[®] X stored electrodes reached a maximum level after day 1, remaining constant thereafter. This implied that Triton[®] X was the harshest treatment that the electrodes were subjected to, removing the silicone oil from the CPE immediately.

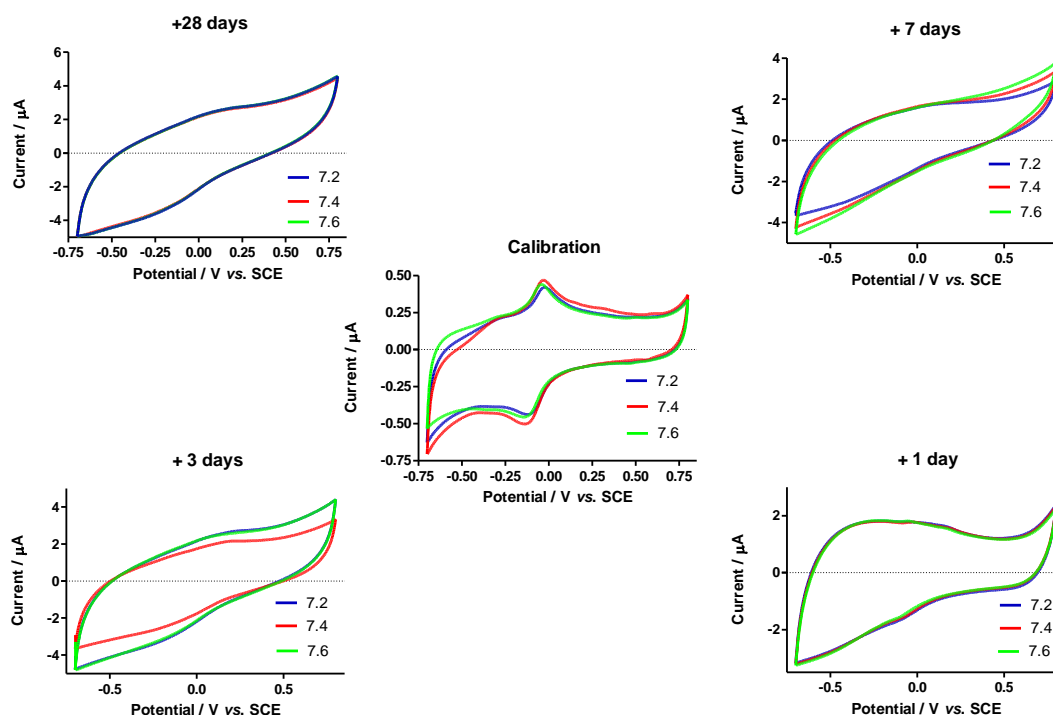


Figure 5.26: CVs showing the effect of storing FBRR/H₂SO₄ modified CPEs in 1% Triton[®]X.

The Triton[®] X had removed some of the silicone oil leaving a concave surface on the electrode. This resulted in an increased surface area which in turn led to higher currents. Also, the removal of oil left a higher carbon: oil ratio at the electrode/solution interface. As the silicone oil is non-conducting the increased carbon: oil ratio resulted in the higher currents achieved. The SEM micrographs in Figure 5.27 show how the removal of oil has caused an increase in the surface area of the electrode from day 1. The reduction in silicone oil content of Triton[®] X modified CPEs will be discussed in Section 5.2.4.1.

The organic FBRR would dissolve in the organic silicone oil, therefore, as the oil was extracted from the electrode surface, some FBRR was taken with it. This is evident from the CVs. The removal of oil alone would result in increased capacitance throughout the CV, with the redox peaks remaining. As the peaks have almost disappeared, it is an indication that the FBRR has also been removed.

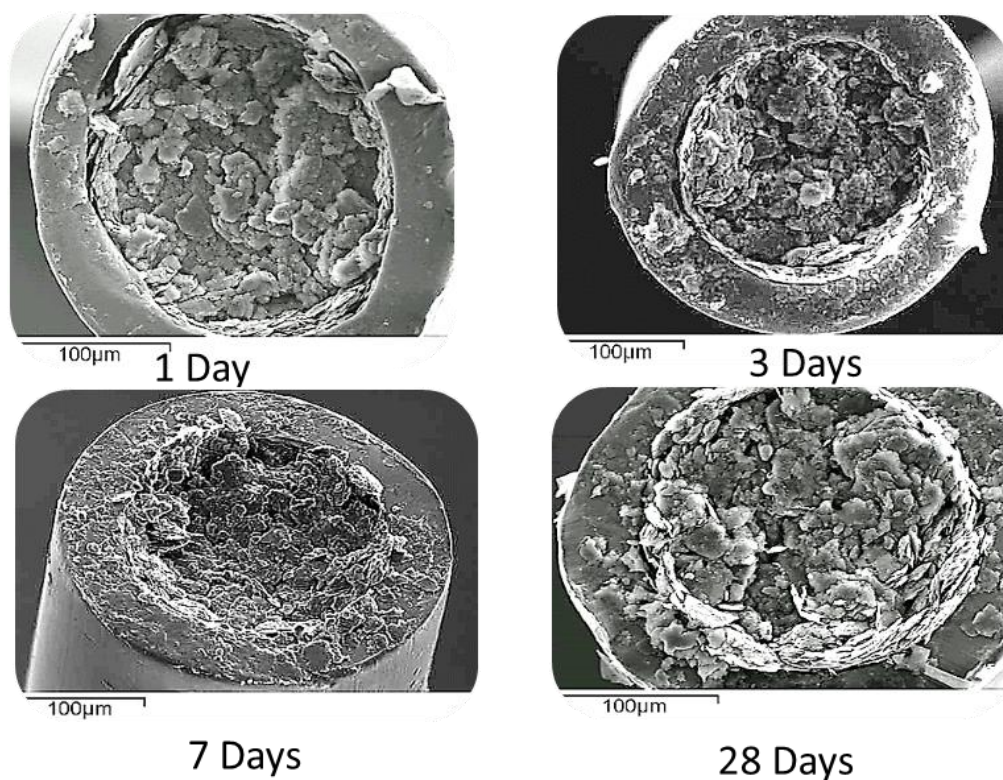


Figure 5.27: SEM micrographs of FBRR/CPEs stored in 1% Triton[®]X for up to 28 days.

An EDX of the surface, after 7 days storage in 1% Triton[®] X, (see Figure 5.28) still shows evidence of silicone oil but this is quantitatively reduced when compared to an EDX of a freshly modified CPE (see Table 5.7). The currents obtained for the Triton[®] X modified electrodes would appear to agree with the % Si quantitative analysis, explored in Section 5.2.4.1 of this chapter, showing an initial drop in % Si after day 1, leading to increased currents that further increase to a maximum level after day 3.

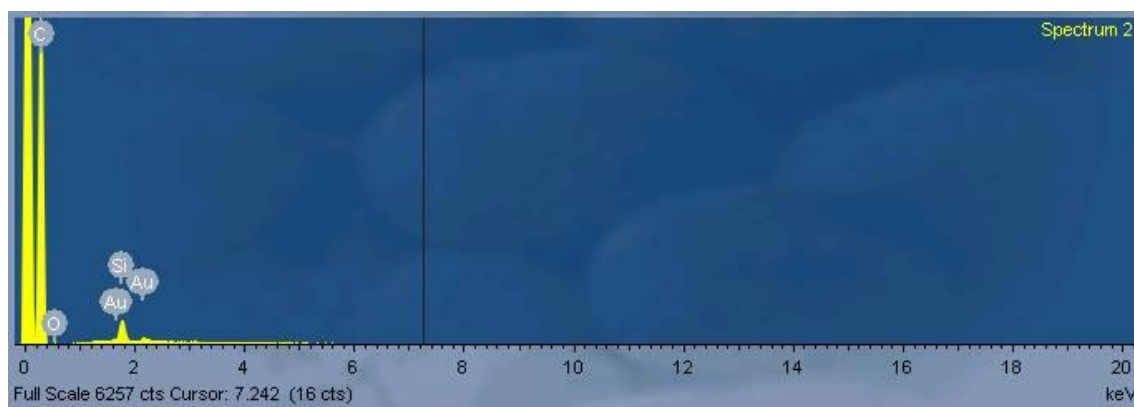


Figure 5.28 EDX of FBRR/CPEs stored in 1% Triton[®]X for 7 days.

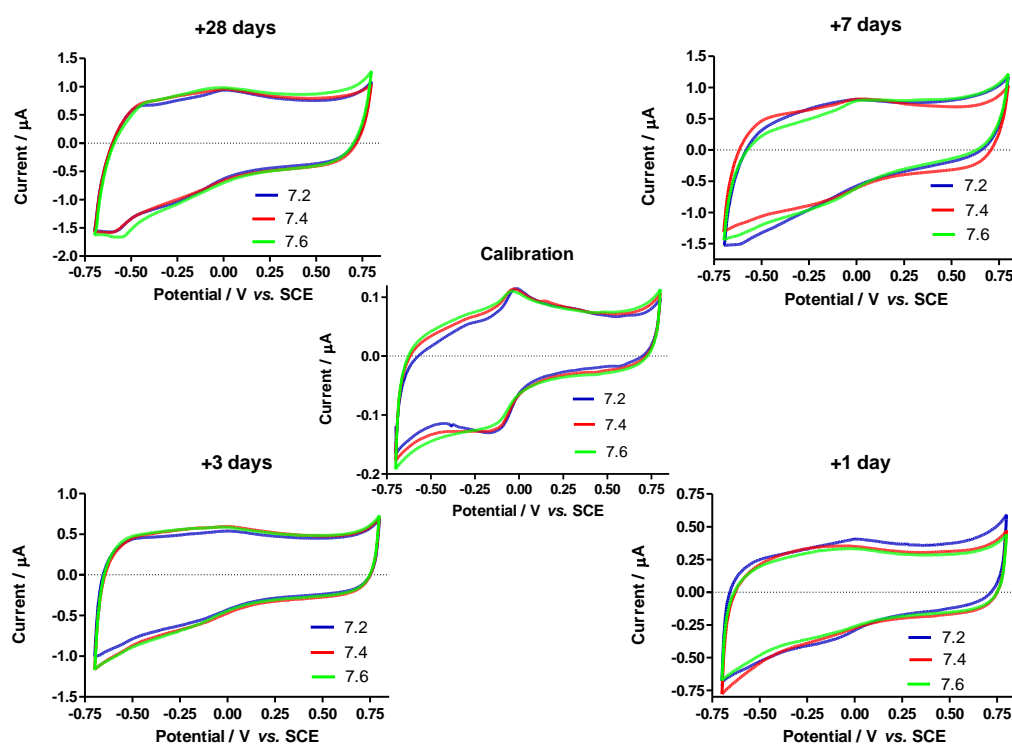
5.2.3.4 Brain Tissue

Sections 5.2.3.1-3 discussed the effect of proteins, lipids and surfactants on FBRR/H₂SO₄ modified electrodes. While these were valid tests to carry out individually, true physiological conditions could only be mimicked by testing the pH sensor in a matrix of all three components. Hence, samples of *ex-vivo* brain tissue, harvested from euthanised Wistar rats used within the research group, were employed as a test model. The biocompatibility studies followed a progression from laboratory prepared solutions of BSA, PEA and Triton[®]X to an *ex-vivo* system. As brain tissue was readily available to the researcher it was deemed a suitable progression step to avail of. It was noted by the researcher that brain tissue and muscle tissue differ in their composition, see Table 5.7.¹⁹ The water content is almost the same and would therefore have very little effect on the resultant CVs. Brain tissue contains substantially more lipid than skeletal muscle tissue, thereby justifying the use of brain tissue as a possible extreme value for the biocompatibility studies carried out in Chapters 5 and 6 of this thesis. The protein content of brain tissue is substantially lower than that of skeletal muscle tissue used in the *in-vivo* application in Chapter 7, however, the fact that *ex-vivo* brain tissue showed lower oxidation peaks than the eventual *in-vivo* muscle tissue, (see Section 7.2.2), meaning it was a harsher environment, the use of brain tissue was justified as an eligible medium in which to carry out testing.

Table 5.7: Comparison of skeletal muscle and whole brain tissue components.¹⁹

	Skeletal Muscle %	Whole Brain %
Water	75	77-78
Lipids	5	10-12
Protein	18-20	8

The centre graph in Figure 5.29 shows typical calibration CVs at pH 7.2, 7.4 and 7.6 with the post-storage CVs surrounding it. Similar to 1% BSA, PEA and Triton[®] X after all days, broad peaks were evident which appeared to shift with pH (non-Nernstian) but at a more positive potential, *ca.* 30 mV *vs.* SCE, than the calibration peaks. The currents increased with time, slightly more than electrodes stored in BSA, (Section 5.2.3.1), but not as much as electrodes stored in PEA or Triton[®] X (Sections 5.2.3.2-3)

**Figure 5.29:** CVs showing the effect of storing FBRR/CPEs in homogenised brain tissue, $n = 4$.

The SEM micrographs in Figure 5.30 show how storing the modified CPEs in homogenised brain tissue affected the surface morphology. After day 1 the electrode

appeared intact, thereafter, the surface became concave, indicating the loss of silicone oil. After 28 days stored in brain tissue, the electrode appeared totally dried out and had pulled away from the Teflon[®] support, leaving a more powdered electrode. There was evidence of brain tissue remaining on the paste and Teflon[®] surfaces, although the electrodes were thoroughly rinsed prior to imaging. It was possible that removing the electrode from the homogenised solution may have removed some paste from the electrode surface.

The EDX of the electrode surface, after 7 days storage in brain tissue, Figure 5.31, still shows evidence of silicone oil, but this quantity has been reduced when compared to the EDX of a freshly modified CPE (see Table 5.7).

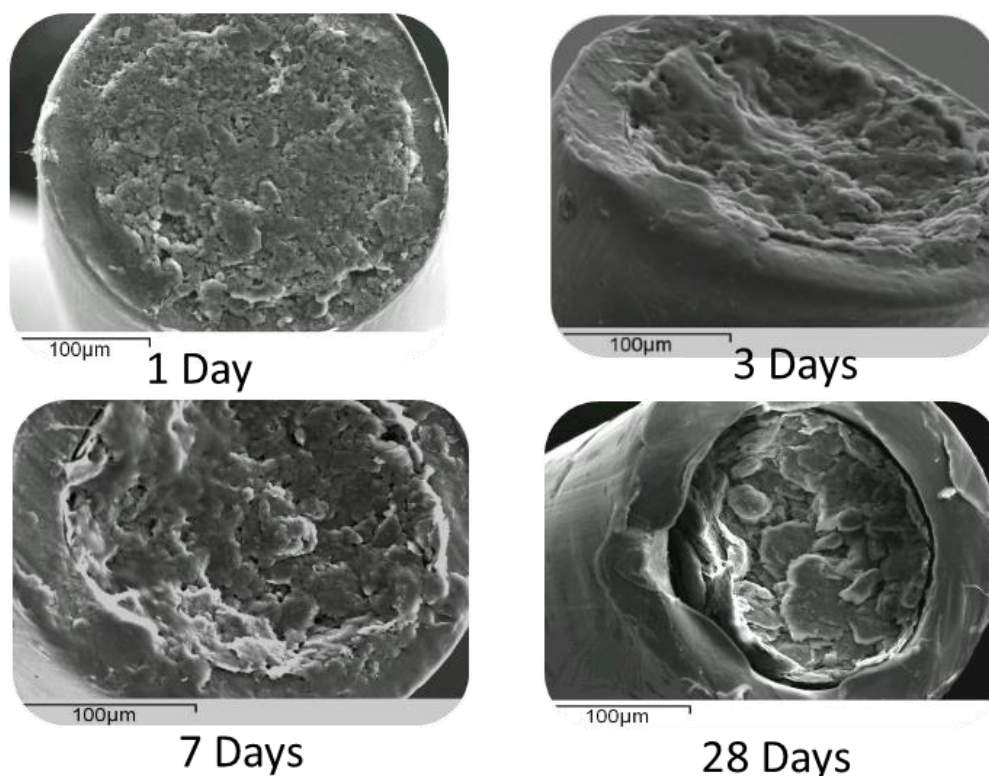


Figure 5.30: SEM micrographs of FBRR/CPEs stored in homogenised brain tissue for up to 28 days.

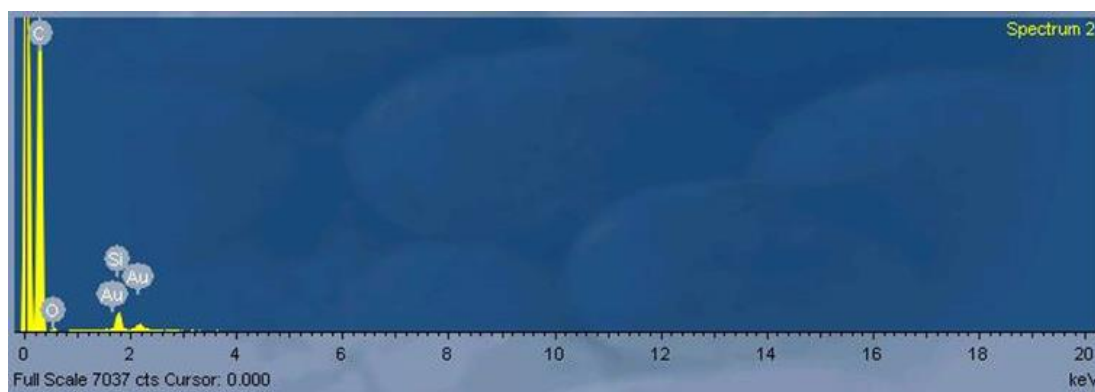


Figure 5.31: EDX of FBRR/CPEs stored in homogenised brain tissue for 7 days.

5.2.4 Silicone Oil Content of CPEs and SMCPEs

As CPEs are composed from a mixture of electrically conducting graphite and non-conducting silicone oil, creating a homogeneous paste, their electrochemical properties vary greatly with the ratio of each component contained within.^{20,21} Many studies have confirmed that some of the binding fluid is removed when CPEs come into contact with proteins and lipids.^{1,22} This could make the use of CPEs problematic for *in-vivo* applications. In an attempt to reduce the silicone oil losses from CPEs SMCPEs were produced. This section discusses the silicone oil content of FBRR/CPEs and FBRR/SMCPEs.

5.2.4.1 *Effect of Physiological Molecules on Oil Content*

It was noted in Section 5.2.3 that the morphology of the modified carbon paste electrodes changed once they had been subjected to the various treatments, (BSA, PEA, Triton[®] X and brain tissue), over a range of time. An EDX study was carried out on all CPEs that had been exposed to the substances and the % silicone oil was analysed. The percentages shown are relative to each other for each sample, this is why it is possible for the percentage of carbon to increase. Day 0 represents freshly modified CPEs which were not stored under any of the aforementioned conditions. All samples used for EDX purposes were modified and stored as required, they were not cycled in PBS at any stage. The % of silicone oil in freshly prepared CPEs was found to be just under 15%. This figure is variable depending on the preparation method²¹ used to make the paste and the age of the paste.²⁰ The initial content of silicone oil

drops off substantially after day 1 for all treatments, with all treatments giving significant differences except brain tissue. ($P_{TX} = 0.0104$, $P_{BSA} = 0.0030$, $P_{PEA} = 0.0041$ and $P_{BT} = 0.0634$). After 3 days of treatment all silicone oil percentages had significantly dropped ($P_{TX} = 0.0034$, $P_{BSA} = 0.0024$, $P_{PEA} = 0.0026$ and $P_{BT} = 0.0038$). This can be seen in Figure 5.32 with the corresponding values for % Si ($n = 6$) in Table 5.8. The results correspond with the findings in Section 5.2.3 which found that Triton[®] X was the most severe treatment applied to the electrode, removing almost all traces of silicone oil from the electrode surface. After day 1, which would correspond to the length of time for physiological recording of pH, brain tissue was found to retain the most silicone oil, (as it did across all days) dropping from 14.50% to 6.41% and not dropping below 2.30% after 28 days. In comparison, the Triton[®] X content dropped below 1% after 7 days (see Section 5.2.3.3), whereas BSA remained relatively +stable from day 3, having initially dropped (see Section 5.2.3.1).

Table 5.8: Quantitative analysis of the Si% contained in Triton[®]X, PEA, BSA and brain tissue modified electrodes, $n = 6$.

Day	Tx%	SEM	BT%	SEM	BSA%	SEM	PEA%	SEM
0	14.50	3.63	14.50	3.63	14.50	3.63	14.50	3.63
1	4.16	0.64	6.41	2.10	2.75	0.25	3.17	0.26
3	2.58	0.13	3.09	0.15	2.36	0.46	2.57	0.21
7	0.11	0.03	2.97	0.51	2.28	0.25	2.55	0.19
28	0.01	0.00	2.33	0.21	1.96	0.36	1.93	0.31

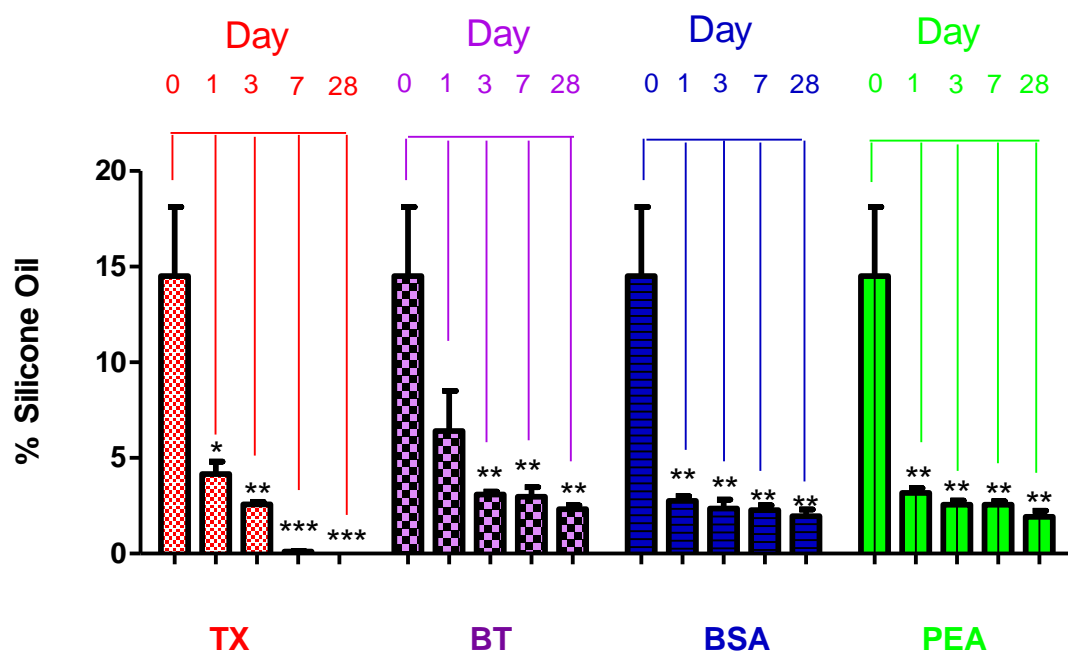


Figure 5.32: Bar chart showing the Si% contained in Triton[®]X, PEA, BSA and brain tissue modified FBRR/CPEs, $n = 6$.

5.2.4.2 Silicone Oil Content During FBRR/CPE Preparation

If the silicone oil content reduced so drastically when in contact with proteins and lipids, surely cycling the electrodes in all media must have an effect on the surface. This was studied by examining the oil content at all stages of preparation of FBRR/H₂SO₄ modified CPEs. The different oil contents resulting from storing and cycling modified CPEs in BSA/PEA was also investigated with the findings presented in Figure 5:33.

EDX analyses were carried out on CPEs to determine the % silicone oil present at various stages during production and after cycling/storage in PEA or BSA. A bare CPE contained about 4%* silicone oil, which dropped to about 3.2% on cycling in PBS (x100) or deposition of FBRR, showing significant differences ($P = 0.0012$ and 0.0013 , respectively). This was expected as some silicone oil leeches out with cycling and when depositing FBRR a percentage of the overall make-up of the surface was now assigned to the constituents of the FBRR. Storing in both BSA and PEA, 1%, for 3.5 hours resulted in a substantial drop in Si % to 1.7 and 1.8%, respectively. When

the FBRR/CPEs were cycled in the same solutions of BSA and PEA the silicone oil loss was reduced to 3.6 and 2.9%, respectively, indicating that storage resulted in a greater loss of oil than cycling.

*This was far lower than the previous Si % of 14.5% for a bare CPE. This was because different batches of carbon paste were used (see Section 5.2.6).

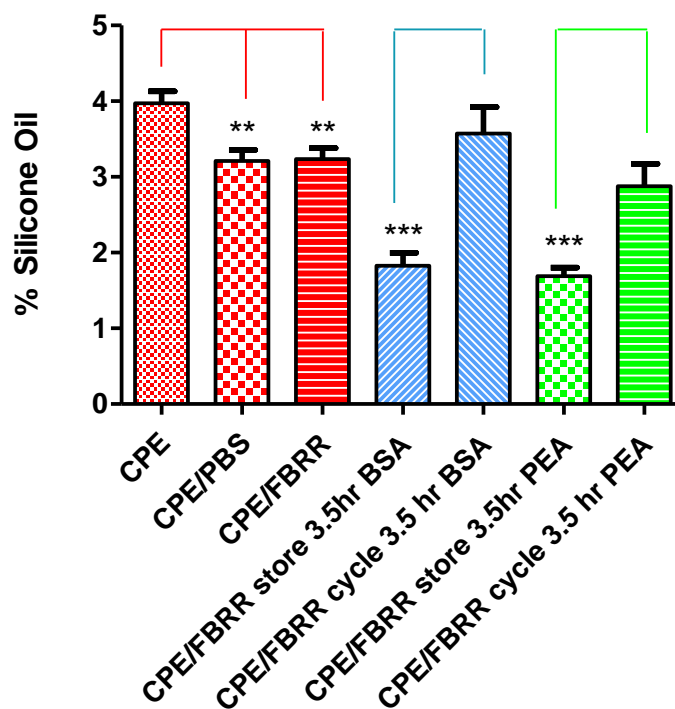


Figure 5.33: Bar chart showing the statistics for silicone oil content during the stages of manufacturing FBRR/CPEs and a comparison of the oil content when cycling or storing modified CPEs in BSA and PEA solutions.

The differences in oil content between storing and cycling the electrodes in the treatments were significant, ($P_{BSA} = 0.0001$ and $P_{PEA} = 0.0007$). This agreed with the findings of Sections 5.2.3.1-2. The increased currents suggested fouling of the electrode surface. The constant application of oxidation and reduction potentials while cycling in the BSA/PEA appears to reduce the amount of electrode fouling hence maintaining a more consistent silicone oil content.

5.2.4.3 Silicone Oil Content of SMCPEs

Section 5.2.4.1-2 reviewed the silicone oil content of FBRR/CPEs, concluding that there was a substantial drop in the oil percentage of electrodes after contact with proteins, lipids, surfactants and brain tissue. The percentage losses after 28 days storage in the media solutions were calculated as BSA: -86%; PEA: - 87% and brain tissue: - 84%. It was also found that a loss of *ca.* 20% resulted from cycling bare CPEs in PBS for 100 cycles and a further loss of < 1% occurred after the electrodeposition of FBRR.

Figure 5.34 shows a bar chart representing the silicone oil content of FBRR/SMCPEs at various stages throughout preparation of the sensor. It also includes the oil content of the modified electrodes having been stored in solutions of BSA, PEA and brain tissue. During preparation the oil percentage dropped from just below 4% to *ca.* 0.4%, an overall drop of -90%, after the CPE was stored in Sty. This recovered by +60% (from 0.4% to 1%) once the electrode was repacked and dried overnight. Similar to CPEs, SMCPEs showed little or no decrease in their oil content after electrodeposition of FBRR. All the results gave significant differences in oil content, with all *P*-values < 0.0001.

Once FBRR was deposited on FBRR/CPEs, they suffered oil losses of -82.5% (BSA), -83% (PEA) and -80% (brain tissue) after storage for 28 days in the media. FBRR/SMCPEs lost -48%, -51% and -38% after 28 days storage in BSA, PEA and brain tissue, respectively. These findings were somewhat disputed by the SEM micrographs in Figure 5.35, which show the concave surfaces resulting from storing sensors in brain tissue and PEA. Sensors stored in BSA for a period of 28 days appeared intact, but some paste had been pulled clear of the Teflon[®] support. The results suggest that modifying the CPEs with Sty reduced oil losses, by approximately 50%, when in contact with biological media. This however, was not sufficient to prevent the loss of FBRR from the surface, which was withdrawn along with the silicone oil. As brain tissue was the most physiologically relevant test medium used, the results obtained in this section could be an indication of how the sensor would behave *in-vivo*.

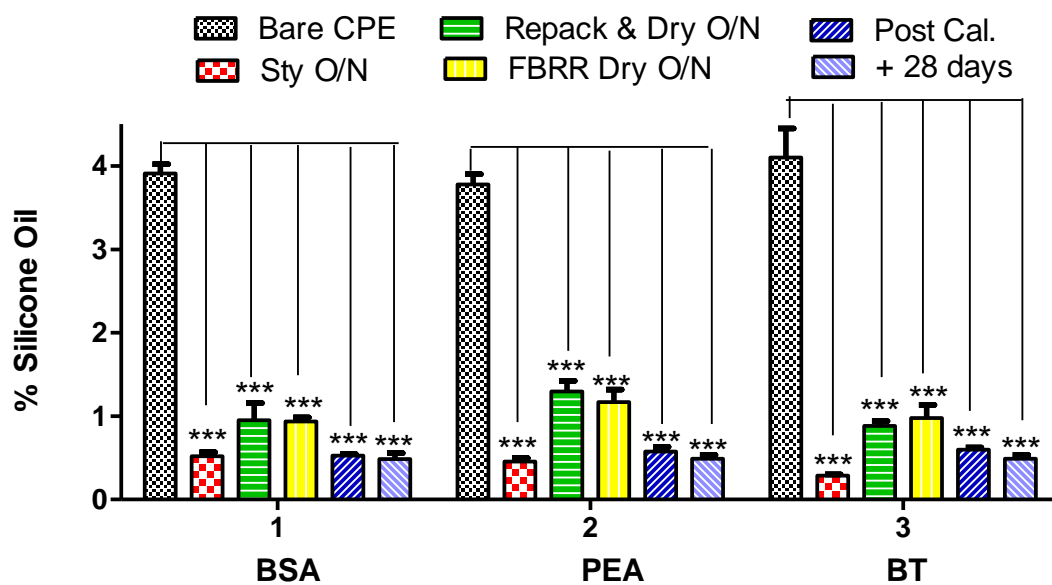


Figure 5.34: Bar chart representing the silicone oil content during preparation of SMCPEs and after storage in BSA, PEA and brain tissue for 28 days.

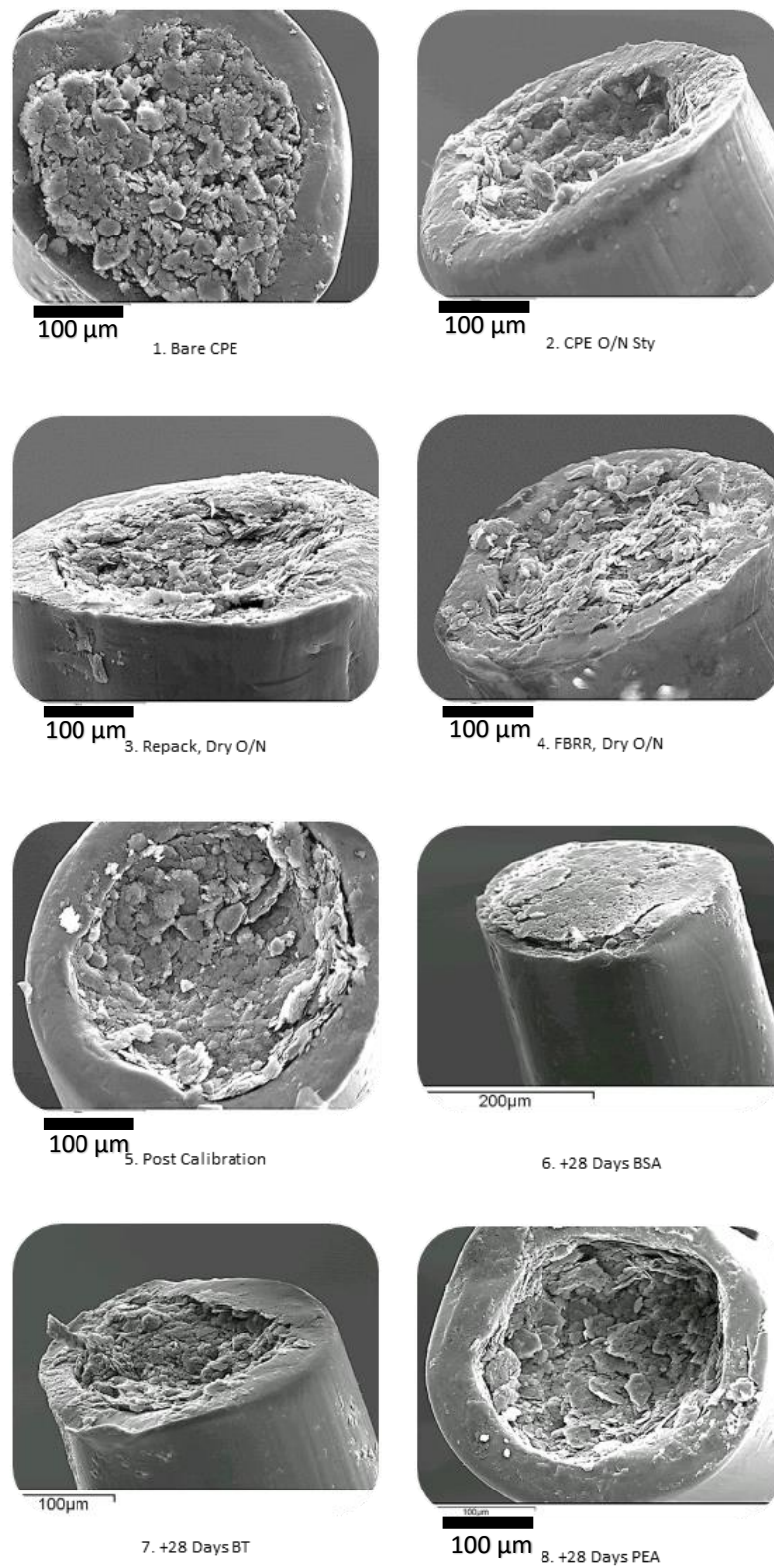


Figure 5.35: SEM micrographs of SMCPs during preparation and after storage in BSA, PEA and brain tissue for 28 days.

5.2.5 Real-Time pH Recording

Real-time pH studies were carried out on FBRR/SMCPEs. The electrodes were allowed to dry overnight at 4°C before being cycled in N₂ saturated PBS. The pH of the solution was altered, between 7.2 and 7.6, by an infusion pump with a constant flow rate, using 0.5 M NaOH or 0.5 M NaH₂PO₄, while being monitored by a commercial pH meter. The results, in Figure 5.36(A), gave a pH response of 59.6 ± 0.8 mV/pH unit, $R^2 = 0.99$, $n = 4$.

When compared to the FBRR/SMCPEs that were pH tested by cycling the electrodes in different pH of PBS (i.e., the electrodes were exposed to air between cycling), the controlled flow method of pH change gave much improved results (-60 mV/pH). This indicated that exposing the electrode to air caused changes to the surface, therefore electrodes took longer to reach steady state.

Figure 5.36(B) shows the comparative results obtained when FBRR/CPEs (Sty unmodified) were exposed to similar controlled flow pH changes. A comparable sensitivity of -56 ± 1 mV/pH ($R^2 > 0.95$, $n = 4$) was achieved, but the inter-electrode variability was reduced as shown by the smaller error bars.

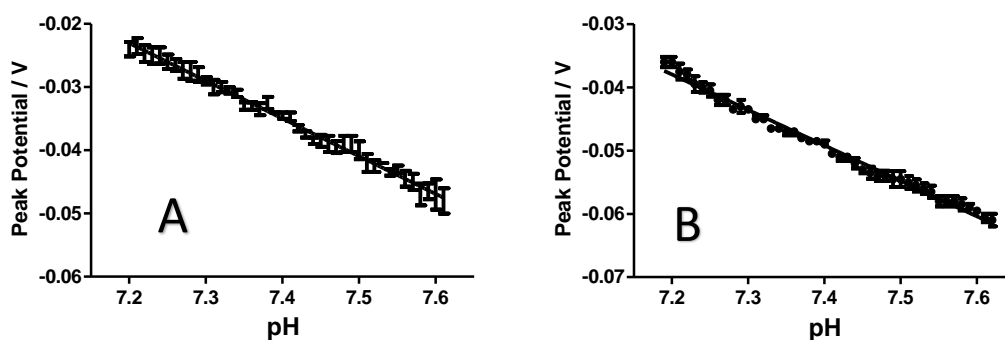


Figure 5.36: (A) Real-time pH response of FBRR/SMCPEs and (B) FBRR/CPEs, $n = 4$.

5.2.6 Carbon Paste Samples

The freshly prepared bare CPE samples examined in Section 5.2.4.1 had an average silicone content of 14.5%. When samples were tested using a different batch of paste the content was found to be *ca.* 4%, (see Section 5.2.4.2). It has been shown that the

age of the paste has an effect on its electrochemical properties^{20, 23} but the samples used were the same age at their time of testing. They were also prepared using the same carbon: silicone oil ratio of 0.71g: 250 μ l. Any differences, therefore, could only be due to the mixing techniques employed. To investigate the effect of mixing technique on the resulting sample, several different batches of carbon paste, some older than others, prepared by other researchers in the group, were examined under EDX and the % silicone oil was estimated. All the micrographs in Figure 5.37 have an identical scale. The silicone oil content and date of manufacture of each sample are displayed in Table 5.9.

Samples 2 and 5 (made by different researchers) were of similar age when tested. There were clear differences in the SEM micrographs, sample 5 being finer, more powder like, therefore it displayed a lower silicone oil content. Similarly, samples 1 and 4 were also of a similar age, made by different researchers. They have a totally different oil content even though they both appear similar. These have a much higher oil content than the powdered samples 3 and 5, made by the same researcher, which have a similar oil content even though there is an age difference of 11 months. These results confirm that the variability in each carbon paste sample is mainly due to the technique employed during preparation by individuals.

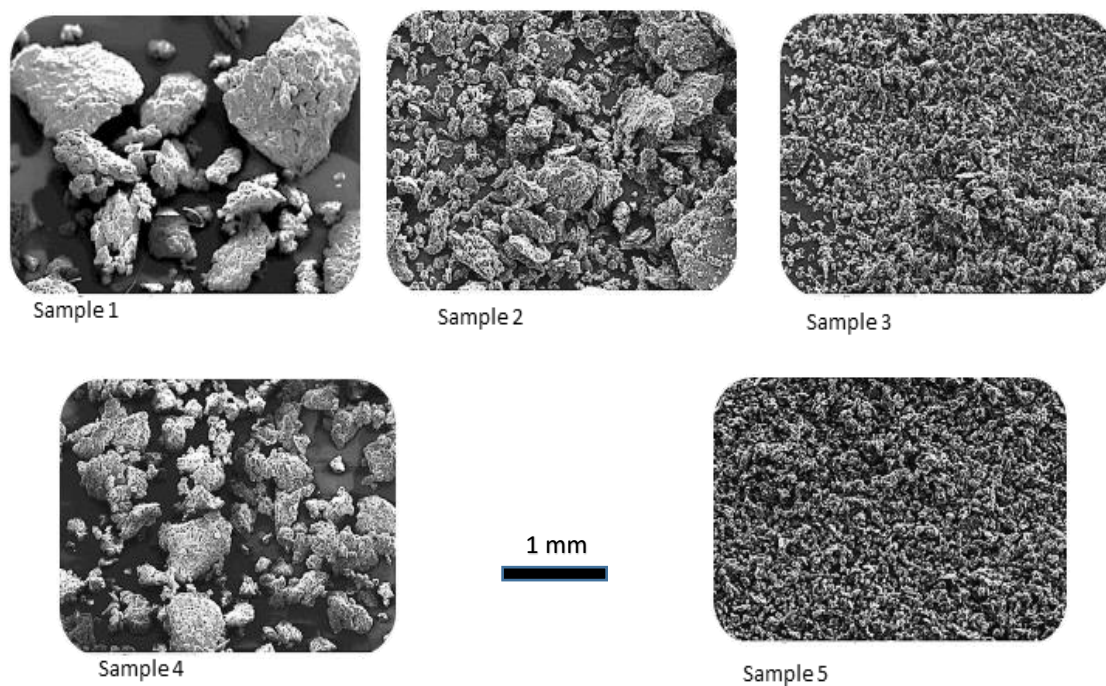


Figure 5.37: SEM micrographs of carbon paste prepared by different group members.

Table 5.9: Silicone oil content of carbon paste samples of varying age, made by different group members.

Sample & Date	Researcher	% Si	SEM
1. 11/2014	1	8.031	1.408
2. 02/2015	2	8.497	0.833
3. 02/2014	3	3.810	0.518
4. 10/2014	3	17.069	1.629
5. 01/2015	3	3.450	0.204

The carbon paste samples were then cycled in PBS (pH 7.4) for 100 cycles to ascertain whether the obtained currents mirrored the silicone oil content of the electrodes. The higher the silicone content the lower the currents generated, as the silicone oil is non-conducting. As the CV plot in Figure 5.38 shows, the paste with the highest silicone % (sample 4: 10/14) results in the lowest currents, whereas the paste with the lowest silicone % gives the highest currents. Sample 5 was noted as being almost 6 months old resulting in the low quantity of oil. This caused the electrode to behave similar to

a carbon electrode and, as such, can have various peaks evident in CV. These peaks were discussed in Chapter 4, Section 4.2.1. In the graph below these peaks are visible in samples 2, 3 and 5.

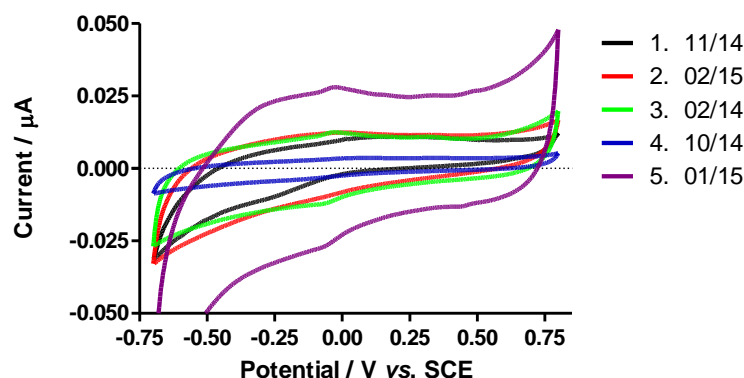


Figure 5.38: CVs of carbon paste samples with varying age, oil content and producers.

These quinone like peaks visible at approximately -0.03V vs. SCE seem to appear on carbon paste that has a lower silicone oil content making them more like carbon electrodes that have exposed carbon edge-plane sites. Literature shows that carbon edge-plane sites can have many functional groups on their surfaces including quinones.²⁴⁻²⁶ It must be noted that even on the same sample of carbon paste these peaks were not always visible or they may appear very broad which would make it difficult to extrapolate a definite peak potential for analysis purposes.

5.2.7 Physiological Interferences

The *in-vivo* environment is loaded with endogenous electroactive species that could interfere with the oxidation of FBRR at CPEs. The FBRR/CPEs were cycled in solutions containing physiologically relevant concentrations of these substances in order to mimic the *in-vivo* environment.

5.2.7.1 Ascorbic Acid (AA)

AA, also known as vitamin C is present in many biological systems.²⁷ Its main use is as an antioxidant.²⁸ The irreversible oxidation of AA at a CPE occurs at approximately 0.20 V vs. SCE^{27, 29} and results in a broad peak indicative of slow electron transfer rates due to fouling of the electrode surface³⁰ by the oxidation product of AA, dehydroascorbic acid.³¹ Blood concentrations of AA are variable, depending on dietary intake, ranging from 200 to 800 μM ,³² whereas brain ECF concentrations can vary between 100 and 500 μM .³³

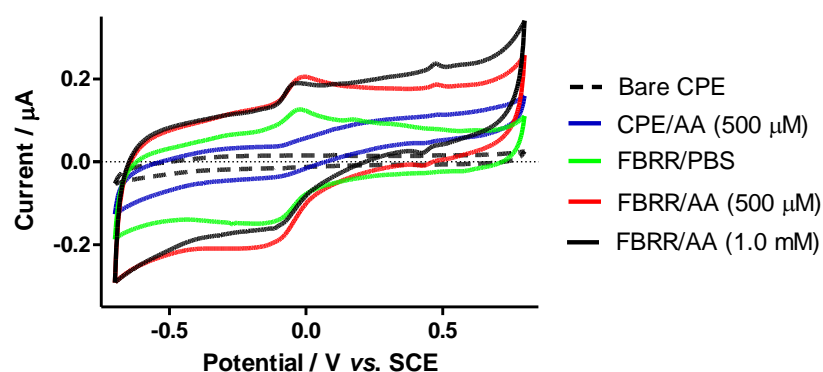


Figure 5.39: CVs showing the effect of 50 μM and 1.0 mM AA on the redox peaks of FBRR/CPEs, $n = 4$.

Figure 5.39 shows the CVs obtained when cycling bare and modified CPEs in AA. The broad oxidation peak of AA was evident at 0.25 V vs. SCE on the bare electrode. This broad wave was also evident, but to a lesser extent, at the FBRR modified electrodes cycled in PBS/AA (500 μM and 1.0 mM). However, the currents increased with increasing concentration. The quinone oxidation peak, resulting from FBRR, was slightly shifted when the modified electrode was cycled in AA, from -0.016 V vs. SCE in PBS to a potential of -0.020 V vs. SCE in PBS/AA (1.0 mM). The mean peak potentials of the FBRR/PBS and FBRR/PBS/AA (1.0 mM) anodic peaks were tested

using unpaired t-tests leading to non-significant differences between the means with a P -value of 0.5006, shown in Table 5.10.

However, the pH of the PBS/AA (1.0 mM) solution was recorded at 7.31. When this pH difference was taken into account the mean peak potential shifted to -0.014 V *vs.* SCE. Repeating the t-test yielded an improved P -value of 0.8637.

Table 5.10: Statistical analyses of the anodic peak potentials of FBRR/CPEs cycled in PBS and PBS/AA (50 μ M and 1.0 mM), $n = 4$.

Mean Peak Potential FBRR (V)	Mean Peak Potential FBRR/AA (V)	P -value	Mean Peak Potential FBRR/AA pH adjusted (V)	P -value
-0.0155 ± 0.0033	-0.0195 ± 0.0045	0.5006	-0.0142 ± 0.0045	0.8637

5.2.7.2 Uric Acid (UA)

UA is an important potential interferent in sensors utilised for *in-vivo* experiments in the brain and peripheral regions of the body.³⁴ UA is present in the blood as an antioxidant and is the final metabolite of purine.³⁵ Blood plasma levels are reported to be up to 0.50 mM,³² with brain ECF levels reported up to 50 μ M.³³ The reversible oxidation of UA at a bare CPE is found at approximately 0.30 V *vs.* SCE.^{27, 30}

Figure 5.40 shows the CVs obtained when cycling bare and modified CPEs in UA. The oxidation peak of UA was clearly visible at 0.28 V *vs.* SCE on the bare electrode. This peak was maintained at the same position on the FBRR modified electrodes. The quinone oxidation peak, resulting from FBRR, was slightly shifted by the UA peak, from -0.027 V *vs.* SCE in PBS to -0.028 V *vs.* SCE in PBS/UA. The mean peak potentials of the FBRR/PBS and FBRR/PBS/UA (100 μ M) anodic peaks were tested using unpaired t-tests leading to non-significant differences between the means with a P -value of 0.9158, shown in Table 5.11. The pH of the PBS/UA (100 μ M) solution was recorded at 7.39 so this would have very little effect on the position of the anodic peaks of FBRR.

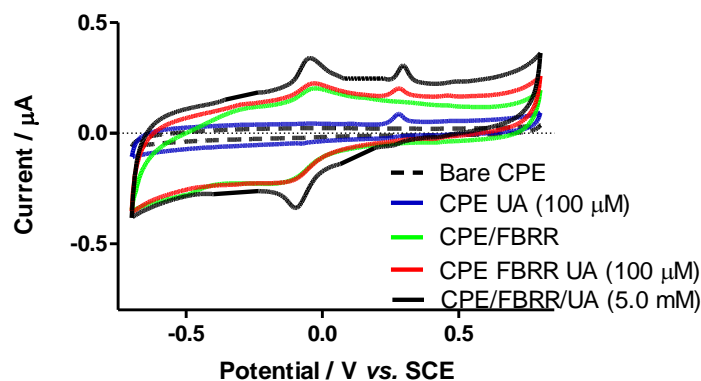


Figure 5.40: CVs showing the effect of 100 μM and 5 mM UA on the redox peaks of FBRR/CPEs, $n = 4$.

Table 5.11: Statistical analyses of the anodic peak potentials of FBRR/CPEs cycled in PBS and PBS/UA (100 μM and 5 mM), $n = 4$.

Mean Peak Potential FBRR (V)	Mean Peak Potential FBRR/UA (V)	<i>P</i> -value
-0.0270 ± 0.0021	-0.0275 ± 0.0040	0.9158

5.2.7.3 Dopamine (DA)

DA is a crucial catecholamine neurotransmitter^{7, 19, 25} of the central nervous system. Mammalian concentrations of DA are low, 0.02-0.05 μM , and as such are difficult to determine.^{2, 22, 33} Anodic peak potentials of DA at a bare CPE are varied in literature, 0.18²⁰, 0.22¹⁷ and up to 0.44 V vs. SCE²⁵, mainly resulting from the differences between carbon paste samples.

The CVs of the bare CPE in PBS, FBRR/CPE in PBS, bare CPE in PBS/ DA and FBRR/CPE in PBS/ DA are shown in Figure 5.41. The oxidation peak for DA at the bare CPE was not observed. There was no evidence of any DA oxidation at the FBRR/modified CPE. The currents obtained for the modified CPE cycled in DA were slightly reduced when compared to those for the FBRR/CPE in PBS. This was indicative of electrode fouling by the oxidation product of DA.^{14, 35} However, as there was no evidence of DA oxidation, this potential shift probably resulted from the solution pH change rather than electrode fouling. The anodic peak of FBRR/H₂SO₄ in

PBS was located at -0.024 V vs. SCE and shifted to a more negative potential of -0.027 V vs. SCE when the DA was added to the PBS solution. The mean peak potentials of the FBRR anodic peaks were tested using unpaired t-tests leading to a non-significant difference between the means with a P -value of 0.3053, shown in Table 5.12.

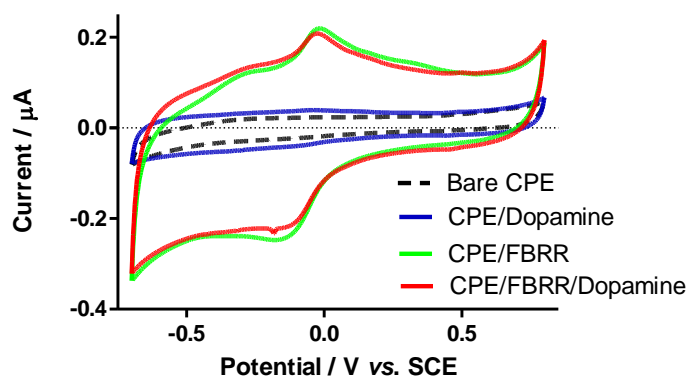


Figure 5.41: CVs showing the effect of $0.1 \mu\text{M}$ DA on the redox peaks of FBRR/CPEs, $n = 4$.

However, the pH of the PBS/DA solution was recorded at 7.35. When this pH difference was taken into account the mean peak potential shifted to -0.024 V vs. SCE. Repeating the t-test yielded an improved P -value of 1.00.

Table 5.12: Statistical analyses of the anodic peak potentials of FBRR/CPEs cycled in PBS and PBS/DA ($0.1 \mu\text{M}$), $n = 4$.

Mean Peak Potential FBRR (V)	Mean Peak Potential FBRR/DA (V)	P -value	Mean Peak Potential FBRR/DA pH adjusted (V)	P -value
-0.0235 ± 0.0025	-0.0265 ± 0.0010	0.3053	-0.0235 ± 0.0010	1.0000

5.2.7.4 L-Cysteine

L-Cysteine is a non-essential amino acid³⁶ that is present in blood at concentrations between $3\text{--}15 \mu\text{M}$.³² At a CPE the oxidation generally yields a poorly defined peak at

approximately 0.50 V vs. SCE.³⁷ The CVs of bare CPEs in PBS, FBRR/CPEs in PBS, bare CPEs in PBS/ L-Cysteine and FBRR/CPEs in PBS/ L-Cysteine are shown in Figure 5.42. The oxidation peak for L-Cysteine at the bare CPE was not observed. There was no evidence of any L-Cysteine oxidation at the FBRR/modified CPE. The anodic peak of FBRR/H₂SO₄ in PBS was located at -0.023 V vs. SCE and shifted to a more negative potential of -0.032 V vs. SCE when the L-Cysteine was added to the PBS solution. The mean peak potentials of the FBRR anodic peaks were tested using unpaired t-tests leading to a significant difference between the means, with a *P*-value of 0.0161, shown in Table 5.13.

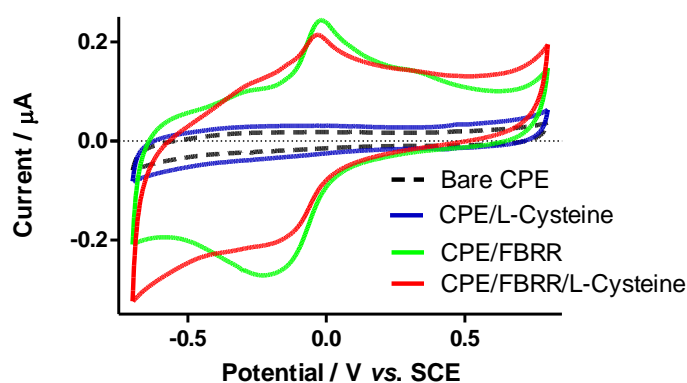


Figure 5.42: CVs showing the effect of 100 μM L-Cysteine on the redox peaks of FBRR/CPEs, $n = 4$.

However, the pH of the PBS/L-Cysteine solution was recorded at 7.34. When this pH difference was taken into account the mean peak potential shifted to -0.028 V vs. SCE. Repeating the t-test yielded an improved *P*-value of 0.0992, indicating no significant difference with the addition of L-Cysteine.

Table 5.13: Statistical analyses of the anodic peak potentials of FBRR/CPEs cycled in PBS and PBS/ L-Cysteine (100 μM), $n = 4$.

Mean Peak Potential FBRR (V)	Mean Peak Potential FBRR/L-Cys (V)	<i>P</i> -value	Mean Peak Potential FBRR/L-Cys pH adjusted (V)	<i>P</i> -value
-0.0230 \pm 0.0019	-0.0315 \pm 0.0017	0.0161	-0.0280 \pm 0.0017	0.0992

5.2.7.5 L-Tyrosine

Tyrosine, 4-hydroxyphenylalanine, is an aromatic amino acid³⁸ that is a precursor for adrenaline, dopamine and melanine.³⁹ Normal blood concentrations have been documented as 100 μM .⁴⁰ The electrochemical oxidation of tyrosine occurs at its hydroxyl groups and involves the transfer of $2\text{H}^+/2\text{e}^-$ resulting in the formation of quinone-like products.⁴¹ Experiments were carried out to investigate whether the oxidation products of tyrosine could influence the FBRR anodic peak. The resulting CVs are shown in Figure 5.43. No anodic peak was observed at the bare CPE as this would generally be found slightly above 1000 mV *vs.* SCE at a CPE.⁴² There was also no evidence of the oxidation products of L-Tyrosine at the bare CPE. However, when the FBRR/CPE was cycled in PBS/L-Tyrosine, a broad peak at approximately 0.30 V *vs.* SCE was evident, that had not been observed when cycling in PBS alone. The FBRR anodic peaks underwent a slight shift in potential between cycling in PBS and PBS/L-Tyrosine, from -0.022 to -0.024 V *vs.* SCE, see Table 5.14. The mean peak potentials of the FBRR peaks (in PBS and PBS/L-Tyrosine) were tested using unpaired t-tests leading to a non-significant difference between the means with a *P*-value of 0.4128, shown in Table 5.14.

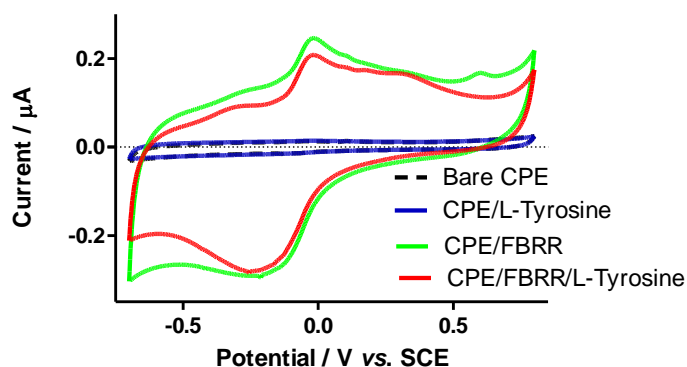


Figure 5.43: CVs showing the effect of 200 μM L-Tyrosine on the redox peaks of FBRR/CPEs, $n = 4$.

However, the pH of the PBS/L-Tyrosine solution was recorded at 7.38. When this pH difference was taken into account the mean peak potential shifted to -0.022 V vs. SCE . Repeating the t-test yielded an improved P -value of 0.7306.

Table 5.14: Statistical analyses of the anodic peak potentials of FBRR/CPEs cycled in PBS and PBS/L-Tyrosine (200 μM), $n = 4$.

Mean Peak Potential FBRR (V)	Mean Peak Potential FBRR/L-Tyr (V)	P -value	Mean Peak Potential FBRR/L-Tyr pH adjusted (V)	P -value
-0.0215 ± 0.0013	-0.0235 ± 0.0019	0.4128	-0.0223 ± 0.0019	0.7306

5.2.7.6 Serotonin (5-HT)

5-HT, 5-hydroxytryptamine, is produced from the amino acid tryptophan in the human body where it acts as a neurotransmitter.⁴³ Predicted brain ECF concentrations, for 5-HT, are extremely low, up to 10 nM,³³ however, almost all serotonin is located in the gastro-intestinal tract, where it is used to regulate intestinal movements. The anodic peak of 5-HT is generally located close to 0.35 V vs. SCE.^{44, 45} Figure 5.44 shows the CVs obtained when cycling bare and modified CPEs in 5-HT. The 5-HT anodic peak was observed at 0.36 V vs. SCE at the bare CPE. This peak was retained at a similar

potential for the FBRR/CPE. The anodic peak for FBRR/PBS was apparent at -0.030 V vs. SCE. This was retained when both 1 and 10 μM concentrations of 5-HT were added to the PBS, although the peak became broader with increased concentration indicating slower electron kinetics due to fouling of the electrode surface by the 5-HT oxidation product.⁴⁴ A metabolite of 5-HT, 5-HIAA, could cause this broadening of the anodic peak, although the concentrations examined in this section far exceed any possible biological levels. The effects of 5-HIAA will be examined separately in Section 5.44.

There was a slight shift in the anodic peak potential for the FBRR/CPEs when 1 μM 5-HT was added, to approximately -0.031 V vs. SCE. When 10 μM 5-HT was added the peak potential shifted to approximately 0.010 V vs. SCE. The mean peak potentials of the FBRR peaks (in PBS and PBS/ 1 μM 5-HT) were tested using unpaired t-tests leading to a non-significant difference between the means with a P -value of 0.6202 , shown in Table 5.15. The pH of the PBS and PBS/ 1 μM 5-HT solutions were both 7.40 .

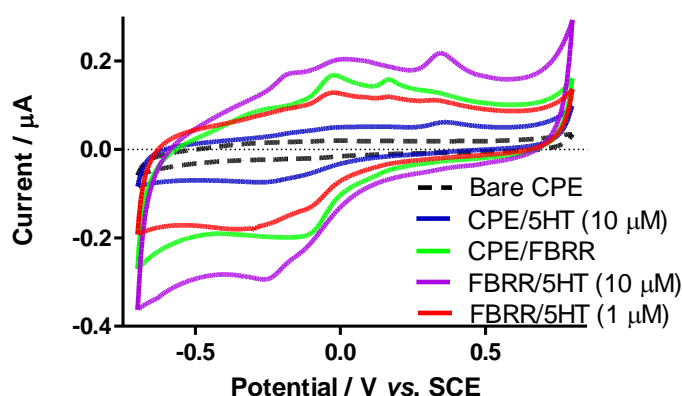


Figure 5.44: CVs showing the effect of 1.0 and 10 μM 5-HT on the redox peaks of FBRR/CPEs, $n = 4$.

Table 5.15: Statistical analyses of the anodic peak potentials of FBRR/CPEs cycled in PBS and PBS/5-HT (1.0 μM), $n = 4$.

Mean Peak Potential FBRR (V)	Mean Peak Potential FBRR/5-HT (V)	P -value
-0.0300 ± 0.0014	-0.0310 ± 0.0013	0.6202

5.2.7.7 L-Glutathione

L-Glutathione is an antioxidant³¹ which plays an important role in the scavenging of physiologically generated free radicals.⁴⁶ The normal blood concentration of L-Glutathione is in the millimolar range while that of plasma is in the micromolar range.⁴⁶ The irreversible oxidation of L-Glutathione at a CPE generally occurs at 1.05 V vs. SCE,⁴⁶ well removed from the FBRR/H₂SO₄ anodic peak and so would not be expected to interfere with the FBRR peak of interest. However, the oxidation of L-Glutathione at a FBRR/CPE was thought to be undocumented, so it was examined here to eliminate the possibility of the FBRR modification facilitating the oxidation of the L-Glutathione bringing it to a lower peak potential.

The CVs of the bare CPE in PBS, FBRR/CPE in PBS, bare CPE in PBS/ L-Glutathione and FBRR/CPE in PBS/ L-Glutathione are shown in Figure 5.45. The oxidation peak for L-Glutathione at the bare CPE was, as expected, outside the range of the CV. There was no evidence of any L-Glutathione oxidation at the FBRR/modified CPE. The anodic peak of FBRR/H₂SO₄ in PBS was located at -0.034 V vs. SCE and shifted to a more negative potential of -0.036 V vs. SCE when the L-Glutathione was added to the PBS solution. The mean peak potentials of the FBRR anodic peaks were tested using unpaired t-tests leading to a non-significant difference between the means with a *P*-value of 0.2347, shown in Table 5.16.

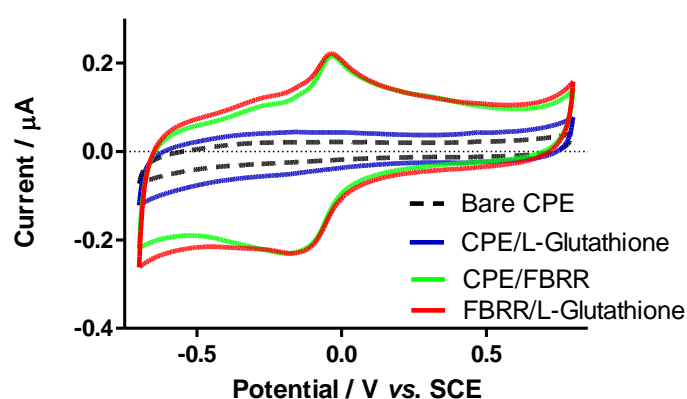


Figure 5.45: CVs showing the effect of 100 μ M L-Glutathione on the redox peaks of FBRR/CPEs, $n = 4$.

As the pH of the PBS/ L-Glutathione solution was recorded at 7.36, this caused a shift of potential for the redox peaks of FBRR. When this pH difference was taken into account the mean peak potential was adjusted to -0.034 V vs. SCE. Repeating the t-test gave an improved *P*-value of 0.9596.

Table 5.16: Statistical analyses of the anodic peak potentials of FBRR/CPEs cycled in PBS and PBS/ L-Glutathione, *n* = 4.

Mean Peak Potential FBRR (V)	Mean Peak Potential FBRR/L-Glut (V)	<i>P</i> -value	Mean Peak Potential FBRR/L-Glut pH adjusted (V)	<i>P</i> -value
-0.0335 ± 0.0017	-0.0360 ± 0.0008	0.2347	-0.0336 ± 0.0008	0.9596

5.2.7.8 Homovanillic Acid (HVA)

HVA is a catecholamine metabolite of DA,^{15, 22} with ECF concentrations of up to 10 μM.³³ The oxidation potential of HVA at a CPE is located at approximately 0.60 V vs. SCE, and is irreversible due to the cleavage of the methoxy bond.²²

The CVs of bare CPEs in PBS, FBRR/CPEs in PBS, bare CPEs in PBS/HVA and FBRR/CPEs in PBS/HVA are shown in Figure 5.46. The redox peaks for HVA appeared at 0.16 and 0.09 V vs. SCE. The anodic peak of FBRR/H₂SO₄ in PBS fell at -0.025 V vs. SCE and shifts to a more negative potential of -0.028 V vs. SCE when the HVA was added to the PBS solution. The mean peak potentials of the FBRR anodic peaks were tested using unpaired t-tests leading to a non-significant difference between the means with a *P*-value of 0.1428, shown in Table 5.17.

As the pH of the PBS/ HVA solution was recorded at 7.37, this caused a shift of potential for the redox peaks of FBRR. When this pH difference was taken into account the mean peak potential was adjusted to -0.027 V vs. SCE. Repeating the t-test gave an improved *P*-value of 0.1762.

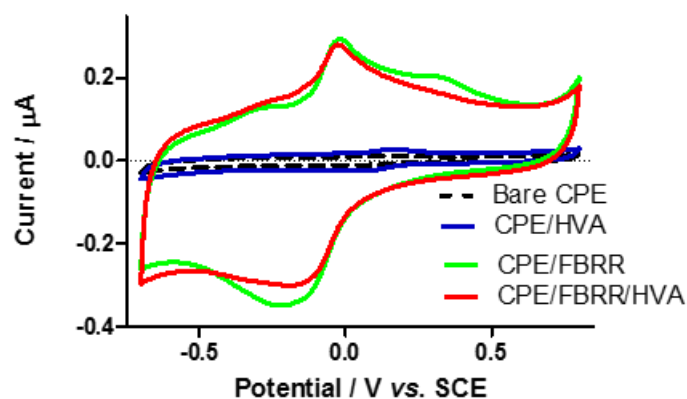


Figure 5.46: CVs showing the effect of 50 μM HVA on the redox peaks of FBRR/CPEs, $n = 4$.

Table 5.17: Statistical analyses of the anodic peak potentials of FBRR/CPEs cycled in PBS and PBS/HVA, $n = 4$.

Mean Peak Potential FBRR (V)	Mean Peak Potential FBRR/HVA (V)	<i>P</i> -value	Mean Peak Potential FBRR/HVA pH adjusted (V)	<i>P</i> -value
-0.0245 ± 0.0013	-0.0275 ± 0.0013	0.1428	-0.0266 ± 0.0005	0.1762

The anodic peak potential of 0.16 V vs. SCE for HVA at a CPE was not in good agreement with literature values of 0.60 V vs. SCE. Further investigation revealed that HVA oxidation resulted in the formation of DOPAC.^{22, 31} As the CVs in Figure 5.46 were recorded after 100 cycles, the peaks observed at the bare CPE corresponded with DOPAC, not HVA. The oxidation of HVA is shown in Figure 5.47. The first cycle shows the oxidation of HVA at approximately 0.65 V vs. SCE, forming its oxidation product, DOPAC. The reverse sweep of the first cycle shows an unexpected reduction peak at approximately 0.10 V vs. SCE, this was the reduction of DOPAC formed from the oxidation of HVA. The second forward cycle shows another oxidation peak at 0.15 V vs. SCE, corresponding to DOPAC oxidation.

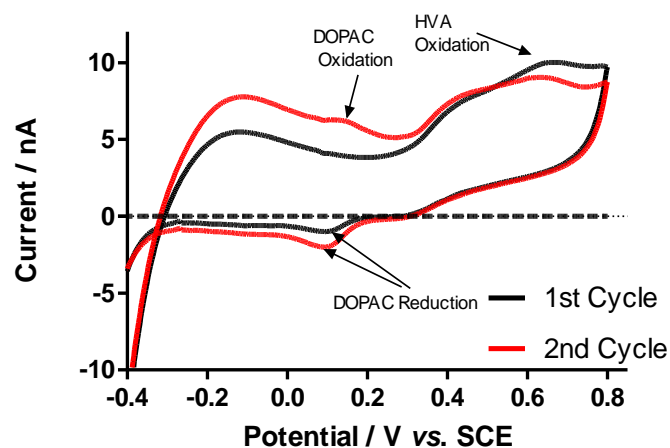


Figure 5.47: First and second cycles of CVs showing the formation of DOPAC by the electrochemical oxidation of HVA at CPEs, $n = 4$.

5.2.7.9 DOPAC

DOPAC, is a metabolite resulting from the oxidation of HVA,²² with expected ECF concentrations between 1 and 20 μM .³³ This was previously shown in Section 5.2.7.8. The CVs of bare CPEs in PBS, FBRR/CPEs in PBS, bare CPEs in PBS/DOPAC and FBRR/CPEs in PBS/DOPAC are shown in Figure 5.48. The redox peaks for DOPAC occurring at 0.15 and 0.05 V vs. SCE are broad due to the slow electron transfer at the paste surface. The anodic peak of FBRR/ H_2SO_4 in PBS falls at -0.026 V vs. SCE and shifts to a slightly more negative potential when the DOPAC was added. The mean peak potentials of the FBRR anodic peaks were tested using unpaired t-tests leading to a non-significant difference between the means with a P -value of 0.3867, shown in Table 5.18.

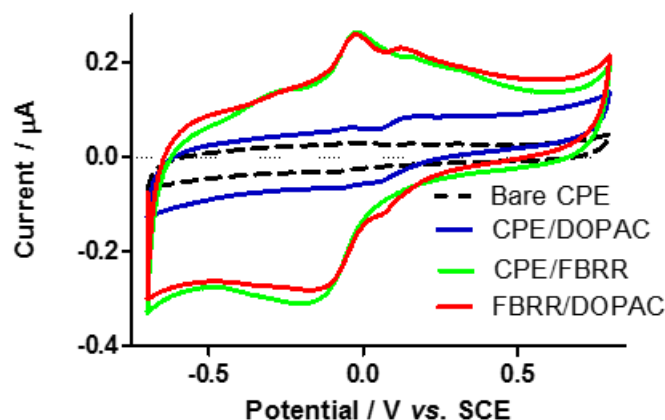


Figure 5.48: CVs showing the effect of 100 μM DOPAC on the redox peaks of FBRR/CPEs, $n = 4$.

As the pH of the PBS/ DOPAC solution was recorded at 7.34, this resulted in a shift of potential for the redox peaks of FBRR. When this pH difference was taken into account the mean peak potential shifted to -0.024 V vs. SCE . Repeating the t-test also gave a P -value of 0.3867.

Table 5.18: Statistical analyses of the anodic peak potentials of FBRR/CPEs cycled in PBS and PBS/DOPAC, $n = 4$.

Mean Peak Potential FBRR (V)	Mean Peak Potential FBRR/DOPAC (V)	P -value	Mean Peak Potential FBRR/DOPAC pH adjusted (V)	P -value
-0.0255 ± 0.0010	-0.0270 ± 0.0013	0.3867	-0.0240 ± 0.0013	0.3867

5.2.7.10 5-Hydroxy-Indole Acetic Acid (5-HIAA)

5-HIAA is a primary metabolite of 5-HT. Normal levels are variable depending on age and the bio fluid being tested (urine, blood, CSF) and are found in the range of $0.05\text{-}55.0 \mu\text{M}$.⁴⁷ The anodic peak resulting from the oxidation of 5-HIAA presents between 0.30 and 0.40 V vs. SCE ⁴⁸ at a bare CPE and is generally broad due to the slow electron transfer rate at the homogeneous CPE surface.⁴⁹

Figure 5.49 shows the CVs obtained when cycling bare and modified CPEs in 5-HIAA. The innermost plot shows a bare CPE, moving outwards the next plot is the bare CPE cycled in a PBS solution with added 5-HIAA (100 μM). The characteristic oxidation peak is apparent at 0.30 V vs. SCE. The next CV, moving outwards, displays the anodic peak of FBRR/ H_2SO_4 at -0.014 V vs. SCE. In the outermost CV both the FBRR and 5-HIAA anodic peaks are evident. The 5-HIAA has remained at the same potential but the FBRR peak has moved to a slightly more positive potential of -0.013 V vs. SCE. The mean peak potentials of the FBRR peaks were tested using unpaired t-tests leading to a non-significant difference between the means with a P -value of 0.1466, shown in Table 5.19.

However, the pH of the PBS/ 5-HIAA solution was recorded at 7.34. When this pH difference was taken into account the mean peak potential shifted to -0.013 V vs. SCE. Repeating the t-test yielded an improved P -value of 0.5298.

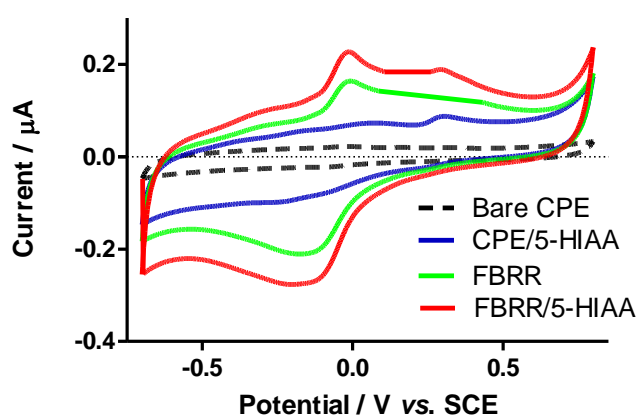


Figure 5.49: CVs showing the effect of 100 μM 5-HIAA on the redox peaks of FBRR/CPEs, $n = 4$.

Table 5.19: Statistical analyses of the anodic peak potentials of FBRR/CPEs cycled in PBS and PBS/5-HIAA, $n = 4$.

Mean Peak Potential FBRR (V)	Mean Peak Potential FBRR/5-HIAA (V)	P -value	Mean Peak Potential FBRR/5-HIAA pH adjusted (V)	P -value
-0.0135 ± 0.0013	-0.0160 ± 0.0008	0.1466	-0.0125 ± 0.0008	0.5298

5.2.8 Pharmacological Interferences

There are a wide range of medications that could possibly interfere with the peak potential at which FBRR oxidises at a CPE, or any, electrode surface. If these oxidise at a similar potential then the resulting peak may be broadened to incorporate both peaks or may be shifted to a more positive or negative potential. Two of the most commonly used drugs are acetaminophen (ACOP) and acetylsalicylic acid (ASA). The effects that these two pharmacological interferences may have on FBRR/CPEs are examined in the following sections.

5.2.8.1 Acetaminophen (ACOP)

ACOP is one of the most common drugs used for a wide variety of ailments and at various concentration levels. It is a main ingredient of paracetamol. Therapeutic levels of 0.2 mM have been reported.³²

Figure 5.50 shows the reversible oxidation and reduction peaks of ACOP at a bare CPE at 0.30 and 0.16 V *vs.* SCE, respectively. These potentials were in agreement with literature values.⁵⁰ The FBRR anodic peak in PBS falls at -0.021 V *vs.* SCE. When the ACOP was added the FBRR anodic peak shifted to -0.027 V *vs.* SCE and was broader. This indicated that the added ACOP did not facilitate the oxidation of FBRR at the CPE surface. The ACOP peak was well separated from the FBRR peak. The mean peak potentials were tested using unpaired t-tests leading to a significant difference between the means with a *P*-value = 0.0225 shown in Table 5.20.

However, the pH of the PBS/ ACOP solution was recorded at 7.34. When this pH difference was taken into account the mean peak potential shifted to -0.023 V *vs.* SCE. Repeating the t-test yielded non-significant differences with an improved *P*-value of 0.3097.

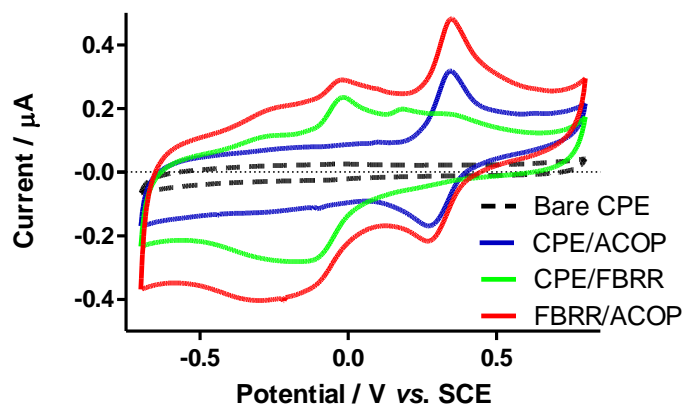


Figure 5.50: CVs showing the effect of 0.50 mM ACOP on the redox peaks of FBRR/CPEs, $n = 4$.

Table 5.20: Statistical analyses of the anodic peak potentials of FBRR/CPEs cycled in PBS and PBS/ACOP, $n = 4$.

Mean Peak Potential FBRR (V)	Mean Peak Potential FBRR/ACOP (V)	<i>P</i> -value	Mean Peak Potential FBRR/ACOP pH adjusted (V)	<i>P</i> -value
-0.0210 ± 0.0013	-0.0265 ± 0.0008	0.0225	-0.0230 ± 0.0013	0.3097

5.2.8.2 Acetylsalicylic Acid (ASA)

ASA, a component of aspirin, may be present in biological systems at concentrations (0.5 mM)⁵¹ that could interfere with the FBRR signal. Figure 5.51 shows no distinct oxidation or reduction peaks of ASA at a bare CPE. This would normally be apparent at approximately 0.80 V vs. SCE, so would appear just outside the potential range used here. The FBRR anodic peak in PBS falls at -0.026 V vs. SCE. The shift to a more negative potential could indicate that the ASA facilitated the oxidation of the FBRR, making it more thermodynamically viable. When the ASA was added the FBRR anodic peak shifted to -0.0285 V vs. SCE. The mean peak potentials were tested using unpaired t-tests leading to a non-significant difference between the means with a *P*-value of 0.1466, shown in Table 5.21.

However, the pH of the PBS/ASA solution was recorded at 7.34. When this pH difference was taken into account the mean peak potential shifted to -0.023 V vs. SCE. Repeating the t-test yielded an improved P -value of 0.5188.

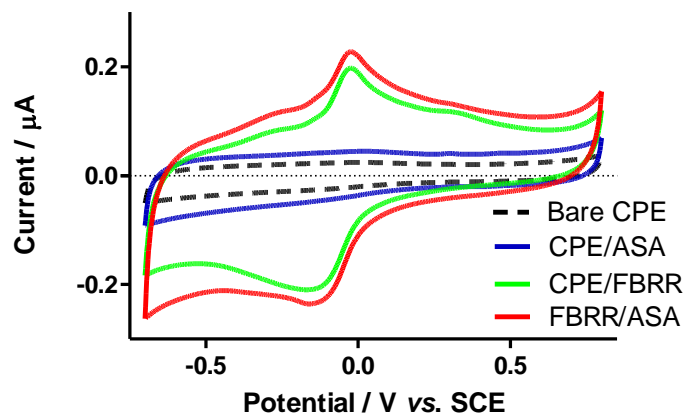


Figure 5.51: CVs showing the effect of 0.50 mM ASA on the redox peaks of FBRR/CPEs, $n = 4$.

Table 5.21: Statistical analyses of the anodic peak potentials of FBRR/CPEs cycled in PBS and PBS/ASA, $n = 4$.

Mean Peak Potential FBRR (V)	Mean Peak Potential FBRR/ASA (V)	P -value	Mean Peak Potential FBRR/ASA pH adjusted (V)	P -value
-0.0260 ± 0.0014	-0.0285 ± 0.0005	0.1466	-0.0249 ± 0.0005	0.5188

5.2.9 Ionic Strength

Many pH sensors, especially those based on optical measurements,⁵² have a fundamental disadvantage of measuring a signal that depends on the ionic strength of the sample. Changes in the ionic strength gives rise to changes in the conductivity of a solution. Decreasing the ionic strength of a solution decreases the conductivity, hence increasing the solution resistance. This results in an increased IR drop causing a subsequent potential increase (Ohm's Law: $V = IR$) which modifies the observed potential. The effect of ionic strength on the FBRR functionalised electrodes was tested by cycling the modified electrodes in PBS of altered ionic strength with pH values of 7.2, 7.4 and 7.6. The ionic strength of the solutions was calculated using the formula:

$$I = 0.5 \sum Z_i^2 C_i \quad 5.1$$

Where, Z_i = ion charge

C_i = ion concentration (M)

Using Equation 5.1 the ionic strength of the PBS used throughout this thesis was calculated as 0.46 M. This was altered to give ionic strengths of 0.92 M and 0.23 M.

Electrodes were modified by electrodeposition of 2 mM FBRR in 0.1 M H_2SO_4 (LSV 5 sweeps, from 0.40 to -0.80 V vs. SCE at 100 mV/s) and calibrated in PBS ($I = 0.46$ M) pH 7.2, 7.4 and 7.6. They were then cycled in PBS with ionic strengths of 0.92 M and 0.23 M pH 7.2, 7.4 and 7.6. The pH responses were determined, see Figure 5.52, and compared using two-tailed t-tests. A P -value of 0.4984 was obtained when comparing ionic strengths of 0.46 M with 0.92 M, and $P = 0.1339$ when comparing ionic strengths of 0.46 M with 0.23 M indicating no significant differences in the pH response between modified electrodes cycled in PBS of various ionic strengths, see Table 5.22.

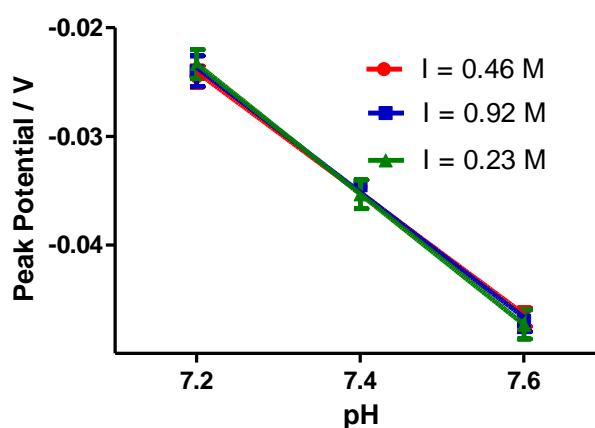
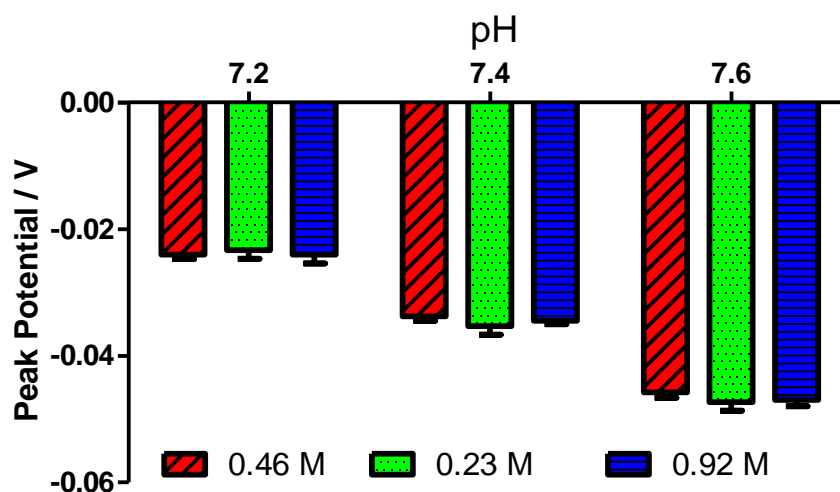


Figure 5.52: Linear regressions comparing the pH responses of FBRR/ H_2SO_4 modified CPEs in solutions of varying ionic strength, $n = 4$.

Table 5.22: Comparison of the pH sensitivities of FBRR/H₂SO₄ modified CPEs in solutions of varying ionic strength, $n = 4$.

	Slope (mV/pH)	SEM	R ²	P-value
I = 0.23 M	-60.00	1.00	1.00	0.1339
I = 0.46 M	-54.37	3.25	0.99	—
I = 0.92 M	-57.50	2.89	0.99	0.4984

The location of the anodic peak potentials remained stable in all solutions tested. This was confirmed upon analysis, shown in the bar chart in Figure 5.53. As the standard PBS solution used throughout this thesis had an ionic strength of 0.46 M, the solutions with ionic strengths of 0.23 M and 0.92 M were examined, using unpaired t-tests, against the standard solution, at each pH. All analyses resulted in non-significant differences, ($P > 0.05$).

**Figure 5.53:** Bar chart showing no effect resulting from changes in ionic strength on the anodic peak potential of FBRR/CPEs, $n = 4$.

5.2.10 Ion Effect

The effect of the introduction of metal ions to the PBS solutions was examined. Mg²⁺ and Ca²⁺ are among the most prevalent cations found in biological systems with average concentrations of 5 mM^{53,54} and 1.2 mM,⁵⁵ respectively. They are also known

to form coordinate bonds, complexes, with several quinones^{18, 56} and could therefore affect their redox peak potentials. Commercially available artificial cerebrospinal fluid, aCSF, contains between 1.3 and 21 mM MgCl₂ and 1.2 to 1.6 mM CaCl₂.

Figure 5.54 shows the resulting pH responses of the calibrated electrodes with the added Mg²⁺ (A) and Ca²⁺ (B).

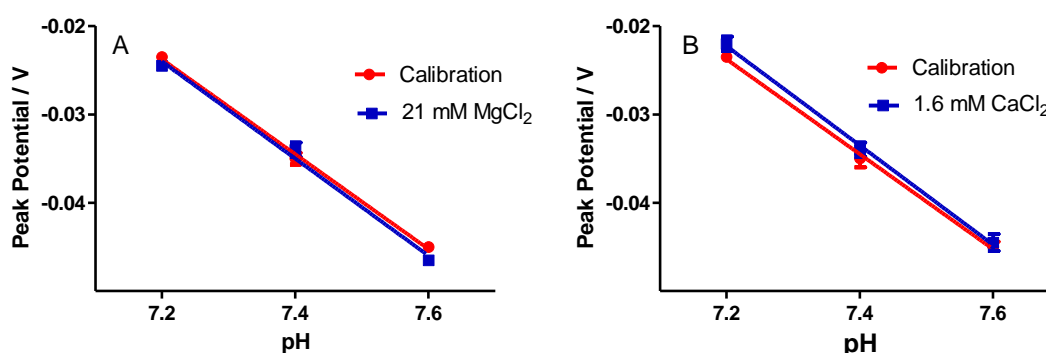


Figure 5.54: pH responses of FBRR/H₂SO₄ modified CPEs in PBS solutions with added MgCl₂ (A) and CaCl₂ (B), $n = 4$.

The pH as a function of peak potential is given in Table 5.23 and was recorded at -54 ± 2 mV/pH, $R^2 > 0.99$, for the calibrations and -55 ± 4 mV/pH, $R^2 > 0.99$, and -56 ± 2 mV/pH, $R^2 > 0.99$, with Mg²⁺ and Ca²⁺ ions added, respectively. These pH responses were compared to the calibrations using unpaired t-tests and it was found that there were no significant differences obtained when the Mg²⁺ and Ca²⁺ ions were added, giving P -values of 0.7760 and 0.4862, respectively.

Table 5.23: Analyses of the pH responses of FBRR/H₂SO₄ modified CPEs cycled in PBS solutions with added MgCl₂ and CaCl₂, $n = 4$.

Calibration (mV/pH)	R ²	+ MgCl ₂ (mV/pH)	R ²	P -value	+ CaCl ₂ (mV/pH)	R ²	P -value
-54 ± 2	0.998	-55 ± 4	0.994	0.7760	-56 ± 2	0.999	0.4862

5.2.11 Temperature

The main aim of this project was to develop a pH sensor suitable for measuring pH changes in a physiological environment, therefore the FBRR/CPEs were tested for their pH response at 37°C. All previous experiments were carried out at room temperature, *ca.* 22°C. The CVs (anodic peaks only) in Figure 5.55 show the resulting peaks and their corresponding potentials when cycling in PBS with pH values of 7.2, 7.4 and 7.6. The first difference observed was the increased currents obtained with increased temperature, as a result of higher energy in the system allowing the formation of more ions in solution. The second was the shift to a more negative potential for the values obtained between the two temperatures. This is because pH changes with temperature, according to the Rosenthal Correction Factor, by 0.015 pH units per °C. This results in a shift of 0.225 pH units for the temperature difference of 15°C.

Assuming a Nernstian response of -59 mV/pH then the expected shift in peak potential is -13 mV. So, if the peak potential at 22°C is -34 mV, the expected peak potential at 37°C would be -47 mV. Comparing the peak potentials at similar pH values between 22°C and 37°C in Figure 5.55 gave potential shifts of approximately -18 mV.

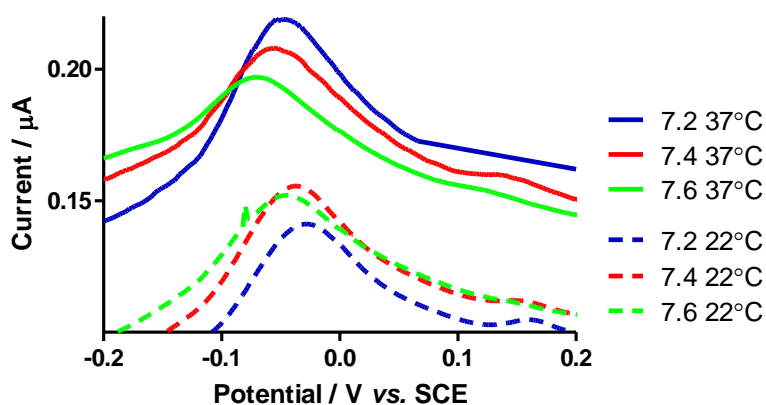


Figure 5.55: Anodic peaks of FBRR/CPEs cycled in various pH PBS showing the shift in potential due to temperature differences at 22°C and 37°C, $n = 4$.

Also, the pH response is dependent on temperature according to:

$$m = 2.303RT/F \quad 5.2$$

Where m is the slope or pH response, R is the universal gas constant ($J K^{-1} mol^{-1}$), T represents the temperature (K) and F denotes the Faraday constant ($C mol^{-1}$). This results in a pH response of -61.55 mV/pH at a temperature of $37^\circ C$.

The pH responses at both temperatures are shown in Figure 5.56. They demonstrate good pH sensitivities with slopes of -58.75 ± 2 and -62.50 ± 1 mV/pH for $22^\circ C$ and $37^\circ C$, respectively, with R^2 values > 0.99 . This is in good agreement with the theoretical value of -61.55 mV/pH unit, at $37^\circ C$, obtained from the Nernst equation (Eqn. 5.2) for a 2 electron, 2 proton transfer at $37^\circ C$. These sensitivities, again highlight the temperature dependence of the Nernst equation.²⁴

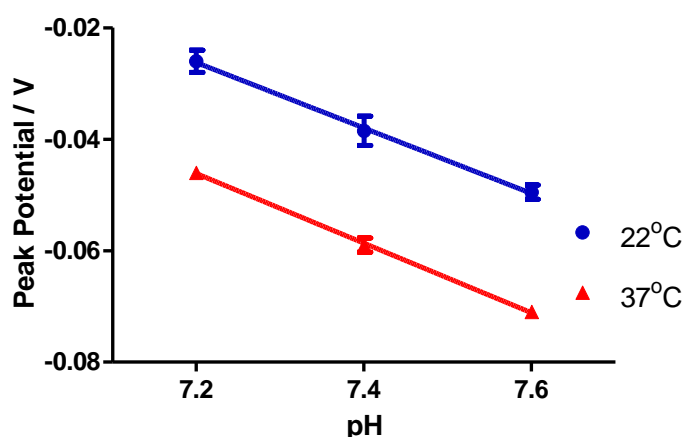


Figure 5.56: pH responses of FBRR/CPEs at $22^\circ C$ and $37^\circ C$, $n = 4$.

Table 5.24: Statistical analyses of the pH responses of FBRR/CPEs comparing temperatures of $22^\circ C$ and $37^\circ C$, $n = 4$.

22°C			37°C		
Slope (mV/pH)	SEM	R ²	Slope (mV/pH)	SEM	R ²
-58.75	0.22	0.9986	-62.50	0.14	0.9995

5.2.12 Reference Electrode

All previous *in-vitro* experiments in this thesis were performed using a SCE reference electrode. This type of electrode is based on the reaction between elemental mercury and mercury(I) chloride, Hg_2Cl_2 , which is in contact with a saturated KCl solution and is all contained in a glass tubing using a Pt wire as the external contact. When carrying out electrode characterisations such a reference should be used as it has a known, pre-determined, stable electrode potential.⁵⁷ When carrying out *in-vivo* experiments a SCE cannot be used because of their size and the toxic mercury⁵⁸ contained within, so an adapted, or pseudo, Ag/AgCl reference is used. In general, Ag/AgCl references consists of a silver wire coated with silver chloride kept in contact with a KCl solution of known concentration. This is all contained within a glass tube and separated from the test solution by a membrane. Ag/AgCl references are easier to miniaturise than a SCE⁵⁹. In a conventional Ag/AgCl microelectrode, the Ag/AgCl wire is usually isolated from the solution by a porous ceramic or glass frit/membrane and kept in a KCl solution of a defined concentration, but in the quasi (or pseudo) Ag/AgCl version, used here, the reference electrode is simply a silver wire plated with silver chloride. It does not contain the inner filling solution of KCl which means it can lead to unstable potentials⁶⁰ depending on the solution.⁶¹ However, it has been reported that pseudo reference electrodes in PBS pH 7 maintain a constant potential.⁶² This makes them suitable for use in areas where the pH is regulated, e.g., biological systems. Other advantages include their biocompatibility and mechanical stability. The SEM micrographs in Figure 5.57

shows the surface morphology of a silver wire, $\varnothing = 0.2$ mm, coated with silver chloride. The accompanying EDX gives further evidence of this coating.

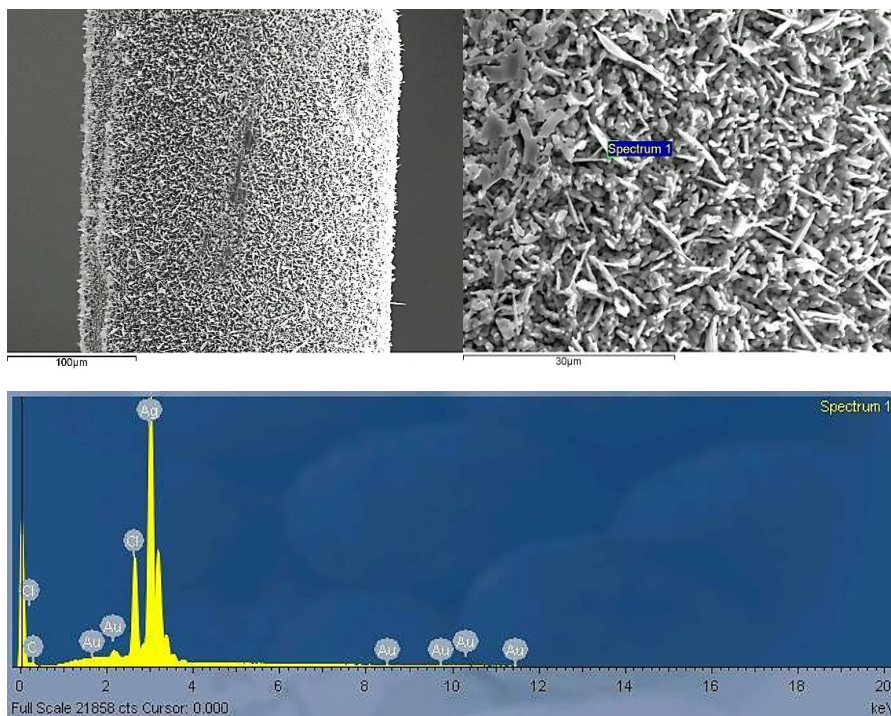


Figure 5.57: SEM micrographs and the corresponding EDX of a quasi Ag/AgCl electrode used as the reference electrode to mimic *in-vivo* experimental conditions.

The anodic peaks from the resulting CVs are shown in Figure 5.58. They clearly show the shift in potential caused by using the Ag/AgCl reference electrodes, of approximately -34 mV compared to SCE. Literature values for the potential difference between Ag/AgCl and SCE reference electrodes suggest a shift of -44 mV.⁵⁹ There is also a clear shift in peak potentials when changing the solution pH between 7.2 and 7.6.

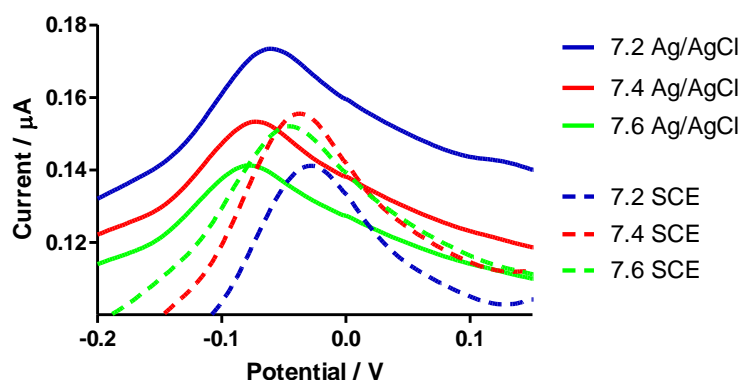


Figure 5.58: Anodic peaks of FBRR/CPEs cycled in PBS solution of varying pH using SCE and Ag/AgCl reference electrodes, $n = 4$.

The pH response of both systems, Ag/AgCl and SCE reference electrodes, is shown in Figure 5.59 with the corresponding values given in Table 5.25. The pH responses were -57.50 mV/pH when using an SCE and -56.25 mV/pH when using an Ag/AgCl electrode. Despite there being discrepancies in peak potentials between the two reference electrode systems, the extremely comparable sensitivities negate this issue. However, it is imperative that the difference in expected peak potentials is characterised prior to deployment of this system in physiological media.

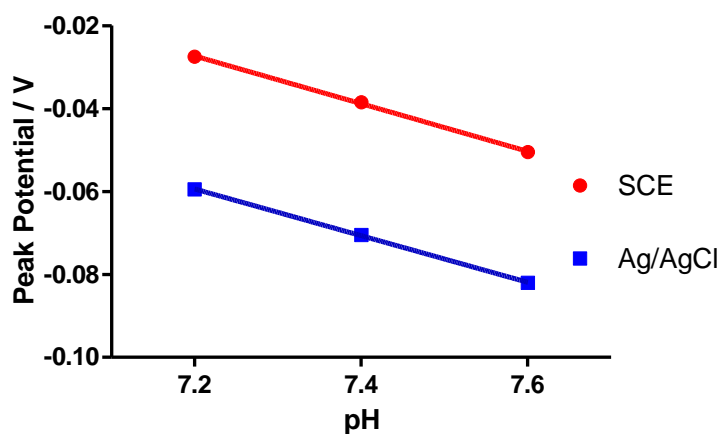


Figure 5.59: pH responses of FBRR/CPEs using SCE and Ag/AgCl reference electrodes, $n = 4$.

Table 5.25: Statistical analyses of the pH responses of FBRR/CPEs comparing SCE and Ag/AgCl reference electrodes, $n = 4$.

	Peak Potential 7.2 (mV)	Peak Potential 7.4 (mV)	Peak Potential 7.6 (mV)	n	Slope (mV/pH)	P -value
SCE	-27 ± 0.50	-38 ± 0.96	-50 ± 0.50	4	-57 ± 1.44	0.4679
Ag/AgCl	-59 ± 0.50	-70 ± 0.96	-82 ± 1.15	4	-56 ± 0.72	

5.3 Conclusion

Throughout this chapter, a rigorous regime of test conditions was applied to the previously designed pH sensor, to evaluate its suitability for use in the challenging *in-vivo* environment.

Section 5.2.1 considered the long-term stability of the FBRR/CPE, when stored at 4°C in either air or N₂, for up to 1 month. Storage in N₂ produced erratic results, with significant differences uncovered, ($P < 0.05$). On the other hand, sensors stored in air displayed similar pH sensitivities pre and post storage. No significant differences were observed, with all P -values > 0.05 . It was, therefore, concluded that the optimum storage conditions for FBRR/CPEs was at 4°C with no further treatment required.

Section 5.2.2 introduced the FBRR/SMCPEs in an attempt to increase the biocompatibility of the pH sensor. The preparation method was discussed, including storage times required between the various steps, and the requirement of repacking the electrodes. The Sty: paste ratio was also examined. The procedure for the preparation of SMCPEs was described in this section.

Section 5.2.3 investigated the biocompatibility of the FBRR/CPE and FBRR/SMCPE sensors, by examining the effects of storing or cycling the electrodes in solutions of protein, lipid, surfactant and *ex-vivo* brain tissue. All FBRR/CPE experiments resulted in increased capacitance caused by electrode fouling, and removal of silicone oil from the paste. The comparative FBRR/SMCPE biocompatibility studies resulted in broad anodic peaks but lower currents were observed, indicating that less silicone oil may have been lost. Cycling the FBRR/CPE sensors in the media proved less severe than storage, the constant application of anodic and cathodic potentials appeared to prevent fouling of the electrode surface. In fact, electron transfer was improved by the deposition of trace amounts of, e.g., lipid on the sensor. The corresponding FBRR/SMCPEs showed no substantial improvement and because of the extra 2 days required for preparation, they were deemed unsuitable for use with this particular sensor. Brain tissue was, physiologically, the most relevant test medium used, resulting in visible anodic peaks even after storage for 28 days. As *in-vivo* voltammetry would involve cycling the electrodes in tissue, rather than storing them, it was concluded that the FBRR/CPE sensor would be suitable for recording in living tissue.

Section 5.2.4 discussed the variability in silicone oil content of FBRR/CPEs and FBRR/SMCPEs stored in lipids, proteins, surfactants and brain tissue. All electrodes exhibited a drop in oil content after storing for one day in the various media. The oil content after storing and cycling the electrodes in BSA and PEA solutions was examined. This confirmed results from Section 5.3.2, that cycling FBRR/CPEs removed less silicon oil from the surface. The silicone oil content of SMCPEs was examined. Direct comparisons with FBRR/CPEs revealed that oil losses were improved over FBRR/CPEs, but did not prevent the loss of FBRR. Real-time pH testing of FBRR/SMCPEs in Section 5.2.5 revealed excellent sensitivity of *ca.* -60 mV/pH. This result compared well with the corresponding result for FBRR/CPEs, showing a detrimental effect occurred when exposing the sensors to air between measurements.

Section 5.2.6 revealed that the silicone oil content of carbon paste samples varied with the age and manufacturing technique used in the production of CPEs. It was shown that CPEs with a higher silicone oil: carbon ratio displayed higher background currents.

Sections 5.2.7 and 5.2.8 considered the effects of physiological and pharmacological interferences on the anodic peaks of FBRR/CPEs, indicating that the sensor performed well in all media. How the sensor responded to changes in ionic strength, introduction of metal ions and temperature differences was also investigated, Sections 5.2.9-11. The findings confirmed the ability of the sensor to function well in all situations tested. Then, in Section 5.2.12, a reference electrode suitable to *in-vivo* voltammetry was introduced into the recording set-up, resulting in an expected shift in potential but similar pH sensitivity.

In conclusion, FBRR/CPEs were deemed suitable for use in an *in-vivo* environment. FBRR/SMCPEs did not improve the biocompatibility of the pH sensor, only adding 2 days to the manufacturing process.

5.4 References

1. R. D. O'Neill, *Sensors*, 2005, **5**, 317-342.
2. P. D. Lyne and R. D. O'Neill, *Analytical Chemistry*, 1990, **62**, 2347-2351.
3. S. Zheng, Y. Huang and G. Chen, *Electrochimica Acta*, 2013, **88**, 117-122.
4. R. R. Nayak, K. Y. Lee, A. M. Shanmugaraj and S. H. Ryu, *European Polymer Journal*, 2007, **43**, 4916-4923.
5. T. E. Chang, A. Kisliuk, S. M. Rhodes, W. J. Brittain and A. P. Sokolov, *Polymer*, 2006, **47**, 7740-7746.
6. A. M. Wynne, NUI Maynooth, 2014.
7. K. Kalcher, *Electroanalysis* 1990, **2**, 419-433.
8. I. Svancara, K. Vytras, J. Barek and J. Zima, *Critical Reviews in Analytical Chemistry*, 2001, **31**, 311-345.
9. Y.-M. Zhang, W. You, Z.-N. Gao and T.-L. Yang, *Croatica Chemica Acta*, 2013, **86**, 309-315.
10. K. Kalcher, J. M. Kauffmann, J. Wang, I. Svancara, K. Vytras, C. Neuhold and Z. Yang, *Electroanalysis*, 1995, **7**, 5-22.
11. Q. J. Chi, W. Gopel, T. Ruzgas, L. Gorton and P. Heiduschka, *Electroanalysis*, 1997, **9**, 357-365.
12. I. Svancara, M. Hvizdalova, K. Vytras, K. Kalcher and R. Novotny, *Electroanalysis*, 1996, **8**, 61-65.
13. G. G. Wildgoose, P. Abiman and R. G. Compton, *Journal of Materials Chemistry*, 2009, **19**, 4875-4886.
14. D. Shin, D. A. Tryk, A. Fujishima, A. Merkoci and J. Wang, *Electroanalysis*, 2005, **17**, 305-311.
15. M. C. Blanco-Lopez, M. J. Lobo-Castanon, A. J. M. Ordieres and P. Tunon-Blanco, *Electroanalysis*, 2007, **19**, 207-213.
16. S. S. Shankar, B. E. K. Swamy and B. N. Chandrashekar, *Journal of Molecular Liquids*, 2012, **168**, 80-86.
17. K. R. Mahanthasha, B. E. K. Swamy, U. Chandra, S. S. Shankar and K. V. Pai, *Journal of Molecular Liquids*, 2012, **172**, 119-124.
18. G. G. Wildgoose, M. Pandurangappa, N. S. Lawrence, L. Jiang, T. G. J. Jones and R. G. Compton, *Talanta*, 2003, **60**, 887-893.
19. H. McIlwain and H. S. Bachelard, *Biochemistry and the Central Nervous System*, Churchill Livingstone, Edinburgh, 1985.
20. I. Svancara and K. Schachl, *Chemické Listy*, 1999, **93**, 490-499.

21. K. Kalcher, I. Svancara, M. Buzuk, K. Vytras and A. Walcarius, *Monatshefte für Chemie*, 2009, **140**, 861-889.
22. I. Al Mulla, J. P. Lowry, P. A. Serra and R. D. O'Neill, *Analyst* 2009, **134**, 893-898.
23. C. Olson and R. N. Adams, *Analytica Chimica Acta*, 1960, **22**, 582-589.
24. H. C. Leventis, I. Streeter, G. G. Wildgoose, N. S. Lawrence, L. Jiang, T. G. J. Jones and R. G. Compton, *Talanta*, 2004, **63**, 1039-1051.
25. M. Lu and R. G. Compton, *Analyst*, 2014, **139**, 2397-2403.
26. M. Lu and R. G. Compton, *Analyst* 2014, **139**, 4599-4605.
27. S. Chitravathi and N. Munichandraiah, *Journal of the Electrochemical Society*, 2015, **162**, B163-B172.
28. S. Shahrokhian and E. Asadian, *Electrochimica Acta*, 2009, **55**, 666-672.
29. K. R. Mahanthesha and B. E. Kumara Swamy, *Journal of Electroanalytical Chemistry*, 2013, **703**, 1-8.
30. K. R. Mahanthesha, B. E. K. Swamy, U. Chandra, T. V. Sathisha, S. Sarojini and K. V. K. Pai, *Analytical and Bioanalytical Electrochemistry*, 2013, **5**, 130-138.
31. C. Apetrei, I. M. Apetrei, J. A. De Saja and M. L. Rodriguez-Mendez, *Sensors*, 2011, **11**, 1328-1344.
32. K. E. Toghill and R. G. Compton, *International Journal of Electrochemical Science*, 2010, **5**, 1246-1301.
33. J. P. Lowry and R. D. O'Neill, *Encyclopedia of Sensors*, 2006.
34. E. P. de Oliveira and R. C. Burini, *Diabetology & Metabolic Syndrome*, 2012, **4**, 12.
35. J. C. Chen, H. H. Chung, C. T. Hsu, D. M. Tsai, A. S. Kumar and J. M. Zen, *Sensors and Actuators, B*, 2005, **110**, 364-369.
36. K. K. Aswini, A. M. V. Mohan and V. M. Biju, *Materials Science and Engineering, C*, 2014, **37**, 321-326.
37. J. B. Raoof, F. Chekin, R. Ojani and S. Barari, *Journal of Chemical Science* 2013, **125**, 283-289.
38. K.-Q. Deng, J.-h. Zhou and X.-F. Li, *Colloids and Surfaces, B*, 2013, **101**, 183-188.
39. Q. Wang, A. Vasilescu, P. Subramanian, A. Vezeanu, V. Andrei, Y. Coffinier, M. Li, R. Boukherroub and S. Szunerits, *Electrochemical Communications*, 2013, **35**, 84-87.
40. R. J. Wurtman, C. M. Rose, C. Chou and F. F. Larin, *New England Journal of Medicine*, 1968, **279**, 171-175.

41. W. Li, C. Li, Y. Kuang, P. Deng, S. Zhang and J. Xu, *Microchimica Acta*, 2012, **176**, 455-461.
42. P. Deng, Z. Xu and Y. Feng, *Materials Science and Engineering, C*, 2014, **35**, 54-60.
43. W. Wang, B. Qiu, X. Xu, L. Zhang and G. Chen, *Electrophoresis*, 2005, **26**, 903-910.
44. S.-G. Park, J.-E. Park, E.-I. Cho, J.-H. Hwang and T. Ohsaka, *Research on Chemical Intermediates*, 2006, **32**, 595-601.
45. J. Oni and T. Nyokong, *Analytica Chimica Acta*, 2001, **434**, 9-21.
46. J. C. Harfield, C. Batchelor-McAuley and R. G. Compton, *Analyst* 2012, **137**, 2285-2296.
47. G. Alfredsson and F. A. Wiesel, *Psychopharmacology*, 1989, **99**, 322-327.
48. F. Crespi, T. Sharp, N. T. Maidment and C. A. Marsden, *Brain Research*, 1984, **322**, 135-138.
49. C. G. Nan, Z. Z. Feng, W. X. Li, D. J. Ping and C. H. Qin, *Analytica Chimica Acta*, 2002, **452**, 245-254.
50. B. J. Sanghavi and A. K. Srivastava, *Electrochimica Acta*, 2010, **55**, 8638-8648.
51. G. M. Borthwick, A. S. Johnson, M. Partington, J. Burn, R. Wilson and H. M. Arthur, *Federation of American Societies for Experimental Biology Journal*, 2006, **20**, 2009-2016.
52. B. M. Weidgans, C. Krause, I. Klimant and O. S. Wolfbeis, *Analyst* 2004, **129**, 645-650.
53. D. Veloso, R. W. Guynn, M. Oskarsson and R. L. Veech, *Journal of Biological Chemistry*, 1973, **248**, 4811-4819.
54. M. Walser, *Ergebnisse der Physiologie*, 1967, **59**, 185-296.
55. M. M. Dvorak, A. Siddiqua, D. T. Ward, D. H. Carter, S. L. Dallas, E. F. Nemeth and D. Riccardi, *Proceedings of the National Academy of Sciences of the United States of America* 2004, **101**, 5140-5145.
56. M. C. Mahedero, M. Roman Ceba and A. Fernandez-Gutierrez, *Analytical Letters*, 1986, **19**, 1725-1730.
57. A. J. Bard and L. R. Faulkner, *Electrochemical Methods: Fundamentals and Applications*, John Wiley & Sons, 2001.
58. M. W. Shinwari, D. Zhitomirsky, I. A. Deen, P. R. Selvaganapathy, M. J. Deen and D. Landheer, *Sensors*, 2010, **10**, 1679-1715.
59. D. Desmond, B. Lane, J. Alderman, J. D. Glennon, D. Diamond and D. W. M. Arrigan, *Sensors and Actuators, B*, 1997, **44**, 389-396.

60. B. J. Polk, A. Stelzenmuller, G. Mijares, W. MacCrehan and M. Gaitan, *Sensors and Actuators, B*, 2006, **114**, 239-247.
61. A. Yakushenko, D. Mayer, J. Buitenhuis, A. Offenhaeusser and B. Wolfrum, *Lab on a Chip*, 2014, **14**, 602-607.
62. T. Matsumoto, A. Ohashi and N. Ito, *Analytica Chimica Acta*, 2002, **462**, 253-259.

Chapter 6

In-Vitro Characterisation of CFE/FBRR pH Sensor

6.1 Introduction

Chapters 4 and 5 discussed the use of CPEs as suitable substrates for the electrodeposition of FBRR, and their efficacy for utilisation as a real-time pH sensor. The CPE used had a diameter of 0.27 mm, inclusive of the Teflon[®] insulation. Some problems, inherent in CPEs, include the formation of an irregular surface leading to inconsistent currents; and the loss of silicone oil resulting in a change in the surface morphology. To overcome these issues, and possibly produce an improved sensor of smaller diameter, carbon fibre electrodes (CFEs) were investigated.

Carbon electrodes are widely used in electroanalytical chemistry due to their low residual currents over a wide potential range.¹ Modifications of carbon surfaces include the electrochemical grafting of organic molecules onto the substrate, for example, the one electron reduction of aryl diazonium salts.²⁻⁴ Quinone modified carbon electrodes have previously been used to produce electrochemical sensors capable of the accurate pH measurement of buffered solutions.⁵⁻⁷ These advancements have enabled the development of electrodes for pH monitoring that have distinct advantages, compared to other common methods used for the determination of solution pH.⁸

The use of carbon fibres in electro-analysis is well reported, with electrodes consisting of a single carbon fibre introduced for electrochemical measurement in 1979.⁹⁻¹¹ Since then, they have been used extensively in electrochemistry, predominantly in applications requiring small recording volumes, such as *in-vivo* monitoring.¹²

In this chapter, the electrochemical deposition of FBRR, in the presence of organic and aqueous solvents, onto CFEs is discussed. This was achieved by utilising the optimum deposition conditions obtained in Chapter 4. The modified electrode characteristics and redox properties were subsequently analysed using CV.

The CFEs used in this thesis consisted of a 7 μm diameter carbon fibre that was held in a 1.5 mm diameter borosilicate glass capillary tubing. The carbon tip was conically shaped and protruded from the glass insulation by $20 \mu\text{m} \pm 5 \mu\text{m}$, leaving a cylindrical surface. There are two main advantages to a cylindrical surface of a CFE over a disc surface. The first advantage is that cylindrical electrodes are less sensitive to acquiring an imperfect seal between the electroactive surface and the surrounding insulator,¹²

while the second advantage relates to the increased surface area, enabling the electrode to yield currents that provide a sufficiently high signal: noise ratio.¹³

As well as the physical advantage of using working electrodes with a smaller diameter, making them more suitable for *in-vivo* experiments, the CFEs used in this thesis had the added benefits of microelectrodes, i.e., the contribution of radial diffusion to the Faradaic current,¹⁴ as the diffusion layer becomes larger than the electrode surface over time. The main limitation with CFEs is the inability to polish or renew the surface once used so, in general, new CFEs were used for each experiment.

6.2 Results and Discussion

In this section, the characterisation of FBRR/CFEs for use as voltammetric pH sensors was performed. FBRR was electrodeposited onto the CFEs by LSV using the CPE/FBRR/H₂SO₄ deposition parameters described in Section 4.3. An investigation was then carried out, regarding the effect of electrode pre-treatment, on the redox peaks formed. The supporting electrolyte was varied from acidic, (H₂SO₄) to organic (TEABF₄/ACN) before the optimised redox peaks were obtained. The pH sensitivity of the sensor and stability for up to 28 days were examined. The FBRR/CFEs were then subjected to a rigorous *in-vitro* testing regime, similar to that applied in Chapter 5 for CPEs, to check their suitability for deployment in the *in-vivo* environment.

6.2.1 Untreated CFEs

CFEs possess good mechanical and electrical properties making them suitable for electrochemical and electrophysiological applications.¹⁵ Their biological compatibility and size, generally < 10 μm, make them ideal substrates for *in-vivo* applications, as they cause less tissue damage than larger conventional electrodes. The background CV (100th cycle) for a bare CPE in N₂ saturated PBS is shown in Figure 6.1, along with the CV of the same electrode subsequently cycled in 0.1 M H₂SO₄. The CV of the bare CFE in PBS is almost sigmoidal,¹⁶ which is typical for single fibre electrodes.^{17, 18} This was in direct contrast to the more conventional background signal obtained in Section 4.2.1 for CPEs. The currents obtained were in the nA range, so the resistance had a

negligible effect on the observed electrochemical reactions.¹⁷ Higher currents were observed when the CFE was subsequently cycled in H₂SO₄. When bare, previously unused, CFEs were cycled in H₂SO₄ the resulting CVs were almost identical to those resulting from CFEs cycled in PBS. This indicated that a bare CFE, initially cycled in PBS, resulted in a pre-treatment effect, either causing scratches on the surface thereby increasing the surface area,¹⁴ or by forming oxides on the surface.¹²

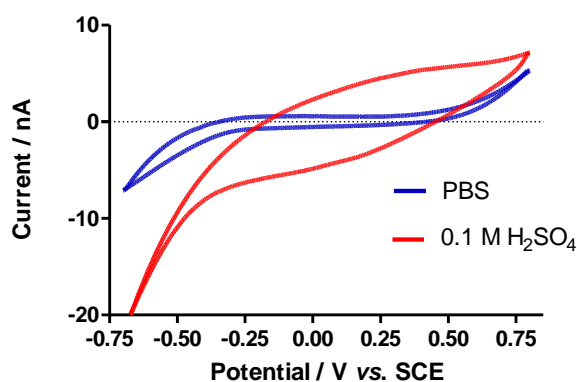


Figure 6.1: CVs (100th cycle) of CFEs cycled in PBS and subsequently cycled in 0.1 M H₂SO₄, $n = 4$.

6.2.1.1 Electro-reduction of FBRR using CPE Parameters

The electro-reduction of FBRR onto the CFE substrate involved the optimised CPE deposition parameters obtained in Section 4.3; LSV x 5, from 0.80 to -0.40 V vs. SCE, at 100 mV/s in 2 mM, N₂ saturated, FBRR/0.1 M H₂SO₄. Figure 6.2 shows a slight reduction wave, during the 1st deposition sweep, at *ca.* -0.20 V vs. SCE, however, this reduction profile was not evident for all electrodes. This wave, when evident, disappeared in the second and subsequent sweeps, showing that the reduction of the diazonium salt to its radical, occurred in the first sweep only.¹⁹

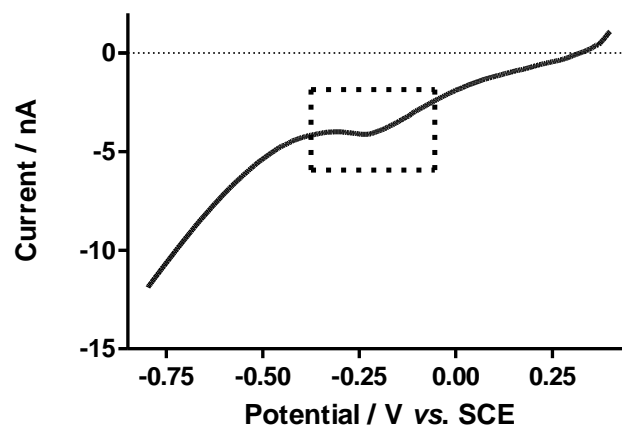


Figure 6.2: Voltammogram showing the 1st reduction wave of FBRR/H₂SO₄ onto untreated CFEs, $n = 4$.

These FBRR modified CFEs were then tested for their pH sensitivity, by cycling in PBS solutions, of variable pH, from -0.70 to 0.80 V vs. SCE, for 100 cycles in each solution. The order of cycling was randomly selected to avoid any hysteresis effects. The resulting CVs are shown in Figure 6.3 (A), with the corresponding linear regression in Figure 6.3 (B). Although Figure 6.3 (A) shows a clear shift in peak potential with pH, a super-Nernstian response of -130 ± 39 mV/pH was obtained, ($R^2 = 0.9194$). This value was not consistent with a $2e^-/2H^+$ redox reaction.²⁰

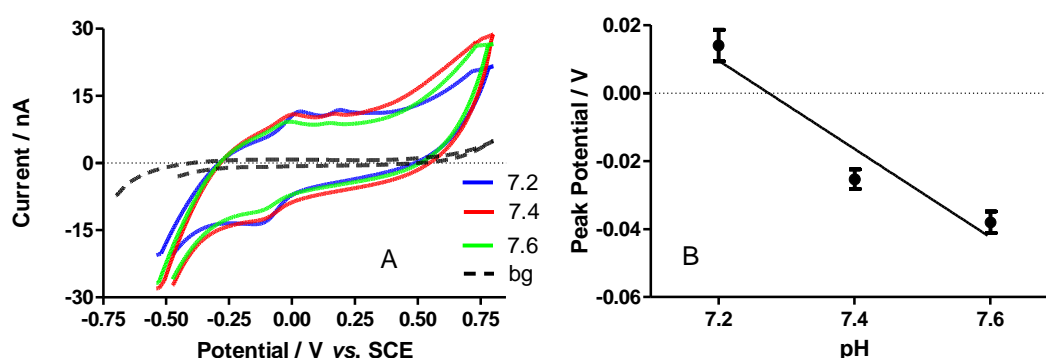


Figure 6.3: (A) CVs of untreated CFEs modified with FBRR/H₂SO₄, cycled in PBS solutions, pH 7.2, 7.4 and 7.6. (B) Linear regression of the peak potentials response with changing pH, $n = 4$.

A requirement of a successful pH sensor is that its response remains stable over a specified time period, e.g., 12-24 hours. To further examine these electrodes, they were cycled for 400 cycles (3.5 hours). This would give a good indication as to how the electrodes would behave over time. It was clear, from Figure 6.4, that the FBRR redox peaks had disappeared with cycling, an indication that a covalent bond had not successfully formed between the salt and the carbon substrate.

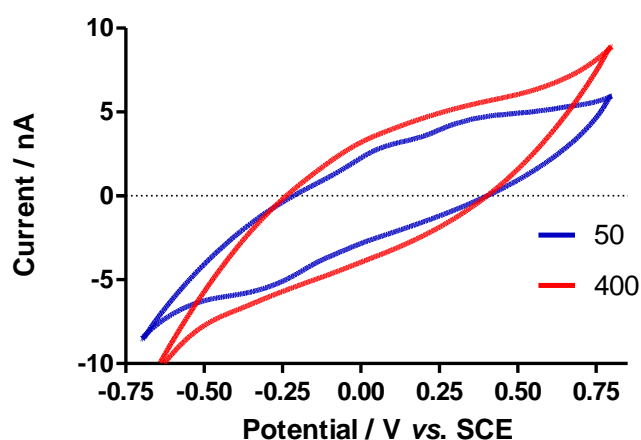


Figure 6.4: Stability, over 400 cycles, of the oxidation and reduction peaks of FBRR/H₂SO₄ deposited on untreated CFEs, $n = 4$.

6.2.2 Pre-treating CFEs

The electrochemical pre-treatment of carbon electrodes by oxidation and reduction of the electrode surface, has been widely used to improve electrode response.^{21, 22} Furthermore, the electrochemical oxidation of single carbon fibre micro cylinders has been reported as increasing electron transfer kinetics.²³ Improvements to CFEs have been achieved by pre-treating the electrodes prior to the attachment of quinones.²⁴ Functional groups generated at the carbon surface, during pre-treatment, may promote electron transfer by participating in a proton-exchange mechanism, causing electrostatic interactions with redox centres, therefore acting as catalytic sites for adsorption or electron transfer.²⁵ Surface oxidation can be achieved by the application

of a constant potential, among other methods.²² The main variables of the pre-treatment process are the oxidation and reduction potentials applied,²⁶ the composition and pH of the electrolyte solution,²¹ and the length of time of oxidation and reduction.²⁴ Many literature electrochemical pre-treatments of CFEs applied a positive potential, up to 3.0 V *vs.* SCE for a period of time, followed by a shorter cathodic potential.^{23,27} The application of 3 V in aqueous solutions has been reported as “overkill” for surface oxidation,²² so for this reason, as well as limitations of the potentiostat used, an anodic potential of 2.0 V *vs.* SCE was applied for 30 s. A cathodic potential of -2.0 V *vs.* SCE was then applied for 10 s.²⁸ Because the surface oxides formed during electrochemical pre-treatment may include H atoms, the pH of the solution used plays an important role, as it can determine the type of oxides formed on the electrode surface.²¹ In the following sections, the pre-treatments were carried out in neutral (PBS pH 7.4), basic (NaOH) and acidic (H₂SO₄) electrolyte solutions.

6.2.2.1 Pre-treatment with PBS

Phosphate buffer, pH 7.4, is reportedly the most common electrolyte for the pre-treatment of CFEs.⁹ Figure 6.5 shows the CVs resulting from the electrochemical pre-treatment of CFEs in PBS (pH 7.4). The applied potential was held at + 2.0 V *vs.* SCE for 30 s followed by a cathodic potential of -2.0 V *vs.* SCE for 10 s. After pre-treatment, the electrodes were cycled in PBS for 400 cycles. When compared to the background signals in Section 6.2.1, the CVs were less sigmoidal, with evidence of the formation of surface oxides in the anodic sweep. This is a feature referred to as an “electrochemical graphitic oxide film” caused by exposing the electrode to high positive potentials in either neutral or acidic electrolytes.²¹ There was little variation in the resulting CVs over time. The first 100 cycles show slightly higher currents at a higher potential, but this settled to a constant response after 100 cycles. This could indicate that the electrodes take a period of time or cycling to settle. All electrodes, henceforth, were cycled for a minimum of 100 cycles before any recordings were taken.

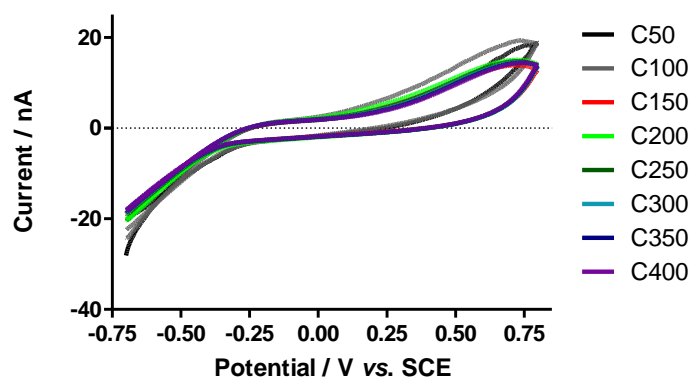


Figure 6.5: CVs of CFEs pre-treated in PBS, pH 7.4, at 2.0 V vs. SCE for 30 s followed by -2.0 V vs. SCE for 10 s, $n = 4$.

In Section 4.2.1, the CVs of CPEs displayed increasing currents with time, caused by the leeching of silicone oil from the electrode surface. CFEs, which do not contain any oil, did not exhibit a similar phenomenon, with their currents remaining stable.

The PBS pre-treated CFEs were then modified with FBRR/ H_2SO_4 using the conditions obtained in Section 4.3. The resulting CVs, 400 cycles, are shown in Figure 6.6(A), with the highlighted anodic peaks in Figure 6.6(B). The peaks were clearly formed, but there was a substantial potential drift over time. A ΔE_p value of 0.2 V vs. SCE between the anodic and cathodic peaks was indicative of quasi-reversible electrode kinetics. Diazonium salts at CFEs generally exhibit a reversible redox reaction, the pre-treatment had caused a slowing down of the electrode response.²⁹ It was also notable that the redox peak currents decreased with time, indicating that the FBRR on the surface was being depleted. This was in contrast to CPEs, see Section 4.2.3.11, where the currents gradually increased over the same time period.

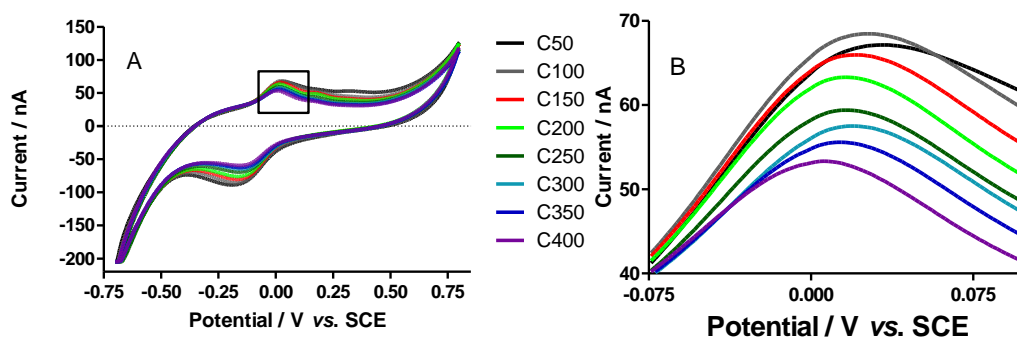


Figure 6.6: (A) CVs of FBRR modified CFEs, pretreated in PBS and (B) the highlighted anodic peaks, showing the potential drift over cycle number, $n = 4$.

The above electrodes were then tested for their pH sensitivities, by cycling them in PBS solutions, of varying pH between 7.2 and 7.6. The order of cycling in each pH solution was randomly selected to reduce any hysteresis effects. Figure 6.7 shows the relationship between the peak potential and pH for (A) the anodic and (B) the cathodic peaks. The FBRR oxidation peak, Figure 6.7(A), yielded a slope of $+16.5 \pm 45$ mV/pH, $R^2 = 0.1197$, with the reduction peak, Figure 6.7 (B) having a response of -37 ± 4 mV/pH, $R^2 = 0.9882$. The reduction peak showed some promise for use as a pH sensor, but because of the amount of drift over time it was deemed unsuitable.

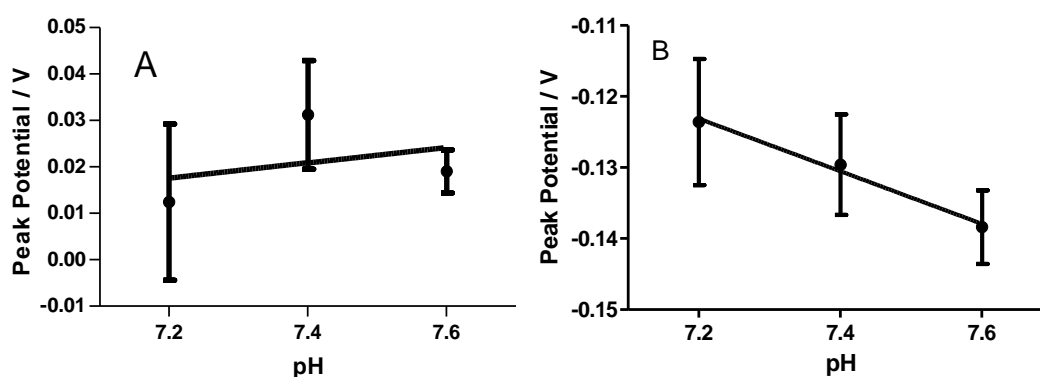


Figure 6.7: pH sensitivities of (A) anodic and (B) cathodic peaks for PBS pre-treated FBRR/CFEs, $n = 4$.

6.2.2.2 Pre-treatment with NaOH

Adjusting the electrochemical pre-treatment applied to CFEs can improve their sensitivities and resolution.⁹ Employing PBS, pH 7.4, as the chosen electrolyte gave mixed results, so the PBS was replaced by a basic electrolyte (0.1 M NaOH, pH \approx 13.0). The reduction of FBRR/H₂SO₄ onto the CFE surface was carried out as described in Section 4.3. The resulting CVs, 400 cycles, are shown in Figure 6.8(A) with the highlighted anodic peak Figure 6.8 (B). The CVs in Figure 6.8(A) show oxide formation at *ca.* 0.50 V vs. SCE. In Section 6.2.2.1, these peaks were said to result from the formation of a graphitic oxide film. The same paper reports that this film is removed in basic solutions, but surface oxides remain.²¹ On closer examination of the FBRR anodic peak, see Figure 6.8 (B), there is an obvious drift in the peak potential. It also shows the disappearance of the anodic peak after 300 cycles, indicating that the FBRR had not formed the desired covalent bond with the electrode surface. As the FBRR appeared to fall away from the electrode with continuous cycling, it was concluded that it would not be suitable as use for the pH sensor, as recording for 12-24 hours was a pre-requisite.

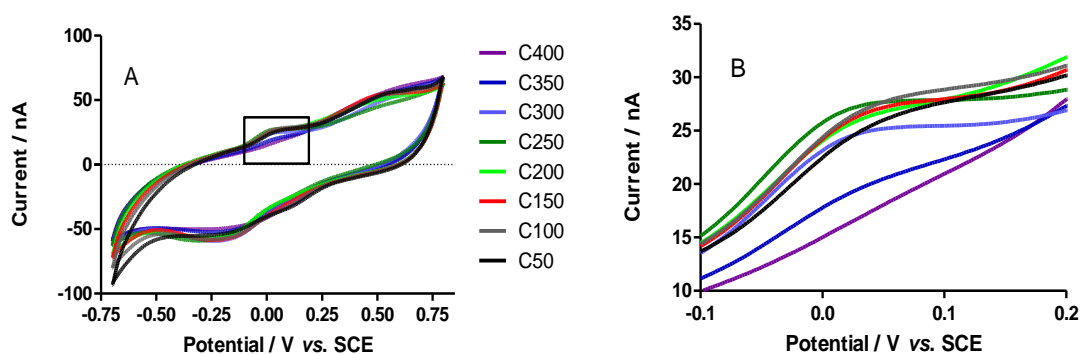


Figure 6.8: (A) CVs of FBRR modified CFEs pretreated in 0.1 M NaOH and (B) the highlighted anodic peaks showing the potential drift over cycle number and eventual disappearance of the peak, $n = 4$.

6.2.2.3 Pre-treatment with H₂SO₄

Sections 6.2.2.1-2 examined pre-treating CFEs with neutral and basic electrolyte solutions, prior to the electro-reduction of FBRR/H₂SO₄, with only limited success

obtained. The electrochemical pre-treatment of CFEs in acidic media (H_2SO_4) has been reported.^{30, 31} Here, CPA was used to pre-treat the carbon surfaces by applying 2.0 V *vs.* SCE for 30 s followed by -2.0 V *vs.* SCE for 10 s in a 0.1 M acid solution ($\text{pH} \approx 1.0$). The resulting CVs, over 400 cycles, are shown in Figure 6.9(A) with the highlighted anodic peak in Figure 6.9(B). The redox peaks displayed quasi-reversible electrode kinetics, $\Delta E \approx 0.25$ V *vs.* SCE, indicating that the pre-treatment had resulted in a slowing of the electron transfer rate.²⁹ On examination of the anodic peak, it was found to be well defined and stable over the time period tested, *ca.* 3.5 hours.

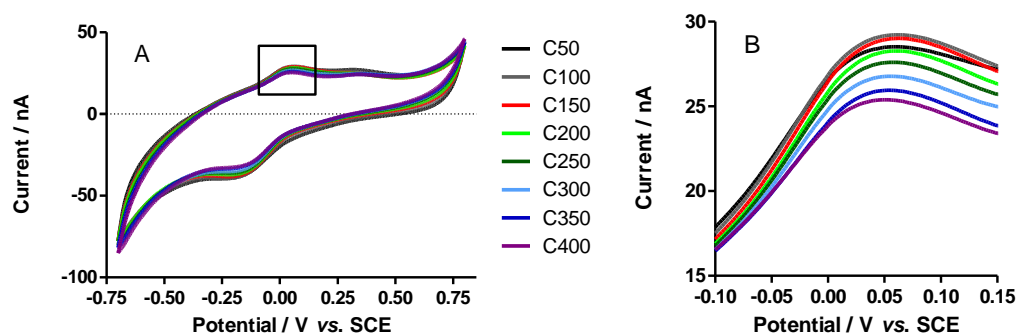


Figure 6.9: (A) CVs of FBRR modified CFEs pretreated in 0.1 M H_2SO_4 and (B) the highlighted anodic peaks showing the peak stability over cycle number, $n = 4$.

Section 4.2 discussed the electrodeposition of FBRR, in organic and aqueous media, onto CPEs, and found better results when using the aqueous H_2SO_4 as the supporting electrolyte. This was due to interactions between the organic silicone oil and TEABF₄/ACN possibly resulting in a multilayer coverage of the electrode surface, therefore, increasing the diffusion layer thickness and reducing the electron transfer rate. As there was no silicone oil present in CFEs and the fact that the majority of research papers, viewed by this researcher, electrodeposited diazonium salts via an organic electrolyte, it was decided to modify the H_2SO_4 pre-treated electrodes using TEABF₄/ACN.

The CVs in Figure 6.10, 100th cycle, show CFEs that were pre-treated in 0.1 M H_2SO_4 for 30 s at 2.0 V *vs.* SCE followed by -2.0 V *vs.* SCE for 10 s, before being modified

with FBRR using either 0.1 M H₂SO₄ or 0.1 M TEABF₄/ACN as the supporting electrolyte. The redox peaks were better defined when the organic electrolyte was used.

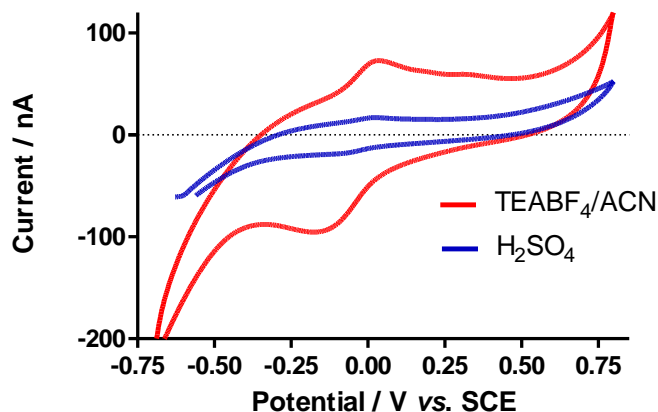


Figure 6.10: CVs of CFEs pretreated in 0.1 M H₂SO₄ before modification with FBRR using H₂SO₄ or TEABF₄/ACN as the supporting electrolyte, $n = 4$.

The FBRR/TEABF₄/ACN modified CFEs were then cycled for up to 3.5 hours, to check the stability of the anodic peak over time. A stable peak potential, with little or no drift over time is required for a successful pH sensor. As Figure 6.11(A) shows, the redox peaks were well defined. The electrode kinetics had improved from those displayed in Section 6.2.2.3, where the ΔE value was *ca.* 0.25 V *vs.* SCE, to demonstrating near reversible kinetics with $\Delta E \approx 0.10$ V *vs.* SCE. Close examination of the anodic peak, Figure 6.11(B) indicated that the peak potential remained stable over the time period of interest, with little fluctuation in the currents obtained.

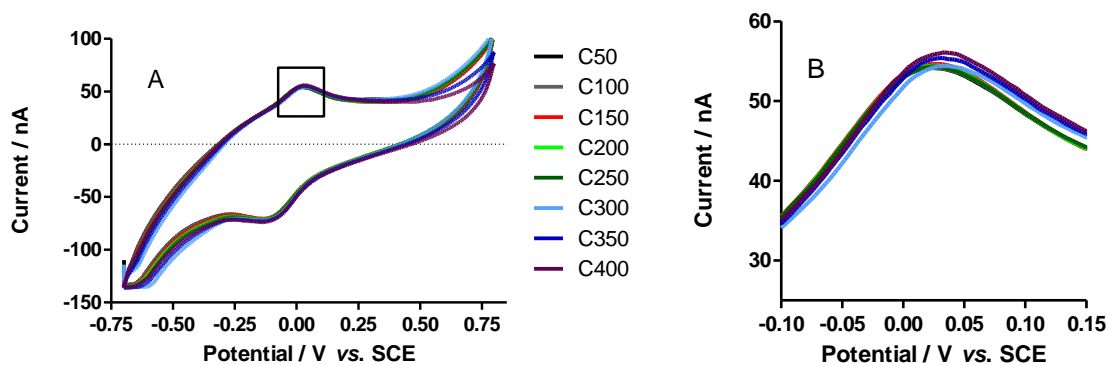


Figure 6.11: (A) CVs of FBRR/TEABF₄/ACN modified CFEs pretreated in 0.1 M H₂SO₄ and (B) the highlighted anodic peaks showing the peak stability over cycle number, $n = 4$.

6.2.3 Characterising FBRR Modified CFEs

Section 6.2.2 optimised the electrochemical pre-treatment of CFEs to best reduce FBRR onto the electrode surface. This was achieved by applying a constant potential of 2.0 V vs. SCE for 30 s followed by a cathodic potential of -2.0 V vs. SCE for 10 s in a 0.1M H₂SO₄ solution. The redox peaks were further improved by changing from an aqueous to an organic supporting electrolyte. In this section the deposition of FBRR onto the electrode surface is discussed. Following this, the pH sensitivity of the functionalised electrode and its stability over time, up to 28 days is examined. Finally, how the sensor behaves under real-time pH changes is analysed.

6.2.3.1 Deposition of FBRR

As described in Section 4.3, the electrochemical reduction of FBRR was carried out using LSV, however, a solution containing 2 mM FBRR in 0.1 M TEABF₄ dissolved in ACN was used as the supporting electrolyte, in this instance. Figure 6.12 shows the reduction profiles obtained using the pre-treated CFE as the working electrode. The recorded voltammogram presented a single electron, irreversible reduction wave at potential $E_p = -0.50$ V vs. SCE. This wave disappeared upon a second sweep and was not recovered in the subsequent scans. This behaviour was attributed to the reduction of the diazonium salt during the first reduction sweep, producing the formation of its

corresponding radical,¹⁹ leading to the grafting of the FBRR onto the substrate. The disappearance of the reduction wave after the first cycle suggested the formation of a thin layer, or monolayer of FBRR, strongly attached to the CFE surface.³² It was noted that this reduction wave was not always evident, resulting in poorly modified electrodes, that did not adequately display well defined redox peaks.

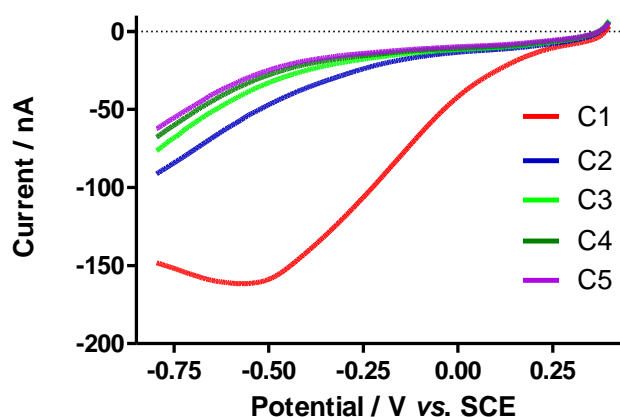


Figure 6.12: Reduction profiles for FBRR/TEABF₄/ACN, sweeps 1-5, showing the deposition occurring during the 1st sweep only, $n = 8$.

6.2.3.2 pH Response

In order to examine the pH response, CFEs were modified with 2 mM FBRR from a 0.1 M TEABF₄/ACN solution by LSV, 5 sweeps, from 0.40 to -0.80 V vs. SCE at 100 mV/s. Each modified electrode was then cycled in PBS, pH 7.2, 7.4 and 7.6, for 100 cycles from -0.70 to 0.80 V vs. SCE at 100 mV/s. The order of the different pH solutions was randomly selected to eliminate any hysteresis effects. The resulting CVs are shown in Figure 6.13(A) with Figure 6.13(B) showing close-up views of the anodic peaks of interest. They clearly show a shift in the peak potential on changing the pH of the PBS solution between 7.2 and 7.6.

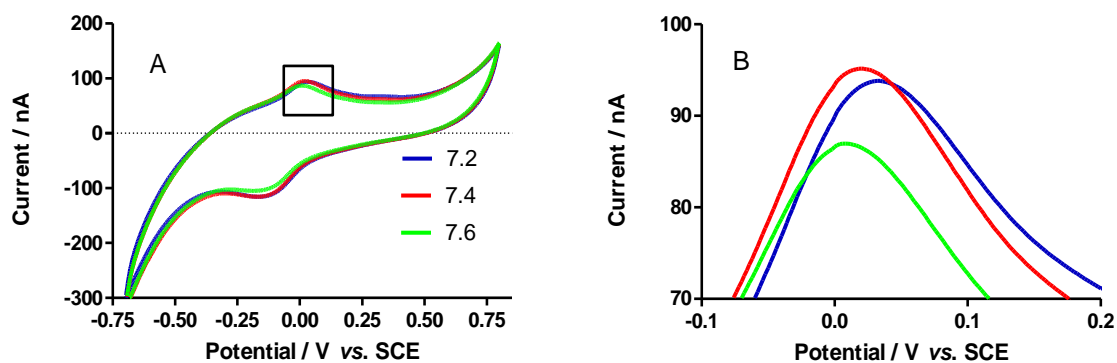


Figure 6.13: (A) CVs of the variation of peak potential with changing pH, (B) close-up of the anodic peaks formed, $n = 20$.

The linear regression of the peak potential response to changing pH is shown in Figure 6.14. It displays an almost ideal sensitivity of -55 ± 0.7 mV/pH, ($R^2 = 0.998$). The error bars signify a large inter-electrode variability, the peak potential values almost overlapping for neighbouring pH values. This inter-electrode variability was much larger for CFEs than those achieved for CPEs in Section 4.2.3.15, and proved to be a limitation when designing the FBRR/CFE pH sensor.

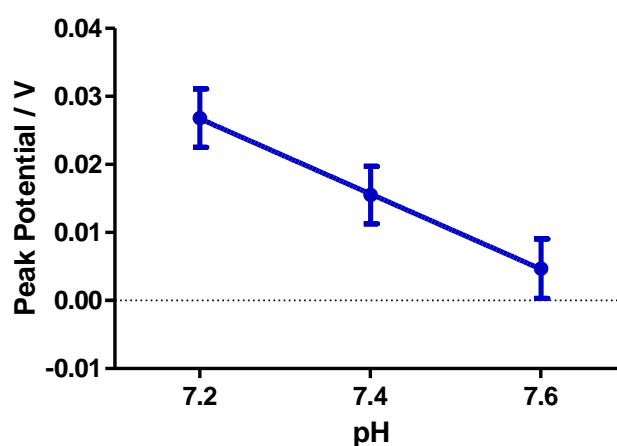


Figure 6.14: pH sensitivity of FBRR/TEABF₄/ACN modified CFEs, $n = 20$.

6.2.3.3 Stability of FBRR/TEABF₄/ACN Modified CFEs in Air

FBRR/TEABF₄/ACN modified CPEs were prepared, as specified in Section 6.2.3.1, and calibrated for their pH sensitivity on the day of modification. These electrodes were then stored at 4°C for 1, 3, 7 and 28 days, before being recalibrated. Figure 6.15 shows the resulting pH responses, before and after storage.

Table 6.1 shows analysed data for all the calibrations, pre and post storage. The slopes of each set of electrodes, before and after storage, have been compared using unpaired t-tests. Although the results in Figure 6.15 suggested a change in the peak potential achieved after storage, due to the large inter-electrode variability obtained when modifying CFEs, the analyses of the sensitivities indicate that there was no significant difference in the pH responses of the modified electrodes after storage at 4°C, for the times specified, ($P > 0.05$).

The changing pH response over time is shown in Figure 6.16. The sensitivity of the modified electrodes remained relatively stable, pre and post storage, for all days examined. These results were similar to those found for CPEs in Section 5.2.1.1.

Table 6.1: Statistical analyses of modified CFEs pH response before and after storage at 4°C.

	Slope (mV/pH)	SEM	R ²	n	P-value
Calibrate	-57.50	2.88	0.9975	4	0.7942
+ 1 Day	-58.33	0.96	0.9997	4	
Calibrate	-60.00	1.92	0.9990	4	0.1966
+ 3 Days	-55.00	2.89	0.9973	4	
Calibrate	-58.75	3.61	0.9962	4	0.0725
+ 7 Days	-66.67	0.48	0.9999	4	
Calibrate	-57.50	2.89	0.9975	4	0.2544
+ 28 Days	-61.25	0.72	0.9999	4	

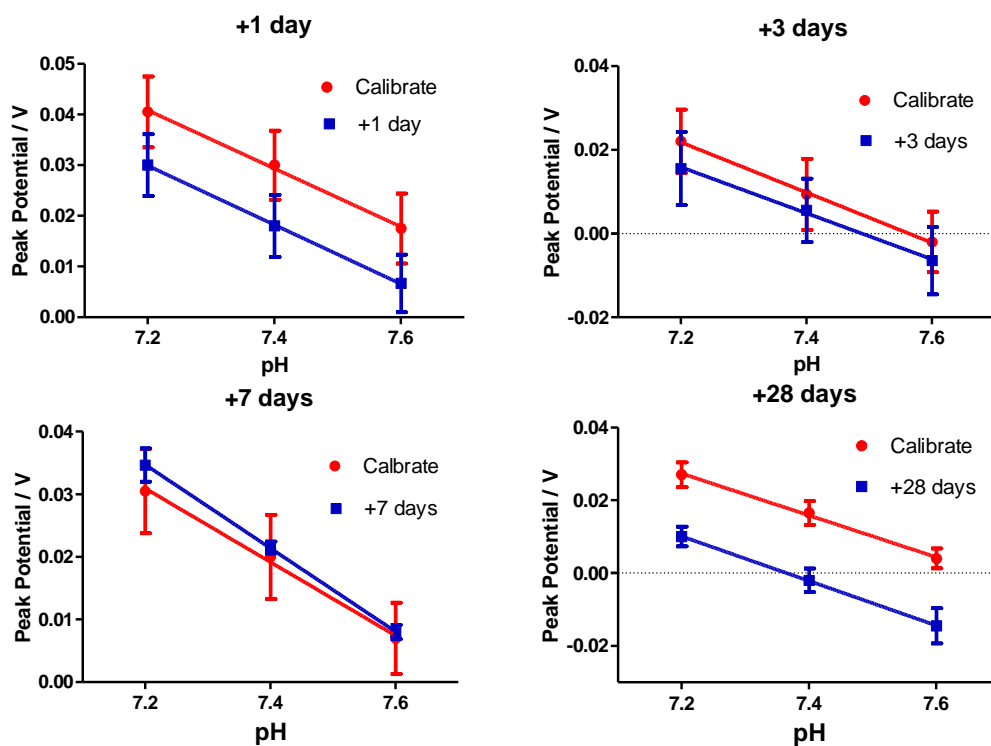


Figure 6.15: pH response of modified CFEs calibrated and stored at 4°C for 1, 3, 7 and 28 days, $n = 4$.

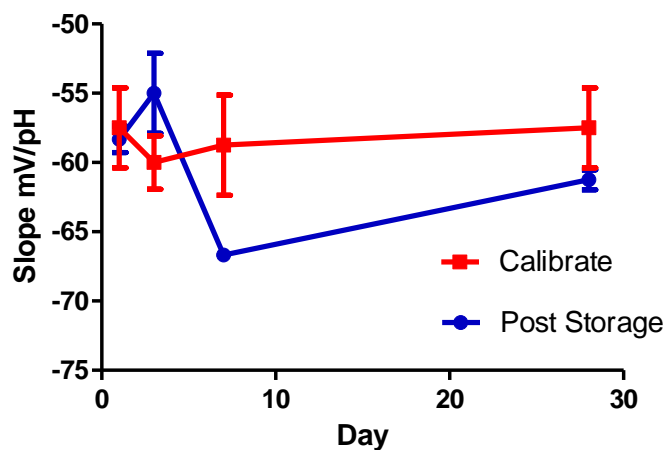


Figure 6.16: Variability in pH sensitivities of FBRR/TEABF₄/ACN modified CFEs, pre and post storage, at 4°C.

Figure 6.17 shows the isolated anodic peaks of the FBRR/TEABF₄/ACN modified electrodes cycled in pH 7.2, 7.4 and 7.6 for 100 cycles each, before and after storage

for 3 days (A) and 28 days (B). They clearly indicate that there was a potential shift with changing pH and that although the peak potentials had shifted after 28 days, the difference in the pH response was insignificant ($P = 0.2544$).

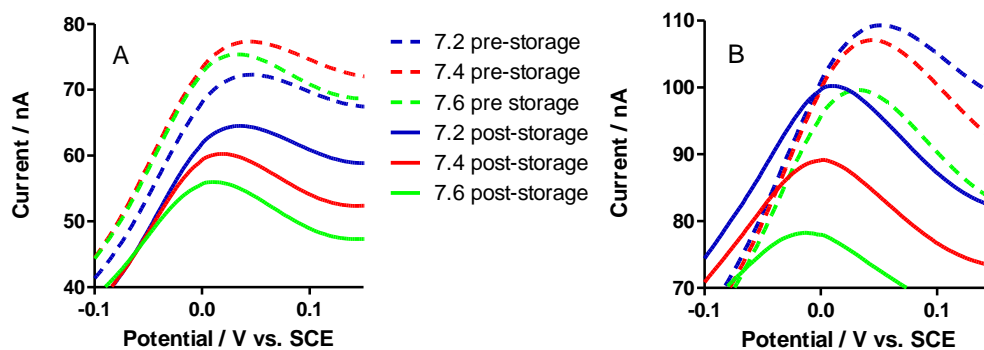


Figure 6.17: Modified CFEs cycled in PBS pH 7.2, 7.4 and 7.6, before and after storage for 3 days (A) and 28 days (B) at 4°C, $n = 4$.

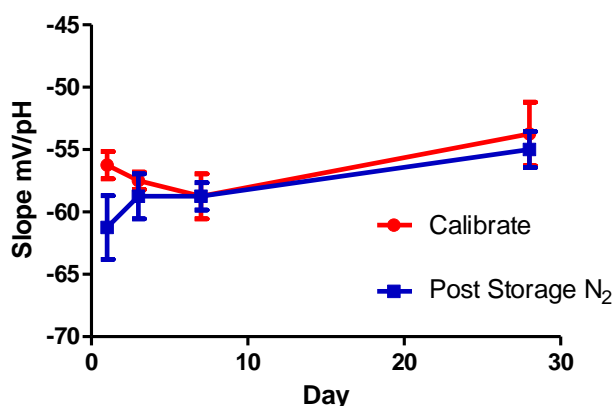
6.2.3.4 Stability of FBRR/TEABF₄/ACN Modified CFEs in N₂

A similar procedure to Section 6.2.3.3 was performed here, except the calibrated FBRR/CFEs were stored at 4°C under N₂. Table 6.2 shows the analysed data for all the calibrations, pre and post storage. The slopes of each data set, before and after storage, were compared using unpaired t-tests and they showed no significant differences in the pH responses of the modified electrodes, after storage at 4°C under N₂, for the times specified, ($P > 0.05$). This was an improvement over CPEs stored in a similar manner, see Section 5.2.1.2, where some significant differences were identified ($P < 0.05$).

Table 6.2: Statistical analyses of modified CFEs pH response before and after storage at 4°C in N₂.

	Slope (mV/pH)	SEM	R ²	n	P-value
Calibrate	-56.25	2.2	0.9985	4	0.1219
+ 1 Day N ₂	-61.25	5.1	0.9932	4	
Calibrate	-57.50	1.4	0.9994	4	0.5414
+ 3 Days N ₂	-58.75	3.6	0.9962	4	
Calibrate	-58.75	3.6	0.9962	4	1.0000
+ 7 Days N ₂	-58.75	2.2	0.9986	4	
Calibrate	-53.75	5.1	0.9912	4	0.6849
+ 28 Days N ₂	-55.00	2.9	0.9973	4	

The change in the pH sensitivity of the FBRR/CFEs was monitored over a 28 day period and the resulting plot is shown in Figure 6.18. They exhibit very stable pH responses both before and after storage in N₂. Also clearly shown is a reduced inter-electrode variability when compared to those in Section 6.2.3.3.

**Figure 6.18:** Variability in pH sensitivities of FBRR/TEABF₄/ACN modified CFEs, pre and post storage, at 4°C under N₂ conditions, $n = 4$.

6.2.3.5 Real-Time pH Study

Section 6.2.2.1 explained that the CFEs required a settling period equivalent to 100 cycles before any data was recorded. This was due to the exposure of the electrodes to air. In all previous pH testing of FBRR/CFEs, the electrodes were cycled in each solution for 100 cycles, giving the sensor an extended response time. In order to reduce the response time of the electrodes, a real-time study of changing pH was undertaken, similar to that for CPEs in Section 4.2.3.19.

CFEs were pre-treated as described in Section 6.2.2.3, before being modified with FBRR as described in Section 6.2.3.1. The calibration process was performed by changing the PBS solution pH using a micro pump, with a constant flow rate of 5 $\mu\text{l}/\text{min}$. The electrodes were allowed to settle for 100 cycles prior to any pH recordings. As physiological pH is so closely regulated³³ the sensor was required to record pH changes to within 0.01 pH units. 0.5 M NaOH or 0.5 M NaH_2PO_4 was used to gradually change the pH of the recording solution. The CV was continuously recorded between the two pH limits, (7.20 and 7.60), while the solution was slowly stirred (45 rev/min). The cycle number and time were noted on each pH change of 0.01 pH units. The peak potentials were extrapolated after the experiment was completed. The results are shown in Figure 6.19 and show that the FBRR/CFEs had a sensitivity of $-67 \pm 2 \text{ mV}/\text{pH}$ ($R^2 = 0.9805$, $n = 4$). These results, when compared to the corresponding CPE results, show increased electrode variability and a significant difference between the sensitivities obtained ($P = 0.0007$), see Table 6.3, with FBRR/CPEs exhibiting a pH response closer to the ideal Nernstian value. Although these results demonstrated that the FBRR/ H_2SO_4 modified CFE continuously measured pH changes *in-vitro*, the large errors indicated that it was not as reliable as the FBRR/CPEs. The error bars in Figure 6.19 correspond to *ca.* 12 mV, or $\pm 6 \text{ mV}$, which is equivalent to $\pm 0.1 \text{ pH}$ units, indicating that this sensor cannot precisely identify a change in pH. When compared to the corresponding results using CPEs, see Section 4.2.3.19, the error bars corresponded to *ca.* 2 mV, or $\pm 1 \text{ mV}$, equivalent to $\pm 0.016 \text{ pH}$ units. These values compounded the limitation, of large inter-electrode variability, in the design of FBRR/CFEs. It should be noted here, that 2 mV was the smallest increment that the potentiostat software could measure.

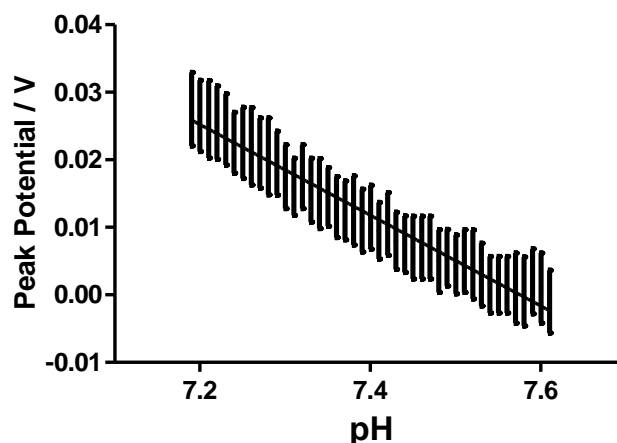


Figure 6.19: pH sensitivity of FBRR/CFEs using a controlled flow micro pump system to alter pH, $n = 4$.

Table 6.3: Comparison of real-time pH sensitivities for FBRR modified CPEs and CFEs, $n = 4$.

Substrate	pH Sensitivity (mV/pH)	R ²	P-value
CPE	-56 ± 1	0.9539	0.0007
CFE	-67 ± 2	0.9805	

6.2.4 Factors Affecting the Operation of a pH Sensor

The FBRR/CFE pH sensor has been characterised in an *in-vitro* environment. The next step in the development of a sensor, for use in physiological samples, was to examine how the sensor might behave when *in-vivo* conditions were mimicked. These conditions included varying the ionic strength of solutions, testing the effect of ions that are prevalent in physiological samples, the operating temperature of the sensor and the suitability of the reference electrode used in the electrochemical set up.

The effects of various physiological and pharmacological interferences on the FBRR/CFE pH sensor will also be discussed in this section.

6.2.4.1 Ionic Strength

Many pH sensors, especially those based on optical measurements,³⁴ have issues when measuring a signal that depends on the ionic strength of the sample. The effect of ionic strength on the FBRR/CFEs was tested by cycling the modified electrodes in PBS of altered ionic strength with pH values of 7.2, 7.4 and 7.6. The ionic strength of the solutions was calculated using Equation 5.1, see Section 5.2.9. All previous PBS solutions had an ionic strength of 0.46 M, recordings were subsequently taken using PBS with ionic strengths of 0.23 and 0.92 M.

FBRR/CFEs were calibrated in PBS solutions, pH 7.2, 7.4 and 7.6. They were then cycled in PBS with ionic strengths of 0.92 M and 0.23 M with the same pH values. The pH responses were determined, see Figure 6.20, and compared using two tailed t-tests. A *P*-value of 1.00 was obtained when comparing ionic strengths of 0.46 M with both 0.92 M and 0.23 M indicating no significant differences in the pH response between modified electrodes cycled in PBS of various ionic strengths, see Table 6.4.

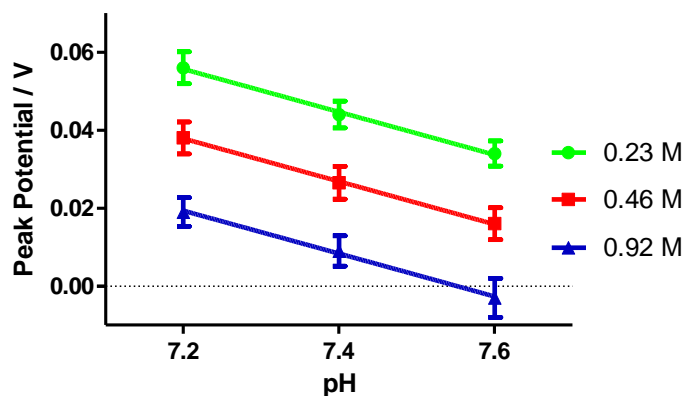
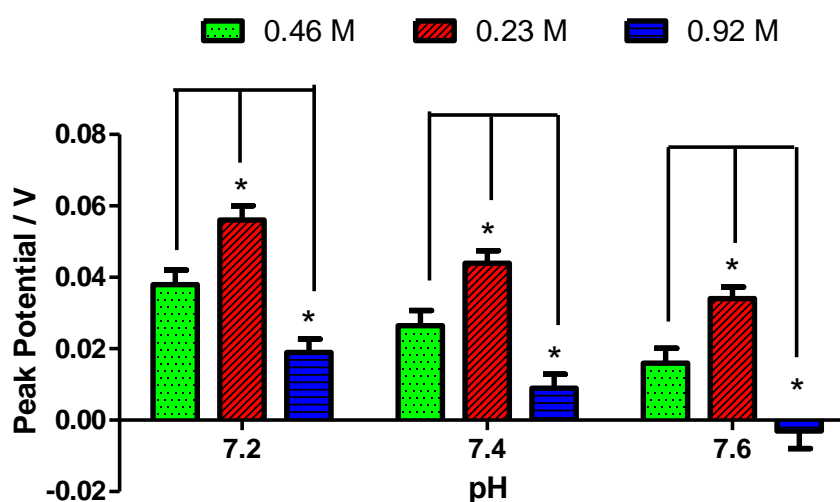


Figure 6.20: Linear regressions comparing the pH responses of FBRR/TEABF₄/ACN modified CFEs in solutions of varying ionic strength, *n* = 4.

Table 6.4: Comparison of the pH sensitivities of FBRR/TEABF₄/ACN modified CFEs in solutions of varying ionic strength, $n = 4$.

	Slope (mV/pH)	SEM	R ²	P-value
I = 0.23 M	-55.00	2.89	0.9973	1.0000
I = 0.46 M	-55.00	1.44	0.9993	—
I = 0.92 M	-55.00	2.89	0.9973	1.0000

**Figure 6.21:** Bar chart of the differences in the anodic peak potential obtained in solutions of different ionic strength, $n = 4$.

However, Figure 6.20 clearly showed that the ionic strength of the solution affected the potential at which the anodic peak was located. This showed a contribution of the ions to the peak potentials of FBRR/CFEs. Figure 6.21, evaluates the differences between the potentials obtained. As 0.46 M was the ionic strength of the standard PBS solution used throughout this thesis, the solutions with ionic strength values of 0.23 M and 0.92 M were compared to the standard value. When the potentials at each pH, 7.2, 7.4 and 7.6 were compared, at each of the ionic strengths, significant differences were obtained for all, see Table 6.5. Similar tests on FBRR/CPEs, see Section 5.2.9, yielded

no difference in the potentials obtained, confirming that the effect of solution ionic strength was a limiting factor when designing FBRR/CFEs.

Table 6.5: Evaluation of the contribution of ionic strength to the peak potential obtained when cycling FBRR/CFEs in solutions with varying ionic strengths, $n = 4$.

pH	P-value	
	(0.46 M vs. 0.23 M)	(0.46 M vs. 0.92 M)
7.2	0.0190	0.0153
7.4	0.0114	0.0238
7.6	0.0114	0.0250

6.2.4.2 Ion Effect

Metal ions are prevalent in living systems. Calcium and magnesium ions (Ca^{2+} and Mg^{2+}) are two alkaline-earth-metal ions physiologically essential to almost all living organisms, with average concentrations of 5 mM^{35, 36} and 1.2 mM,³⁷ respectively. They are also known to form coordinate bonds and complexes, with several quinones.^{5,38} To examine the effect of these ions on the FBRR/CFE pH sensor, they were introduced into the PBS solutions, once the electrodes had been calibrated.

FBRR/CFEs were prepared and calibrated in PBS solutions with pH values of 7.2, 7.4 and 7.6. They were then cycled in the same PBS solutions with added MgCl_2 (21 mM) and CaCl_2 (1.6 mM). This concentration of MgCl_2 was used as some commercially available aCSF contains up to 21 mM. Figure 6.22 shows the resulting pH sensitivities of the calibrated electrodes, with the added Ca^{2+} (A) and Mg^{2+} (B).

The pH sensitivities are assigned in Table 6.6 and were recorded as -58 ± 5 mV/pH, $R^2 > 0.99$, for the calibrations and -56 ± 4 , $R^2 > 0.99$, and -59 ± 2 mV/pH, $R^2 > 0.99$, with Mg^{2+} and Ca^{2+} ions added, respectively. These pH responses were compared to the calibrations using unpaired t-tests and it was found that there were no significant differences obtained when the Mg^{2+} and Ca^{2+} ions were added, giving P -values of 0.8012 and 0.7434, respectively.

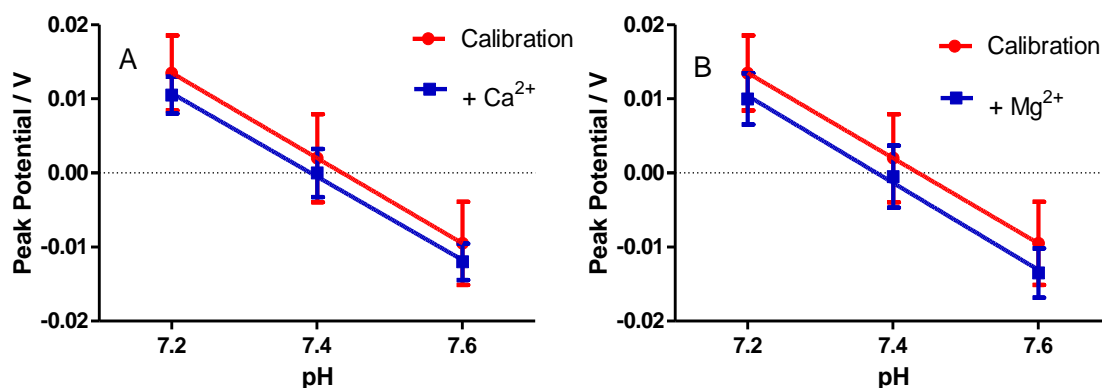


Figure 6.22: pH responses of FBRR/TEABF₄/ACN modified CFEs in PBS solutions with added CaCl₂ (A) and MgCl₂ (B), $n = 4$.

Table 6.6: Analyses of the pH responses of FBRR/CFEs cycled in PBS solutions with added MgCl₂ and CaCl₂, $n = 4$.

Calibration (mV/pH)	R ²	+ MgCl ₂ (mV/pH)	R ²	P-Value	+ CaCl ₂ (mV/pH)	R ²	P-value
57.50 ± 5	0.9958	56.25 ± 4	0.9962	0.8012	58.75 ± 6	0.9985	0.7434

6.2.4.3 Temperature

So far, the FBRR/CFEs were examined in solutions at room temperature, 22°C. In order to develop a successful sensor, suitable for real-time testing of physiological pH, the sensor must be capable of operating at a temperature of 37°C.

Prepared FBRR/CFEs were firstly calibrated in PBS solutions, pH 7.2, 7.4 and 7.6, at 22°C. The solutions were subsequently heated to, and maintained at, 37°C for the re-calibration of electrodes. The CVs, anodic peaks only, Figure 6.23, show the resulting peaks and their corresponding potentials when cycling in PBS with pH values of 7.2, 7.4 and 7.6.

There was a shift to a more negative potential for the values obtained between the two temperatures. This is because pH changes with temperature, according to the Rosenthal Correction Factor, by 0.015 pH units per °C. This results in a shift of 0.225 pH units for the temperature difference of 15°C. Assuming a Nernstian response of -59 mV/pH

then the expected shift in peak potential is -13 mV. So, if the peak potential at 22°C is -34 mV, the expected peak potential at 37°C would be -47 mV. Comparing the peak potentials at similar pH values between 22°C and 37°C, in Figure 6.24, gave potential shifts of approximately -12 mV, corresponding to a non-significant difference ($P = 0.2070$).

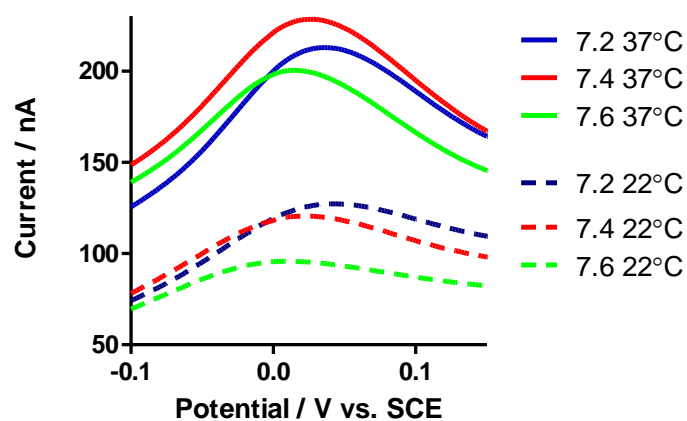


Figure 6.23: Anodic peaks of FBRR/CFEs cycled in various pH PBS showing the shift in potential due to temperature differences at 22°C and 37°C, $n = 4$.

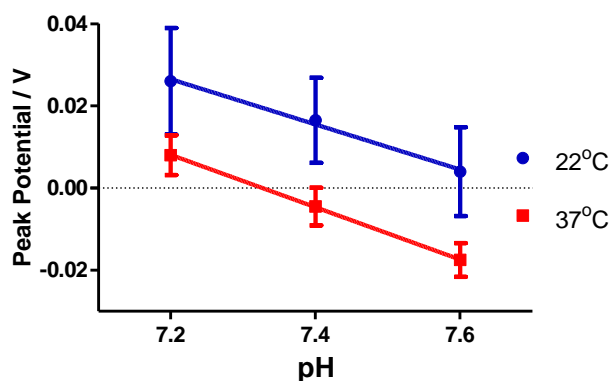


Figure 6.24: pH responses of FBRR/CFEs at 22°C and 37°C, $n = 4$.

Also, the pH response is dependent on temperature according to Equation 5.2, (see Section 5.2.11), giving a pH sensitivity of -61.55 mV/pH at 37°C, compared to -59

mV/pH at 22°C. These sensitivities, highlight the temperature dependence of the Nernst equation.⁶

The pH responses at both temperatures are shown in Figure 6.24, with the corresponding analyses in Table 6.7. They demonstrated good pH sensitivities with slopes of -55 ± 4 and -63.75 ± 1 mV/pH for 22°C and 37°C, respectively, with R^2 values > 0.99 . A significant difference was found when the theoretical value of -61.55 mV/pH was compared with the sensitivity achieved, -63.75 mV/pH, ($P = 0.0208$).

Table 6.7: Statistical analyses of the pH responses of FBRR/CPEs comparing temperatures of 22°C and 37°C, $n = 4$.

22°C			37°C		
Slope (mV/pH)	SEM	R ²	Slope (mV/pH)	SEM	R ²
-55.00	4.33	0.9938	-63.75	0.72	0.9999

6.2.4.4 Reference Electrode

The reference electrode, used so far in this chapter, was a SCE. Section 5.2.12 discussed the reasons for its unsuitability as an *in-vivo* reference electrode, mainly size and toxicity, and why it was replaced by a pseudo Ag/AgCl reference electrode.

In order to examine the effect of changing the reference electrode, FBRR/CFEs were calibrated in PBS solutions with pH values of 7.2, 7.4 and 7.6, using a SCE reference, before being cycled under the same conditions using a Ag/AgCl pseudo reference electrode. To further mimic *in-vivo* conditions, a 5 mm cylinder silver wire was used as the auxiliary electrode. The anodic peaks from the resulting CVs are shown in Figure 6.25. They clearly show the shift in potential caused by using the Ag/AgCl reference electrodes, of approximately -33 mV compared to SCE. Literature values for the potential difference between Ag/AgCl and SCE reference electrodes suggest a shift of -44 mV.³⁹ A significant difference was found between the literature and actual values, ($P < 0.0001$), nonetheless, the comparable sensitivities negate this issue.

However, it is imperative that the difference in expected peak potentials is characterised prior to deployment of this system in physiological media.

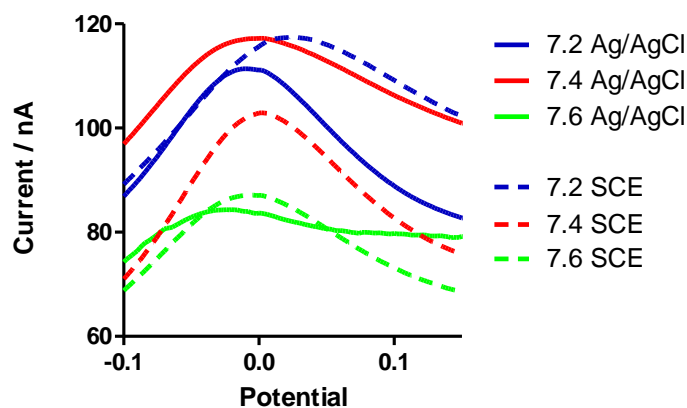


Figure 6.25: Anodic peaks of FBRR/CFEs cycled in PBS solution of varying pH using SCE and Ag/AgCl reference electrodes, $n = 4$.

The pH response of both systems, Ag/AgCl and SCE reference electrodes, is shown in Figure 6.26, with the corresponding statistical analyses given in Table 6.8. The pH responses were -55.00 ± 1 mV/pH when using a SCE and -53.75 ± 1 mV/pH when using a Ag/AgCl reference electrode. Analyses disclosed that these differences in sensitivity were non-significant, ($P = 0.4679$).

Table 6.8: Statistical analyses of the pH responses of FBRR/CFEs comparing SCE and Ag/AgCl reference electrodes, $n = 4$.

	Peak Potential 7.2 (mV)	Peak Potential 7.4 (mV)	Peak Potential 7.6 (mV)	n	Slope (mV/pH)	P -value
SCE	16 ± 5.50	6 ± 6.63	-5 ± 5.62	4	-55.00 ± 1.44	0.4679
Ag/AgCl	-16 ± 4.65	-27 ± 5.26	-38 ± 8.3	4	-53.75 ± 0.72	

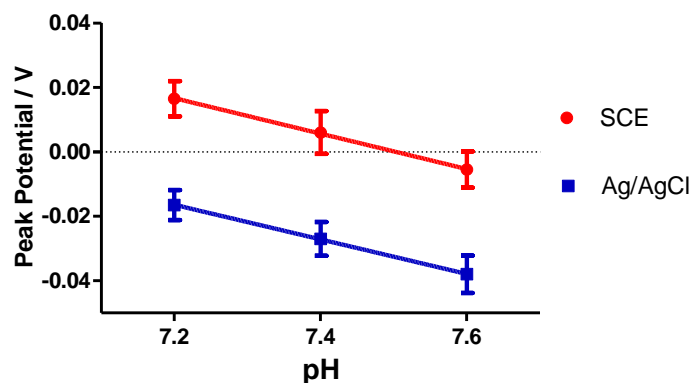


Figure 6.26: pH responses of FBRR/CFEs using SCE and Ag/AgCl reference electrodes, $n = 4$.

6.2.4.5 Physiological Interferences

Good sensitivity is not the only desirable characteristic in sensor design. Selectivity between different analytes is also an important factor to consider. This is of importance here, as many physiological interference molecules in biological media are electroactive, possibly with similar oxidation potentials to FBRR at a CFE surface. To examine any possible effects of these interfering molecules, physiologically relevant concentrations of the individual interferences were added to the PBS solution, before the modified electrodes were recycled in the solution. All recordings involved the 100th cycle. Section 5.2.3 detailed all the analytes examined, along with their relevant physiological concentrations that were used in this section.

The peak potentials pre and post treatment were recorded, $n = 4$, and the differences were compared using t-tests. As in Section 5.2.3, some analytes caused a change in solution pH, which resulted in a shift of the peak potential. An adjustment was made to allow for this. To avoid repetition of Section 5.2.3, the results obtained were tabulated, see Table 6.9. When analysed, all treatments caused a slight shift in the peak potentials, which were deemed non-significant, ($P > 0.05$). The corresponding P -values, obtained for FBRR/CPEs cycled in the same analytes, are shown alongside the CFE results. They conclude that both FBRR modified electrodes, CPEs and CFEs, were not affected by the analytes examined, or their metabolites.

Table 6.9: Effect of chemical interferences on FBRR/CFE peak potentials, showing also the corresponding results for FBRR/CPEs, $n = 4$.

Interference	FBRR/CFE			FBRR/CPE
	Peak Potential Without Interference (V vs. SCE)	Peak Potential With Interference (V vs. SCE)	<i>P</i> -value	<i>P</i> -value
AA	0.047 ± 0.010	0.049 ± 0.010	0.8761	0.8637
UA	0.025 ± 0.003	0.018 ± 0.002	0.0950	0.9158
DA	0.020 ± 0.002	0.021 ± 0.001	0.7735	1.0000
L-Cysteine	-0.002 ± 0.002	0.001 ± 0.001	0.3512	0.0992
L-Tyrosine	0.033 ± 0.002	0.022 ± 0.001	0.6355	0.7306
5-HT	0.011 ± 0.005	0.007 ± 0.004	0.5496	0.6202
L-Glutathione	-0.034 ± 0.002	-0.035 ± 0.002	0.6994	0.9596
HVA	-0.014 ± 0.009	-0.016 ± 0.012	0.8871	0.1762
DOPAC	0.056 ± 0.006	0.050 ± 0.003	0.3982	0.3867
5-HIAA	0.024 ± 0.007	0.040 ± 0.007	0.1256	0.5298

6.2.4.6 Pharmacological Interferences

Like physiological interferences, pharmacological interferences may affect the location and definition of FBRR/CFE peak potentials. This would generally result from fouling of the electrode surface, and the electroactive nature of the interferences. Acetaminophen (ACOP) and acetylsalicylic acid (ASA) are two of the most commonly used medications, so their effects on the modified sensors were investigated.

Both ACOP and ASA caused a change in the solution pH, so an adjustment to the peak potential was made, see Section 5.2.8. The peak potentials, pre and post treatment, were analysed using t-tests and the significance of any differences found were quoted as *P*-values. The results are located in Table 6.10, along with the corresponding results for FBRR/CPEs. Details of the analytes examined, along with their relevant physiological concentrations that were used in this section, can also be found in Section 5.2.8.

When analysed, both treatments caused a slight shift in the peak potentials, which were deemed non-significant, ($P > 0.05$). The corresponding *P*-values, obtained for FBRR/CPEs cycled in ACOP and ASA, are shown alongside the CFE results. They conclude that both FBRR modified electrodes, CPEs and CFEs were not affected by the analytes examined.

Table 6.10: Effect of pharmacological interferences on FBRR/CFE peak potentials, showing also the corresponding results for FBRR/CPEs, $n = 4$.

Interference	CFE			CPE
	Peak Potential Pre-Treatment (V vs. SCE)	Peak Potential Post-Treatment (V vs. SCE)	P-value	P-value
ACOP	0.042 ± 0.008	0.040 ± 0.005	0.0866	0.3097
ASA	0.025 ± 0.005	0.019 ± 0.004	0.03858	0.5188

6.2.5 Biocompatibility

Biological tissue presents as a very hostile environment for electrochemical sensors. In Section 5.2.3, the biocompatibility of FBRR/CPEs was examined. It concluded that proteins and lipids pulled the silicone oil, along with FBRR, from the electrode surface. They also caused electrode fouling. CFEs on the other hand, do not contain oil, so improved biocompatibility was expected.

To test the effect of various physiological substances (e.g., proteins, lipids and surfactants) on FBRR/CFEs, calibrated electrodes were stored, in solutions of BSA, 1% (protein), PEA, 1% (lipid), Triton® X 1% (surfactant) or homogenised brain tissue, overnight at 4°C, before being recalibrated in the PBS solutions. Although the end application for this sensor involved skeletal muscle tissue, *ex-vivo* brain tissue was deemed a suitable medium for characterisation due the similarities displayed in Table 5.7 and the fact that *in-vivo* studies showed the homogenised brain tissue to be a harsher environment than the *in-vivo* muscle tissue, see Section 7.2.2.

In the corresponding section on biocompatibility of FBRR/CPEs, see Section 5.2.3, the modified electrodes were treated for up to 28 days. Such lengthy treatments were not considered for CFEs. A problem uncovered when developing the FBRR/CFE sensor was the lack of reproducibility. This was evident when electrodepositing FBRR onto the pre-treated electrodes, as not all reductions led to successful formation of the FBRR layer. Often, when well defined redox peaks were obtained, the location of the peak potentials led to large inter-electrode variability. This was highlighted in Section 6.2.3.5, where the errors displayed were equivalent to 0.2 pH units. Section 6.2.4.1 uncovered a limiting effect, on the location of the peak potential, caused by the ionic

strength of the solution. Later, in this thesis it will be discovered that the fragility of CFEs in the *in-vivo* environment meant that they were unsuitable for use as a biological real-time pH sensor, see Section 7.2.1. For these reasons, preliminary biocompatibility studies on FBRR/CFEs were performed over a 24 hour period only.

6.2.5.1 Bovine Serum Albumen

Figure 6.27(A) shows the resulting CVs having stored FBRR/CFEs in BSA, 1%, overnight at 4°C. The anodic peaks of interest, Figure 6.27(B), were clearly still visible after storage. This was in contrast to CPEs stored in BSA, see Section 5.2.3.1, where the peaks were broad and barely distinguishable after storing in BSA, for 1 day. The peak currents dropped after storing CFEs, this was an indication of electrode fouling, increasing the diffusion layer thickness, and therefore reducing the electron transfer kinetics. CFEs, bare and pre-treated, had previously shown fouling effects due to BSA.²⁸

There was an obvious shift in the peak potential with changing pH. Linear regression plots of the pH sensitivities are shown in Figure 6.28, giving sensitivities of -56.25 ± 2 and -57.50 ± 4 mV/pH for pre and post treatment, respectively. When compared using t-tests, no significant difference was found between the electrode responses, ($P = 0.8049$). These values are given in Table 6.11.

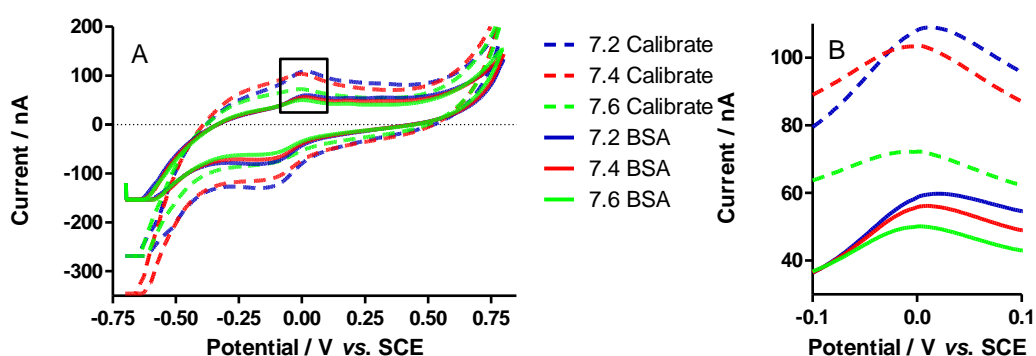


Figure 6.27: (A) CVs pre and post storage of FBRR/CFEs in BSA, (B) close-up view of the anodic peaks, $n = 4$.

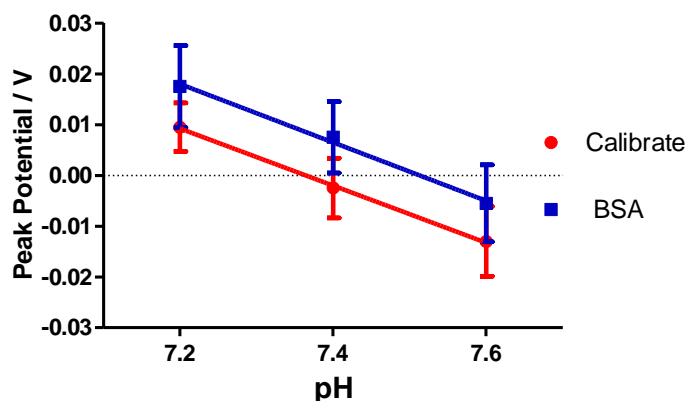


Figure 6.28: pH sensitivities of FBRR/CFEs stored overnight in BSA, 1%, $n = 4$.

Table 6.11: Analyses of the pH responses of FBRR/CFEs pre and post treatment in BSA, $n = 4$.

	Slope (mV/pH)	SEM	R ²	n	P -value
Calibrate	-56.25	2.17	0.9985	4	0.8049
+ 1 Day BSA	-57.50	4.33	0.9944	4	

6.2.5.2 Phosphatidylethanolamine

CFEs, stored in PEA, 1%, overnight were calibrated pre and post storage, resulting in the CVs shown in Figure 6.29(A). Enhanced views of the anodic peaks obtained are shown in Figure 6.29(B). The peaks, post storage, were clearly defined with little difference in the currents obtained, indicating negligible electrode fouling. This was not expected as PEA was previously found to poison pre-treated CFEs.²⁸ Section 5.2.3.2 showed the effect of storing CPEs in PEA. In contrast to CFEs, the CPE peaks post storage were ill-defined, due to electrode fouling, and FBRR removal along with silicone oil.

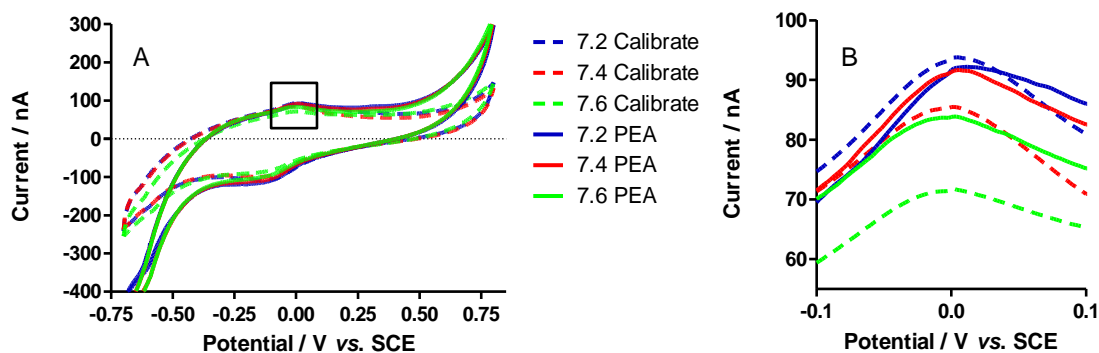


Figure 6.29: (A) CVs pre and post storage of FBRR/CFEs in PEA, (B) close-up view of the anodic peaks, $n = 4$.

When the anodic peaks for CFEs stored in PEA were analysed, they had pH sensitivities of -61.25 ± 0.7 and -65.00 ± 4 mV/pH, pre and post treatment, respectively. The linear regression for the pH response, shown in Figure 6.30, indicated a shift in potential for the modified electrodes after storage, and improved inter-electrode variability, i.e., smaller error bars. The pH responses were compared using unpaired t-tests, resulting in non-significant differences between the electrode responses before and after storage in PEA, ($P = 0.4257$), shown in Table 6.12.

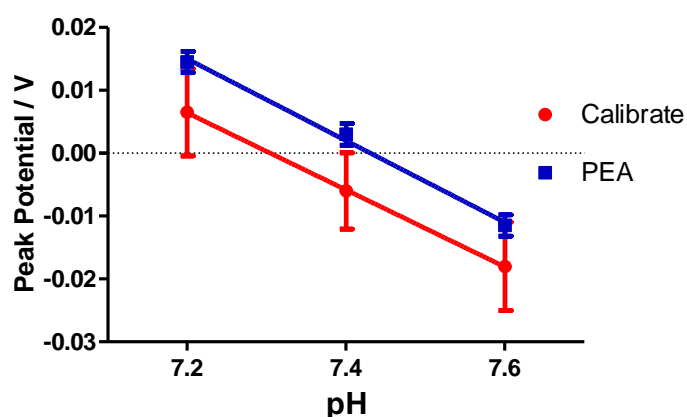


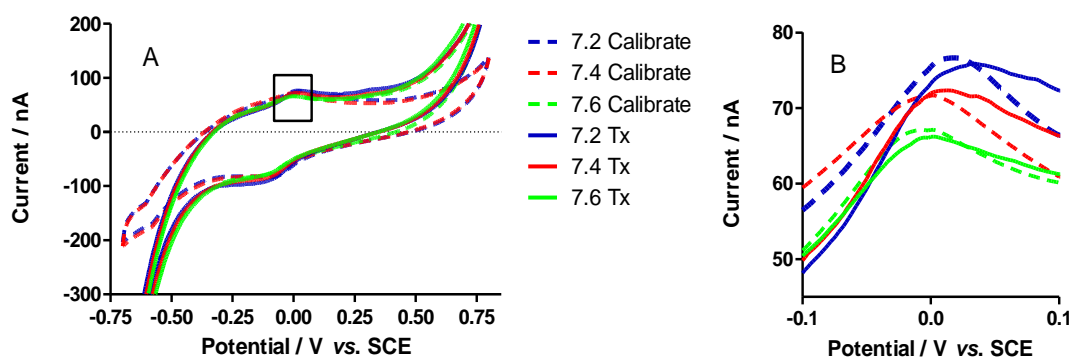
Figure 6.30: pH sensitivities of FBRR/CFEs stored overnight in PEA, 1%, $n = 4$.

Table 6.12: Analyses of the pH responses of FBRR/CFEs pre and post treatment in PEA, $n = 4$.

	Slope (mV/pH)	SEM	R ²	n	P -value
Calibrate	-61.25	0.72	0.9999	4	0.4257
+ 1 Day PEA	-65.00	4.33	0.9956	4	

6.2.5.3 Triton[®]X

Section 5.2.3.3 found Triton[®]X to be the most severe of the treatments applied to CPEs, with a vast increase in electrode capacitance and no anodic peaks visible in the resulting post storage CVs. When pre-treated FBRR/CFEs were exposed to the same treatment, the CVs formed were almost identical pre and post storage, see Figure 6.31(A). On closer examination of the anodic peaks, in Figure 6.31(B), it can be seen that the peaks were clearly defined, with no change in the current output, consistent with no electrode fouling. This enhances the results from Section 5.2.3.3, indicating that the increased capacitive currents resulted from the loss of silicone oil from the CPE matrix, which in turn removed the FBRR.

**Figure 6.31:** (A) CVs, pre and post storage of FBRR/CFEs in Triton[®]X, (B) close-up view of the anodic peaks, $n = 4$.

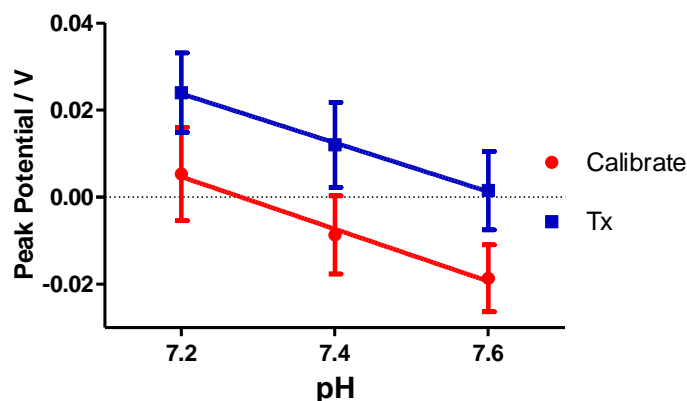


Figure 6.32: pH sensitivities of FBRR/CFEs stored overnight in Triton[®]X, 1%, $n = 4$.

Table 6.13: Analyses of the pH responses of FBRR/CFEs pre and post treatment in Triton[®]X, $n = 4$.

	Slope (mV/pH)	SEM	R ²	n	P -value
Calibrate	-60.00	5.77	0.9908	4	0.5653
+ 1 Day Triton [®] X	-56.20	2.17	0.9985	4	

The anodic peaks potentials, for CFEs stored in Triton[®]X, were analysed, see Figure 6.32, resulting in pH sensitivities of -60.00 ± 6 and -56.20 ± 2 mV/pH, pre and post treatment, respectively. The pH responses were compared using unpaired t-tests, resulting in non-significant differences between the electrode responses before and after storage in Triton[®]X, ($P = 0.5653$), shown in Table 6.13.

6.2.5.4 Brain Tissue

Although Sections 6.2.5.1-3 investigated the biocompatibility of the FBRR/CFEs in solutions of lipids, proteins and surfactants, the medium that best mimics the *in-vivo* environment is *ex-vivo* brain tissue. To examine the effect of brain tissue on the pH sensor, CFEs were modified with FBRR then calibrated, for 100 cycles in PBS of pH 7.2, 7.4 and 7.6. The resulting, calibrated, electrodes were stored in homogenised brain tissue, at 4°C overnight, before being recycled using the same calibration conditions. Figure 6.33(A) shows the resulting CVs pre and post treatment, with the anodic peaks magnified in Figure 6.33(B).

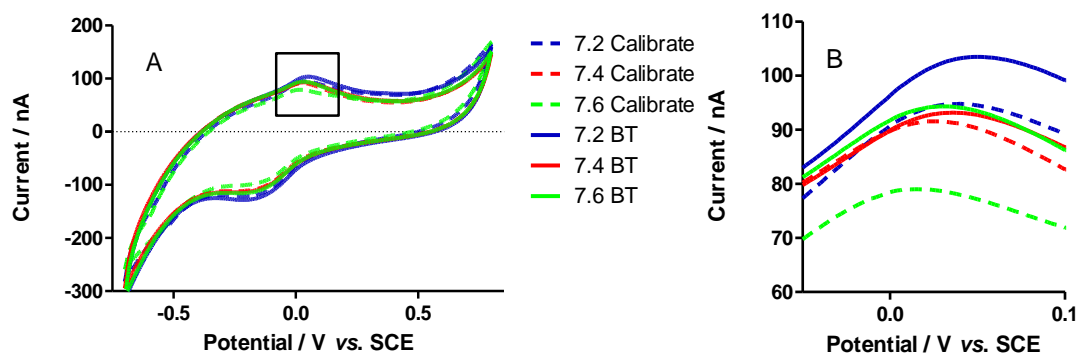


Figure 6.33: (A) CVs showing the effect of storing FBRR/CFEs in homogenised brain tissue, (B) close up view of the anodic peaks, $n = 4$.

It was observed that the CVs formed, were almost identical pre and post storage, see Figure 6.33(A). On closer examination of the anodic peaks, see Figure 6.33(B), it can be seen that the peaks were clearly defined, with no change in the current output, which indicated little or no electrode fouling.

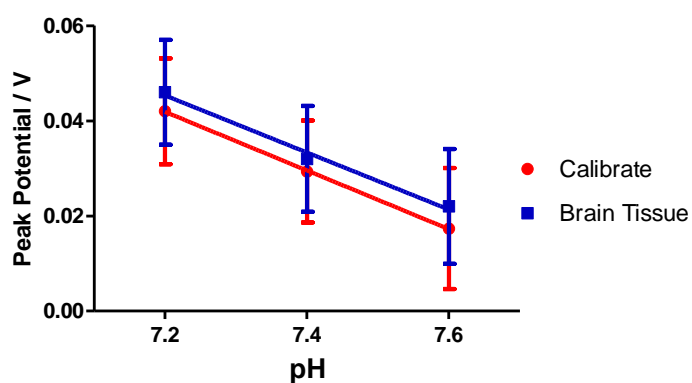


Figure 6.34: pH sensitivities of FBRR/CFEs stored overnight in *ex-vivo* brain tissue, 1%, $n = 4$.

The anodic peaks potentials, for CFEs stored in *ex-vivo* brain tissue, were analysed, see Figure 6.34, resulting in pH sensitivities of -61.67 ± 1 and -60.00 ± 6 mV/pH, pre and post treatment, respectively. The pH responses were compared using unpaired t-

tests, resulting in non-significant differences between the electrode responses before and after storage in brain tissue, ($P = 0.7850$), shown in Table 6.14.

Table 6.14: Analyses of the pH responses of FBRR/CFEs pre and post treatment in *ex-vivo* brain tissue, $n = 4$.

	Slope mV/pH	SEM	R²	<i>n</i>	<i>P</i>-value
Calibrate	-61.67	0.96	0.9998	4	0.7850
+ 1 Day BT	-60.00	5.77	0.9908	4	

6.3 Conclusion

Chapter 6 of this thesis examined the possibility that FBRR/CFEs were suitable for use as real-time pH sensors. Section 6.2.1 discussed the suitability of untreated CFE modified with FBRR, using the optimised CPE parameters from Chapter 4, but this proved unsuccessful, mainly due to their small surface area and fragility causing possible fractures during cycling. The reduction profile showed a small wave, in the first linear sweep, which was not consistently formed. The pH sensitivity, of electrodes that had been functionalised, displayed a super-Nernstian response of -130 ± 39 mV/pH.

Section 6.2.2 discussed the electrochemical pre-treatment of CFEs and the resulting effects on the electrodeposition of FBRR onto the electrode surfaces. The pre-treatment can cause scratches on the electrode surface, thereby increasing the electroactive surface area, or alternatively it leads to the formation of surface oxides that can facilitate electron transfer rates.¹⁴

Neutral, basic and acidic media were employed as the pre-treatment electrolytes, before the electro-reduction of FBRR onto the already modified surfaces. The most stable, consistent anodic peaks resulted from CFEs that were pre-treated in 0.1 M H₂SO₄ at 2.0 V *vs.* SCE for 30 s, followed by -2.0 V *vs.* SCE for 10 s. The anodic peaks were further improved by depositing the FBRR from a solution of 0.1 M TEABF₄/ACN.

The optimised conditions for producing FBRR/CFEs was:

- Pretreat CFEs in 0.1 M H₂SO₄ by applying a potential of 2.0 V vs. SCE for 30 s followed by a potential of -2.0 V vs. SCE for 10 s.
- Prepare 2 mM solution of FBRR in 0.1 M TEABF₄/ACN. Store at 4°C when not in use.
- N₂ saturate FBRR/ TEABF₄/ACN prior to use.
- Electro-reduce FBRR onto CFEs (LSV x5, 0.40 to -0.80 V vs. SCE at 100 mV/s).
- Cycle modified CFEs in N₂ saturated PBS for 100 cycles to stabilise (-0.70 to 0.80 V vs. SCE at 100 mV/s).

It must be noted, at this stage, that many literature sources state that the important parameter when pre-treating electrodes is not the potential applied, but the current density passed during the process.^{9, 21} This was a limitation imposed on the work in this chapter, due to the potentiostat used not being designed for the high currents involved.

Section 6.2.3 of this thesis examined the suitability of FBRR/CFEs for use as real-time voltammetric pH sensors, capable of distinguishing pH values to within 0.01 units. The deposition parameters from Chapter 4 were adapted to include TEABF₄/ACN as the supporting electrolyte. The electrodeposition of the diazonium salt onto the substrate was confirmed by the 1 electron reduction wave, leading to a monolayer coverage, although this reduction was not always evident. The pH response was reported as -55 ± 0.7 mV/pH ($R^2 = 0.998$, $n = 4$), and in a real-time situation was recorded as -67 ± 6 mV/pH ($R^2 = 0.980$, $n = 4$). The stability of the modified electrodes was investigated over a period of 28 days, storing the sensors in either air or N₂. All resulting sensitivities, when compared pre and post storage, yielded no significant differences ($P > 0.05$). When monitoring pH in a real-time situation, the pH response was -67 ± 6 mV/pH. The reproducibility of the sensor became apparent, with large inter-electrode variability also an issue. The CFE sensor was not as reliable as its CPE counterpart.

Section 6.2.4 examined some factors that might affect the functionality of the developed FBRR/CFE pH sensor. The factors included ionic strength, which is a particular weakness with many optical based pH sensors. It was shown that in solutions with ionic strengths of 0.23, 0.46 and 0.92 M, the pH sensitivities of the sensors was exactly the same. However, the ionic strength of the solution contributed to a shift in the peak potential that was not evident for CPEs. Solution ionic strength was therefore a limitation in designing the pH sensor when using CFEs.

Also discussed were the effects of metal ions, which are prevalent in living tissue, on the FBRR/CFEs. The pH sensitivities, before and after treatment with Mg^{2+} and Ca^{2+} ions showed no significant differences, ($P = 0.8012$ and 0.7434 , respectively). Section 6.2.4.3 detailed the effect of using the sensor at the physiologically relevant temperature of $37^{\circ}C$. As the Nernst equation is temperature dependent, a change in the pH sensitivity was expected. However, when the theoretical value was compared to the obtained sensitivity, a significant difference was uncovered, ($P = 0.0208$). The use of a reference electrode suitable for the *in-vivo* environment, pseudo Ag/AgCl was examined and compared to the SCE used in all previous experiments. A shift in peak potential was observed, and the compared pH responses yielded no significant difference ($P > 0.05$). Finally, the effects of various chemical and pharmacological interferences on the sensor were examined. Similar to FBRR/CPEs in Sections 5.2.7 and 5.2.8, all the analytes tested revealed no significant differences between the pH sensitivities before and after treatment, ($P > 0.05$).

Finally, in Section 6.2.5, the biocompatibility of FBRR/CFEs was discussed. Because of reproducibility and reliability concerns, treatment in BSA, PEA, Triton[®]X and brain tissue was only reported over a 24 hour period. All treatments showed excellent results in the aforementioned media, the CVs before and after treatment remaining almost identical. This was as a result of the absence of silicone oil, which in CPEs, was withdrawn along with FBRR, resulting in increased capacitance and a loss of the FBRR redox peaks. Although the CFE sensors showed improved biocompatibility over CPEs, they were deemed not suitable for use as a voltammetric pH sensor, due to their large inter-electrode variability, the contribution of solution ionic strength to the location of the anodic peak potentials, and reproducibility problems.

6.4 References

1. P. Takmakov, M. K. Zachek, R. B. Keithley, E. S. Bucher, G. S. McCarty and R. M. Wightman, *Analytical Chemistry*, 2010, **82**, 9892-9900.
2. A. J. Downard, *Electroanalysis*, 2000, **12**, 1085-1096.
3. P. A. Brooksby and A. J. Downard, *Langmuir*, 2004, **20**, 5038-5045.
4. J. Pinson and F. Podvorica, *Chemical Society Reviews*, 2005, **34**, 429-439.
5. G. G. Wildgoose, M. Pandurangappa, N. S. Lawrence, L. Jiang, T. G. J. Jones and R. G. Compton, *Talanta*, 2003, **60**, 887-893.
6. H. C. Leventis, I. Streeter, G. G. Wildgoose, N. S. Lawrence, L. Jiang, T. G. J. Jones and R. G. Compton, *Talanta*, 2004, **63**, 1039-1051.
7. C. Batchelor-McAuley, B. R. Kozub, D. Menshkykau and R. G. Compton, *Journal of Physical Chemistry C*, 2011, **115**, 714-718.
8. H. Kahlert, *Journal of Solid State Electrochemistry*, 2008, **12**, 1255-1266.
9. J. P. Lowry and R. D. O'Neill, *Encyclopedia of Sensors*, 2006.
10. R. D. O'Neill, J. P. Lowry and M. Mas, *Critical Reviews in Neurobiology*, 1998, **12**, 69-127.
11. M. Armstrong-James and J. Millar, *Journal of Neuroscience Methods*, 1979, **1**, 279-287.
12. L. Agui, A. Guzman, P. Yanez-Sedeno and J. M. Pingarron, *Analytical Chimica Acta*, 2002, **461**, 65-73.
13. D. Budai, *Intelligent and Biosensors*, 2010.
14. Z. Bartosova, D. Riman, P. Jakubec, V. Halouzka, J. Hrbac and D. Jirovsky, *Science World Journal.*, 2012, 295802-295806.
15. M. L. Huffman and B. J. Venton, *Analyst*, 2009, **134**, 18-24.
16. L. Nemcova, H. Dejmekova, J. Barek and J. Zima, *International Journal of Electrochemical Science*, 2011, **6**, 6373-6384.
17. M. A. Dayton, J. C. Brown, K. J. Stutts and R. M. Wightman, *Analytical Chemistry*, 1980, **52**, 946-950.
18. M. A. Dayton, A. G. Ewing and R. M. Wightman, *Analytical Chemistry*, 1980, **52**, 2392-2396.
19. M. Delamar, G. Desarmot, O. Fagebaume, R. Hitmi, J. Pinson and J. M. Saveant, *Carbon*, 1997, **35**, 801-807.

20. N. S. Lawrence, M. Pagels, S. F. J. Hackett, S. McCormack, A. Meredith, T. G. J. Jones, G. G. Wildgoose, R. G. Compton and L. Jiang, *Electroanalysis*, 2007, **19**, 424-428.
21. A. L. Beilby, T. A. Sasaki and H. M. Stern, *Analytical Chemistry*, 1995, **67**, 976-980.
22. J. X. Feng, M. Brazell, K. Renner, R. Kasser and R. N. Adams, *Analytical Chemistry*, 1987, **59**, 1863-1867.
23. P. M. Kovach, M. R. Deakin and R. M. Wightman, *Journal of Physical Chemistry*, 1986, **90**, 4612-4617.
24. F. G. Gonon, C. M. Fombarlet, M. J. Buda and J. F. Pujol, *Analytical Chemistry*, 1981, **53**, 1386-1389.
25. C. D. Allred and R. L. McCreery, *Analytical Chemistry*, 1992, **64**, 444-448.
26. P. Surmann and B. Peter, *Electroanalysis*, 1996, **8**, 692-697.
27. L. Agui, D. Vega-Montenegro, P. Yanez-Sedeno and J. M. Pingarron, *Analytical and Bioanalytical Chemistry*, 2005, **382**, 381-387.
28. D. A. Kane and R. D. O'Neill, *Analyst*, 1998, **123**, 2899-2903.
29. M.-F. Suaud-Chagny, *Methods*, 2004, **33**, 322-329.
30. E. Desimoni, G. I. Casella, T. R. I. Cataldi, A. M. Salvi, T. Rotunno and E. Di Croce, *Surface and Interface Analysis*, 1992, **18**, 623-630.
31. A. H. Holm, K. H. Vase, B. Winther-Jensen, S. U. Pedersen and K. Daasbjerg, *Electrochimica Acta*, 2007, **53**, 1680-1688.
32. M. Janin, J. Ghilane, H. Randriamahazaka and J.-C. Lacroix, *Electrochemical Communications*, 2009, **11**, 647-650.
33. O. Korostynska, K. Arshak, E. Gill and A. Arshak, *IEEE Sensors Journal*, 2008, **8**, 20-28.
34. B. M. Weidgans, C. Krause, I. Klimant and O. S. Wolfbeis, *Analyst*, 2004, **129**, 645-650.
35. D. Veloso, R. W. Guynn, M. Oskarsson and R. L. Veech, *Journal of Biological Chemistry*, 1973, **248**, 4811-4819.
36. M. Walser, *Ergebnisse der Physiologie*, 1967, **59**, 185-296.
37. M. M. Dvorak, A. Siddiqua, D. T. Ward, D. H. Carter, S. L. Dallas, E. F. Nemeth and D. Riccardi, *Proceedings of the National Academy of Sciences of the United States of America* 2004, **101**, 5140-5145.

38. M. C. Mahedero, M. Roman Ceba and A. Fernandez-Gutierrez, *Analytical Letters*, 1986, **19**, 1725-1730.
39. D. Desmond, B. Lane, J. Alderman, J. D. Glennon, D. Diamond and D. W. M. Arrigan, *Sensors and Actuators, B*, 1997, **44**, 389-396.

Chapter 7

In-Vivo Characterisation of Carbon/FBRR pH Sensors

7.1 Introduction

In Chapters 4-6, the FBRR modification of CPEs and CFEs was optimised, resulting in sensors capable of measuring potential changes, attributed to pH changes, *in-vitro*. The final results chapter of this thesis evaluates the application of these sensors, under physiological conditions, and their ability to function as real-time, voltammetric, pH sensors *in-vivo*. Living muscle tissue was the chosen medium for all *in-vivo* experiments in this chapter.

Muscle pH monitoring has been shown to effectively correlate with decreased tissue perfusion,^{1, 2} and provides an earlier indication of possible tissue damage than monitoring blood pH.³ This is because blood contains a highly efficient buffering system and so could fail to reveal potential damage.

Although FBRR modified electrodes were extensively tested *in-vitro*, these results are not expected to be the same *in-vivo*. Living tissue provides an anatomically and chemically challenging environment that includes lipids, proteins and a wide variety of electrochemically active species, such as AA, UA and DA. The composition of tissue matrix leads to a highly resistive medium, that restricts mass transport to the electrode surface,⁴ as well as reacting to the physical implantation of a foreign object (sensor).⁵ Literature has shown that temperature influences the oxidation potential of several physiological interferences, including DOPAC and AA.⁶ Hence, the detailed characterisation of CFEs and CPEs carried out in the previous chapters may be insufficient to mimic the real-time *in-vivo* application of these sensors. As such, the modified CPEs and CFEs were implanted into the adductor femoris muscle in the hind limb of Wistar rats. Localised changes in pH were brought about by either a) inducing ischemia to reduce the pH or b) injection of bicarbonate ions to increase pH. After a short recording time period, the tissue pH was allowed to recover.

Reduced blood flow results in tissue ischemia, causing insufficient oxygen and nutritional requirements, starving the affected tissue of its metabolic needs. The efficient removal of waste products, H₂O, CO₂ and ions, is also reduced. The reduced oxygen supply to the tissue causes cell metabolism to change from aerobic to anaerobic,⁷ which results in the production of lactic acid.⁸ This, along with increased levels of CO₂, induces a decrease in pH levels.⁹ If the episode of ischemia is prolonged

the tissue will eventually die.⁸ Reperfusion is the re-establishment of blood flow to the affected tissue. The surgical procedure for induction of hind limb ischemia, commonly referred to as the hind limb ischemic model, proceeds as follows. Once the animal was sufficiently anaesthetised, the needle tip, containing the three electrodes, was inserted through the skin of an exposed area of the hind leg, deep enough to reach tissue. The needle tip was then retracted from the muscle, and the recording electrodes were left *in-situ*. A sterilised tourniquet was placed around the top of the animal's limb to allow for occlusion of the blood supply. To induce ischemia, the tourniquet was tightened around the upper leg for a 10 minute period, after which it was released to allow reperfusion of the muscle tissue.

The acid-base balance of tissue is tightly regulated. The main buffering ion, HCO_3^- , controls pH changes by interconversion with CO_2 in the reaction:¹⁰



The plasma bicarbonate concentration in humans is 24 mM.^{10, 11} An increase in pH can be brought about by simply adding a strong base to the system.¹² However, complications can arise due to the effect of the increase in CO_2 levels leading to acidosis.¹³ Therefore salts of weak bases should be used. Bicarbonate therapy is a known treatment administered to patients suffering from the effects of acidosis.¹³⁻¹⁶ Although an increase in CO_2 levels is still possible, these effects are reduced by efficient exhalation, i.e., where there is no respiratory distress displayed.¹³ In order to induce an increase in pH levels, in the following *in-vivo* study, injections of sodium bicarbonate,^{13, 17, 18} a weak base, were administered locally to the hind limb of the animals.

7.2 Results and Discussion

In this section, the *in-vivo* testing of FBRR/CFEs and FBRR/CPEs, for use as real-time voltammetric pH sensors, was performed. FBRR was electrodeposited onto the pre-treated CFEs by LSV using the deposition parameters optimised in Section 6.3, whereas CPEs were modified with FBRR according to the protocol set out in Section 4.3. The modified electrodes were calibrated by cycling in PBS solutions with pH

values of 7.2, 7.4 and 7.6 for 100 cycles each. The electrodes were then surgically implanted into the hind limbs of Wistar rats, using a three electrode set-up, including a pseudo Ag/AgCl reference electrode and a bare silver wire as the auxiliary electrode (see Section 5.2.12). CVs were recorded from -0.80 to 0.70 V vs. Ag/AgCl at 100 mV/s, for 90 cycles, (45 minutes), to ensure the electrodes had settled. A local increase or decrease in pH was then induced for 10 minutes, after which the treatment was removed and the CV recordings were continued for a further 45 minutes, to see if the pH returned to the pre-treatment level. The animal remained under anaesthesia throughout the experiment.

7.2.1 FBRR Modified CFEs

CFE microelectrodes are mainly used *in-vivo* as neurochemical sensors,^{19, 20} and have many advantages for use in biological applications. These include their biocompatibility, good electrochemical properties, low cost, ease of modification and small size which leads to less tissue damage upon implantation. In this section, their suitability as functioning pH sensors was examined, by monitoring the shift in the peak potential, as ischemia was induced in an animal, causing a decrease in the pH.

7.2.1.1 Effect of Lowering Tissue pH

In order to examine the suitability of FBRR/CFEs to function as real-time voltammetric pH sensors, the fibres were pre-treated and modified as described in Section 6.5, before being calibrated in PBS solutions of pH 7.2, 7.4 and 7.6. The order of solution pH was randomly selected to remove any hysteresis effects. The pH sensitivity of the electrodes is shown in Figure 7.1, with the corresponding linear regression data in Table 7.1. These show a response of -56.25 ± 2 mV/pH, ($R^2 = 0.9985$, $n = 5$). As in the results found throughout Chapter 6, a large inter-electrode variability of FBRR/CFEs was again evident by the size of the error bars.

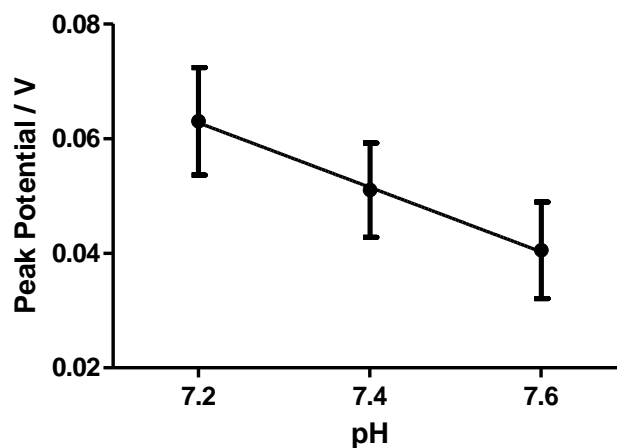


Figure 7.1: pH sensitivities for the calibration of FBRR/CFEs prior to *in-vivo* testing, $n = 5$.

Table 7.1: Linear regression data for FBRR/CFE calibrations.

	Slope (mV/pH)	SEM	n	R^2
Calibrate	-56.25	2.17	5	0.9985

The modified CFEs, $n = 5$, were then inserted into the hind limb of the animals, $n = 3$, under anaesthesia, along with the pseudo reference and auxiliary electrodes, according to the hind limb ischemia model described in Section 7.1. Although the diameter of the working electrode was $7 \mu\text{m}$, the glass capillary surrounding it had a diameter of 1.5 mm. Because of this, the working electrode was inserted into the muscle tissue using a 14 gauge needle, (inner $\text{Ø} = 1.60 \text{ mm}$) and the reference and auxiliary electrodes were inserted separately, using an 18 gauge needle, (inner $\text{Ø} = 0.84 \text{ mm}$), as close in proximity to the CFE as possible. Recording lasted for 200 cycles, (equivalent to 100 minutes), as follows:

Cycles 1-90: Electrode settling period.

Cycles 91-110: Induction of ischemia/ tourniquet applied.

Cycles 111-200: Treatment reversed/tourniquet released.

A selection of the resulting CVs is shown in Figure 7.2, demonstrating how inconsistently the sensors behaved, with the output currents continuously surging and

dropping. This was attributed to the distance between the fibres and the reference/auxiliary electrodes, and that they were inserted through separate needles. Muscle tissue is a highly resistive medium, restricting mass transport to the electrode surface,⁵ and any movement of the electrodes could cause an increase in the distance between the working electrode and the reference/auxiliary electrodes, meaning a larger resistance, resulting in a corresponding decrease in the current output. If the electrodes were inserted together in one needle, any movement would more likely move all three electrodes in unison, (see Section 7.2.2). Movement of the reference/auxiliary electrodes may cause them to touch the glass capillary surrounding the fibre, affecting the resulting currents. The fragility of carbon fibres can also make them unsuitable for the application of muscle tissue pH sensors, as any movement, particularly that resulting from the application or removal of the tourniquet, can cause the small fibre to break. The heterogeneity of tissues makes it necessary to specify the exact anatomical location²¹ and orientation²² of microelectrodes, however, due to the location of electrodes through separate sites, this could not be guaranteed.²³

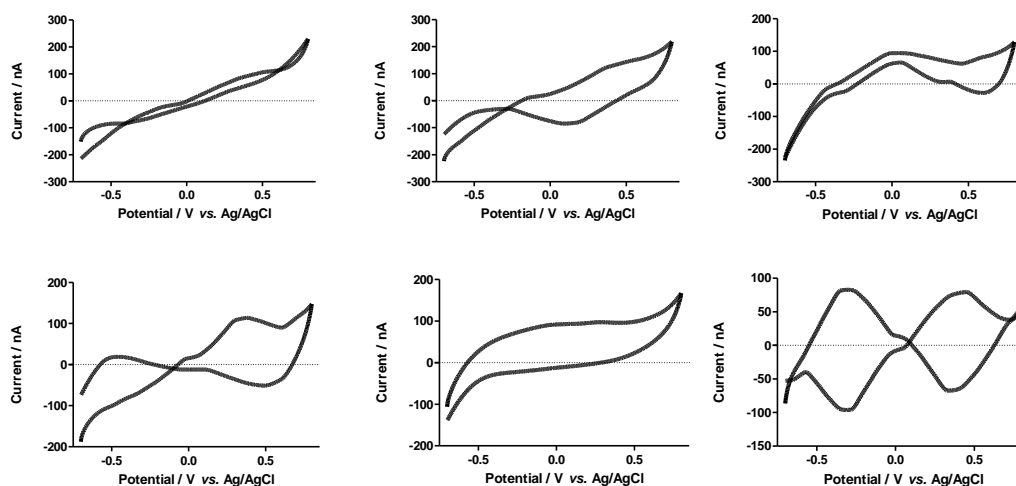


Figure 7.2: CVs showing the instability of FBRR/CFEs implanted in muscle tissue.

The post-surgical electrodes were then recycled in PBS, *in-vitro*, to evaluate whether they were still functioning. As Figure 7.3 demonstrates, the post-surgery electrodes

exhibited similar CVs to those of bare electrodes, resulting from the possible fracture of the fibres, this was confirmed by examination under a light microscope.

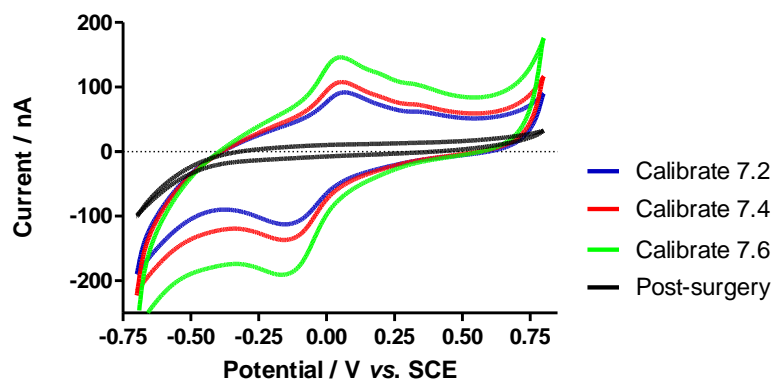


Figure 7.3: CVs, calibration and post-surgery, of FBRR/CFEs indicating the fracture of the fibre.

7.2.2 FBRR Modified CPEs

CPEs have been well documented for *in-vivo* applications.^{22, 24, 25} The leeching of pasting oil from their surface, when in contact with proteins and lipids, leads to their long term stability during *in-vivo* monitoring techniques.^{4, 26} Their application as real-time pH sensors, in muscle tissue, is discussed in this section. Perturbations in pH were incurred through the hind limb ischemia model leading to a drop in pH, or injection of NaHCO_3 to inflict a rise in pH.

7.2.2.1 Effect of Lowering Tissue pH

In order to examine the suitability of FBRR/CPEs for use as real-time voltammetric pH sensors, the electrodes were modified as described in Section 4.4, and subsequently calibrated in PBS solutions of pH 7.2, 7.4 and 7.6. The order of solution pH was randomly selected to remove any hysteresis effects. The linear regression data obtained are shown in Table 7.2. These show a response of -57.00 ± 2 mV/pH, ($R^2 = 0.9991$, $n = 5$). When compared to the corresponding results for CFEs in Figure 7.1, the error bars for FBRR/CPEs show a far improved inter-electrode variability, see Figure 7.4.

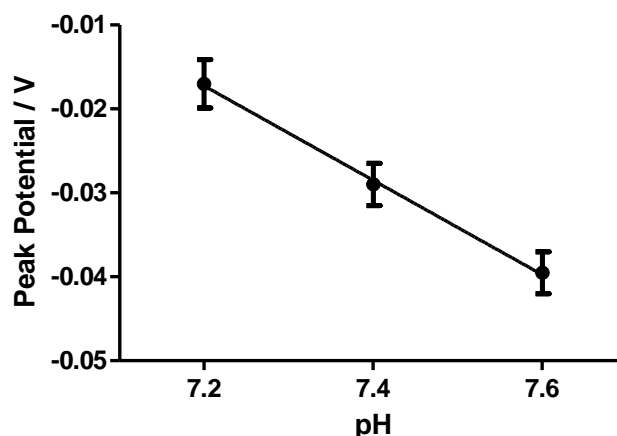


Figure 7.4: pH sensitivities for the calibration of FBRR/CPEs prior to *in-vivo* testing, $n = 5$.

Table 7.2: Linear regression data for FBRR/CPE calibrations.

	Slope (mV/pH)	SEM	n	R^2
Calibrate	-57.00	1.73	5	0.9991

The modified CPE sensors, $n = 4$, were then inserted into the hind limb muscle of anaesthetised animals, along with an Ag/AgCl pseudo reference electrode and a silver wire auxiliary electrode. All three electrodes were inserted together, within an 18 gauge needle, (inner $\varnothing = 0.84\text{mm}$). Recording lasted for 200 cycles, (equivalent to 100 minutes), from -0.80 V to 0.70 V vs. Ag/AgCl at 100 mV/s as follows:

Cycles 1-90: Electrode settling period, see Figure 7.5(B).

Cycles 91-110: Induction of ischemia/ tourniquet applied, see Figure 7.5(C).

Cycles 111-200: Treatment reversed/tourniquet released, see Figure 7.5(D).

The selected partial CVs in Figure 7.5 show that the oxidation peaks were well defined. Figure 7.5(A) shows a selection from all stages of the experiment. The 90th cycle, recorded at the end of the settling phase, had its peak potential located at *ca.* -0.070 V vs. Ag/AgCl. Tissue oxygenation is dependent on a constant supply of oxygen and blood circulation carries oxygen to tissues.²⁷ Reduction in oxygen levels leads to a

decrease in tissue pH.²⁸ This was clearly shown by the shift in the anodic peak potential for the recordings, taken 10 and 20 cycles, after the tourniquet was applied, exhibiting a shift in the potential to -0.015 V and 0.00 V vs. Ag/AgCl, respectively. This shift in potential, which likely corresponds to a change in pH, due to the onset of ischemia, highlights the effectiveness of tissue pH monitoring.⁸ This was further corroborated by Takano et al, who demonstrated that monitoring muscle pH, gives an earlier indication of blood flow decrease, than if monitoring blood pH.³ Figure 7.5(A) shows recordings that were made during the recovery period, 50 and 90 cycles after the tourniquet was removed. These show a reverse shift in the peak potential, to -0.02 V and -0.05 V vs. Ag/AgCl, respectively. It was noted that the peak potentials did not return to their original level, in the time allowed for recovery, however, homeostatic levels would have returned soon after.

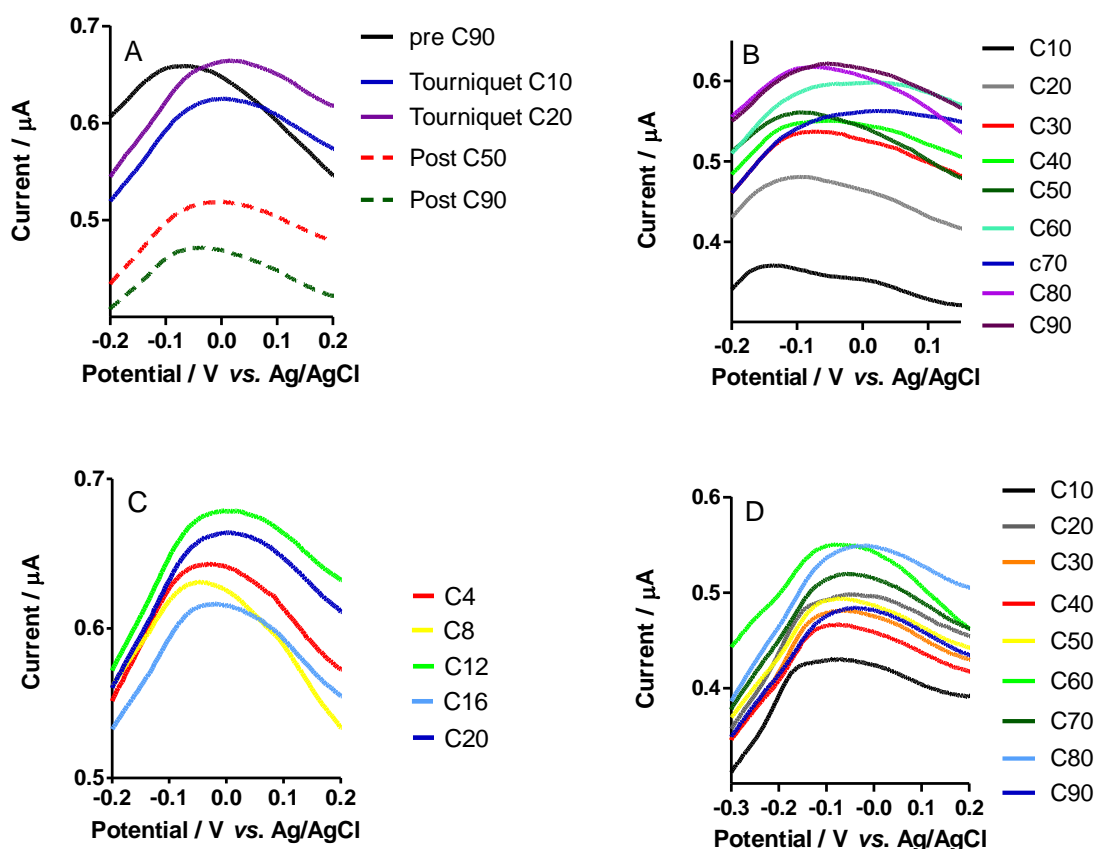


Figure 7.5: Section of oxidation peaks from CVs recorded (A) before during and after the ischemic event, and separately, (B) before ischemia was induced, (C) during the ischemic event and (D) the recovery period, $n = 4$.

Figure 7.5(B) shows the settling period of the electrodes, every 10th cycle, prior to the onset of ischemia. Just like the corresponding *in-vitro* characterisation, see Section 4.2.3.11, they required several cycles to obtain consistent peak potential values, although, as expected, *in-vivo* settling was not as clearly defined as its *in-vitro* counterpart. Figure 7.5(C) shows every 4th cycle during the ischemic episode, with a gradual shift to a more positive potential over time, possibly indicating a decrease in pH, and Figure 7.5(D) shows a gradual shift towards a more negative potential once the tourniquet had been released, indicating a likely increase in pH. This change in potential, and therefore possibly pH, occurred during ischemia, probably due to increased levels of lactate in the tissue, which was gradually decreased upon reperfusion.⁸ These CVs show that the FBRR/CPE sensors have clearly monitored the change in potential, which most likely corresponds to pH, during the onset of ischemia in muscle tissue, and the eventual return towards pre-insult potential levels. During reperfusion, ischemia may not be reversed to the effected tissue immediately. Blood may flow quickly to some areas, releasing oxygen, whereas other areas may be slowly perfused, leaving them hypoxic for several minutes.²⁹ This effect is more pronounced after longer spells of ischemia.⁸

Unlike FBRR/CFEs *in-vivo*, see Section 7.2.1.1, the CPEs displayed consistent CVs. This was likely because the three electrodes were all inserted into the tissue through one needle, maintaining them in the same plane, and hence, they were more likely to record from similar layers of tissue. Movement of the muscle, especially during the application and removal of the tourniquet, had a minimal effect on the currents, as the three electrodes were likely to move in unison, maintaining a constant distance between the working, reference and auxiliary electrodes.

Figure 7.6(A) shows how the peak potential changed over the duration of the 200 cycles, (100 minutes), of the experiment, with Figure 7.6(B) showing the inset area where the tourniquet was applied, inducing ischemia. The significant potential increase, from pre-insult levels of *ca.* -0.052 V to -0.017 V vs. Ag/AgCl, ($P < 0.0001$) was clearly evident immediately after the tourniquet was applied. These electrodes were calibrated as having a pH sensitivity of -57 ± 2 mV/pH, (see Table 7.2). Using these values, a proposed pH shift of *ca.* 0.65 pH units resulted from the ischemic

episode, causing in a drop to pH 6.75, assuming a pre-ischemia pH value of 7.4. This decrease is consistent with literature values reporting a pH drop of 0.70 pH units after 60 minutes.³⁰ During ischemia, tissue pH can drop to as low as 6.0 – 6.5 *in-vivo*.³¹ Post-ischemic tissue was shown to return to a pH value of 7.25, indicated by a potential shift from -0.015 V to -0.044 V *vs.* Ag/AgCl ($P = 0.0926$), not quite making a full recovery to the pre-ischemic value, in the allocated recording time.

As temperature causes a shift in pH, and therefore a potential shift, part of the observed potential should be attributed to temperature. However, the Rosenthal correction factor allows for a shift of 0.015 pH units per °C. As the pH shift in Figure 7.6 was estimated at 0.65 pH units (a temperature change of 43.3°C), a substantial proportion of the shift obtained can be attributed to pH.

During ischemia anaerobic metabolism ensues as there is insufficient oxygen to carry out aerobic processes for ATP generation. During anaerobic metabolism energy is produced at a lower rate than it is consumed resulting in a decrease in ATP levels and decreased heat generation within the tissue. Because of reduced perfusion levels and decrease in metabolic heat generation, tissue temperatures can be lower than the surrounding tissue.³² However, infection can result in a localised increase in temperature at the wound/injection site. Changes of up to 4°C have been reported between periwound skin temperature and local wound infection temperature.³³ As the highlighted area in Figure 7.6(A) indicates a potential change of 0.0316 V *vs.* Ag/AgCl, a temperature change of *ca.* 4°C would account for 0.060 pH units. This is equivalent to 0.0035 V (using the calibration response of -57 mV/pH). The estimated potential change is then 0.028 V *vs.* Ag/AgCl, which equates to 0.49 pH units, a substantial pH shift in biological terms. Figure 7.4 indicates an error of *ca.* 0.006 V *vs.* SCE for the calibration potentials observed, resulting in a potential shift of 0.028 ± 0.006 V, equivalent to a pH change of 0.49 ± 0.10 .

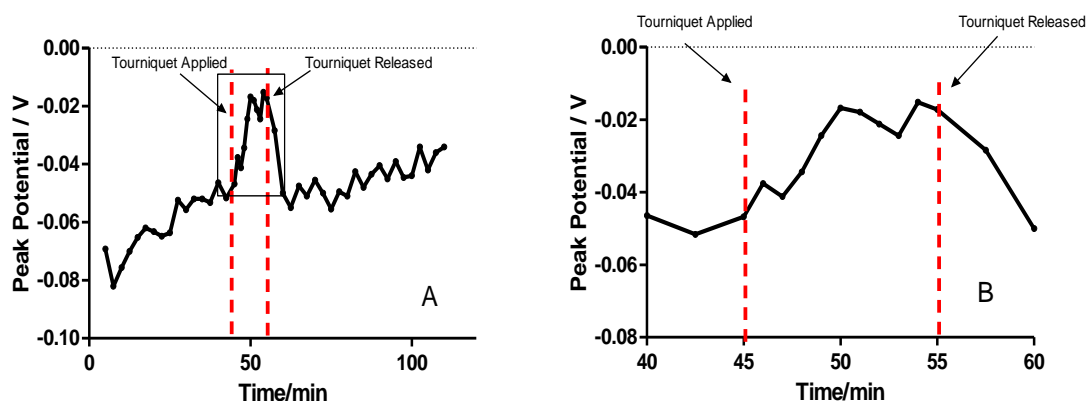


Figure 7.6: (A) Plot of the change in peak potential with time, pre-, during and post-ischemia, for *in-vivo* recordings using FBRR/CPEs, (B) Close up showing the ischemic event, $n = 4$.

The post-surgical FBRR/CPEs were removed and rinsed with water. They were subsequently cycled under the *in-vitro* calibration conditions. Figure 7.7(A) shows the resulting CVs along with the calibration CVs at pH 7.2, 7.4 and 7.6. The increase in currents obtained when cycling the modified CPEs *in-vivo* is evident, possibly due to electrode fouling by the tissue matrix, affecting mass transport at the electrode surface, and the more resistive nature of the tissue. When compared to FBRR/CPEs stored in homogenised brain tissue, (see Section 5.2.3.4), the currents obtained *in-vivo* were similar to those obtained after 1 day *ex-vivo*. The peak potentials also shifted to a more positive potential when cycling *in-vivo*, similar to *ex-vivo*, indicating that the surface fouling caused the oxidation of FBRR to be less thermodynamically stable.³⁴ Figures 7.7(B) and (C) show the isolated oxidation peaks for the calibration and post-surgery, respectively. The potential, x-axis, scales show identical ranges, to emphasise the difference in peak widths pre- and post-surgery, due to electrode fouling in the tissue matrix. However, these peaks were still clearly defined and information on the location of the peak potentials could be extrapolated. The pH sensitivities are shown in Figure 7.8, with the corresponding linear regression data in Table 7.3. Pre- and post-surgery electrodes had sensitivities of -57 ± 1.7 and -60 ± 0.7 mV/pH, respectively. These differences were deemed insignificant when compared using unpaired t-tests ($P = 0.1610$). The inter-electrode variability remained similar to pre-surgery levels, demonstrated by the comparable size of the error bars.

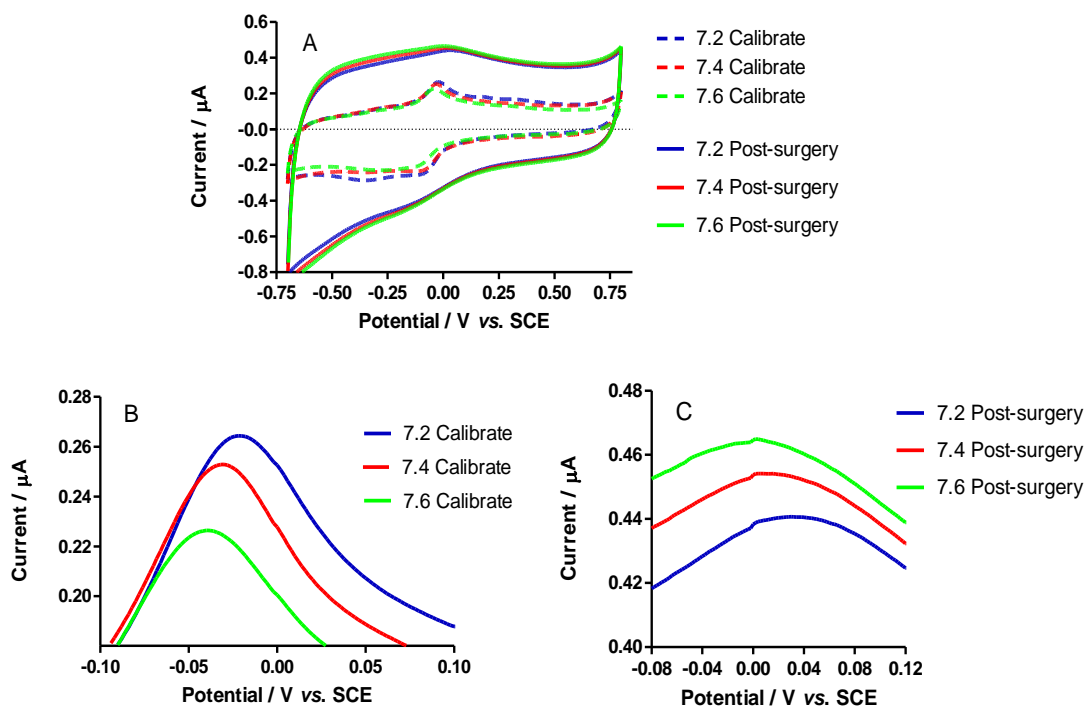


Figure 7.7: (A) Calibration and post-surgery CVs, *in-vitro*, of FBRR/CPEs, with the anodic peaks of the calibration (B), $n = 5$, and post-surgery (C), $n = 4$.

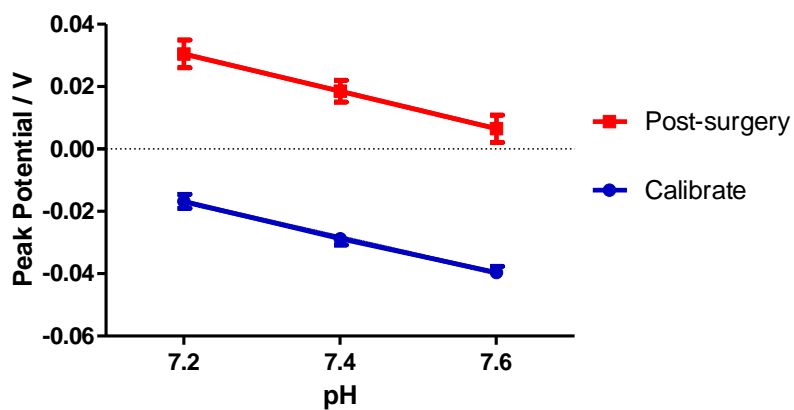


Figure 7.8: Linear regressions of the pH sensitivities of FBRR/CPEs pre- and post-surgery.

Several factors may be involved in the anodic peak potential shift between *in-vitro* and *in-vivo* conditions. One, was the effect of the reference electrode on the peak potentials

obtained. The calibration CVs, at pH 7.4, located the peaks at *ca.* -0.030 V *vs.* SCE, while the *in-vivo* potential, at an assumed pH of 7.4, was -0.070 V *vs.* Ag/AgCl, a difference of *ca.* -40 mV, close to the literature value of -44 mV,³⁵ (see Section 5.2.12). The increased temperature, *in-vivo*, could also cause the peaks to locate to a more negative potential, by *ca.* -18 mV *vs.* SCE, (see Section 5.2.11). However, it was demonstrated in Section 5.2.3.4, that electrode fouling caused the oxidation peaks to relocate to a more positive potential.

Table 7.3: Linear regression data for FBRR/CPEs pre- and post-surgery.

	Slope (mV/pH)	<i>n</i>	R ²	<i>P</i> -value
Calibrate	-57.00 ± 1.7	5	0.9991	0.1610
Post-surgery	-60.00 ± 0.7	4	0.9999	

7.2.2.2 Oxygen and pH

Oxygen is an essential element for sustaining most living organisms. As it is distributed by the vascular system, reduced oxygen levels in tissue can arise from conditions involving defective vasculature. These conditions include ischemic disorders, diabetes and cancer.³⁶ It is well documented that tissue ischemia occurs when blood flow is restricted, resulting in inadequate oxygen supply to the affected region.^{9, 37, 38} This results in a rise in lactic acid⁸ concentrations along with CO₂.³⁹ A relationship has been established between the tissue oxygen supply and the production of the oxidative metabolite, CO₂, which directly affects the pH.^{39, 40}

To further reinforce the data in Section 7.2.2.1, where tissue ischemia resulted in a potential shift, indicating a probable pH change, the change in potential was plotted as a percentage change against time. This was then overlaid on data, acquired within the research group, of the percentage change in oxygen incurred during an ischemic event, see Figure 7.9. The oxygen data was acquired using CPA, this accounted for the smoother response, as more data points were collected, whereas, CV gave a data point, for the anodic peak potential, every 30 s. The oxygen data was for 12 sensors from 6 animals, (courtesy of Dr. Niall Finnerty), while the potential data was for 4 sensors from 4 animals.

Figure 7.9 shows how the % change in potential closely follows the trend for % oxygen. This result endorsed the successful functioning of FBRR/CPE pH sensors and showed that monitoring tissue pH may be used as a reliable indicator of the onset of tissue ischemia, or other conditions caused by reduced oxygen levels, e.g., cancer. Similar trends were also found by Troitzsch et al,³⁰ where comparisons were made between PO₂, (partial pressure of oxygen), and pH.

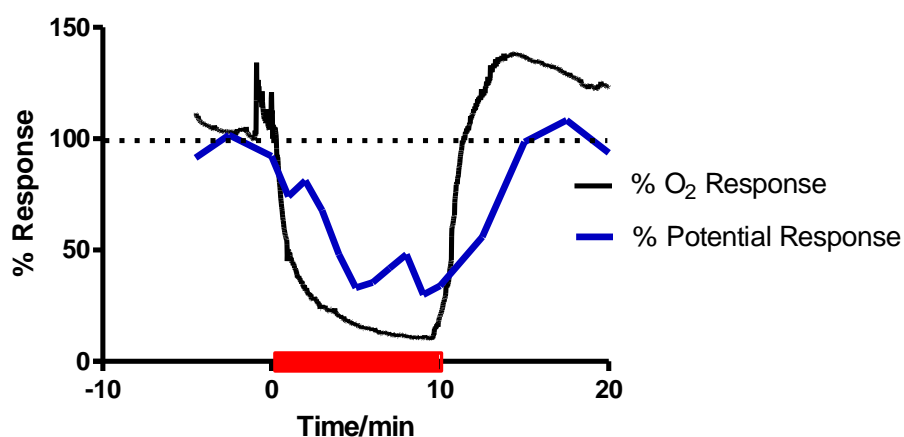


Figure 7.9: Comparison plot of the percentage change in oxygen, and therefore pH, ($n = 12$ sensors from 6 animals) and peak potential/pH, ($n = 4$ sensors from 4 animals), during tissue ischemia.

7.2.2.3 Effect of Increasing Tissue pH

Section 7.2.2.2 demonstrated that the FBRR/CPE pH sensors successfully monitored a potential change which can possibly be attributed to a decrease in tissue pH, caused by the withdrawal of oxygen, with the subsequent partial recovery of the affected tissue. In order to further assess the suitability of the FBRR/CPEs as functioning real-time pH sensors, they were tested, *in-vivo*, while inducing a pH increase. This was implemented by local injection of NaHCO₃. Literature values use between 32 mM⁴¹ and 100 mM¹⁰ solutions of bicarbonate, for the treatment of acidosis. In this section, the concentration used was 45 mM NaHCO₃.^{14, 15}

The CPEs were modified as described in Section 4.3, and then calibrated in PBS solutions of pH 7.2, 7.4 and 7.6. The order of solution pH was randomly selected to

remove any hysteresis effects. The linear regression data obtained are shown in Table 7.4. These show a response of -58.75 ± 4 mV/pH, ($R^2 = 0.9962$, $n = 4$).

The modified CPE sensors. $n = 4$, were then inserted into the hind limb muscle of anaesthetised animals, along with an Ag/AgCl pseudo reference electrode and a silver wire auxiliary electrode. All three electrodes were inserted together, within an 18 gauge needle, (inner $\varnothing = 0.84$ mm). Recording lasted for 200 cycles, (equivalent to 100 minutes), from -0.80 V to 0.70 V vs. Ag/AgCl at 100 mV/s as follows:

Cycles 1-89: Electrode settling period.

Cycles 90: 1st 45 mM NaHCO_3 injection (0.1 ml).

Cycles 100: 2nd 45 mM NaHCO_3 injection (0.1 ml).

Cycles 110: 3rd 45 mM NaHCO_3 injection (0.1 ml).

Cycles 120-200: Tissue recovery.

Table 7.4: Linear regression data for FBRR/CPE calibrations.

	Slope (mV/pH)	SEM	n	R^2
Calibrate	-58.75	4	4	0.9962

The selected partial CVs, in Figure 7.10, show that the oxidation peaks were well defined. Figure 7.10 (A) shows a selection from all stages of the experiment. The 90th cycle, recorded at the end of the settling phase, had its peak potential located at *ca.* -0.074 V vs. Ag/AgCl. The peaks obtained 5 cycles after each of the injections, are also displayed in Figure 7.10 (A) and separately in Figure 7.10 (B). These show a shift to a more negative potential, from *ca.* -0.076 V to -0.094 V vs. Ag/AgCl, inferring an increase in pH. Also shown in Figure 7.10 (A) are the anodic peaks obtained after 50 and 90 cycles of tissue recovery, located at *ca.* -0.072 V and -0.068 V vs. Ag/AgCl, respectively. These results clearly demonstrate the functioning of FBRR/CPEs as successfully monitoring potential changes possibly indicating a pH shift, following an initial increase in potential after injection of NaHCO_3 and the partial recovery thereafter. Analyses of these peak potential shifts are shown in Table 7.5. They show

that the shift in the peak potential did not become significant until after the third injection of NaHCO_3 , ($P = 0.0438$) and had recovered to non-significant levels by the 50th cycle of recovery, ($P = 0.8570$).

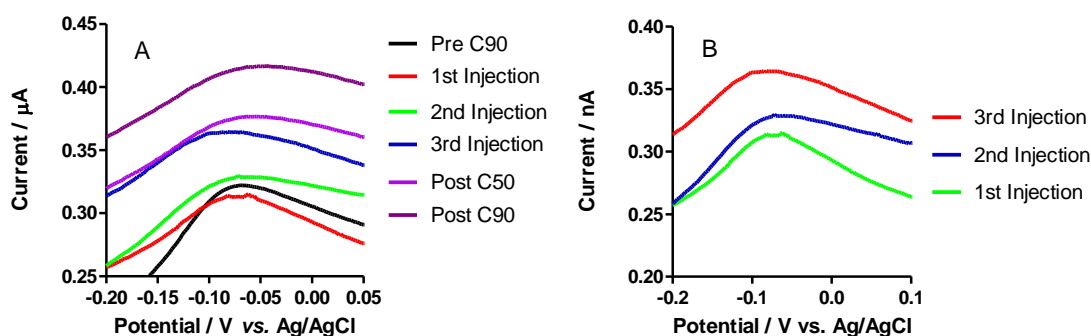


Figure 7.10: (A) Anodic peaks recorded over the course of an *in-vivo* experiment to increase local tissue pH, and (B) the anodic peaks obtained 5 cycles after each injection of 45 mM NaHCO_3 , $n = 4$.

Table 7.5: Statistical analyses of the potential shift achieved 5 cycles after injecting 45 mM NaHCO_3 into muscle tissue *in-vivo*.

	Peak Potential V vs. Ag/AgCl	SEM	n	P -value vs. Pre C90
Pre C90	-0.074	0.007	4	NA
Injection 1	-0.076	0.002	4	0.7927
Injection 2	-0.076	0.003	4	0.8016
Injection 3	-0.092	0.001	4	0.0438
Post C50	-0.072	0.008	4	0.8570
Post C90	-0.068	0.001	4	0.4287

Figure 7.11(A) shows how the peak potential changed over the duration of the 200 cycles of the experiment (100 minutes), with Figure 7.11 (B) showing the inset area where the injections were administered, causing a decrease in the peak potential, probably corresponding to a pH increase. It was noticeable that, immediately after the 1st and 2nd injections, there was an unexpected increase in the peak potential, which was interpreted as injection stress. Contrary to the information displayed in the CVs in

Figure 7.10, a larger drop in anodic peak potential was recorded between the 2nd and third injection, at -0.094 V vs. Ag/AgCl, although this was still not significant, ($P = 0.1338$), and a further drop after the 3rd injection was recorded at -0.110 V vs. Ag/AgCl, ($P = 0.0030$). This showed that it took time for the NaHCO₃ to take effect. The 1st injection showed no response within the 5 minute period between injections, the 2nd caused a drop to a minimum value 3 minutes after injection, before levelling off. The third injection gave an immediate response, possibly masking the injection stress, in this case. The maximum decrease was observed 2 minutes after the 3rd injection, followed by the immediate onset of recovery.

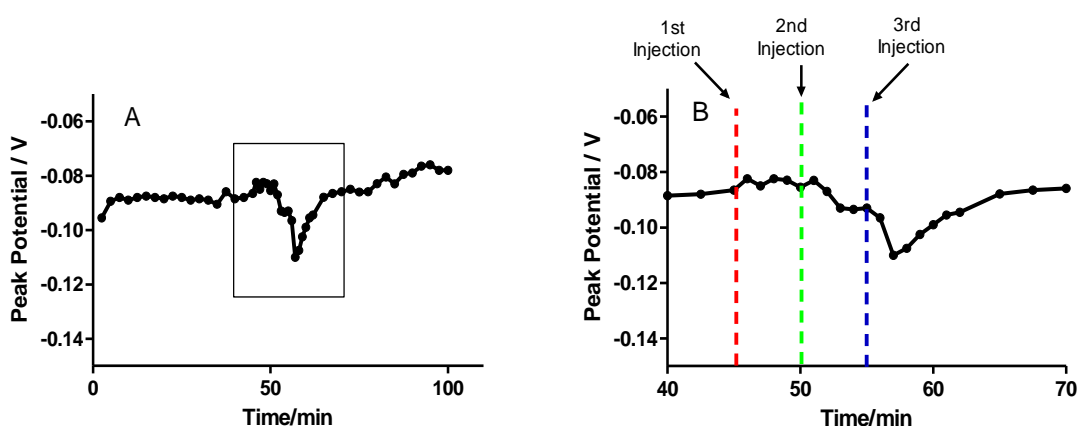


Figure 7.11: (A) Plot of the change in peak potential with time, pre-, during and post- NaHCO₃ injections, for *in-vivo* recording using FBRR/CPEs, (B) Close up showing the effect of the three NaHCO₃ injections, $n = 4$.

The FBRR/CPEs used in this section were calibrated with a pH response of -58.75 ± 4 mV/pH. Assuming a baseline pH of 7.4, the drop in peak potential, from -0.074 V to a minimum -0.110 V vs. Ag/AgCl, corresponded to a pH rise of 0.61 to 8.01 units, resulting in severe alkalemia¹¹ or alkalosis. As discussed in Section 7.2.2.1, some of this shift may be due to a change in temperature, but increasing temperature causes a positive shift in pH, so only decreasing temperature could detract from the shift in potential observed here. Any infection caused by the insertion of the device would result in a local increase in temperature. Also the potential shift here was estimated at 0.61 V vs. Ag/AgCl, corresponding to a temperature change of 40.6°C . Therefore a

substantial proportion of the potential shift can most likely be attributed to a pH change.

The post-surgical FBRR/CPEs were removed and rinsed with water. They were subsequently cycled under the *in-vitro* calibration conditions. Figure 7.12(A) shows the resulting CVs, along with the calibration CVs, at pH 7.2, 7.4 and 7.6. The increase in currents obtained when cycling the modified CPEs *in-vivo* was evident, possibly due to electrode fouling by the tissue matrix, affecting mass transport at the electrode surface and the more resistive nature of the tissue. Figures 7.12(B) and (C) show the anodic peaks of the calibration and post-surgery CVs, respectively. The calibration peaks were more clearly defined, whereas, the post-surgery peaks were broadened, indicative of the slower electron transfer, due to surface fouling by the tissue matrix. It was also apparent that there was a shift in the potentials, post-surgery, to a more positive value as the exposure to physiological conditions caused the oxidation of FBRR to be less thermodynamically stable.¹³

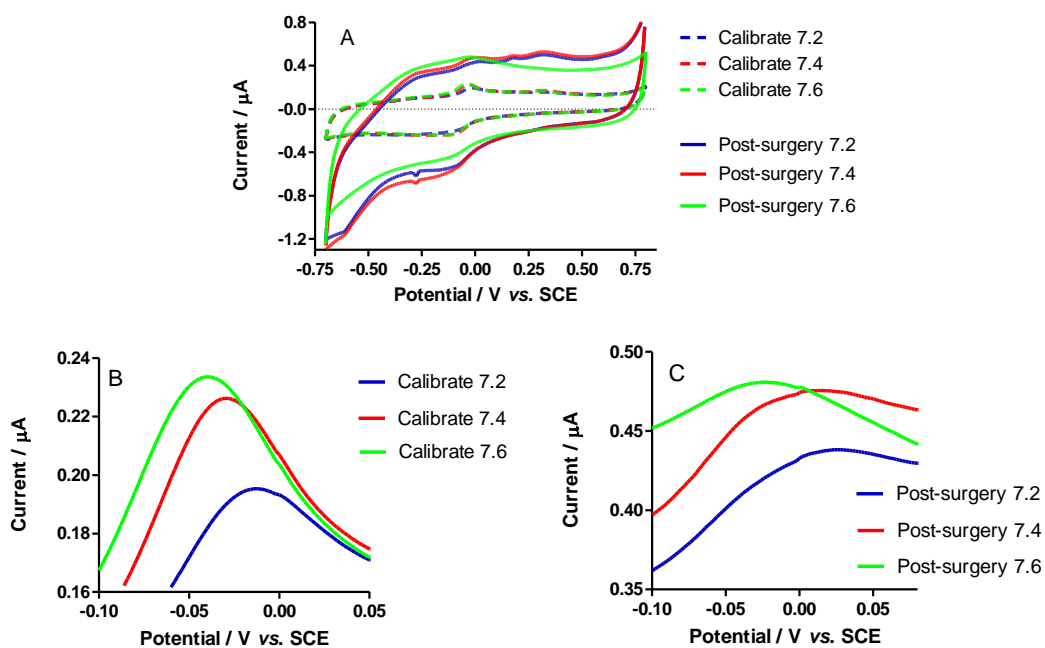


Figure 7.12: (A) Calibration and post-surgery CVs, *in-vitro*, of FBRR/CPEs, with the anodic peaks of the calibration (B), and post-surgery (C), $n = 4$.

The pH sensitivities of FBRR/CPEs pre- and post-surgery are shown in Figure 7.13, with the corresponding statistical analyses in Table 7.6. They show a non-significant change in the sensitivities from -58.75 ± 4 to -50.00 ± 10 mV/pH, respectively, ($P = 0.3811$). The small error bars achieved here, are indicative of the low inter-electrode variability obtained throughout this thesis when using FBRR/CPEs.

Table 7.6: Comparison of the pH sensitivities of FBRR/CPEs, pre- and post-surgery, $n = 4$.

	Slope (mV/pH)	n	R^2	P -value
Calibrate	-58.75 ± 4	4	0.9962	0.3811
Post-surgery	-50.00 ± 10	4	0.9643	

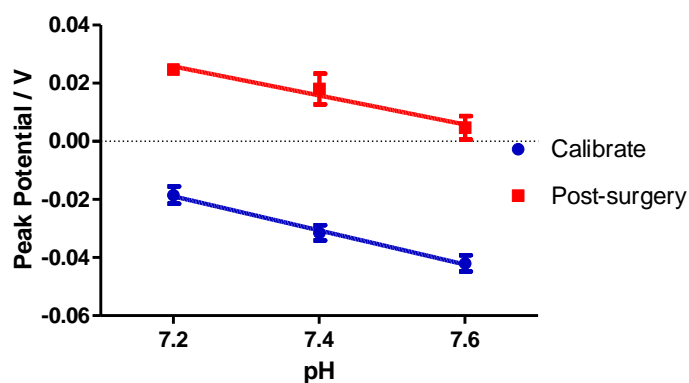


Figure 7.13: Linear regressions comparing the pH responses of FBRR/CPEs, pre- and post-surgery, $n = 4$.

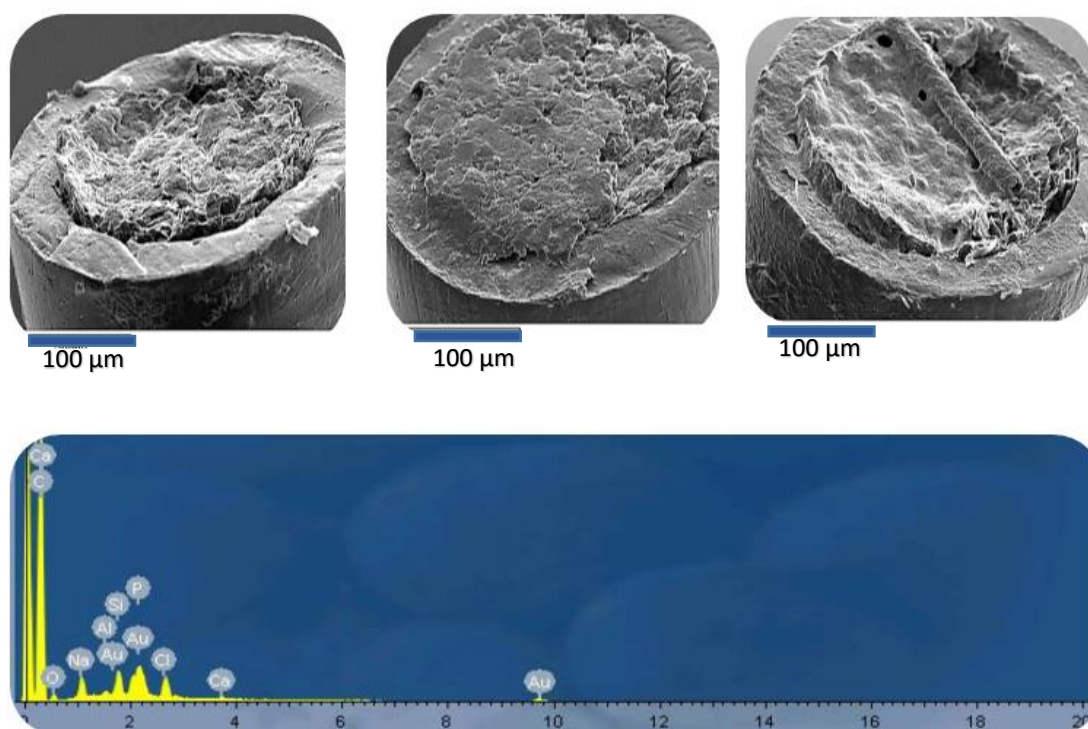


Figure 7.14: SEM micrographs and EDX recorded for FBRR/CPEs after implantation into muscle tissue *in-vivo*.

Figure 7.14 shows a selection of SEM micrographs of FBRR/CPEs post-surgery, along with a typical EDX. The surface morphology, after implantation in the tissue, appears similar to those in Figure 5.30, after storage in homogenised brain tissue. The surface oil has been drawn out pulling the paste away from the Teflon[®] insulation, leaving a more powder-like carbon surface. CPEs have been found to be stable *in-vivo* for several months,²² due to the interaction between the pasting oil and lipids, restricting electrode fouling caused by proteins.⁴ There was also evidence that the carbon paste may have been pulled outwards from the Teflon[®] insulation during the removal of the electrode, along with some muscle tissue.

7.3 Conclusion

Chapter 7 of this thesis discussed the *in-vivo* application of FBRR modified carbon sensors, under physiological conditions, and their ability to function as real-time, voltammetric, pH sensors. Section 7.2.1 considered CFEs, and found that although the *in-vitro* calibration resulted in near Nernstian sensitivities, once the electrodes were surgically inserted the ensuing CVs were erratic, and no recordable data was obtained. This was because, although the fibre diameter was 7 μm , the glass capillary surrounding them had a diameter of 1.5 mm. This necessitated their implantation, into the tissue, through a large bore needle, and the reference/auxiliary electrode bundle was inserted separately. The distance between the working electrode and the reference/auxiliary electrodes varied with movement of the muscle, resulting in sudden increases and decreases in the current output, as the tissue matrix provides a highly resistive medium. Any increases in resistance, restricted the mass transport to the electrode surface, causing lower currents. On examination of the electrodes post-surgery, they were found to have broken at some stage during the procedure. It was concluded that FBRR/CFEs were unsuitable for use in muscle tissue under the surgical protocol that was licensed to the research team. As such, no further *in-vivo* testing of FBRR/CFEs was carried out.

Section 7.2.2, discussed the performance of FBRR/CPEs during *in-vivo* testing. A decrease in tissue pH was induced by the onset of ischemia, caused by the application of a tourniquet to the hind limb of the animal, cutting off the oxygen supply. Consistent CVs were obtained as all three electrodes were inserted within the same introduction needle, reducing the distance between them, and the effect of movement, keeping the current output stable. Upon ischemia, a significant shift in potential to a more positive value, i.e., lower pH, was observed, ($P < 0.0001$), which did not fully recover when the tourniquet was released. Although the local muscle temperature was not monitored during the surgery, only a small fraction of the potential shift can be attributed to a temperature change. Following on from the *in-vitro* studies carried out throughout this thesis, the change in potential is most like caused by a shift in pH. Pre- and post-surgical calibrations of the electrodes, *in-vitro*, showed no difference in their pH sensitivities, ($P = 0.1610$).

The data obtained in Section 7.2.2.1 were adapted to show the percentage change in the anodic peak potential. These were overlaid with data, from the research team, showing the percentage change in oxygen during similar ischemic events, resulting in similar trends, confirming the relationship between tissue oxygen concentration and the potential shift probably caused by changing pH.

Finally, the FBRR/CPEs were examined under conditions where the pH was increased, by the addition of NaHCO_3 to the muscle tissue. Prior to the 1st injection of 45 mM NaHCO_3 , steady CVs were recorded. A change in the potential was not evident until 3 minutes after the 2nd injection, but a significant difference was not found until after the 3rd injection ($P = 0.0030$). Recovery of the potential was almost immediate, fully recovering to the original value within 50 cycles, (25 minutes). Pre- and post-surgical calibrations of the electrodes showed no difference in their pH sensitivities, ($P = 0.3811$).

The results from this chapter show a clear advantage of CPEs over CFEs due to the design and fragility of the fibres used. The FBRR/CPEs functioned exceptionally well during *in-vivo* testing, compounding their ability to monitor the potential shift most likely attributed to real-time changes in pH.

7.4 References

1. J. R. Pineyro, *Journal of Pediatric Surgery*, 1979, **14**, 77-79.
2. R. M. Filler, J. B. Das, G. M. Haase and P. K. Donahoe, *Journal of Pediatric Surgery*, 1971, **6**, 535-542.
3. K. Takano, S. Yosii, S. Hosaka, R. Hashimoto, T. Matsukawa and Y. Tada, *Journal of Pediatric Surgery*, 1993, **28**, 1376-1379.
4. R. D. O'Neill, *Sensors*, 2005, **5**, 317-342.
5. R. D. O'Neill, *Analyst*, , 1993, **118**, 433-438.
6. F. Crespi, *Biosensors and Bioelectronics*, 1996, **11**, 743-749.
7. A. Jabre, Y. Bao and E. L. Spatz, *Surgical Neurology*, 2000, **54**, 55-58.
8. A. Kabaroudis, T. Gerassimidis, D. Karamanos, B. Papaziogas, V. Antonopoulos and A. Sakantamis, *Journal of Investigative Surgery*, 2003, **16**, 219-228.
9. S. Kun, B. Ristic, R. A. Peura and R. M. Dunn, *IEEE Transactions on Biomedical Engineering*, 2003, **50**, 1352-1359.
10. F. A. Gallagher, M. I. Kettunen, S. E. Day, D.-E. Hu, J. H. Ardenkjaer-Larsen, R. in't Zandt, P. R. Jensen, M. Karlsson, K. Golman, M. H. Lerche and K. M. Brindle, *Nature* 2008, **453**, 940-943.
11. H. J. Adroque and N. E. Madias, *New England Journal of Medicine*, 1998, **338**, 107-111.
12. G. L. Smith, C. Austin, C. Crichton and S. Wray, *Cardiovascular Research*, 1998, **38**, 316-331.
13. E. M. Ostrea, Jr. and G. B. Odell, *Journal of Pediatrics*, 1972, **80**, 671-680.
14. J. Levraut, C. Giunti, J.-P. Ciebiera, G. De Sousa, R. Ramhani, P. Payan and D. Grimaud, *Critical Care Medicine*, 2001, **29**, 1033-1039.
15. J. Levraut, Y. Labib, S. Chave, P. Payan, M. Raucoules-Aime and D. Grimaud, *Kidney International*, 1996, **49**, 1262-1267.
16. H. J. Adroque and N. E. Madias, *New England Journal of Medicine*, 1998, **338**, 26-34.
17. D. W. Richardson, A. J. Wasserman and J. L. Patterson, Jr., *Journal of Clinical Investigation*, 1961, **40**, 31-43.

18. S. A. Grant, K. Bettencourt, P. Krulevitch, J. Hamilton and R. Glass, *Sensors and Actuators, B*, 2001, **72**, 174-179.
19. M. L. Huffman and B. J. Venton, *Analyst* 2009, **134**, 18-24.
20. P. Takmakov, M. K. Zachek, R. B. Keithley, E. S. Bucher, G. S. McCarty and R. M. Wightman, *Analytical Chemistry*, 2010, **82**, 9892-9900.
21. I. A. Silver, *Philosophical Transactions of the Royal Society of London*, 1987, **316**, 161-167.
22. J. P. Lowry, M. G. Boutelle and M. Fillenz, *Journal of Neuroscienc Methods*, 1997, **71**, 177-182.
23. X.-r. Huang, Q.-q. Ren, X.-j. Yuan, W. Wen, W. Chen and D.-p. Zhan, *Electrochemistry Communications*, 2014, **40**, 35-37.
24. R. D. O'Neill, R. A. Gruenewald, M. Fillenz and W. J. Albery, *Neuroscience*, 1982, **7**, 1945-1954.
25. J. P. Lowry, M. G. Boutelle, R. D. O'Neill and M. Fillenz, *Analyst*, 1996, **121**, 761-766.
26. D. A. Kane and R. D. O'Neill, *Analyst*, 1998, **123**, 2899-2903.
27. M. C. Brahim-Horn and J. Pouyssegur, *FEBS Letters*, 2007, **581**, 3582-3591.
28. E. Gnaiger, G. Mendez and S. C. Hand, *Proceedings of the National Academy of Sciences* 2000, **97**, 11080-11085.
29. M. Erecinska and I. A. Silver, *Respiration Physiology*, 2001, **128**, 263-276.
30. D. Troitzsch, S. Vogt, H. Abdul-Khaliq and R. Moosdorf, *Journal of Surgical Research*, 2005, **128**, 9-14.
31. A.-D. Andersen, K. A. Poulsen, I. H. Lambert and S. F. Pedersen, *American Journal of Physiology*, 2009, **296**, C1227-C1242.
32. A. Bhargava, A. Chanmugam and C. Herman, *Diagnostic Pathology*, 2014, **9**, 36.
33. M. Fierheller and R. G. Sibbald, *Advances in Skin and Wound Care*, 2010, **23**, 369-379; quiz 380-361.
34. M. C. Blanco-Lopez, M. J. Lobo-Castanon, A. J. M. Ordieres and P. Tunon-Blanco, *Electroanalysis*, 2007, **19**, 207-213.
35. D. Desmond, B. Lane, J. Alderman, J. D. Glennon, D. Diamond and D. W. M. Arrigan, *Sensors and Actuators, B*, 1997, **44**, 389-396.

-
36. A. Abbaspour and E. Mirahmadi, *Fuel*, 2013, **104**, 575-582.
 37. D. Uhlmann, U.-C. Pietsch, S. Ludwig, J. Hess, B. Armann, G. Gaebel, E. Escher, L. Schaffranietz, A. Tannapfel, M. Fiedler, J. Hauss and H. Witzigmann, *Microvascular Research*, 2004, **67**, 38-47.
 38. O. Korostynska, K. Arshak, E. Gill and A. Arshak, *IEEE Sensors Journal*, 2008, **8**, 20-28.
 39. A. J. Brooks, J. S. Hammond, K. Girling and I. J. Beckingham, *Journal of Surgical Research*, 2007, **141**, 247-251.
 40. Y. Ha, D. Myung, J. H. Shim, M. H. Kim and Y. Lee, *Analyst* 2013, **138**, 5258-5264.
 41. A. S. Allegretti, J. E. Flythe, V. Benda, E. S. Robinson and D. M. Charytan, *BioMed Research International*, 2015, 1-9.

Chapter 8

General Conclusions

8.1 Conclusions

Chapter 3 of this thesis involved the investigation of the electrochemical properties of different morphologies of PPy. Pyrrole was electrodeposited onto gold electrodes in two conformations, bulk and nanowire. The polymers were deposited from the same conditions, but altering the electrolyte solution pH, to obtain the different morphologies. CV studies revealed that the bulk polymer had a much higher capacitance than the nanowires due to its larger surface area. A second bulk polymer with a similar surface area to that of the nanowire polymer was subsequently deposited, CV showed these two polymers to have similar capacitances.

The electrochemical properties of the polymers were compared using EIS. Bare gold electrodes were compared to the PPy modified electrodes. The Nyquist plots revealed considerable differences in the resulting impedance spectra. The results were fitted to the same equivalent circuit, enabling easy comparison of the electrical properties. Modification with both morphologies of PPy, nanowire and bulk, improved the electronic properties of the films, illustrated by the reduction of the polymer resistances.

The impedance experiments were carried out over various potentials to examine the effect of the applied potential on the polymers. The bulk polymer, grown for 300 s, displayed characteristics of over-oxidation at an applied potential of 0.50 V *vs.* SCE, which were not evident in the nanowire film. There was a clear change in the shape of the Nyquist plots with the negative shift in potential, indicating that the electrochemical properties of PPy films varied as the polymer changed from an oxidised to a reduced state. The effect of the electrolyte pH on the electronic characteristics of the films revealed that the polymers stored less charge in an alkaline solution.

It must be stated clearly here, that the bulk and nanowire polymers formed in this section were not optimised for their electrochemical properties. They were specifically designed to form from either the same deposition conditions, or be of similar electroactive surface area.

The main aim of the research carried out in this section was to develop a robust, miniaturised, voltammetric pH sensor, which could accurately detect pH changes in physiological environments. Real-time monitoring of pH levels is important for many reasons. Tissue oxygenation, and therefore pH, is severely disturbed during pathological illnesses such as stroke and cancer.⁴⁰ Tumour pH, for example, is more acidic than that of normal tissue in both animals and humans, due to elevated levels of anaerobic and aerobic glycolysis.⁴¹ Most estimates of tissue pH have been obtained by insertion of pH electrodes,⁴² many of which are too large to obtain precise localised readings. A pH sensitive quinone, FBRR, was electrochemically deposited onto carbon surfaces. The $2e^-/2H^+$ quinone/hydroquinone redox process results in potentiometric equilibrium potentials which vary with pH in a Nernstian manner.

Chapter 4 investigated the optimal deposition parameters of FBRR onto CPEs. The electrochemical techniques of LSV and CV were employed, using either acidic⁴³ (H_2SO_4) or organic⁴⁴ ($TEABF_4/ACN$) electrolyte solutions. Although the reduction of aryl diazonium salts generally results in multilayers,⁴⁵ the formation of a uniformly distributed monolayer of FBRR on the substrate was desirable in order to minimise the diffusion layer thickness⁴⁶ therefore increasing the electron transfer kinetics. This was achieved by optimising the number of deposition sweeps or cycles. Other deposition parameters optimised included the scan rate, age of the deposition solution and potential window applied.

The deposition of FBRR, by LSV in $TEABF_4/ACN$, resulted in broad ill-defined redox peaks, impeding the ability to precisely locate the peak potentials. Similar deposition by CV resulted in improved, yet broad redox peaks, indicative of slow electron transfer, possibly due to the presence of the non-conducting silicone oil in the CPE or due to the formation of multi-layers of FBRR on the surface, increasing the diffusion layer thickness. As the $TEABF_4/ACN$ has a similar polarity to the silicone oil contained in the CPEs, it is likely that some oil is removed from the electrode surface, leaving a more carbon-like electrode. The decrease in the silicone oil content facilitates the reduction of FBRR onto the surface, enabling the formation of multilayers, which increase the diffusion layer thickness. The resulting modified electrodes were cycled in PBS solutions with pH values relevant to biological media, i.e., between 7.2 and 7.6. The cycling parameters were investigated, including scan rate and the optimum

potential window, which would give well defined reproducible redox peaks. All deposition of FBRR in TEABF₄/ACN resulted in inconsistent non-Nernstian pH sensitivities. The existence of a second oxidation peak in all CVs was investigated and it was concluded that it resulted from ZnCl₂, which was present in the FBRR salt. Methods to reduce the interfering effect of the ZnCl₂ were devised. The electrodeposition of FBRR using H₂SO₄ as the supporting electrolyte was also carried out using the techniques of CV and LSV. Although improved pH sensitivities resulted from the CV deposition, the peaks remained broad. However, deposition by LSV, yielded well defined peaks, with Nernstian pH sensitivities of *ca.* -59 mV/pH. The introduction of the acidic electrolyte solution was beneficial to the sensor design, possibly enabling the deposition of FBRR in monolayers. Throughout the optimisation process, the anodic peak, of the resultant CVs, consistently displayed sharper, more defined peaks than the cathodic peaks, facilitating the extrapolation of peak potentials for pH sensitivity analyses. The electrodes remained stable over time, (*ca.* 3.5 hours), with little or no drift in their pH response.

Once the sensor design was optimised and it was capable of recording real-time *in-vitro* pH changes, a rigorous regime of test conditions were applied to the working sensor, in order to evaluate its long term stability and its suitability for use in the harsh *in-vivo* environment. Calibrated, modified CPEs were stored at 4°C in air and N₂, for up to 1 month before being re-calibrated. Storage under N₂ gave inconsistent results with significant differences between pre- and post-storage calibrations, ($P < 0.05$), however, no significant differences were uncovered when the electrodes were stored in air, ($P > 0.05$).

The biocompatibility of the modified electrodes was studied by cycling and storing them in lipid, protein and surfactant solutions. Consistent fouling of the electrodes, along with the removal of silicone oil from the electrode surface, resulted in increased capacitances in all cases examined. It was suggested that some FBRR was also lost along with the oil. However, it was observed that cycling the sensors in the aforementioned solutions proved less detrimental to the appearance of the redox peaks than storage. The constant application of cathodic and anodic potentials seemed to prevent the build-up of material on the electrode surface. A more relevant biocompatibility test was performed using *ex-vivo* brain tissue, which, even after 28

days storage, exhibited pH sensitive redox peaks. As the silicone oil was withdrawn from the electrode surfaces, a study was carried out into the extent of this loss after storage and cycling in the various treatments. Analyses confirmed that more oil was lost during storage. SMCPEs were introduced in an attempt to reduce the amount of oil lost from the sensors.⁴⁷ Once the optimum styrene:paste ratio was attained, the biocompatibility tests were repeated. Upon cycling the resulting electrodes, lower currents were obtained, possibly indicating a reduction in the oil loss. This was confirmed by EDX. Real-time testing of the SMCPEs revealed good pH sensitivity of *ca* -60 mV/pH. However, as the styrene modification added two days to the manufacturing process, without substantially improving their response, the treatment was deemed unnecessary.

Within the *in-vivo* environment exists a substantial number of endogenous electroactive species that could interfere with the oxidation peak of FBRR at CPEs. A full and comprehensive study into their effects, and those of some pharmacological interferences, on the oxidation peak of the modified electrodes was executed. The sensors were cycled in solutions containing physiologically relevant concentrations of these substances in order to mimic the *in-vivo* environment. Some of these interferences caused a shift in pH of the electrolyte solution and when this was incorporated into the analyses, there were no significant differences in pH sensitivities pre- and post- treatment, ($P > 0.05$). A particular limitation of optical pH sensors is their response to changing the solution ionic strength. The voltammetric sensor was subjected to increased and decreased ionic strengths without affecting its sensitivity. As pH is temperature dependent, and all previous tests were performed at room temperature, the sensors were tested at 37°C, to examine their operating viability in living tissue. To further mimic *in-vivo* conditions, a pseudo Ag/AgCl reference electrode replaced the SCE that had been utilised in all previous *in-vitro* testing. Both these tests confirmed the successful operation of the FBRR modified CPEs and deemed them suitable for use in the challenging clinical environment.

Chapter 6 investigated the use of FBRR modified CFEs as pH sensors. As the CPEs had an inherent disadvantage due to the oil loss from their surface, the homogeneous formation of carbon fibres should be advantageous. Also the CPEs had an overall diameter of 0.27 mm, whereas the fibres were only 7 μ m in diameter. This reduced

size would cause less trauma on insertion into living tissue. The optimised deposition parameters obtained for CPEs were applied here, but proved unsuccessful, attaining a non-Nernstian pH sensitivity of -130 ± 39 mV/pH. Also, the redox peaks disappeared over time indicating that covalent attachment of the FBRR to the carbon substrate had not been achieved.

The electrochemical pre-treatment of carbon electrodes has been widely used to improve electrode response⁴⁸ and increase electron transfer kinetics,⁴⁹ by scratching the surface thereby increasing the surface area⁵⁰ or by forming oxides on the electrode surface.⁵¹ Because the surface oxides formed during electrochemical pre-treatment may include H atoms, the pH of the solution used plays an important role,⁴⁸ so electrochemical pre-treatments were performed in acidic, neutral and alkaline solutions, at various potentials and time intervals. The optimum pre-treatment was the application of a constant potential of 2.0 V vs. SCE for 30 s followed by -2.0 V vs. SCE for 10 s, in a 0.1 M H₂SO₄ solution. The anodic peaks were further improved by depositing the FBRR from a solution of 0.1 M TEABF₄/ACN, and not H₂SO₄ as for CPEs and achieved a pH sensitivity of -55 ± 0.7 mV/pH, $n = 20$. However, the modified CFEs were not as reliable as their CPE counterpart. Inter-electrode variability became an issue, leading to large errors when the sensor was subjected to real-time pH testing, with a sensitivity of -67 ± 6 mV/pH.

The main reason for developing the pH sensor on CFEs was to eliminate the oil loss that occurred with CPEs. The modified CFEs were subjected to treatment in protein, lipid and a surfactant, giving almost identical results pre- and post-treatment after 24 hours. This outcome gave the CFEs an advantage over modified CPEs. The long term stability was examined by storing the electrodes in air and N₂ for up to 1 month, with no change in their sensitivities. The CFE pH sensor was then subjected to a similar regime of tests to ascertain the suitability for its use in the physiological environment. These tests included physiological and pharmacological interferences, temperature, ionic strength and changing the reference electrode. All resulted in non-significant differences, before and after treatment, ($P > 0.05$), except increasing the temperature to 37°C ($P = 0.0208$). The issue with reproducibility remained for the CFE sensor, and proved to be a major limitation in the sensor design.

Finally, Chapter 7 introduced a working application of the miniaturised, voltammetric pH sensors, where the working, auxiliary and reference electrodes were inserted, through a catheter, into the hind limb of anaesthetised rats. The modified CFEs proved problematic. Due to the glass capillary, surrounding the fibre, insertion of the working electrode was through a separate catheter. The proximity of the electrodes in the system could not be guaranteed, due to movement and the highly resistive nature of the muscle. This caused fluctuations in the currents obtained. The fragility of the CFEs also resulted in fracture of the sensors.

CPEs, on the other hand, proved very successful at recording pH fluctuations in living tissue. Perturbations in pH were incurred through the hind limb ischemia model leading to a drop in pH, or injection of NaHCO_3 to inflict a rise in pH. On insertion, the sensors were allowed to equilibrate before inducing ischemia by application of a tourniquet. The ischemic event was continued for a period of 10 minutes and showed a significant change in pH, ($P < 0.0001$), corresponding to a drop of 0.65 pH units, before the tourniquet was released and the tissue pH was allowed to recover. The modified CPEs were calibrated *in-vitro* before implantation and then post-surgery resulting in no significant difference in their pH sensitivities ($P = 0.1610$).

Tissue ischemia occurs when blood flow is restricted, resulting in inadequate oxygen supply to the affected region.³⁵ Tissue oxygen data, acquired during ischemic events, was supplied by Dr. Niall Finnerty, Maynooth University, and was compared directly with the potential response from the CPE pH sensor. The pH sensor closely mirrored the oxygen data, demonstrating the successful operation of the sensor and that monitoring tissue pH can be used as a reliable indicator of the onset of tissue ischemia.

To confirm the ability of the designed sensor to detect pH changes, injections of NaHCO_3 were administered to the anaesthetised animals. This caused a shift in the peak potential, corresponding to a pH increase of 0.61 pH units, before the onset of recovery. Evidence of injection stress was also uncovered. Each sensor was calibrated pre- and post-surgery and revealed no significant difference in their pH sensitivities, ($P = 0.3811$).

In conclusion, a miniaturised, voltammetric pH sensor was successfully developed. Modification of CPEs and CFEs with the quinone containing FBRR salt, resulted in

sensors with Nernstian pH sensitivities. The CPEs proved to be the optimal sensor substrate. These sensors remained calibrated for a period of at least 1 month, they showed little or no drift, were reliable, biocompatible, temperature and ionic strength stable and showed no ill-effects when subjected to physiological and pharmacological interferences. *In-vivo* testing revealed their successful monitoring of inflicted pH changes, increases and decreases, on anaesthetised animals. Their simple design and easy electrochemical modification makes their production cost and time efficient.

8.2 References

1. J. R. Pineyro, *Journal of Pediatric Surgery*, 1979, **14**, 77-79.
2. R. M. Filler, J. B. Das, G. M. Haase and P. K. Donahoe, *Journal of Pediatric Surgery*, 1971, **6**, 535-542.
3. K. Takano, S. Yosii, S. Hosaka, R. Hashimoto, T. Matsukawa and Y. Tada, *Journal of Pediatric Surgery*, 1993, **28**, 1376-1379.
4. R. D. O'Neill, *Sensors*, 2005, **5**, 317-342.
5. R. D. O'Neill, *Analyst*, , 1993, **118**, 433-438.
6. F. Crespi, *Biosensors and Bioelectronics*, 1996, **11**, 743-749.
7. A. Jabre, Y. Bao and E. L. Spatz, *Surgical Neurology*, 2000, **54**, 55-58.
8. A. Kabaroudis, T. Gerassimidis, D. Karamanos, B. Papaziogas, V. Antonopoulos and A. Sakantamis, *Journal of Investigative Surgery*, 2003, **16**, 219-228.
9. S. Kun, B. Ristic, R. A. Peura and R. M. Dunn, *IEEE Transactions on Biomedical Engineering*, 2003, **50**, 1352-1359.
10. F. A. Gallagher, M. I. Kettunen, S. E. Day, D.-E. Hu, J. H. Ardenkjaer-Larsen, R. in't Zandt, P. R. Jensen, M. Karlsson, K. Golman, M. H. Lerche and K. M. Brindle, *Nature* 2008, **453**, 940-943.
11. H. J. Adroque and N. E. Madias, *New England Journal of Medicine*, 1998, **338**, 107-111.
12. G. L. Smith, C. Austin, C. Crichton and S. Wray, *Cardiovascular Research*, 1998, **38**, 316-331.
13. E. M. Ostrea, Jr. and G. B. Odell, *Journal of Pediatrics*, 1972, **80**, 671-680.
14. J. Levraut, C. Giunti, J.-P. Ciebiera, G. De Sousa, R. Ramhani, P. Payan and D. Grimaud, *Critical Care Medicine*, 2001, **29**, 1033-1039.
15. J. Levraut, Y. Labib, S. Chave, P. Payan, M. Raucoules-Aime and D. Grimaud, *Kidney International*, 1996, **49**, 1262-1267.
16. H. J. Adroque and N. E. Madias, *New England Journal of Medicine*, 1998, **338**, 26-34.
17. D. W. Richardson, A. J. Wasserman and J. L. Patterson, Jr., *Journal of Clinical Investigation*, 1961, **40**, 31-43.
18. S. A. Grant, K. Bettencourt, P. Krulevitch, J. Hamilton and R. Glass, *Sensors and Actuators, B*, 2001, **72**, 174-179.
19. M. L. Huffman and B. J. Venton, *Analyst* 2009, **134**, 18-24.
20. P. Takmakov, M. K. Zachek, R. B. Keithley, E. S. Bucher, G. S. McCarty and R. M. Wightman, *Analytical Chemistry*, 2010, **82**, 9892-9900.

21. I. A. Silver, *Philosophical Transactions of the Royal Society of London*, 1987, **316**, 161-167.
22. J. P. Lowry, M. G. Boutelle and M. Fillenz, *Journal of Neuroscienc Methods*, 1997, **71**, 177-182.
23. X.-r. Huang, Q.-q. Ren, X.-j. Yuan, W. Wen, W. Chen and D.-p. Zhan, *Electrochemistry Communications*, 2014, **40**, 35-37.
24. R. D. O'Neill, R. A. Gruenewald, M. Fillenz and W. J. Albery, *Neuroscience*, 1982, **7**, 1945-1954.
25. J. P. Lowry, M. G. Boutelle, R. D. O'Neill and M. Fillenz, *Analyst*, 1996, **121**, 761-766.
26. D. A. Kane and R. D. O'Neill, *Analyst*, 1998, **123**, 2899-2903.
27. M. C. Brahim-Horn and J. Pouyssegur, *FEBS Letters*, 2007, **581**, 3582-3591.
28. E. Gnaiger, G. Mendez and S. C. Hand, *Proceedings of the National Academy of Sciences* 2000, **97**, 11080-11085.
29. M. Erecinska and I. A. Silver, *Respiration Physiology*, 2001, **128**, 263-276.
30. D. Troitzsch, S. Vogt, H. Abdul-Khaliq and R. Moosdorf, *Journal of Surgical Research*, 2005, **128**, 9-14.
31. A.-D. Andersen, K. A. Poulsen, I. H. Lambert and S. F. Pedersen, *American Journal of Physiology*, 2009, **296**, C1227-C1242.
32. M. C. Blanco-Lopez, M. J. Lobo-Castanon, A. J. M. Ordieres and P. Tunon-Blanco, *Electroanalysis*, 2007, **19**, 207-213.
33. D. Desmond, B. Lane, J. Alderman, J. D. Glennon, D. Diamond and D. W. M. Arrigan, *Sensors and Actuators, B*, 1997, **44**, 389-396.
34. A. Abbaspour and E. Mirahmadi, *Fuel*, 2013, **104**, 575-582.
35. D. Uhlmann, U.-C. Pietsch, S. Ludwig, J. Hess, B. Armann, G. Gaebel, E. Escher, L. Schaffranietz, A. Tannapfel, M. Fiedler, J. Hauss and H. Witzigmann, *Microvascular Research*, 2004, **67**, 38-47.
36. O. Korostynska, K. Arshak, E. Gill and A. Arshak, *IEEE Sensors Journal*, 2008, **8**, 20-28.
37. A. J. Brooks, J. S. Hammond, K. Girling and I. J. Beckingham, *Journal of Surgical Research*, 2007, **141**, 247-251.
38. Y. Ha, D. Myung, J. H. Shim, M. H. Kim and Y. Lee, *Analyst* 2013, **138**, 5258-5264.
39. A. S. Allegretti, J. E. Flythe, V. Benda, E. S. Robinson and D. M. Charytan, *BioMed Research International*, 2015, 1-9.
40. A. Carreau, B. E. Hafny-Rahbi, A. Matejuk, C. Grillon and C. Kieda, *Journal of Cellular and Molecular Medicine*, 2011, **15**, 1239-1253.

41. J. Wike-Hooley, A. v. d. Berg, J. v. d. Zee and H. Reinhold, *European Journal of Cancer and Clinical Oncology*, 1985, **7**, 785-787.
42. I. F. Tannock and D. Rotin, *Cancer Research*, 1989, **49**, 4373-4384.
43. P. A. Brooksby and A. J. Downard, *Langmuir*, 2004, **20**, 5038-5045.
44. M. A. Makos, D. M. Omiatek, A. G. Ewing and M. L. Heien, *Langmuir*, 2010, **26**, 10386-10391.
45. V. Hambate Gomdje, T. R. Ngono, H. Saadane, M. Ennachete, M. Khouili, A. Hafid, L. Benoit and A. Chtaini, *Pharmaceutica Analytica Acta*, 2013, **4**, 1000271/1000271-1000271/1000274, 1000274 pp.
46. M. Raicopol, L. Necula, M. Ionita and L. Pilan, *Surface and Interface Analysis*, 2012, **44**, 1081-1085.
47. A. M. Wynne, NUI Maynooth, 2014.
48. A. L. Beilby, T. A. Sasaki and H. M. Stern, *Analytical Chemistry*, 1995, **67**, 976-980.
49. P. M. Kovach, M. R. Deakin and R. M. Wightman, *Journal of Physical Chemistry*, 1986, **90**, 4612-4617.
50. Z. Bartosova, D. Riman, P. Jakubec, V. Halouzka, J. Hrbac and D. Jirovsky, *Science World Journal.*, 2012, 295802-295806.
51. L. Agui, D. Vega-Montenegro, P. Yanez-Sedeno and J. M. Pingarron, *Analytical and Bioanalytical Chemistry*, 2005, **382**, 381-387.

8.3 Conference Presentations

Karen Herdman, Dr. Niall Finnerty and Prof. Carmel Breslin, “Electrochemical Characterisation of a Real-Time pH Sensor”, 227th Electrochemical Society Meeting, Chicago, Illinois, U.S.A. 24/05/2015 – 28/05/2015. [Oral Presentation].

Karen Herdman, Dr. Niall Finnerty and Prof. Carmel Breslin, “Electrochemical Characterisation of a Real-Time pH Sensor”, Post Graduate Seminar, Maynooth University, Kildare, Ireland, 06/10/2014. [Oral Presentation].

Karen Herdman and Carmel Breslin, “Comparison of Conductivities of Bulk and Nanowire Morphologies of Electrodeposited Polypyrrole”, 224th Electrochemical Society Meeting, San Francisco, California, U.S.A. 27/10/2013 – 01/11/2013. [Poster Presentation].

8.4 Publication

Karen Herdman and Carmel B. Breslin. “Comparison of Conductivities of Bulk and Nanowire Morphologies of Electrodeposited Polypyrrole”. *ECS Transactions*, 2014, **58** (25), 51-58. [Published].

